U.S. Department
of Transportation
**National Highway
Traffic Safety
Administration**

NHTSA
www.nhtsa.gov

DOT HS 812

December 2014

Comparative Biofidelity Assessment of the Large Omnidirectional Child Prototype and Hybrid III 10-Year-Old ATD

DISCLAIMER

Suggested APA Format Citation:

Suntay, B., & Stammen, J. (2014, December). *Comparative biofidelity assessment of the large omnidirectional child prototype and Hybrid III 10-year-old ATD*. (Report No. DOT HS 812). Washington, DC: National Highway Traffic Safety Administration.

Technical Report Documentation Page

1. Report No. DOT HS 812	2. Government Accession No.	3. Recipient's Catalog No.
4. Title and Subtitle Comparative Biofidelity Assessment of the Large Omnidirectional Child Prototype and Hybrid III 10-Year-Old ATD		5. Report Date December 2014
		6. Performing Organization Code NHTSA/NVS-311
7. Authors Brian Suntay of Transportation Research Center Inc. and Jason Stammen, Ph.D., of NHTSA Vehicle Research and Test Center		8. Performing Organization Report No.
9. Performing Organization Name and Address National Highway Traffic Safety Administration Vehicle Research and Test Center P.O. Box 37 East Liberty, OH 43319		10. Work Unit No. (TRAIS) 11. Contract or Grant No.
12. Sponsoring Agency Name and Address National Highway Traffic Safety Administration 1200 New Jersey Avenue SE. Washington, DC 20590		13. Type of Report and Period Covered Final Report 14. Sponsoring Agency Code
15. Supplementary Notes		

Abstract

A new 10-year-old size thorax, referred to as the large omnidirectional child (LODC), has been developed by the NHTSA Vehicle Research and Test Center (VRTC) to improve the overall response of the Hybrid III 10-year-old ATD (HIII-10C). In this study, the LODC was compared to both the HIII-10C and pediatric data in component and sled tests. The LODC displayed improved biofidelity over the HIII-10C in component and low-speed sled test conditions. In medium and high-speed sled tests, the LODC displayed higher head/spine displacements, chest compressions, and head excursions but lower neck loads than the HIII-10C. The LODC was sensitive to restraint condition, with its measurements identifying differences in protection strategies between a 5 point harness and booster seat. The combined effects of a stiff shoulder, soft thorax, and soft cervicothoracic spine joint resulted in the LODC head contacting the upper leg in some tests. Addressing these individual body components in the next version of the LODC, while improving the durability of the shoulder connection to the thorax, should result in improved kinematics. In summary, the LODC shows promise as a potential enhancement to the HIII-10C. In accordance with the multi-year agency research plan for child dummy enhancements, further evaluation testing will be conducted on an improved version of the LODC starting in summer 2014.

17. Key Words:		18. Distribution Statement: Document is available to the public from the National Technical Information Service www.ntis.gov	
19. Security Classif. (of this report) Unclassified	20. Security Classif. (of this page) Unclassified	21. No. of Pages 164	22. Price

Form DOT F 1700.7 (8-72) Reproduction of completed page authorized

EXECUTIVE SUMMARY

A new 10-year-old size thorax, referred to as the large omnidirectional child (LODC), has been developed by the NHTSA Vehicle Research and Test Center (VRTC) to improve the overall response of the Hybrid III 10-year-old ATD (HIII-10C). In this study, the LODC was compared to both the HIII-10C and pediatric data in component and sled tests.

- The LODC displayed improved biofidelity over the HIII-10C in component and low-speed sled test conditions:
    - In frontal thorax testing, the LODC met a 6 year old-based pediatric response corridor that it was designed to represent.
    - In lateral thorax and shoulder tests, the LODC met scaled 10-year-old response requirements, which is encouraging for testing where oblique loading is present.
    - In quasi-static posteromedial shoulder compressions, the LODC was significantly more stiff than pediatric volunteers but considerably softer than the HIII-10C.
    - In abdomen belt pull tests, the LODC met the pediatric corridor.
    - The LODC thoracic spine was stiffer than human biofidelity target data (scaled 10-year-old), but appeared to approach the human data at higher test speeds.
    - In neck tests, the LODC peak moment was closer to pediatric data in flexion than the HIII-10C. In extension, the LODC rotation was increased from the HIII-10C due to the soft T1 joint. The overall response will be improved by a new omnidirectional neck design.
    - The response of the LODC in repeated testing was very consistent.
    - In low-speed testing, the LODC was closer to the pediatric volunteer response than the HIII-10C, but still too stiff. The high shoulder belt forces reflect the difference in shoulder stiffness between the LODC and volunteer data in the quasi-static compression tests. The greater downward displacement component in the LODC may indicate the effect of active neck musculature in the volunteers.

- In medium and high-speed sled tests, the LODC displayed higher head/spine displacements, chest compressions, and head excursions but lower neck loads than the HIII-10C. The LODC was sensitive to restraint condition, with its measurements identifying differences in protection strategies between a 5-point harness and booster seat.

- There was correlation in HIC for the LODC and HIII-10C in the same restraint condition/pulse combination. It is likely that if the LODC were tested in the same conditions where the HIII-10C has exhibited artificially high HIC values, that the LODC would demonstrate more humanlike head accelerations than the HIII-10C. However, at this time, nothing can be definitively concluded about HIC until a wider range of test conditions can be evaluated with a revised LODC.

- The combined effects of a stiff shoulder, soft thorax, and soft thoracic spine resulted in the LODC head contacting the upper leg in some tests. Addressing these individual body components in the next version of the LODC while improving the durability of the shoulder connection to the thorax should result in improved kinematics.

In summary, the LODC shows promise as a potential enhancement to the HIII-10C. Testing beginning in summer 2014 on an improved LODC will include comparison to the Q10 dummy under development in Europe, testing on the same sled as pediatric volunteers, and FMVSS No. 213-type tests on a larger range of booster seats currently on the market.

TABLE OF CONTENTS

LIST OF FIGURES

LIST OF TABLES

1. Introduction

Child anthropomorphic test devices (ATDs) used to assess the protection provided by belt-positioning booster seats in FMVSS No. 213 regulatory tests have been noted to have biofidelity limitations (49 CFR Part 571). The Hybrid III 6-year old (HIII-6C) and Hybrid III 10-year old (HIII-10C) ATDs have been adopted into CFR 49 Part 572 as the best available tools, but there are some notable shortcomings that prevent them from being utilized fully to assess injurious situations for the occupant. Primarily, chin contacts with the ATD's chest often result in high/variable head accelerations, which has both extended the use of the Hybrid II 6-year old in place of the HIII-6C version (76 FR 55825 under 49 CFR 571) and prevented the use of HIC as a head injury criterion for the HIII-10C in FMVSS No. 213 testing (49 CFR Part 571). These contacts have been attributed to non-biofidelic response of the neck, spine, and shoulder producing excessive head rotation in some situations where injury is not expected. The HIII-10C possesses a rigid thoracic spine and stiff shoulders, with the ribcage being coupled separately to the spine and shoulder. It is important to address the spine and shoulder responses to provide improved head kinematics so that the ATD can be used to evaluate head injury risk in child restraint tests.

In late 2010, the NHTSA Vehicle Research & Test Center (VRTC) tasked Denton (now Humanetics) to design and build a 10-year-old-sized thorax, with anthropometry criteria through consultation with UMTRI (25) and response criteria using pediatric biomechanical data from the literature, as a retrofit package for the HIII-10C. This Large Omnidirectional Child (LODC) thorax possesses several differences from the HIII-10C thorax, including a flexible thoracic spine, multi-point thoracic deflection measurement using IR-TRACCs, and anthropometric ribcage, shoulder, and spine geometry based on child postures while seated in belt-positioning boosters (Figure 1). It was designed to exhibit biofidelic response in both frontal and lateral impacts, which could potentially allow it to be used in test environments that produce off-axis loading. The LODC has a thick flesh wrap surrounding the ribcage and shoulders, as opposed to the bib/flesh jacket and rigid sloped shoulder elements in the HIII-10C. The upper arm attachment is a ball and socket joint as opposed to the clevis pivot in the HIII-10C. The abdomen and pelvis geometry remained unchanged from the Hybrid III 10 year old, except that the LODC abdomen was made softer and also heavier to account for the absence of the chest potentiometer plate. In addition, the UMTRI data showed that the pelvis needed to be further forward with respect to the ribcage. Therefore, the lumbar joint was made to be angled to position the pelvis more realistically. Figure 2 gives more detail on the LODC design and how it differs from the Hybrid III design.

Figure 1. Large omni-directional child, LODC

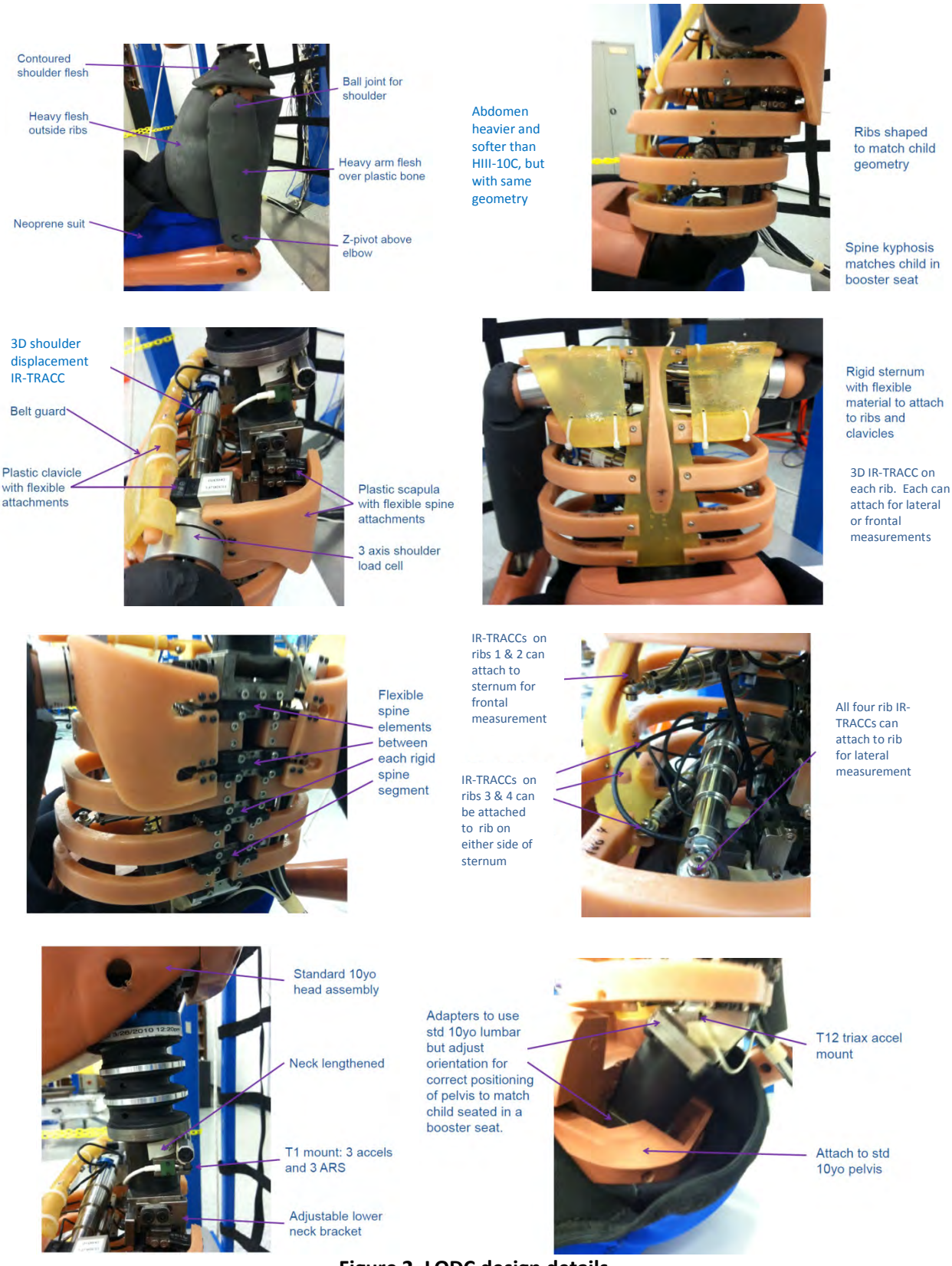

Figure 2. LODC design details

The objective of this study is to evaluate the biofidelity of the HIII-10C equipped with the LODC thorax by comparing component and full-body response to both the standard HIII-10C response and available pediatric biomechanical data.

2. Methods

Table 1 summarizes the sources of pediatric biomechanical criteria for this evaluation. This study focuses on comparing the LODC-equipped HIII-10C with the standard HIII-10C in the frontal condition. The LODC thorax is "omnidirectional" because the shoulder and thorax were designed such that they also matched lateral shoulder and thorax impact criteria specified in Irwin, Mertz, Elhagediab, and Moss (2002). This was done to assure that off-axis loading would be monitored by the ATD in crash scenarios where oblique components are present. Given that the HIII-10C was not designed for lateral impact, it was not tested nor compared with the LODC thorax in these lateral conditions.

Table 1. Summary of pediatric biomechanical criteria for evaluation of 10-year-old size ATDs

Criterion	ATDs Tested	Test Specifications	Source
Frontal Thorax Impact	LODC, HIII-10C	2.9 kg probe impact at 6.0 m/s	Parent et al. (5); Maltese et al. (18); Ouyang et al. (19)
Lateral Thorax Impact	LODC	Low (4.3 m/s) and high (6.0 m/s)-speed impacts with 6.89 kg probe	Irwin et al. (4)
Lateral Shoulder Impact	LODC	6.89 kg probe at 6.0 m/s	Irwin et al. (4)
Shoulder Posteromedial Compression	LODC, HIII-10C	Quasi-static loading of pediatric volunteers	Suntay et al. (6)
Abdomen Belt Loading	LODC	1.5 m/s belt input displacement rate	Kent et al. (7; 8)
Thoracic Spine Flexion	LODC	Isolated segment manipulation (ISM) and fixed spine sled, normalized and scaled	Stammen et al. (9; 10; 11); Donnelly et al. (12; 13); Lopez-Valdes et al. (14; 21); Arbogast et al. (15)
Neck Flexion	LODC, HIII-10C	Pediatric data-validated head neck model in HIII-10C Part 572 neck pendulum test	Dibb et al. (17)
Neck Extension	LODC, HIII-10C	HIII-10C Part 572 neck pendulum	CFR 49 Part 572 Subpart T (2)
Low-speed Kinematics	LODC, HIII-10C	Low-speed frontal sled tests using bumper car-based pulse	Arbogast et al. (15)

2.1. Component Testing

A component biofidelity evaluation was conducted to compare both the standard and LODC-equipped HIII-10C (referred to as "LODC" for the remainder of this report) to available biomechanical targets. Tests included neck flexion and extension, lateral/frontal low and high-speed thorax impact, lateral dynamic impact and posteromedial quasi-static shoulder compression, and frontal dynamic abdomen

belt pulls. To assess the thoracic spine, the LODC was tested in both the system identification-based Isolated Segment Manipulation (ISM) and vertebral fixation upper thoracic spine – pectoral girdle (UTS-PG) setups.

2.1.1. Frontal Thorax

Biomechanical Target

Three studies provide direct examination of pediatric thorax response. Ouyang et al. (2006) conducted pendulum hub impacts to the anterior thorax of pediatric specimens age 2 – 12. This data was later re-processed by Parent et al. (2002) along with cardiopulmonary resuscitation (CPR) data from Maltese et al. (2010) to derive biofidelity targets for 3/6-year-old ATDs. Following the development of the LODC, a more appropriate 10-year-old biofidelity target using a 6.89 kg probe mass was created using the method presented by Irwin et al. (2002). Both corridors are shown in Figure 3.

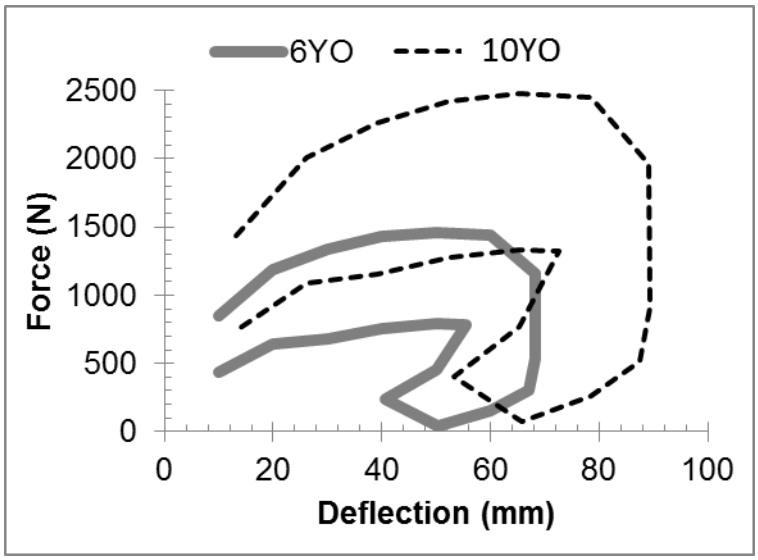

Figure 3. Six and ten-year old ATD thorax impact biofidelity force-deflection corridors. The 6-year-old corridor was developed using a 2.9 kg probe at 6.7 m/s. The 10-year-old corridor was developed using a 6.89 kg probe at 6.0 m/s. Note that deflection is an external measurement.

The LODC was designed to meet the six-year-old force versus displacement response because that was the only target developed directly from human data at the time the LODC was being designed. In this study, the HIII-10C was tested in both the six year old-based (2.9 kg, 6.7 m/s) and higher energy HIII-10C Part 572 (6.89 kg, 6.0m/s) thorax impact conditions. The LODC was tested at the HIII-6C Part 572-speed (6.7 m/s) using a 6-year-old probe (2.9 kg) due to concerns regarding IR-TRACC damage from applying a higher energy condition to a thorax designed to meet the six-year-old biofidelity response. Therefore, in this study there was less emphasis on the comparison of the HIII-10C and LODC with respect to the six-year-old biofidelity corridor and more emphasis on how closely the LODC follows the six year old-based design corridor. In the next phase of this study, the next iteration of the LODC will be tested against the 10-year-old biofidelity corridor shown in Figure 3 for a more appropriate comparison of the two 10-year-old size dummies.

ATD Test Setup

For this lower energy biofidelity condition, the LODC was positioned similar to the HIII-10C ATD position in a Part 572 frontal thorax impact test. The dummy was seated on the test bench with the legs extended and arms held forward parallel to the legs. The torso was positioned so that the dummy was level side to side and the spine was at a 90° angle with the bench surface, which resulted in a pelvis angle of 26° and a neck that was angled slightly forward (Figure 4). The impact point was located along the mid-sagittal plane of the LODC, ½ inch down from the center of the second rib and was impacted by a 2.9 kg probe with an impact face diameter of 121 mm (± 0.25 mm). The impact velocity was 6.0 m/s. The dummy was suited with a neoprene jacket during the test. The test setup is shown in Figure 5.

For frontal thorax testing, the LODC was instrumented with three uniaxial accelerometers and three angular rate sensors mounted in the X, Y, and Z-axis directions at T1; three uniaxial accelerometers mounted in the X, Y, and Z-axis directions at T12; a uniaxial accelerometer mounted in the Y-axis direction on each of the masses of ribs 2 and 3; and two three-dimensional IR-TRACCs mounted in the frontal configuration at ribs 2 and 3. A uniaxial accelerometer was mounted at the rear of the probe to calculate impact force, and a light trap was used to measure impact velocity.

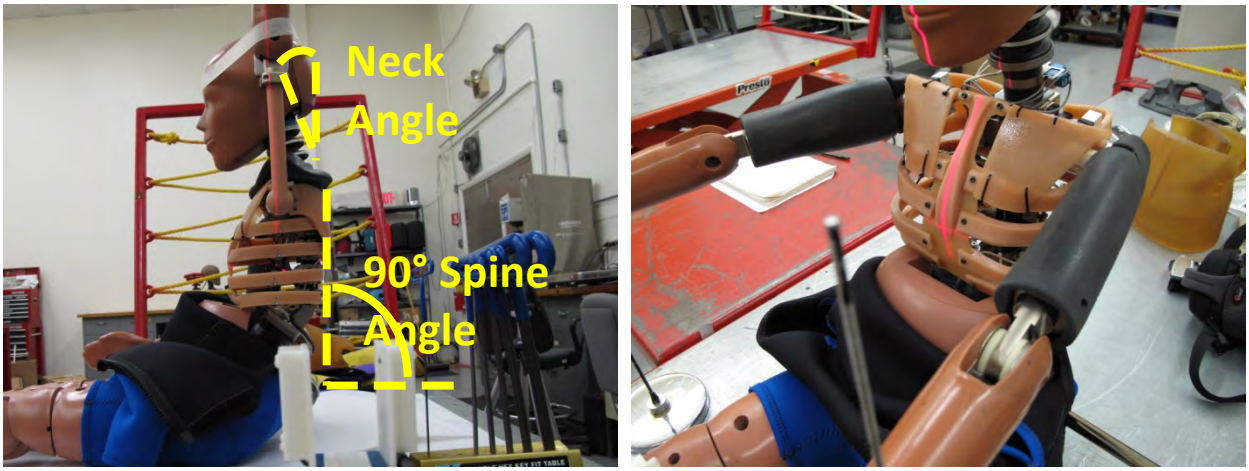

(a) (b)

Figure 4. Dummy posture (a) and location of impact centerline (b) in frontal thorax test

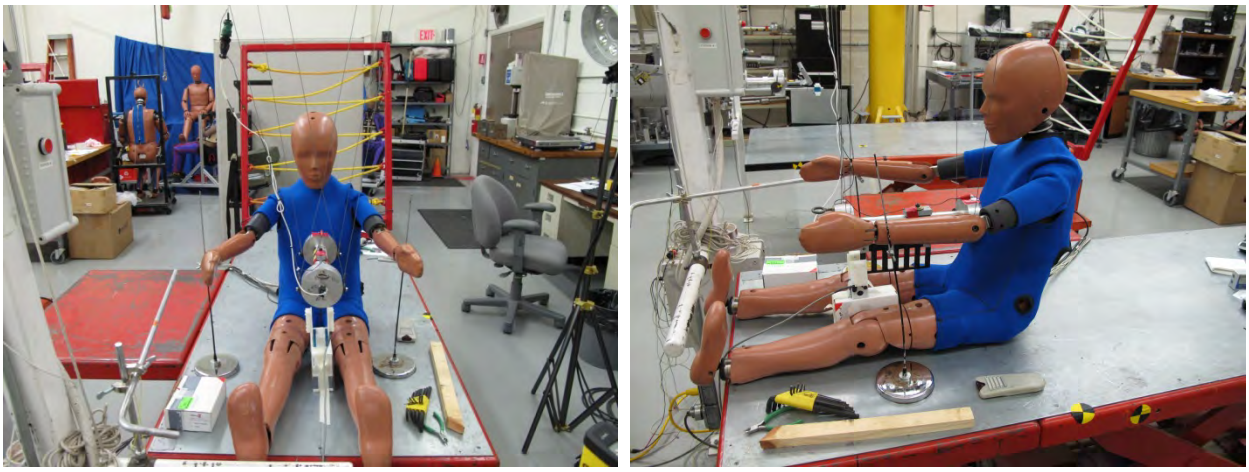

(a) (b)

Figure 5. Front (a) and side (b) views of frontal thorax impact setup

2.1.2. Lateral Thorax

Biomechanical Target

The LODC thorax was designed to meet the low (4.3 m/s) and high (6.0 m/s)-speed scaled side impact response requirements using a 6.89 kg probe (Irwin et al. 2002), as shown in Figure 6 and Figure 7. The HIII-10C thorax is not designed for lateral impact and was therefore not tested or compared with the LODC in this condition.

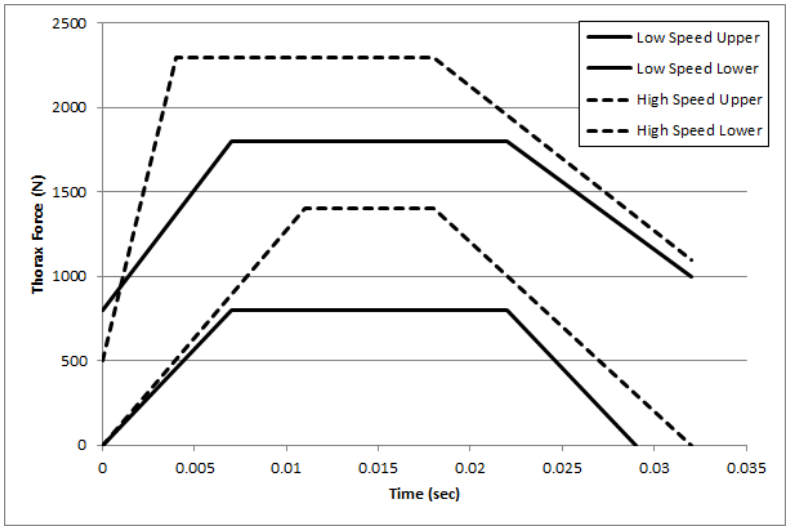

Figure 6. Lateral 10-year-old thorax force corridors (from Irwin et al. (2002)

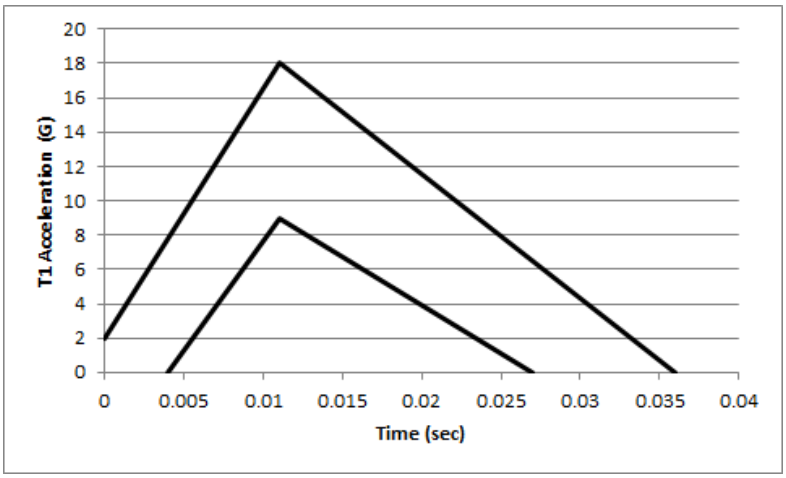

Figure 7. Lateral 10-year-old T1 acceleration corridors (from Irwin et al. 2002)

ATD Test Setup

The LODC was positioned similar to the frontal thorax tests, but rotated 90° so that the dummy's left side was impacted. The dummy was seated on two Teflon sheets with the legs extended. The right arm was held at the dummy's side and bent at the elbow at 90°. The left arm was held up vertically and taped to the head. The torso was positioned so that the dummy was level side to side and the spine was at a 90° angle with the bench surface, which resulted in a pelvis angle of 26° and a neck that was angled slightly forward. The impact point was located along the lateral plane of the LODC, between the second and third rib (Figure 8) and was impacted by a 6.89 kg probe with an impact face diameter of 121 mm (± 0.25 mm). The impact velocity was 4.3 m/s for low-speed tests and 6.0 m/s for high-speed tests.

For lateral thorax testing, the LODC was instrumented with three uniaxial accelerometers and three angular rate sensors mounted in the X, Y, and Z-axis directions at T1; three uniaxial accelerometers mounted in the X, Y, and Z-axis directions at T12; a uniaxial accelerometer mounted in the Y-axis direction on each of the masses of ribs 2 and 3; and two three-dimensional IR-TRACCS mounted in the lateral configuration at ribs 2 and 3. A uniaxial accelerometer was mounted at the rear of the probe to calculate impact force, and a light trap was used to measure impact velocity.

Due to interference with the probe, the upper arm flesh on the impact side was removed and the dummy was not fully suited with a neoprene jacket during the test. However, a small section of neoprene material was taped to the impact point to replicate the response of having a neoprene jacket. The test setup is shown in Figure 9.

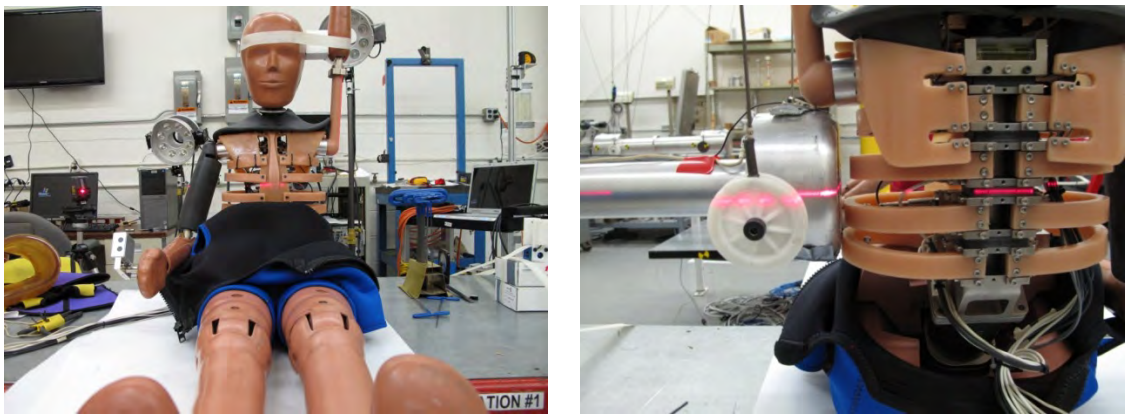

Figure 8. Dummy posture (a) and location of impact centerline (b) in lateral thorax test

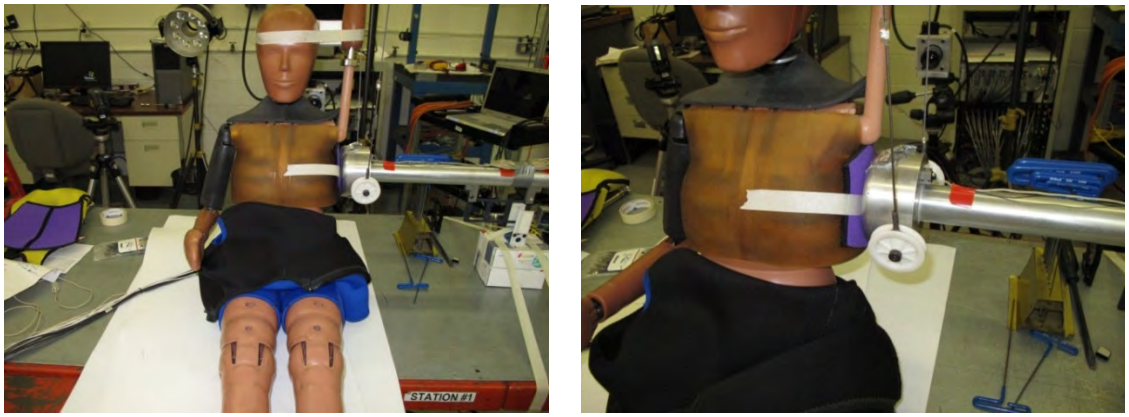

Figure 9. Front (a) and oblique (b) views of lateral thorax impact setup

2.1.3. Shoulder

2.1.3.1. Lateral Pendulum Impacts

Biomechanical Target

The LODC shoulder was designed to meet scaled side impact shoulder response requirements using a 6.89 kg probe (Irwin et al. 2002), as shown in Figure 10. The HIII-10C shoulder is not designed for lateral impact and was therefore not tested or compared with the LODC in this condition.

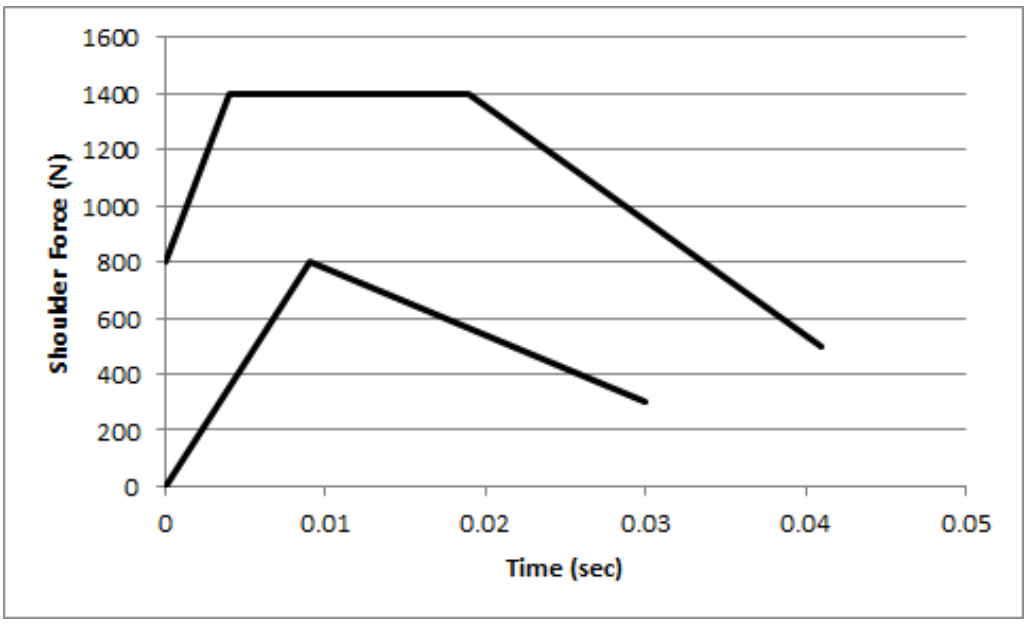

Figure 10. Lateral 10-year-old shoulder force corridor from Irwin et al (2002)

ATD Test Setup

The LODC was positioned similar to the lateral thorax tests so that the dummy's left side was impacted. The dummy was seated on two Teflon sheets with the legs extended. Both arms were held down at the dummy's sides and bent at the elbow at 90°. The torso was positioned so that the dummy was level side to side and the spine was at a 90° angle with the bench surface, which resulted in a pelvis angle of 26° and a neck that was angled slightly forward. The impact point was located along the lateral plane of the LODC and centered at the shoulder load cell socket (Figure 11). The shoulder was impacted by a 6.89 kg probe with an impact face diameter of 121 mm (± 0.25 mm). The impact velocity was 4.5 m/s.

For the lateral shoulder pendulum impacts, the LODC was instrumented with three uniaxial accelerometers and three angular rate sensors mounted in the X, Y, and Z-axis directions at T1; three uniaxial accelerometers mounted in the X, Y, and Z-axis directions at T12; a uniaxial accelerometer mounted in the Y-axis direction on each of the masses of ribs 2 and 3; and two three-dimensional IR-TRACCS mounted in the lateral configuration at ribs 2 and 3. A uniaxial accelerometer was mounted at the rear of the probe to calculate impact force, and a light trap was used to measure impact velocity.

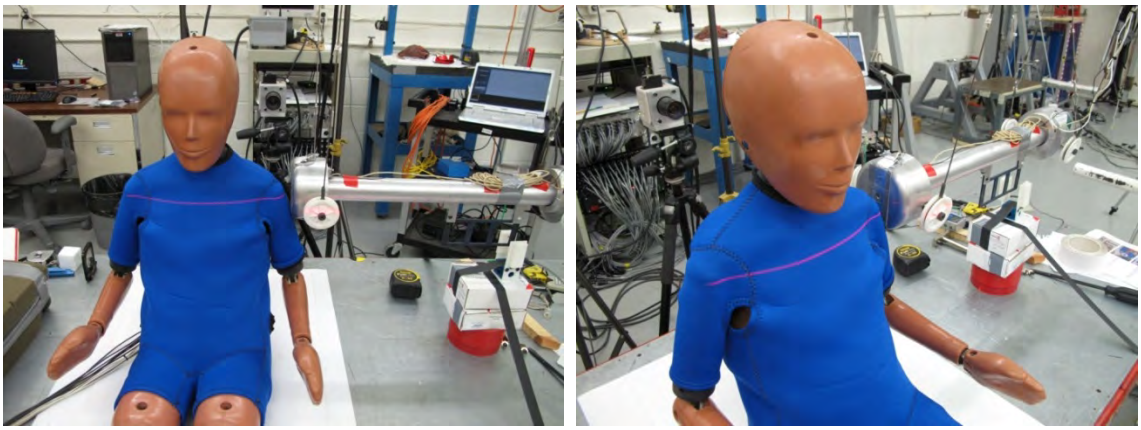

(a) (b)

Figure 11. Lateral shoulder impact setup

2.1.3.2. Quasi-Static Posteromedial Testing

Biomechanical Target

No information exists on the frontal stiffness of the pediatric shoulder at crash-level-speeds. Suntay et al. (2011) investigated the quasi-static shoulder stiffness of pediatric volunteers at a loading angle of 30° anterior of lateral ("posteromedial") and split the data into 6-year-old and 10-year-old age bins for direct comparison with child ATDs (Figure 12).

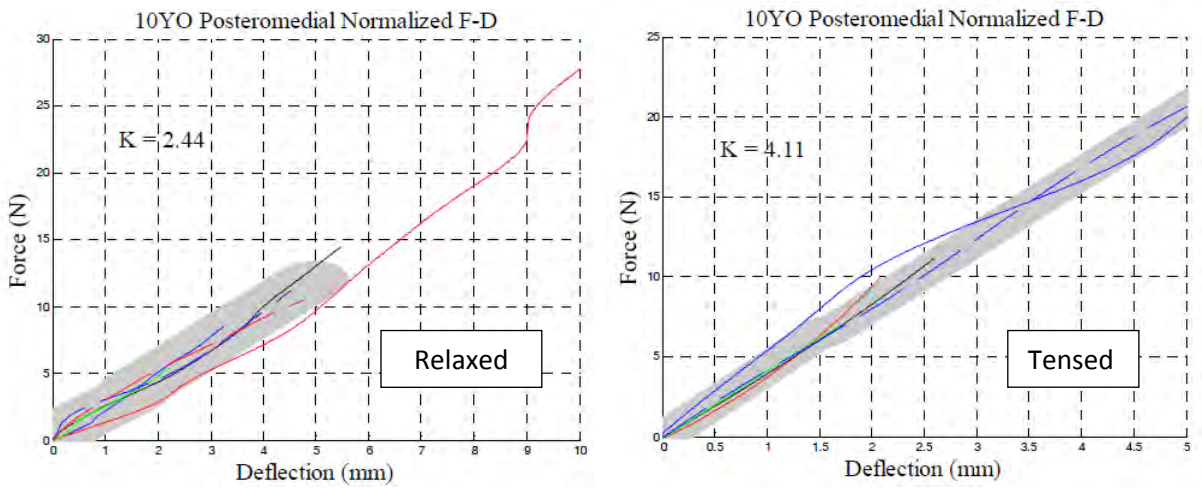

Figure 12. Posteromedial shoulder response target for 10-year-old (from Suntay et al. 2011)

ATD Test Setup

For quasi-static shoulder testing, the LODC was seated on a bench that was placed at the center of an 8-camera, 100 Hz VICON optical motion analysis system (Figure 13). The dummy was seated on the right edge of the bench with the right side of the seatback along the dummy's spine, allowing for a free range of motion of the shoulder (Figure 14). With the LODC in position, a load wall was applied to the

subject's left shoulder and clamped onto the bench to prevent any translational motion of the dummy during testing.

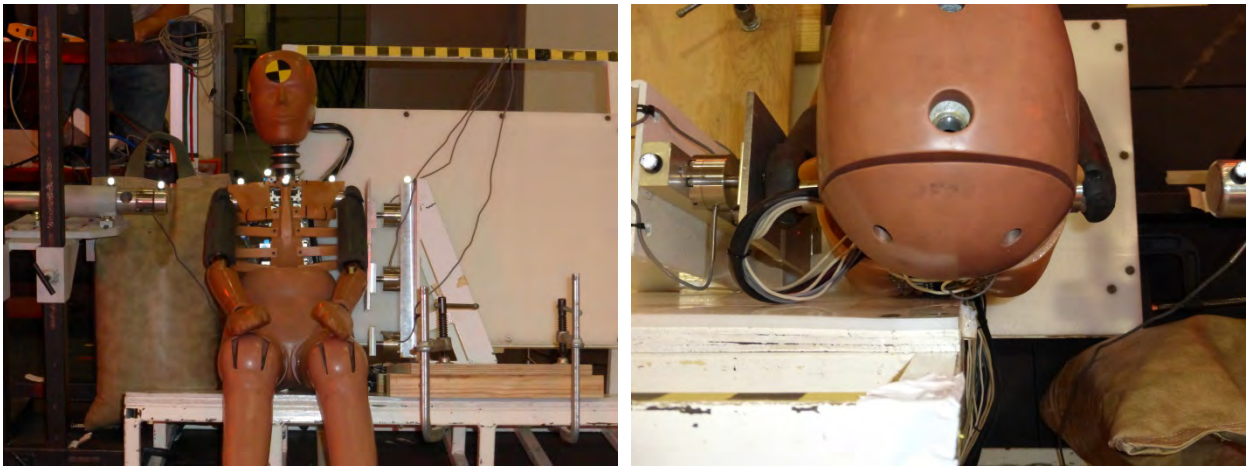

(a) (b)

Figure 13. Front (a) and top (b) views of LODC in quasi-static shoulder test

To measure the forces needed to displace the shoulder, a load cell (Honeywell Model 31 Mid-Range Precision Miniature Load Cell) was attached to a linear force applicator. A frame, with translational motions in the X, Y, and Z-directions, was used to properly align the force applicator at the center of the shoulder socket in the desired direction of loading. To measure shoulder girdle deflection, reflective markers (Figure 15) were placed over the acromion processes of both shoulders, the manubrium, the neck, the force applicator, and the load wall. Quasi-static tests were performed in the same 30° posteromedial direction as the pediatric volunteers.

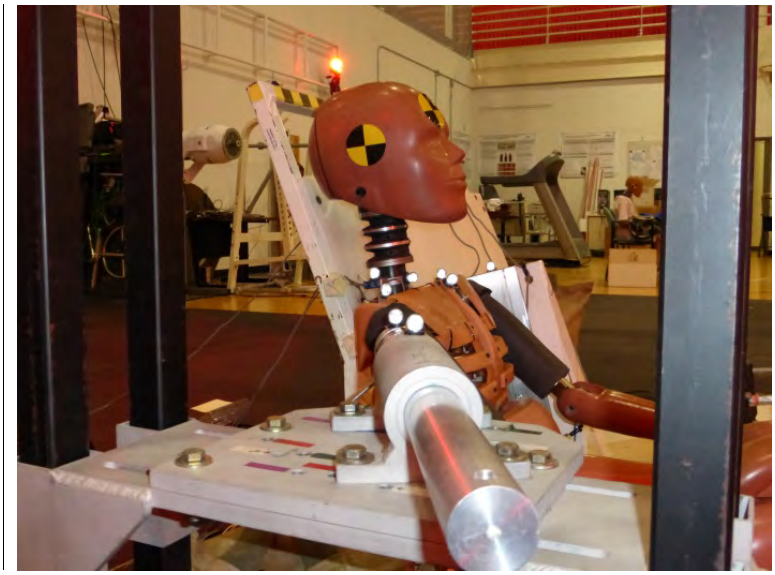

Figure 14. Test direction in quasi-static shoulder test

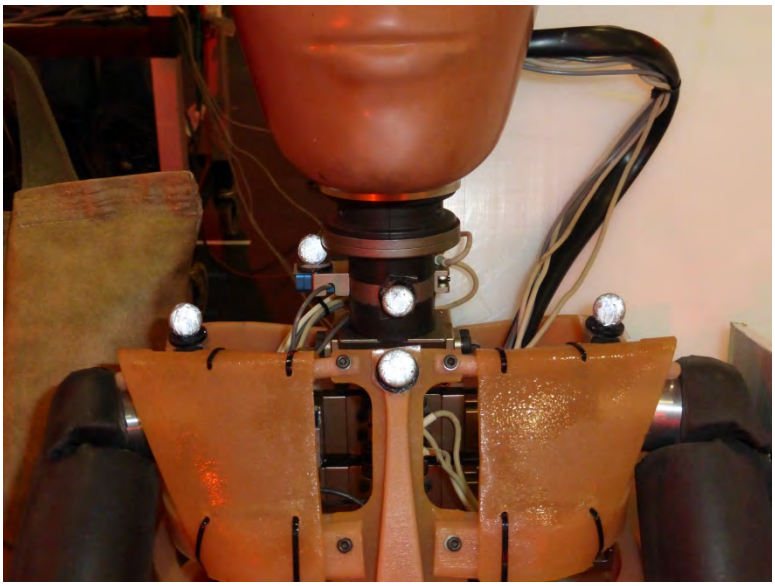

Figure 15. VICON marker locations on LODC

Quasi-static tests were performed with and without the chest jacket (Figure 16). Without the chest jacket, the LODC's arms were both held down with the hands at the knees. The non-impact side upper arm flesh was flush with the load wall. With the chest jacket, the LODC's elbows were pushed outward so that the upper arm was not flush with the load wall. Therefore, to eliminate any gaps between the load wall and the non-impact side of the dummy, the non-impact side arm was held up so that the shoulder was flush with the load wall.

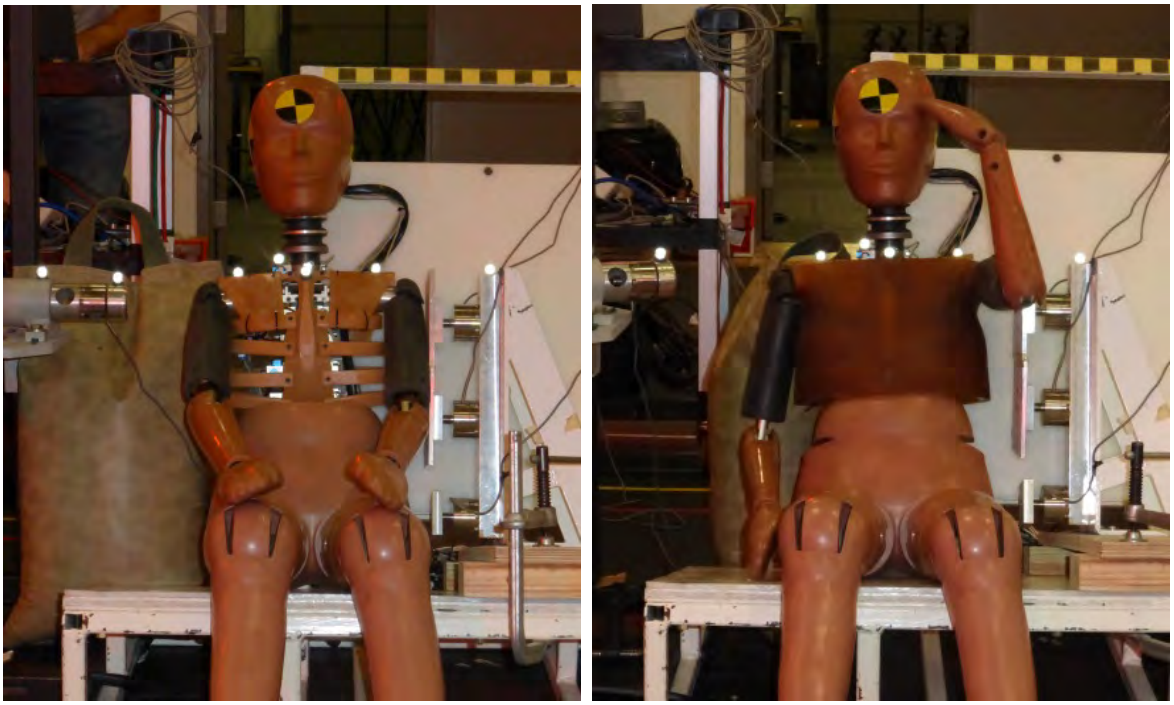

(a) (b)

Figure 16. Test setups without (a) and with (b) the flesh jacket

2.1.4. Abdomen

Biomechanical Target

Kent et al. (7; 8) evaluated the pediatric abdomen stiffness of developmentally-matched porcine specimens and later verified human response equivalence by testing pediatric human specimens in the same conditions. The human 7YO abdominal stiffness was found to be very consistent with porcine data with a force versus penetration value in the range of 50 - 75 N/mm (Figure 17). However, due to the combination of an inertial spike caused by a moving mass and the lack of significant belt penetration until around 500 N, the corridor does not contain the origin (0,0).

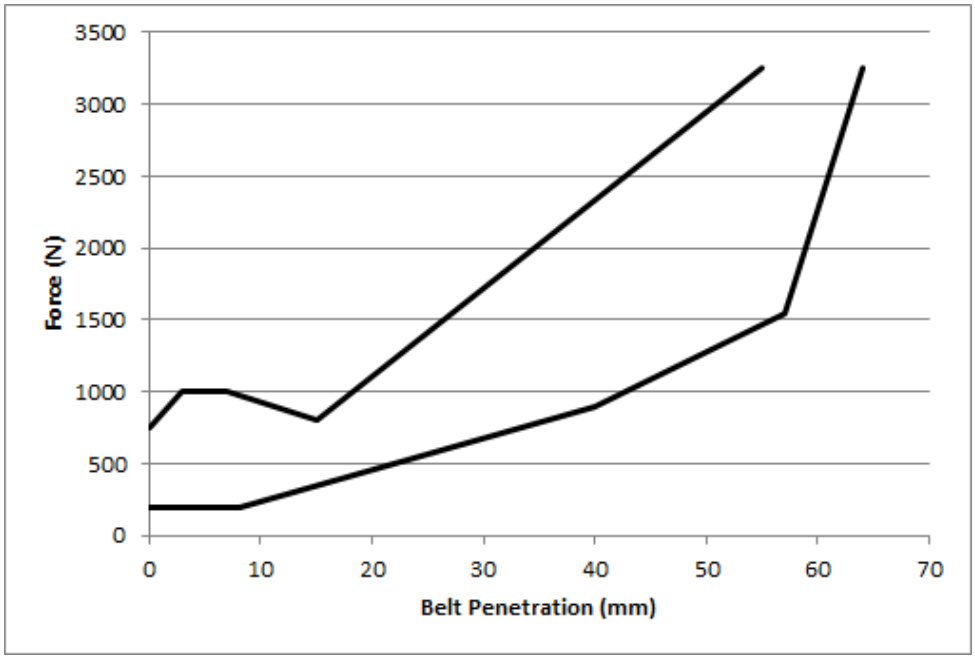

Figure 17. Force versus penetration of pediatric abdomen transverse belt tests (Kent et al., 2006).

ATD Test Setup

The LODC abdomen was tested using a belt pull setup similar to the Kent setup, except that the dummy was seated instead of supine (Figure 18), similar to the setup used by Hardy et al. (2001). This seated setup was used instead of the Kent supine configuration because the test fixture was already constructed by VRTC for adult abdomen loading studies and considered more representative of how the dummy would be loaded in a sled test. The seat belt pull device utilized a pneumatic piston to thrust a seat belt into the abdomen/pelvis of the dummy. Air pressure was adjusted to achieve the desired penetration velocity of 3.0 m/s. Two string potentiometers, attached to the pelvis and seat belt, allowed for calculation of the abdomen penetration due to the belt. Two seatbelt load cells measured the loads applied by the belt. Belt force and penetration were measured, calculated, and compared with a corridor derived from the Kent data (7). No adjustments were required to account for the free back used in this study versus the fixed back used by Kent since peak belt penetration occurred prior to any motion of the spine.

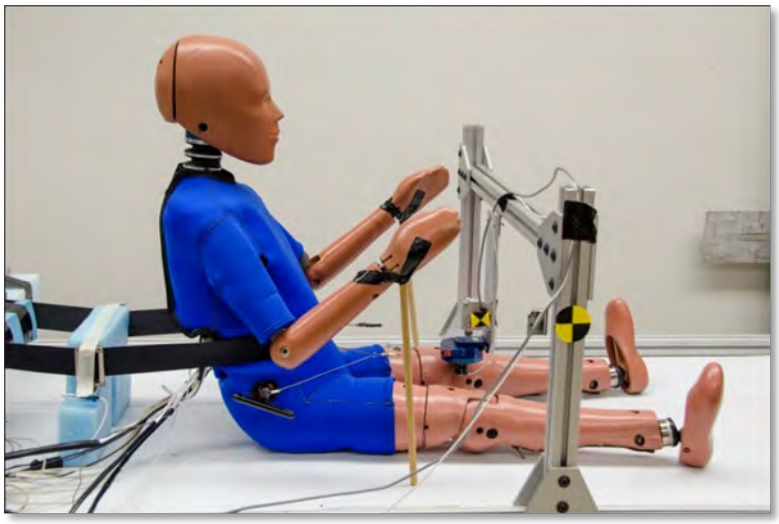

Figure 18. Abdomen belt pull test setup

2.1.5. Thoracic Spine

Biomechanical Target

Stammen et al. (2012) calculated the mechanical properties of the adult PMHS upper thoracic spine – pectoral girdle (UTSPG) body segment at-speeds of 3.8 – 7 m/s in both system identification and frontal sled test configurations (Figure 19) to span both low-speed and high-speed spinal velocities of both pediatric and adult sled tests in the literature. In the three-point belt sled configuration, a natural frequency in the range of 21.7 – 31.7 rad/sec was reported. This data was separated into two-speeds (3.8 m/s and 5.0 m/s), normalized using a method presented by Donnelly et al (13), and scaled using a combination of methodologies (Stammen et al. 2014). The resulting adult and 10-year-old size force versus displacement corridors built using an elliptical method first used in Shaw et al. (2006) and later refined by Donnelly et al. (2013) for the thoracic spine are shown in Figure 20.

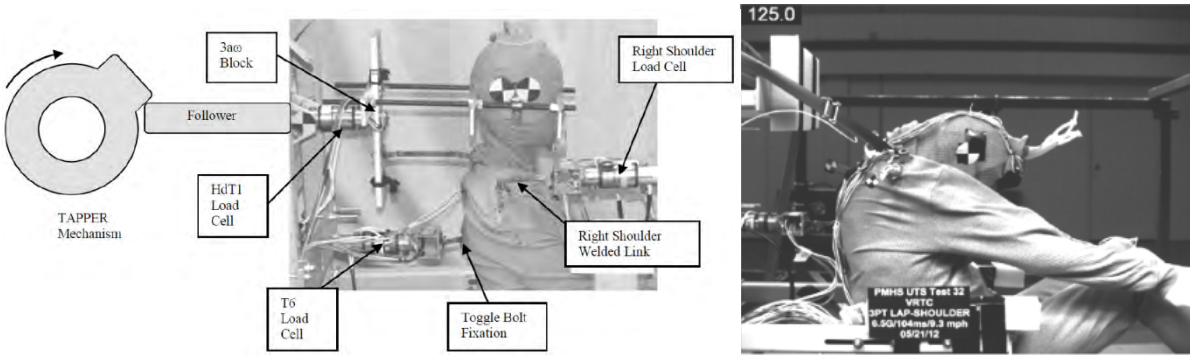

Figure 19. ISM & UTSPG sled setups for characterizing thoracic spine dynamic response (from Stammen et al. 2012).

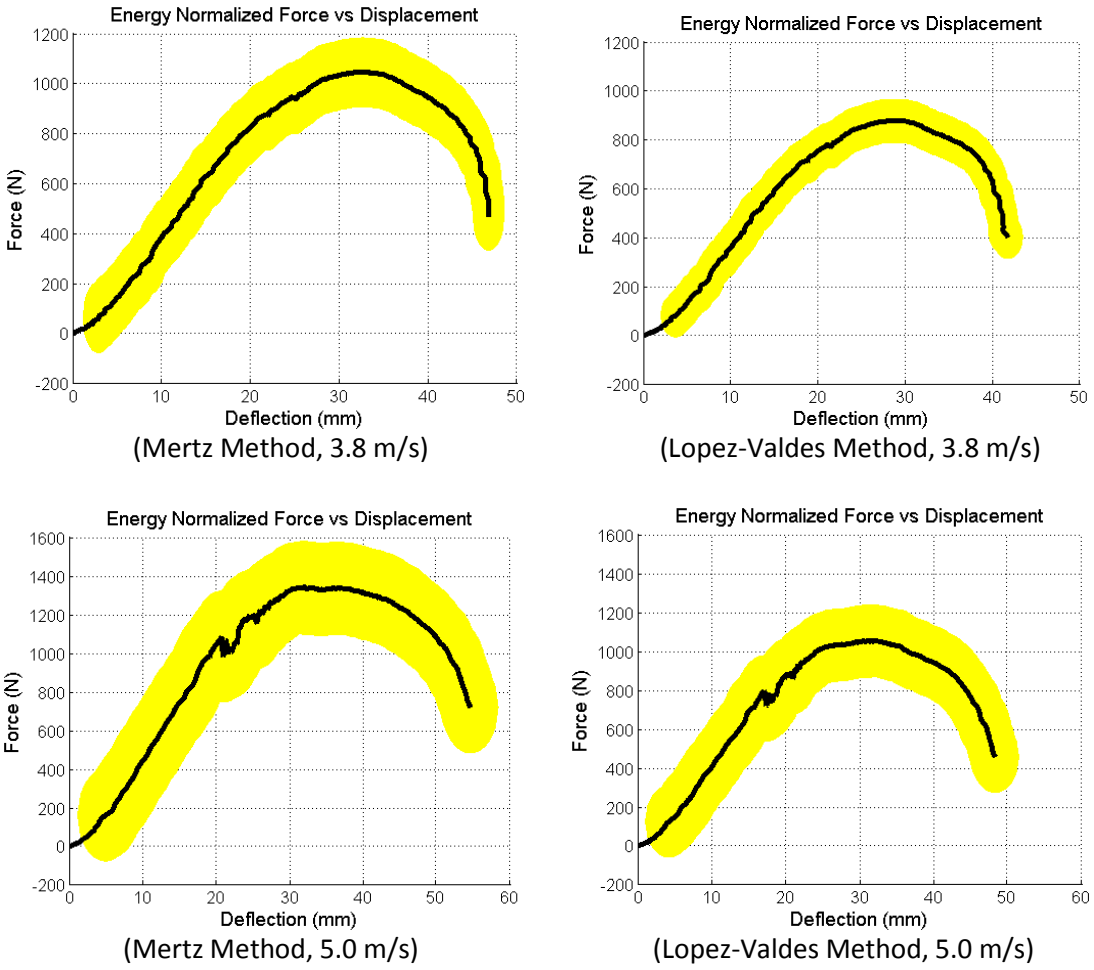

Figure 20. Biofidelity targets for the LODC thoracic spine in the fixed spine sled condition (see Stammen et al. 2014)

ATD Test Setup

The biofidelity of the LODC thoracic spine was evaluated in two conditions used previously for adult PMHS thoracic spine evaluation: Isolated Segment Manipulation (ISM) and fixed spine UTSPG sled. Figure 21 shows the LODC setup for the ISM condition, where the head and neck are coupled together above the T1 location. This head-neck assembly is connected rigidly to the follower, which rides on the TAPPER cam mechanism. The displacement is measured by a 3aω motion block (3 accelerometers and 3 angular rate sensors mounted on a rigid cube) connected to the coupling plate. The force for each perturbation is measured by the HdT1 load cell. The T6 location of the LODC is rigidly fixed to the frame, with reaction loads measured by the T6 load cell. A series of perturbations were obtained at 0.5 m/s linear velocity over a duration of 5 seconds, with no fixation at the pectoral girdle (PG) locations anterior to the thorax. An impulse response function (IRF) was calculated from the force and displacement data obtained over the duration. The IRF was then fit with a parametric model to obtain mechanical properties of the assumed second order system. The properties of the LODC were compared directly to the adult PMHS properties from Stammen et al. (2012).

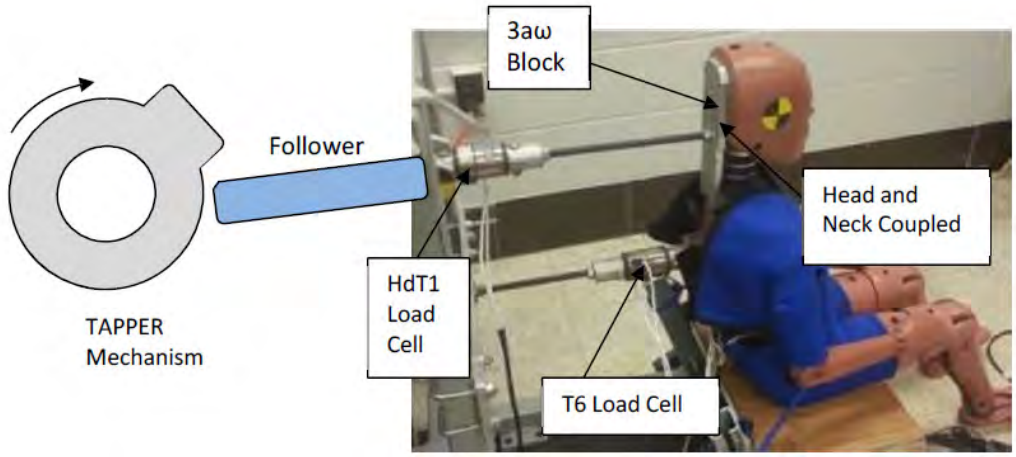

Figure 21. LODC in same ISM test setup used to evaluate adult PMHS

In the fixed spine UTSPG condition (Figure 22), the mid spine is coupled to the sled via a load cell to track the reaction loads while the thoracic spine kinematics are measured. The LODC response was compared to both the normalized adult PMHS and scaled 10-year-old targets at 3.8 m/s and 5.0 m/s, and the mechanical properties were compared in both ISM and sled conditions.

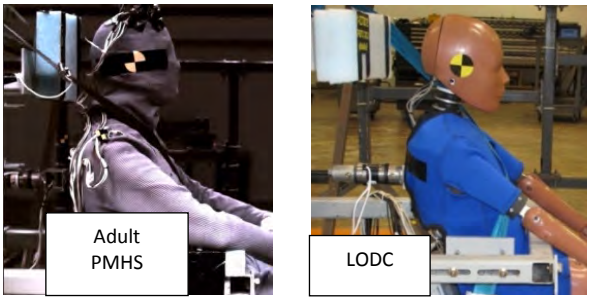

Figure 22. LODC in same vertebral fixation sled setup used to evaluate adult PMHS

Mechanical properties from parametric second order damped system model

A parametric model was used to estimate mechanical properties of both the LODC and adult PMHS in the ISM tests. A parametric model of a second order damped system (Figure 23) was fit to the impulse response function to find the effective mass, stiffness, and damping coefficient of the T1-T6 segment (Stammen et al. 2014).

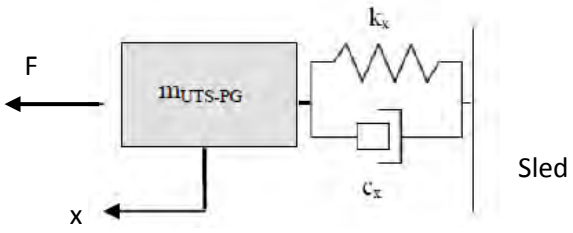

Figure 23. System model of T1-T6 body segment

2.1.6. Neck

Flexion

Biomechanical Target

Dibb et al. (2013) used head and neck models validated with pediatric experimental data to investigate the dynamic bending stiffness of the pediatric human neck during frontal impact induced via HIII-10C ATD neck certification pendulum loading (Figure 24). The pediatric 6- and 10-year-old models were 53 percent and 60 percent less stiff than the HIII ATD, respectively. The models demonstrated nonlinear softening behavior while the HIII ATDs experienced nonlinear stiffening. Figure 25 shows the biofidelity corridor presented for a 10-year-old.

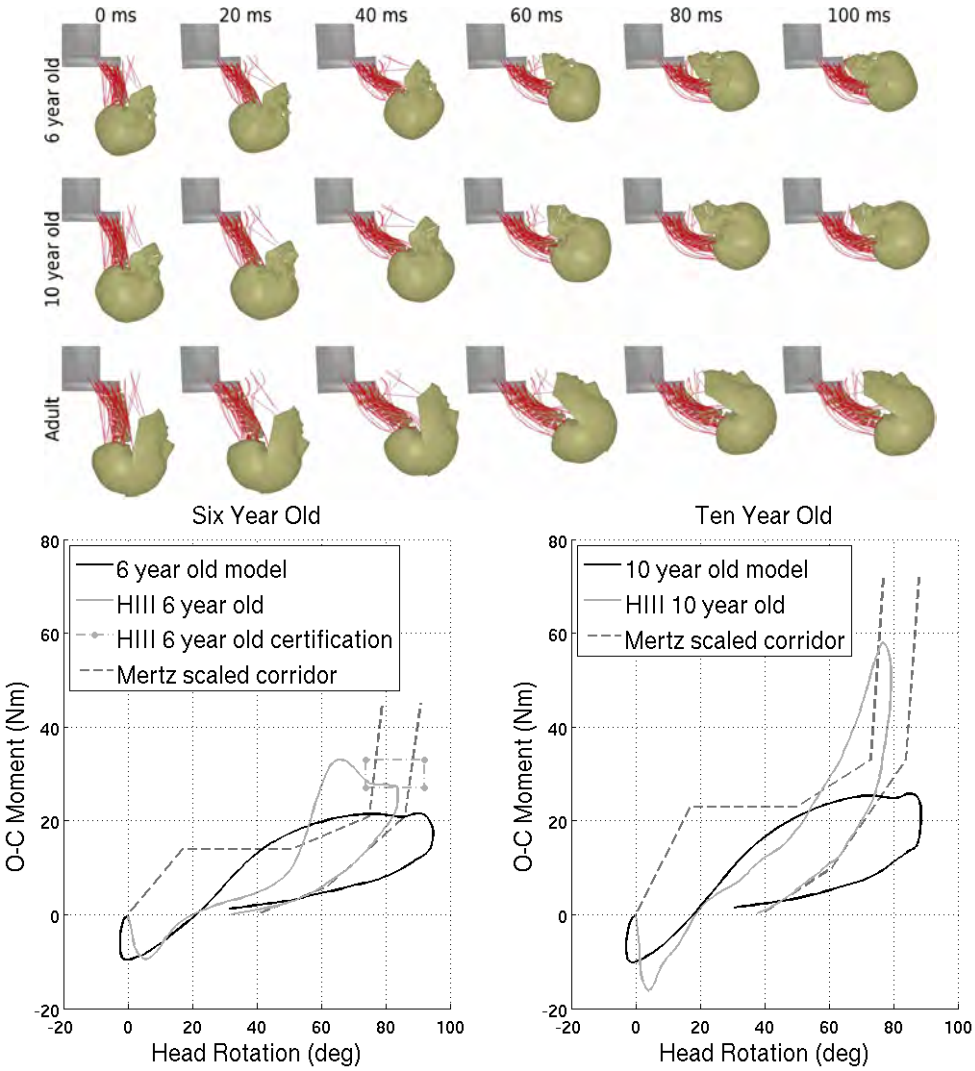

Figure 24. The models were less stiff than the HIII-10C ATDs and their behavior was not predicted by the Irwin and Mertz (1997) scaled flexion corridor (from Dibb et al., 2013).

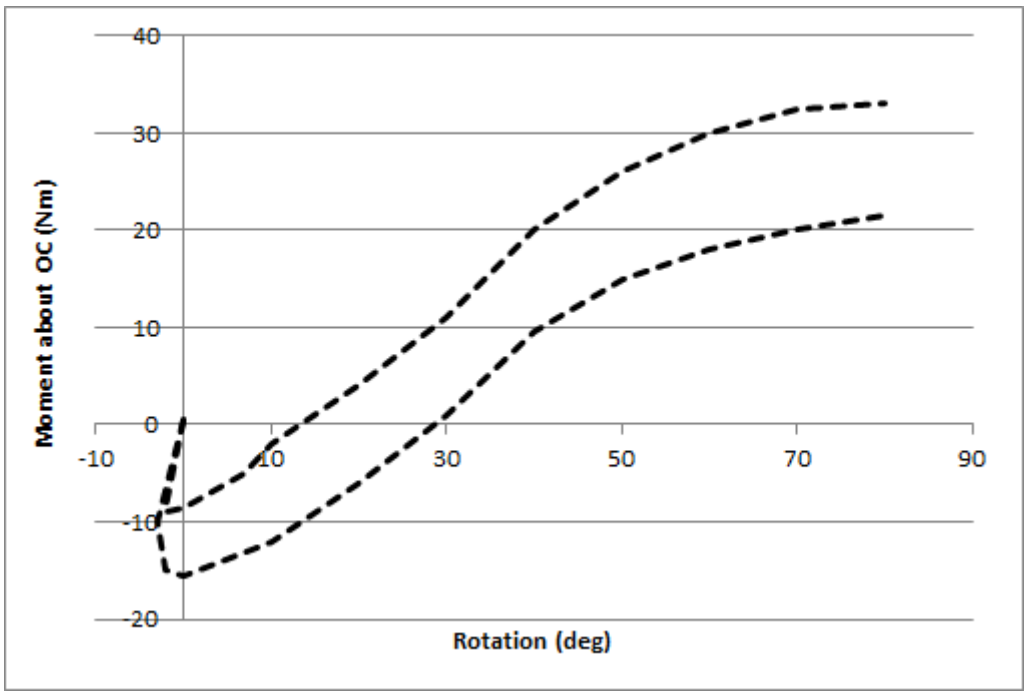

Figure 25. Neck flexion biofidelity target (from Dibb et al., 2013).

ATD Test Setup

The LODC head-neck assembly was tested in flexion similar to a HIII-10C in a Part 572 neck pendulum test (CFR 49 Part 572). The head-neck assembly was mounted on the pendulum so that the leading edge of the lower neck bracket coincided with the leading edge of the pendulum. A bracket was fabricated in order to mount the inverted LODC head-neck assembly to the pendulum just below the T1 location (Figure 26). The pendulum was raised and released from a height so that the head-neck assembly was able to fall freely and achieve an impact velocity of 6.1 m/s (± 0.12 m/s). The pendulum was stopped using Hexcell with an acceleration versus time pulse that met the Part 572 requirements (Figure 27).

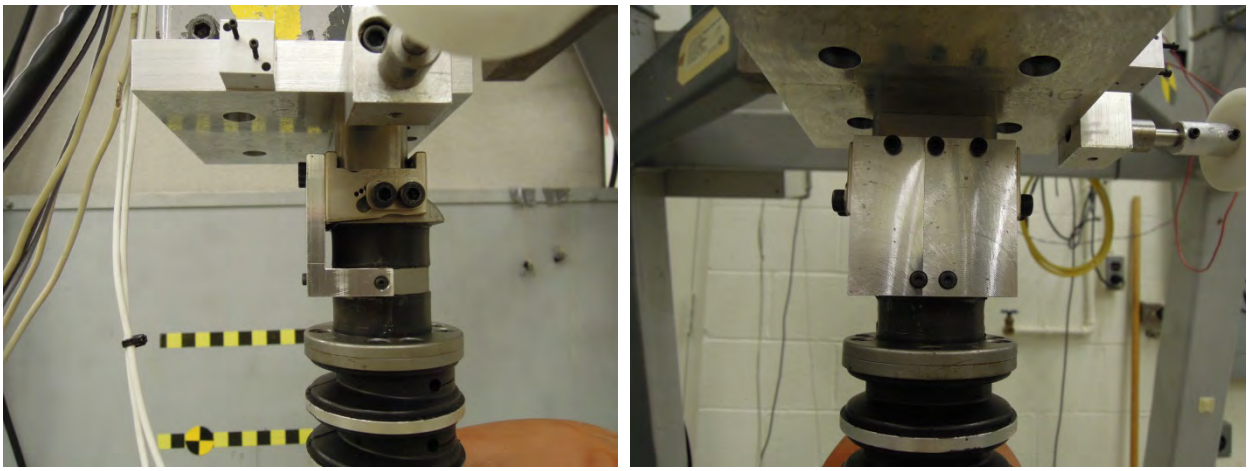

(a) (b)

Figure 26. LODC lower neck attachment to pendulum to isolate lower T1 joint segment

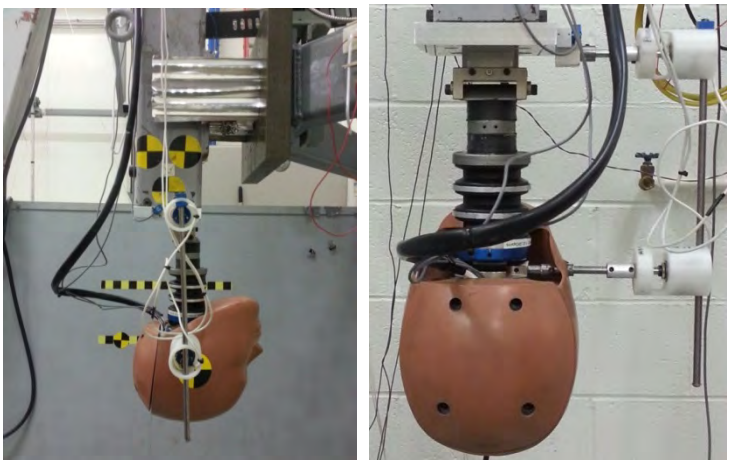

(a) (b)

Figure 27. Lateral (a) and rear (b) views of LODC neck flexion test setup

The head-neck assembly was instrumented with two angular rate sensors inside the head that were mounted in the Y and Z-axis directions, one angular rate sensor that was mounted on the pendulum arm, and an upper neck load cell. Rotation potentiometers were mounted on the occipital condyle pin on the head and on the pendulum arm. Impact velocity was measured using a light trap.

Extension

Biomechanical Target

The only known biofidelity target for 10-year-old neck extension is the scaled corridor presented in Irwin & Mertz (20) shown in Figure 28. The LODC and HIII-10C necks were tested using Part 572 conditions and their responses compared with this corridor. However, given the difference indicated between the Dibb and Mertz corridors in flexion, a modification to this extension biofidelity requirement should be investigated. The next iteration of the LODC will contain a new omnidirectional neck design that is tuned to meet all applicable flexion, extension, lateral, and twist criteria for a 10-year-old size ATD.

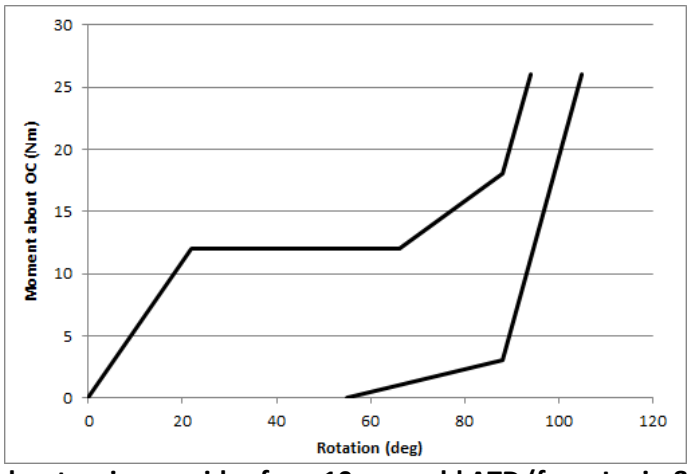

Figure 28. Neck extension corridor for a 10-year-old ATD (from Irwin & Mertz, 1997)

ATD Test Setup

The LODC head-neck assembly was tested in extension similar to a HIII-10C in a Part 572 neck pendulum test. The head-neck assembly was mounted on the pendulum so that the leading edge of the lower neck bracket coincided with the leading edge of the pendulum. The same bracket that was used in the flexion tests to mount the inverted LODC head-neck assembly to the pendulum just below the T1 location was also used in the extension tests. The pendulum was raised and released from a height so that the head-neck assembly was able to fall freely and achieve an impact velocity of 5.03 m/s (± 0.12 m/s). The pendulum was stopped using Hexcell with an acceleration pulse that met the Part 572 requirements.

The head-neck assembly was instrumented with two angular rate sensors inside the head that were mounted in the Y and Z-axis directions, one angular rate sensor that was mounted on the pendulum arm, and an upper neck load cell. Rotation potentiometers were mounted on the occipital condyle pin on the head and on the pendulum arm. Impact velocity was measured using a light trap.

2.2. Low-Speed Kinematics

Biomechanical Target

Arbogast et al. (2009) tested pediatric volunteers in a low-speed frontal sled test condition using a bumper car-based pulse. Two targets from this data (belt tension force versus time and head/spine XZ trajectories) were biofidelity targets for the ATD tests, with the caveat that there were differences between ATD and volunteer setups. The ATD seating position and FMVSS No. 213 bench (stiff foam) were configured to simulate the volunteer test setup as closely as possible.

Figures 29 – 30 show the volunteer belt tension force time history corridor (+/- one standard deviation) and head/spine mean trajectories for the 10-year-old bin of volunteer data.

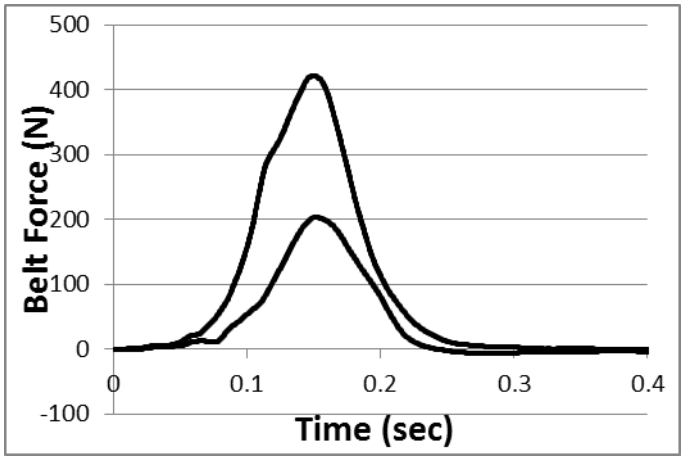

Figure 29. Belt tension force versus time corridor for 10-year-old volunteer dataset.

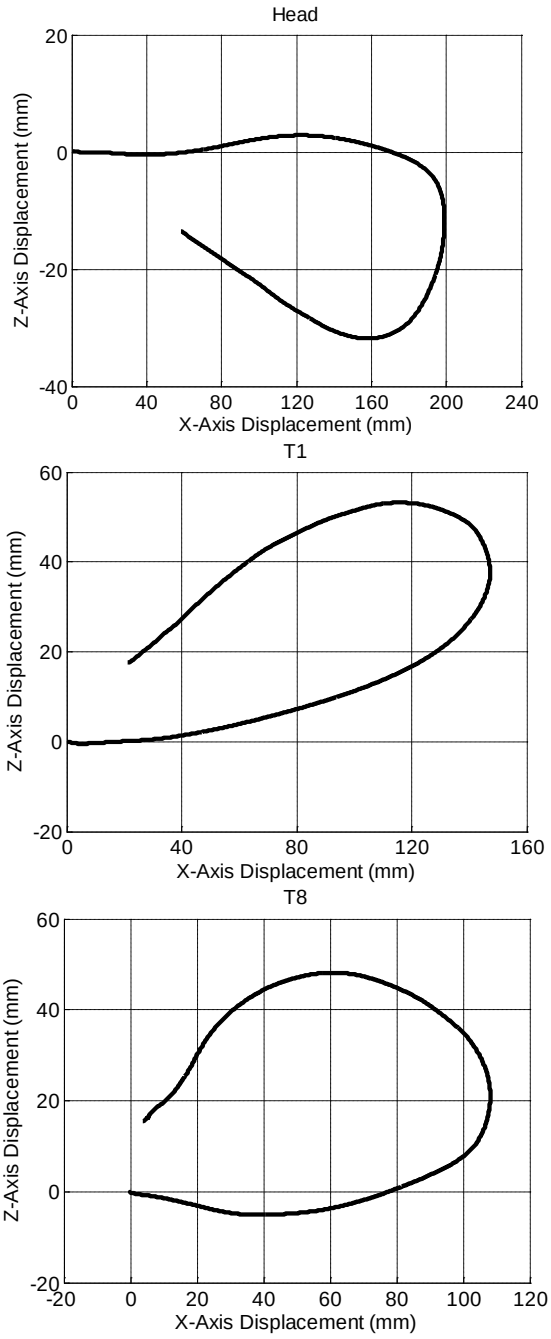

Figure 30. Mean trajectories of the head (top), T1 (center), and T8 (bottom) for the 10-year-old volunteer sled test dataset (from Arbogast et al., 2009).

ATD Test Setup

Both the LODC and standard HIII-10C ATDs were seated on the FMVSS No. 213 bench (stiff foam) using a 3-point belt and were positioned to as closely match the volunteer test setup as possible (Figure 31). The seat pan angle, ATD seating position, and seatbelt routing were made to match the volunteer sled tests as closely as possible.

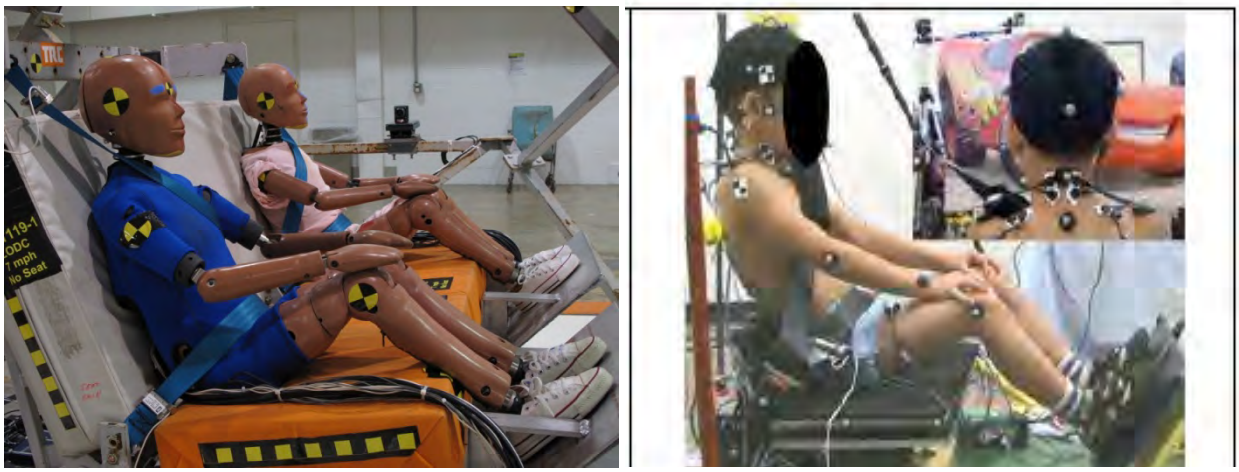

Figure 31. LODC and HIII-10C test setup on revised 213 bench to mimic pediatric volunteer test

The LODC was instrumented with six-axis load cells in the upper neck and lumbar and single-axis load cells in the left and right ASIS. Kinematics measuring units consisting of three linear accelerometers (Endevco/Entran 7264) and three angular rate sensors (DTS ARS-12K) were mounted at the center of gravity of the head, T1, T6, and at the pelvis. Last, ribs 2 and 3 were instrumented with three-dimensional IR-TRACCs to measure chest compression.

The HIII-10C was instrumented with six-axis load cells in the upper neck, lower neck, and lumbar and single-axis load cells in the left and right ASIS. Kinematics measuring units consisting of three linear accelerometers (Endevco and Entran 7264) and three angular rate sensors (DTS ARS-12K) were mounted at the center of gravity of the head, T6, and pelvis. Last, a displacement potentiometer was mounted in the chest to measure chest compression.

Figure 32 shows that the low-speed frontal sled test was performed using a 7 mph (9 km/h) bumper car-based pulse that closely matched the pulse used by Arbogast et al. (2009).

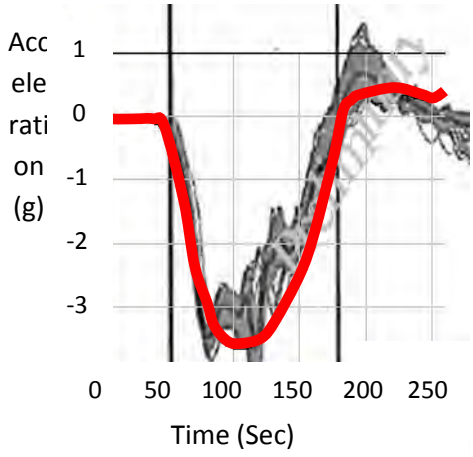

Figure 32. Low-speed sled pulse (red) to mimic pediatric volunteer test pulse (grey)

2.3. High-speed Kinematics

To compare the LODC with the HIII-10C, frontal sled tests were conducted with medium (40 km/h) and high (48 km/h, FMVSS No. 213) energy pulses using four different types of restraint configurations (5-pt harness, high back booster, backless booster, and 3-pt belt with no booster). Both dummies were seated according to UMTRI child seating procedures (23). The test matrix is shown in Table 2 below.

Table 2. Overall test matrix with low, medium, and high energy sled pulses

Test No.	ATD (Driver)	ATD (Passenger)	CRS Type	CRS Make/Model	Speed
1	Standard HIII-10C	LODC	5pt Harness	Britax Frontier 85	40 km/h
2	Standard HIII-10C	LODC	High Back	Graco TurboBooster	
3	Standard HIII-10C	LODC	Backless	Graco TurboBooster	
4	Standard HIII-10C	LODC	3-pt Belt (no booster)	None	
5	Standard HIII-10C	LODC	3-pt Belt (no booster)	None	9 km/h (bumper car)
6	Standard HIII-10C	LODC	3-pt Belt (no booster)	None	
7	Standard HIII-10C	LODC	3-pt Belt (no booster)	None	
8	Standard HIII-10C	LODC	5pt Harness	Britax Frontier 85	40 km/h
9	Standard HIII-10C		5pt Harness	Britax Frontier 85	48 km/h (213 pulse)
		LODC	5pt Harness	Britax Frontier 85	
10		LODC	High Back	Graco TurboBooster	
11		LODC	Backless	Graco TurboBooster	
12	Standard HIII-10C		Highback	Graco TurboBooster	
		LODC	3-pt Belt (no booster)	None	

The 40 km/h pulse is based on a past FMVSS No. 208 sled test condition and has been used to evaluate adult PMHS response in belted frontal sled tests (Lopez-Valdes et al (21)). This pulse was used as a starting pulse to assure the LODC durability would be sufficient before proceeding to the regulatory type FMVSS No. 213 condition. Both pulses are shown below in Figure 33.

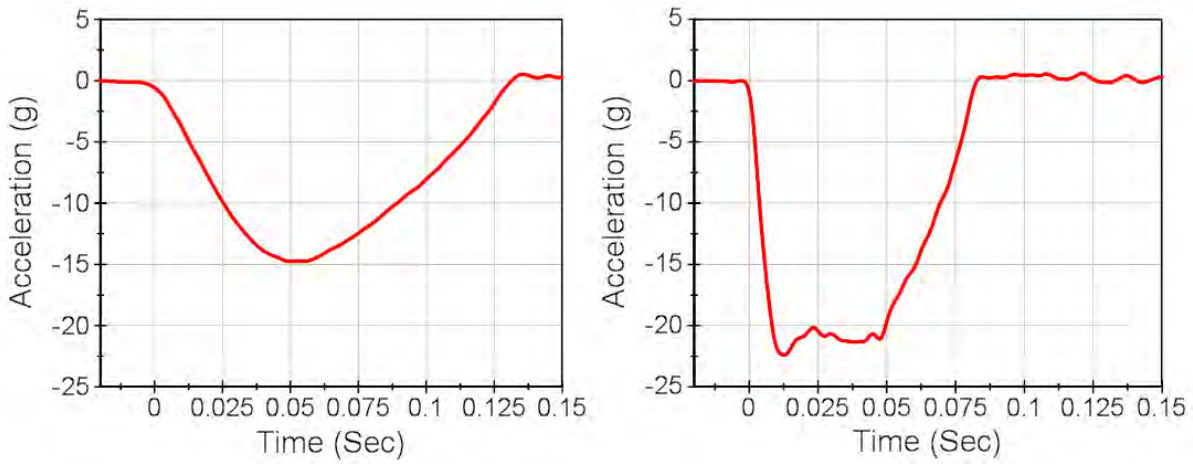

Figure 33. Medium energy (left) and high energy (right) pulses used in sled evaluation.

Tests were conducted with a LODC seated on the passenger side and a HIII-10C seated on the driver side. In the 40 km/h case, both driver and passenger side dummies were seated on the same type of child restraint. For the 48 km/h tests (FMVSS No. 213), the LODC was tested in each of the four different child restraint systems and seated in a similar position to the 40 km/h tests (Figure 34). A FARO three-dimensional coordinate measurement tool was used to seat the dummies in a consistent and similar position. Initial position measurements of the head top, inboard and outboard head centers of gravity, head back, head front, head top, inboard and outboard pelvis, shoulders, shoulder and lap belts, and child seat positions were kept within 10 mm between the two dummies. Pelvis and femur angles were also positioned similarly between the two dummies. The LODC and HIII-10C were instrumented the same way as they were in the low-speed tests.

Figure 34. LODC and HIII-10C in (top left) 5 point harness CRS, (top right) highback belt positioning booster, (bottom left) backless belt positioning booster, and (bottom right) non-CRS condition

3. Results & Discussion

3.1. Component Testing

3.1.1. Frontal Thorax

Figure 35 shows chest deflection and probe force time histories for the 6.0 m/s frontal thorax impacts. Figure 36 shows the force versus displacement of the LODC and HIII-10C against the pediatric corridor from Parent et al. (2002). In Figures 35 and 36, positive chest deflection indicates that the sternum is moving towards the spine.

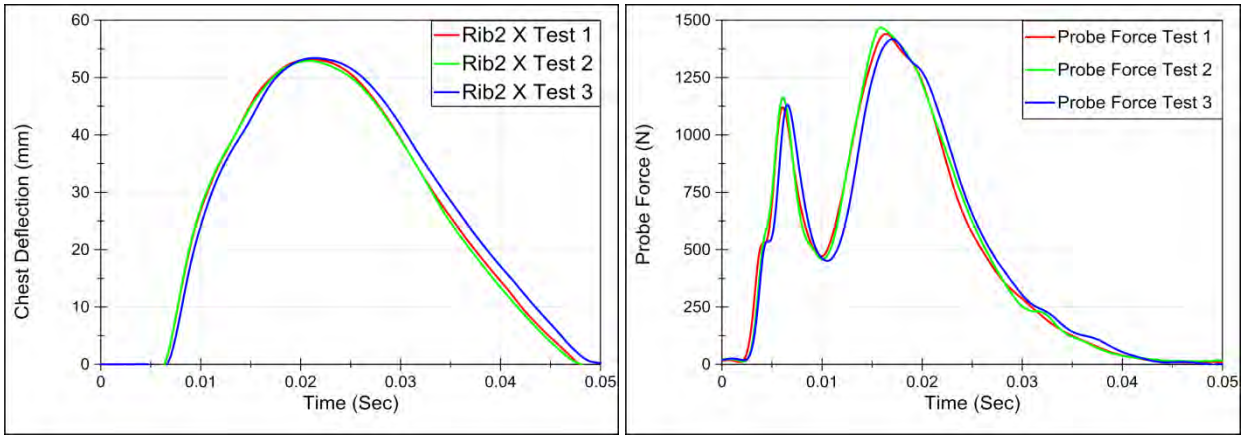

Figure 35. LODC chest deflection and probe force versus time in frontal thorax impact

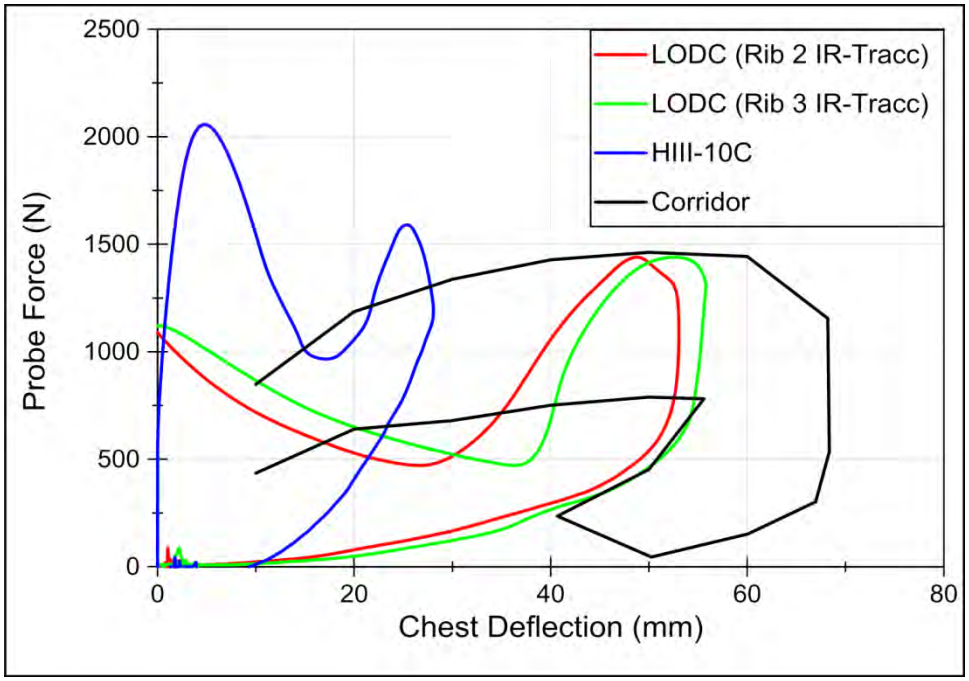

Figure 36. LODC and HIII-10C response versus six year old-based corridor in frontal thorax impact

For the frontal thorax impact, the LODC meets the force-displacement biofidelity corridor pretty well as shown in Figure 36. It should be noted that the LODC was tested with the lighter six-year-old probe instead of the 10-year-old probe due to fear of damaging the thorax and IR-TRACCs. The IR-TRACCs were close to bottoming out against the spine. There are plans to test both dummies in a more recently derived 10YO-based biofidelity condition when the next LODC version is ready.

3.1.2. Lateral Thorax

Low-Speed, 4.3 m/s

Figure 37 shows the T1 resultant acceleration and probe force time histories overlaid with their corresponding biofidelity corridors for the low-speed, 4.3 m/s lateral thorax impacts.

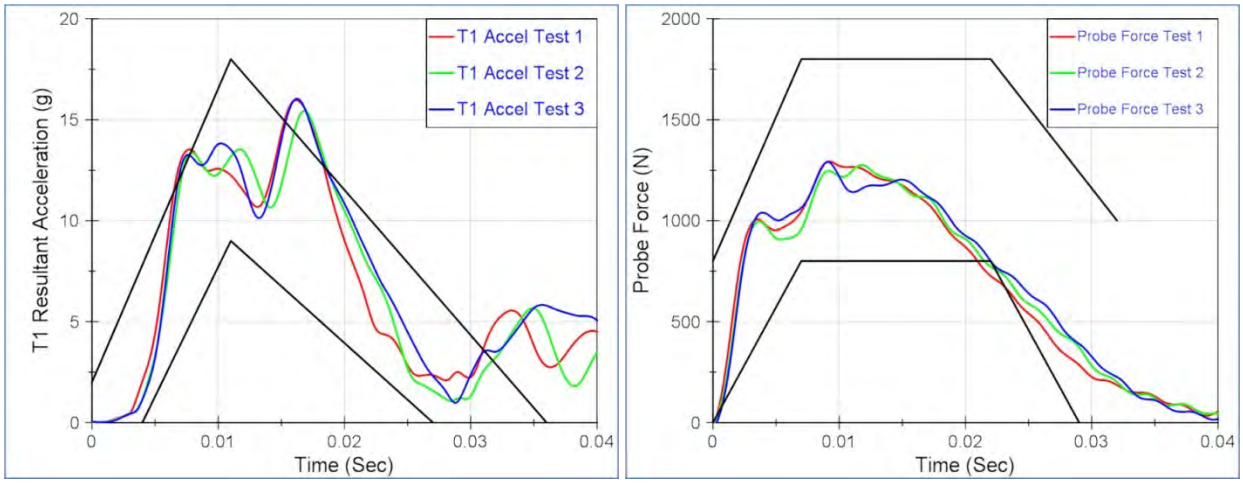

Figure 37. LODC T1 acceleration and probe force versus time in 4.3 m/s lateral thorax impact

High-Speed, 6.0 m/s

Figure 38 shows the probe force time histories overlaid with the corresponding biofidelity corridor for the high-speed, 6.0 m/s lateral thorax impacts.

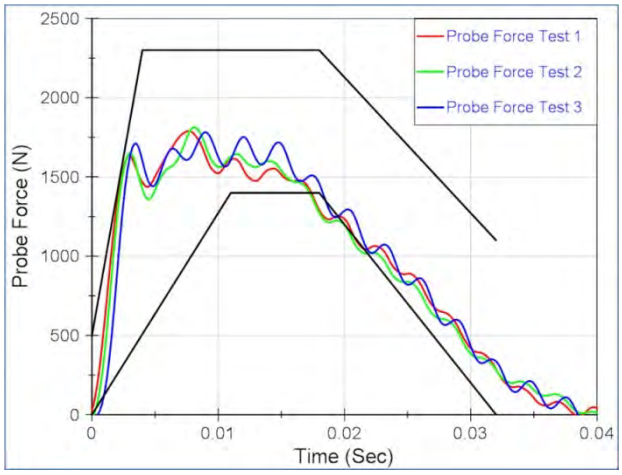

Figure 38. LODC probe force versus time in 6.0 m/s lateral thorax impact

Figures 37-38 shows that the T1 resultant acceleration and probe force time histories were within their corresponding biofidelity corridors for both the low-speed 4.3 m/s and high-speed 6.0 m/s lateral thorax impacts.

3.1.3. Shoulder

Lateral Pendulum Impact, 4.5 m/s

Figure 39 shows the probe force time histories overlaid with the corresponding biofidelity corridor for the 4.5 m/s lateral shoulder impacts.

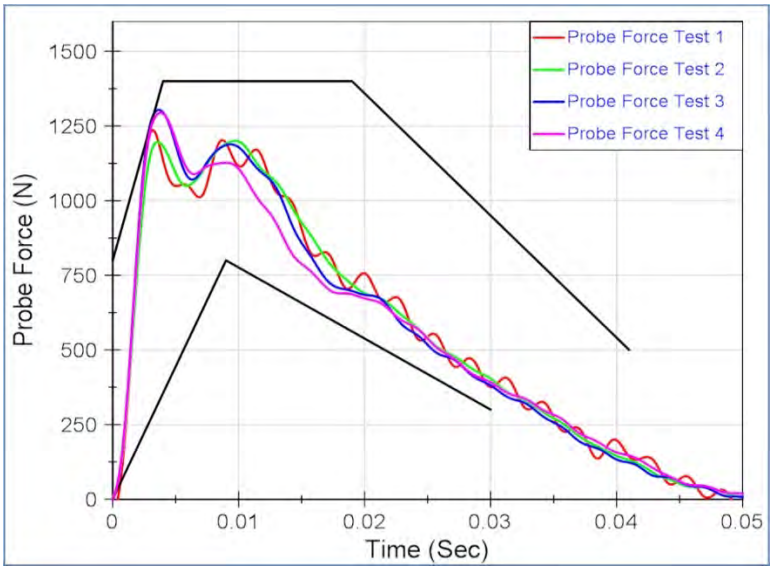

Figure 39. LODC probe force versus time in lateral shoulder impact

Figure 39 shows that the probe force time history was consistent with the corresponding biofidelity corridor for the lateral shoulder impacts. While the focus of this study is on the frontal response of the LODC for FMVSS No. 213 testing, the thorax and shoulder meeting the scaled response corridor is encouraging for the use of this dummy in test scenarios where the direction of loading is not purely frontal.

Quasi-Static Posteromedial Testing

Figure 40 compares the LODC response to pediatric volunteer data (from Suntay et al. 2011) .

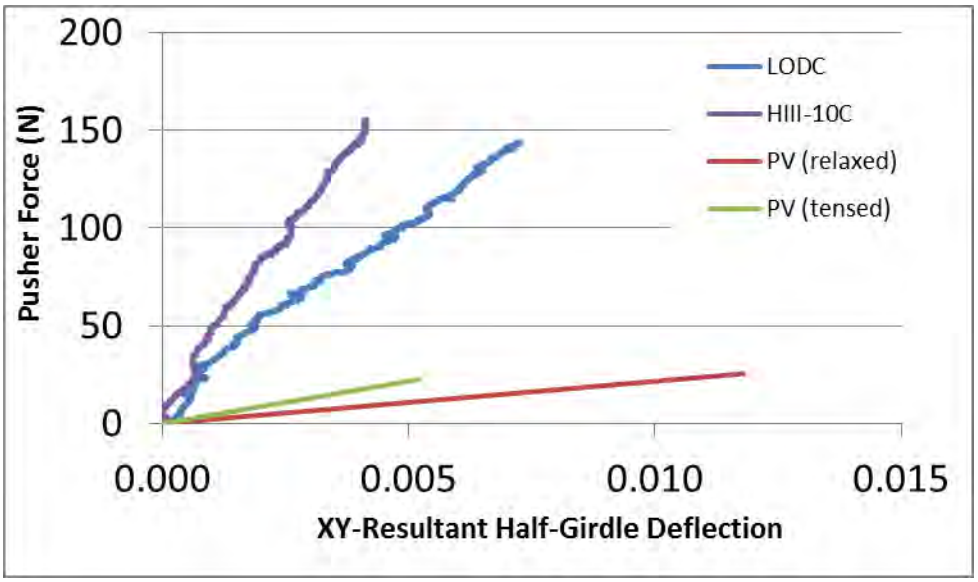

Figure 40. LODC quasi-static shoulder response versus pediatric volunteer data

Figure 40 shows that the LODC is softer than the HIII-10C, but it is still much stiffer than the pediatric volunteers (relaxed and tensed) at a quasi-static rate. It is possible that the quasi-static rates are too low for what ATDs are capable of being designed for. It is expected that the shoulder stiffness of the LODC and pediatric volunteers will converge when tested at higher loading rates. This is evidenced by the LODC falling within the dynamic corridor in the lateral shoulder impact test. Additionally, this test condition is not purely frontal or specific to belt loading. So, like in the case of the lateral thorax and shoulder responses, it is encouraging to know that the oblique response is closer to pediatric volunteers if off-axis loading is present.

3.1.4. Abdomen

Figure 41 shows the belt force and abdomen penetration versus time histories. Figure 42 compares the LODC response to the pediatric corridor from Kent et al. (2006).

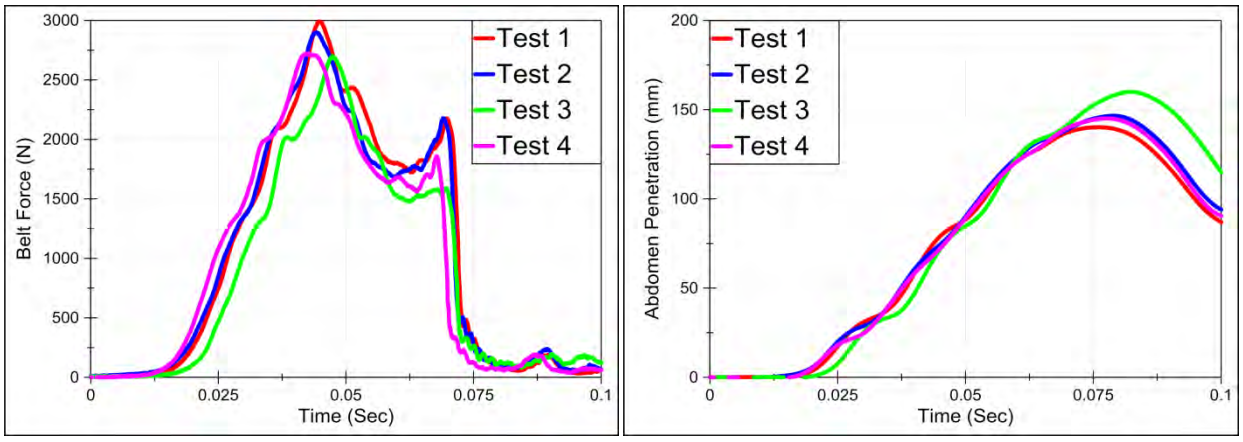

Figure 41. LODC belt force and abdomen penetration versus time in lateral shoulder impact

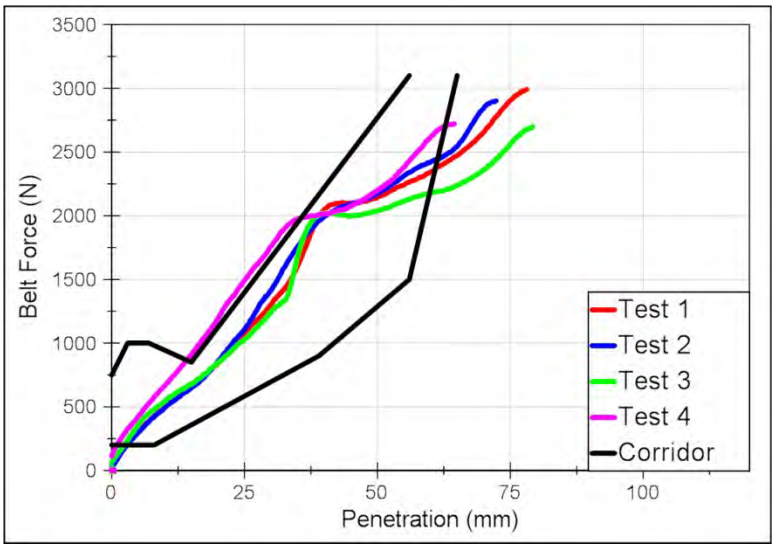

Figure 42. LODC response relative to pediatric corridor in abdomen belt pull test

Even though an abdomen performance specification was not provided to Humanetics during the development of the LODC, the LODC abdomen response was found to match the pediatric abdomen corridor in Figure 42. During the LODC design process, the abdomen was made heavier and softer to account for the loss of mass associated with the removal of the chest potentiometer plate with the LODC having IR-TRACCs for measuring chest compression instead. For the HIII-10C, very little if any belt penetration would be expected, because the HIII-10C abdomen is very stiff and almost completely covered by the rigid pelvis front.

3.1.5. Thoracic Spine

Thoracic Spine TAPPER Tests

Figure 43 shows the non-parametric IRF and parametric model fit with mechanical properties for the LODC test at 0.5 m/s perturbation velocity. The effective mass of the LODC from the parametric model was 20.4 kg, while the stiffness was 14.3 kN/m and damping coefficient was 76 N-s/m.

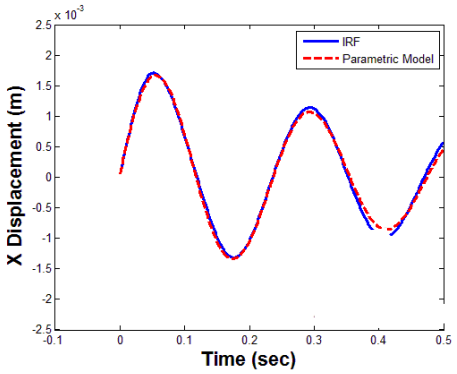

Figure 43. IRF fit for LODC test at 0.5 m/s

Table 3 compares mechanical properties of the LODC to the normalized adult PMHS properties for the ISM condition. The properties in the ISM condition come from a second order system parametric model fit to the impulse response function. The effective stiffness of the LODC is 73 percent of the adult PMHS, which is consistent with the stiffness ratio used to scale the adult PMHS sled data (Stammen et al. 2014).

Table 3. Mechanical properties from parametric model fits

Subject	Test Condition	Speed[1] (m/s)	Effective Mass (kg)	Damping Coefficient (Ns/m)	Stiffness (kN/m)
Adult PMHS [2]	ISM	0.5	43.4	188	19.5
LODC	ISM	0.5	20.4	76	14.3

[1]ISM perturbation velocity representing relative-speed of T1 with respect to T6; sled velocity is T6 with respect to ground
[2]Same three PMHS as used for the 3.8 and 5.0 m/s sled tests

Thoracic Spine UTSPG Testing

Figures 44 and 45 shows LODC response from three repeat tests compared to large child biofidelity targets scaled using two different approaches (Stammen et al. 2014).

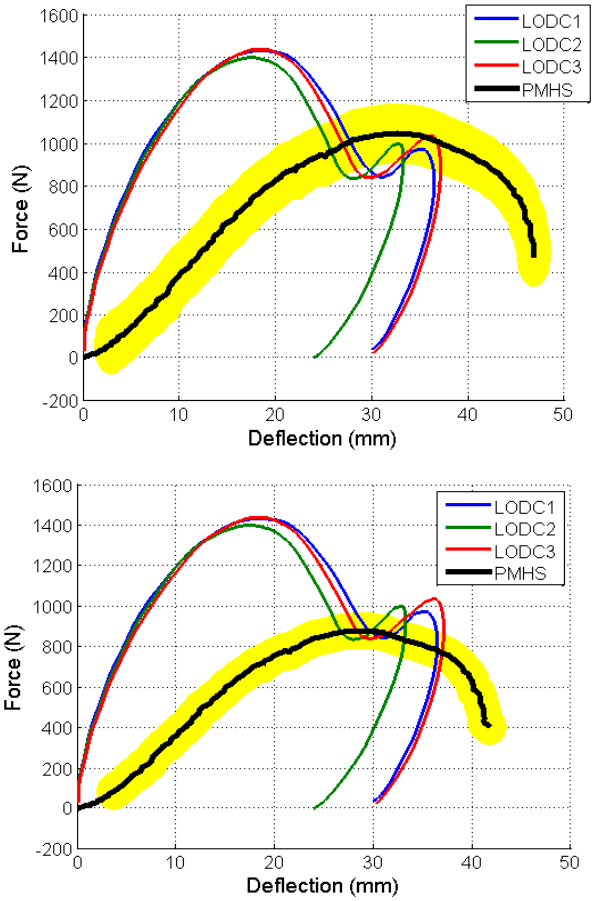

Figure 44. LODC response at 3.8 m/s compared with scaled (top = Mertz method, bottom = Lopez-Valdes method) large child biofidelity targets.

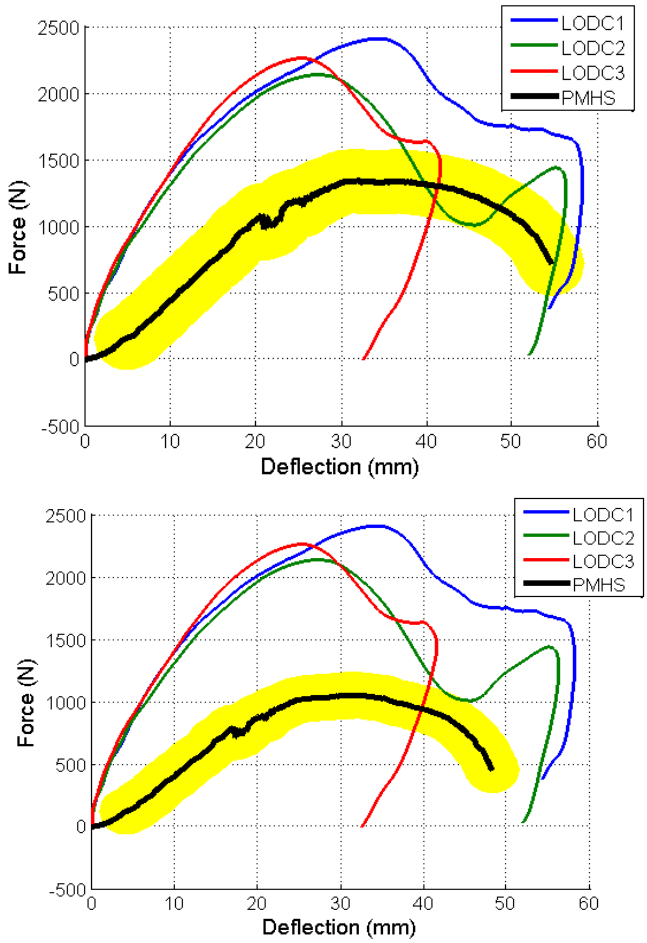

Figure 45. LODC response at 5.0 m/s compared with scaled (top = Mertz method, bottom = Lopez-Valdes method) large child biofidelity targets.

The LODC, with its flexible thoracic spine, appears to possess characteristics that result in dynamic behavior that is more similar to human response than existing child ATDs. The inertial component of the LODC response should be reduced somewhat in order to shift the peak force to a higher displacement level while decreasing the overall stiffness of the LODC. The LODC showed a bi-modal response as opposed to a more uni-modal response displayed by the human. This appears to be related to the very soft T1 joint being pulled forward in the LODC, indicating the need to incorporate a smoother/gradual transition between the contributions of the cervical and thoracic spine components in the dummy. Together, these adjustments should result in a response more closely matching the scaled 10-year-old biofidelity target. This may be accomplished by analyzing the stiffness of the individual LODC rubber elements during the sled tests by tracking the vertebral kinematics. The individual elements in the dummy can be tuned along the spine to simulate the overall displacement of T1 in the human with a different distributed force profile.

3.1.6. Neck

Figure 46 shows moments about the occipital condyle versus head rotations overlaid with the corresponding biofidelity targets for the Part 572 neck flexion and extension tests. Flexion results are plotted against the neck flexion corridor developed by Dibb et al. (2013). Extension results are plotted against the scaled Irwin/Mertz neck extension corridor [20].

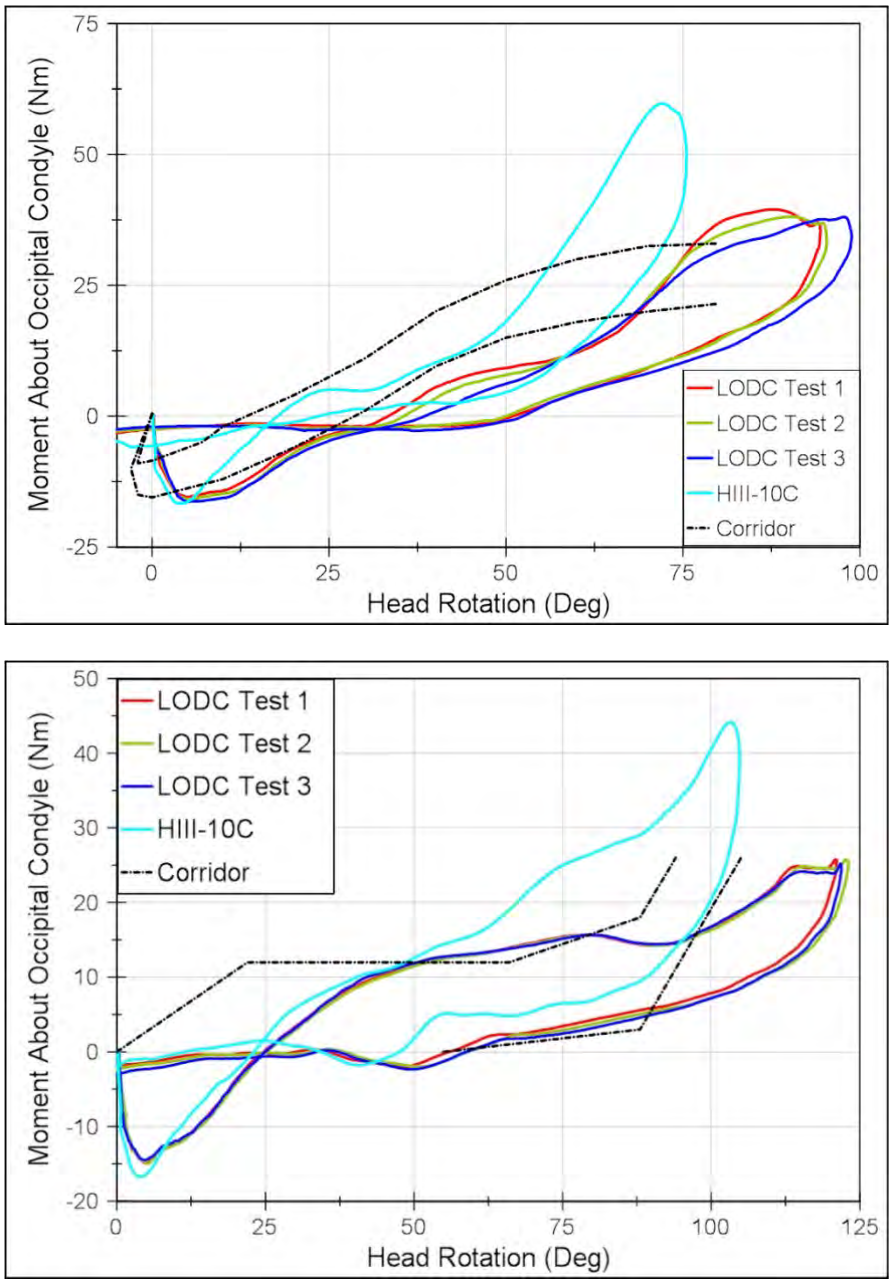

Figure 46. LODC versus HIII-10C (top) neck flexion and (bottom) neck extension plotted against their corresponding biofidelity corridors

The LODC hardware covers everything between the neck and lumbar. To maintain the overall anthropometry of a 10 year old, the HIII-10C neck was shortened by one segment and replaced with a very flexible T1 joint. Since there was no pediatric corridor for the neck at the time of development, no performance specifications were provided to Humanetics for the neck itself, but only for the attachment of the HIII-10C neck to the LODC thorax. However, a response corridor for neck flexion now exists from the Duke head-neck model (Dibb et al. 2013). For flexion in the Part 572 pendulum test, the peak moment matches the corridor, but the overall response needs to the refined (Figure 46). For extension, the overall shape still reflects the scaled Irwin/Mertz corridor, but with more rotation (Figure 46). A new neck is being designed and developed to match current pediatric data and possess omnidirectional characteristics.

3.2. Low-Speed Kinematics

Head trajectory and belt loads from the LODC and HIII-10C (tests 1 and 3 only) are compared to pediatric volunteer data in Figures 47-48. In test 2, a low shoulder belt force and high head excursion were observed and were likely due to the shoulder belt spooling out of the belt anchor plate. This did not occur in any of the other tests for either ATD. All time history data is found in Appendix A. Maximum values for head and knee excursion, chest compression, occipital condyle moment, and belt loads are tabulated in Table 4.

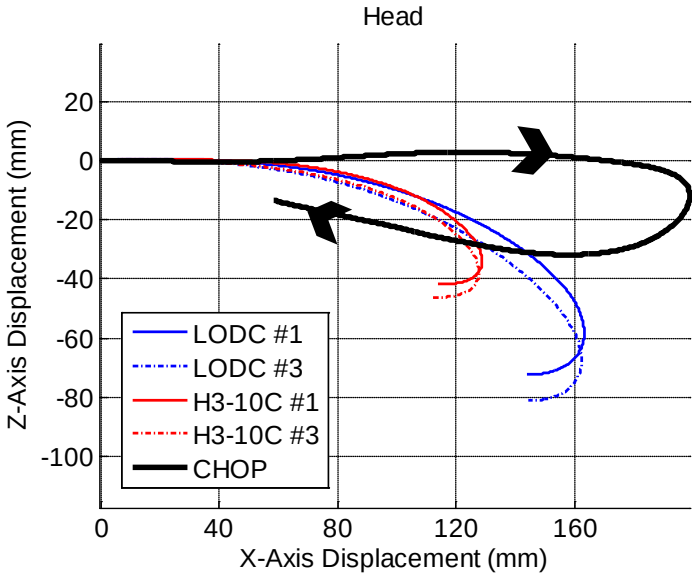

Figure 47. Head CG X-Z trajectories for the LODC (blue) and HIII-10C (red) compared with the average CHOP pediatric volunteer dataset (black).

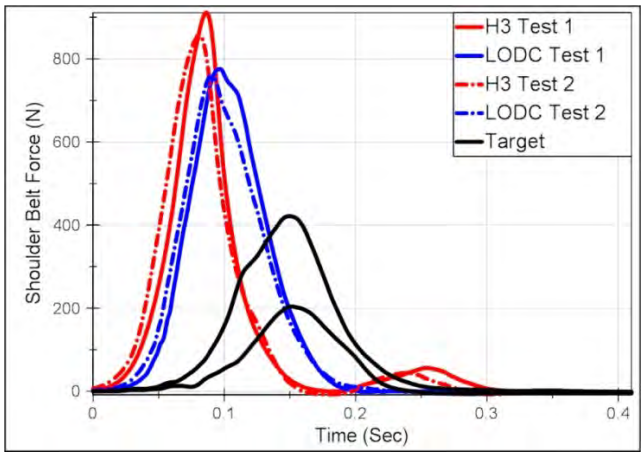

Figure 48. Shoulder belt forces for LODC and HIII-10C versus pediatric volunteer corridor

Dummy kinematics were also calculated for the head, neck (T1), mid-spine, and pelvis for both dummies using the corresponding accelerometers and angular rate sensors and maximum displacements are tabulated in Table 4 along with average pediatric data that was provided by Arbogast et al. (2009). For the HIII-10C dummy, the T1 kinematics were calculated using rigid body translations of the mid-spine transducers. The LODC kinematics are represented by the blue curves and the HIII-10C kinematics are represented by the red curves in Figure 49 below. For the HIII-10C, spine Z displacement data was suspect due to excessive integration error on a very small Z acceleration magnitude and therefore not included in the trajectory plots. Video screen captures correspond to the data point markers shown in the plots.

Table 4. Maximum value comparisons for the low-speed (9 km/h) bumper car tests.

Description		Test 1		Test 2		Test 3		CHOP
		HIII-10C	LODC	HIII-10C	LODC	HIII-10C	LODC	
Head Excursion (mm)		344	360	345	423	345	357	--
Knee Excursion (mm)		594	563	595	569	588	552	--
Head Displacement (mm)	X	129	163	130	216	128	162	199
	Z	-41.9	-72.4	-43.6	-62.3	-46.3	-81.1	-31.9
T1 Displacement (mm)	X	10.1	68.8	11.3	106	9.11	64.3	147
	Z*	--	32.7	--	59.6	--	26.8	53.2
Mid-Spine Displacement (mm)	X	9.72	38.9	10.6	52.3	8.49	34.9	108
	Z*	--	-31.6	--	-13.3	--	-39.1	48.2
Chest Compression (mm)		-2.41	-5.80	-2.03	-4.35	-2.45	-8.36	--
Moment About Occipital Condyle (Nm)		-1.54 14.5	-3.09 12.0	-2.45 14.7	-2.78 9.98	-0.979 14.5	-3.29 12.4	--
Peak Belt Tension (N)	Lap	618	772	554	556	554	741	346
	Shoulder	911	775	825	303	857	758	317

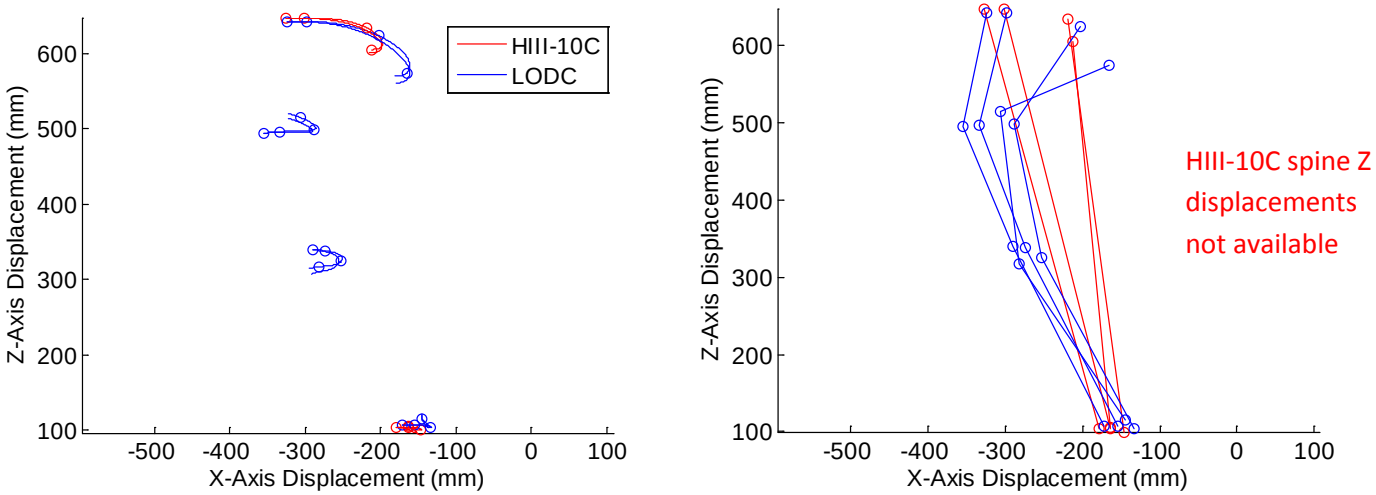

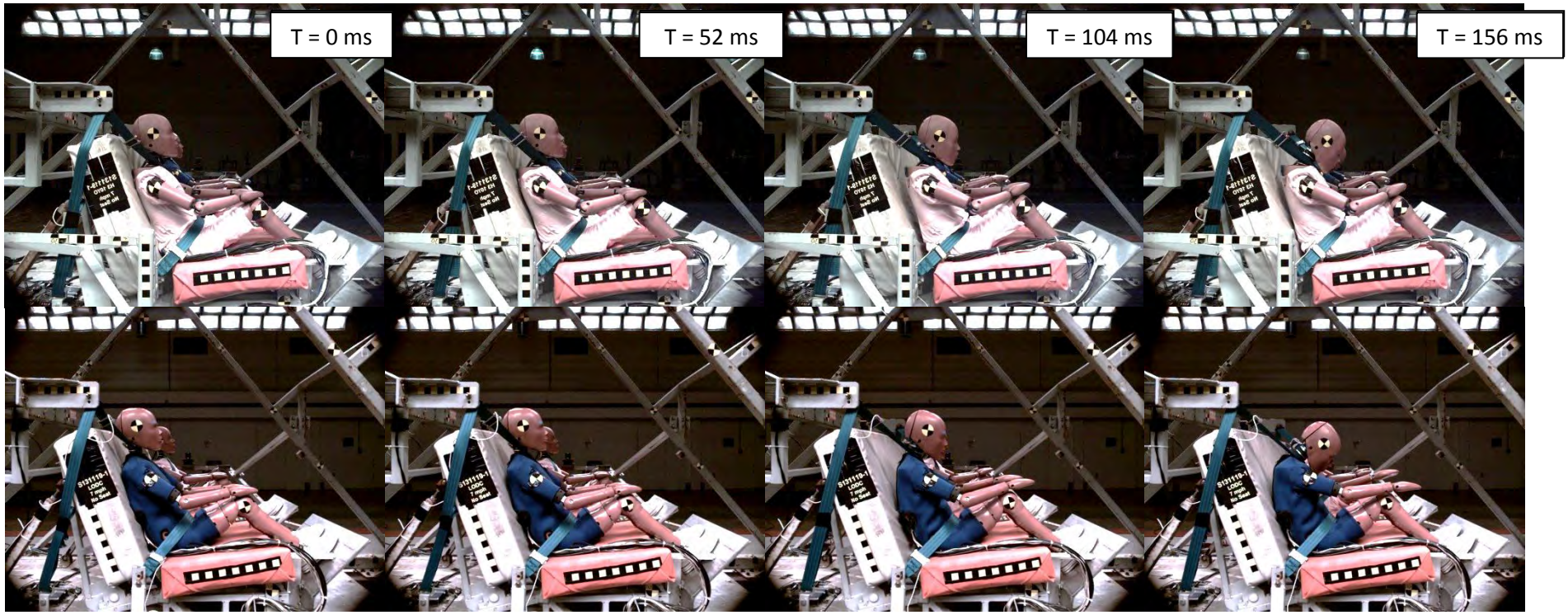

Figure 49. Kinematics of LODC and HIII-10C in Low-Speed Test

Low-Speed Summary

Head CG, T1, and mid-spine forward trajectories of the LODC, HIII-10C, and pediatric volunteers are compared in Figure 50. A comparison of the peak belt tensions are shown in Figure 51 for the two ATDs and volunteer data.

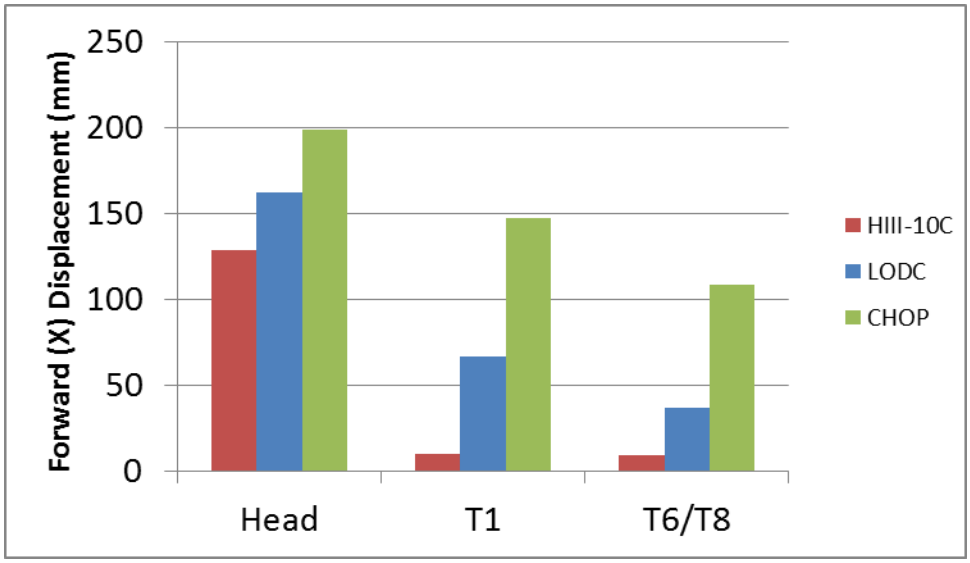

Figure 50. Head CG, T1, and mid-spine forward trajectories of the LODC, HIII-10C, and pediatric volunteers in the low-speed (9 km/h) bumper car tests.

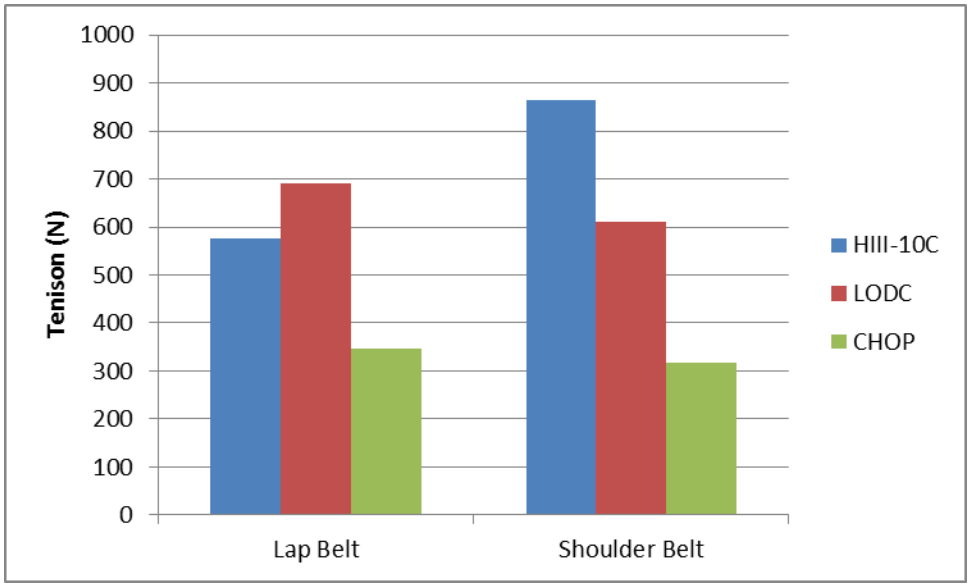

Figure 51. Belt tensions for the LODC, HIII-10C, and pediatric volunteers in the low-speed (9 km/h) bumper car tests.

Figure 50 shows that the HIII-10C has the least amount and the pediatric volunteers have the greatest amount of forward displacement. The LODC lies between the two. The displacement results show that the LODC is stiffer than the pediatric volunteers but less stiff than the HIII-10C. Therefore, the LODC design seems to be moving in the right direction. Figure 47 showed that the volunteers had very little downward motion, which may be due to active musculature. The lack of muscle effect in the ATD in this

low-speed event may also be contributing to the difference in belt tension. Without the presence of active musculature, the full weight of the ATDs may be loading the belts during the event. In contrast, the presence of active musculature in pediatric volunteers may cause only a fraction of the volunteer's weight to load the belts during the event, resulting in much lower belt forces. In addition, the LODC shoulder appears to be stiffer than the pediatric volunteer at low-speed, as shown in Figure 40. This may also be contributing to the higher shoulder belt force in the LODC.

Discrepancies in displacements and belt tensions between the ATDs and volunteer data may also be due to differences in seating position, belt routing, seat cushion thickness and stiffness, and the buck itself. For this test series, the FMVSS No. 213 bench was modified to seat the ATDs as close to the CHOP setup as possible. In addition, a retractor was used by CHOP, whereas a retractor wasn't used in the ATD tests. Results may be different if tested using CHOP's actual bumper car setup, so there are plans to send the LODC to CHOP for testing under the bumper car conditions. It should also be noted that the-speeds performed in these tests may be lower than what ATDs may be capable of being designed for.

3.3. High-Speed Kinematics

3.3.1. Mid-Speed, 40 km/h pulse

5-Point Harness (Britax Frontier 85)

Time histories for head acceleration, chest acceleration, chest compression, and occipital condyle moment are shown in Figures 52-55. Additional time history plots for the LODC and HIII-10C dummies seated in a 5-point harness (Britax Frontier 85) are shown in Appendix B.

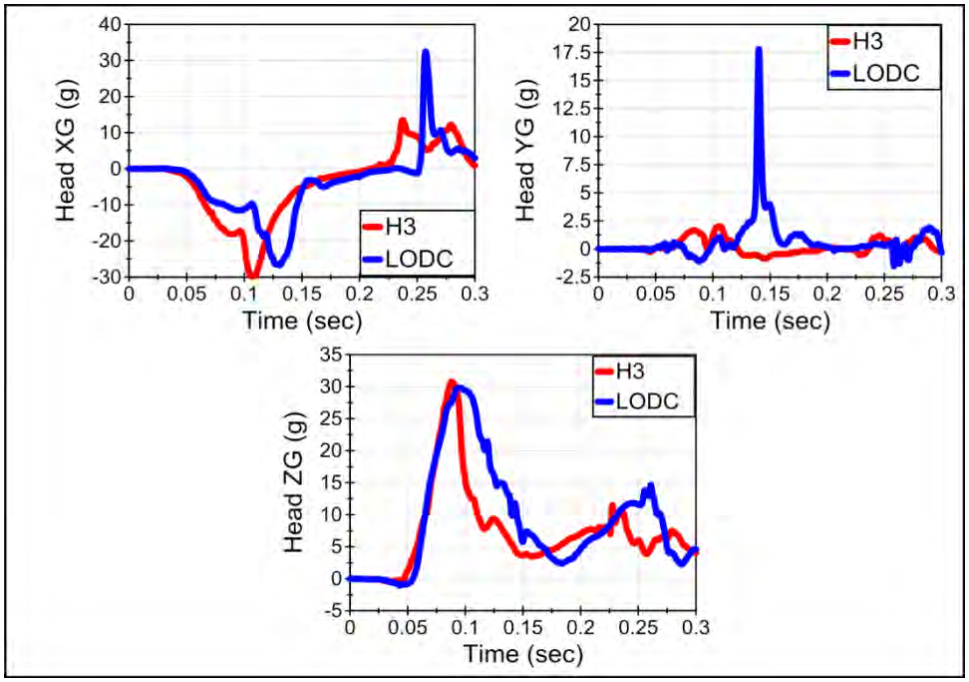

Figure 52. Head accelerations in the LODC and HIII-10C using a 5-point harness (40 km/h)

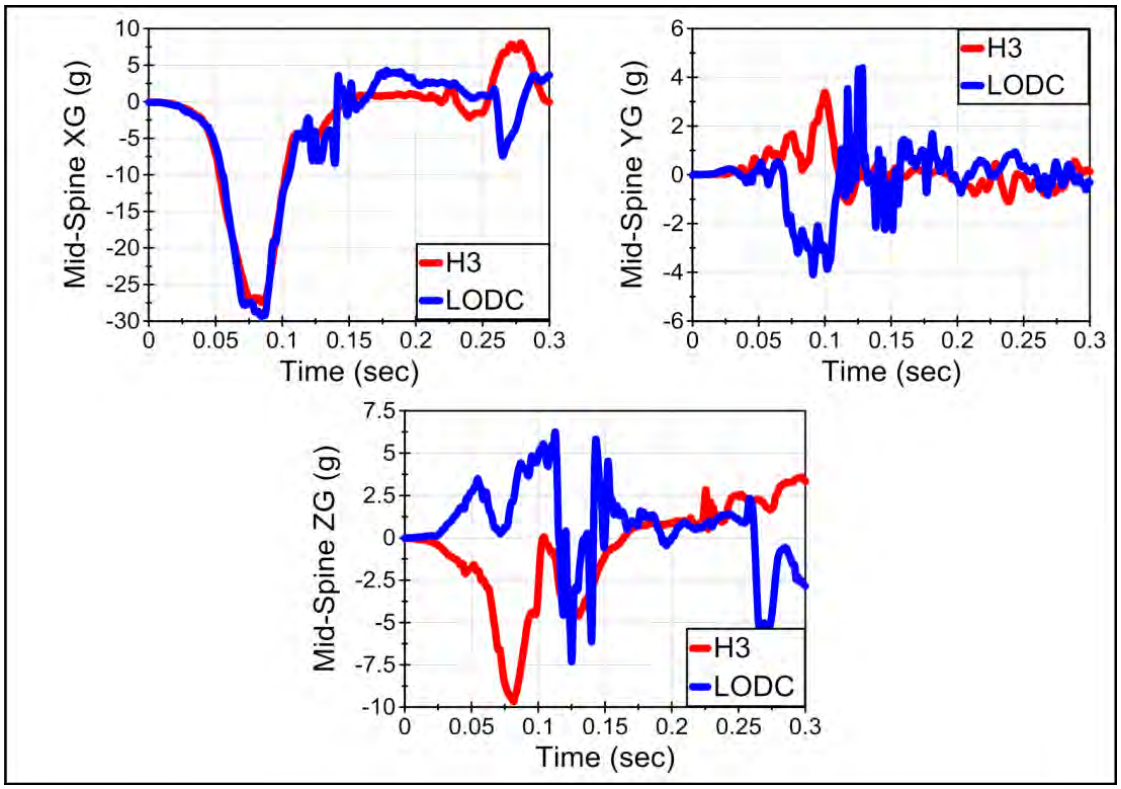

Figure 53. Mid-spine accelerations in the LODC and HIII-10C using a 5-point harness (40 km/h)

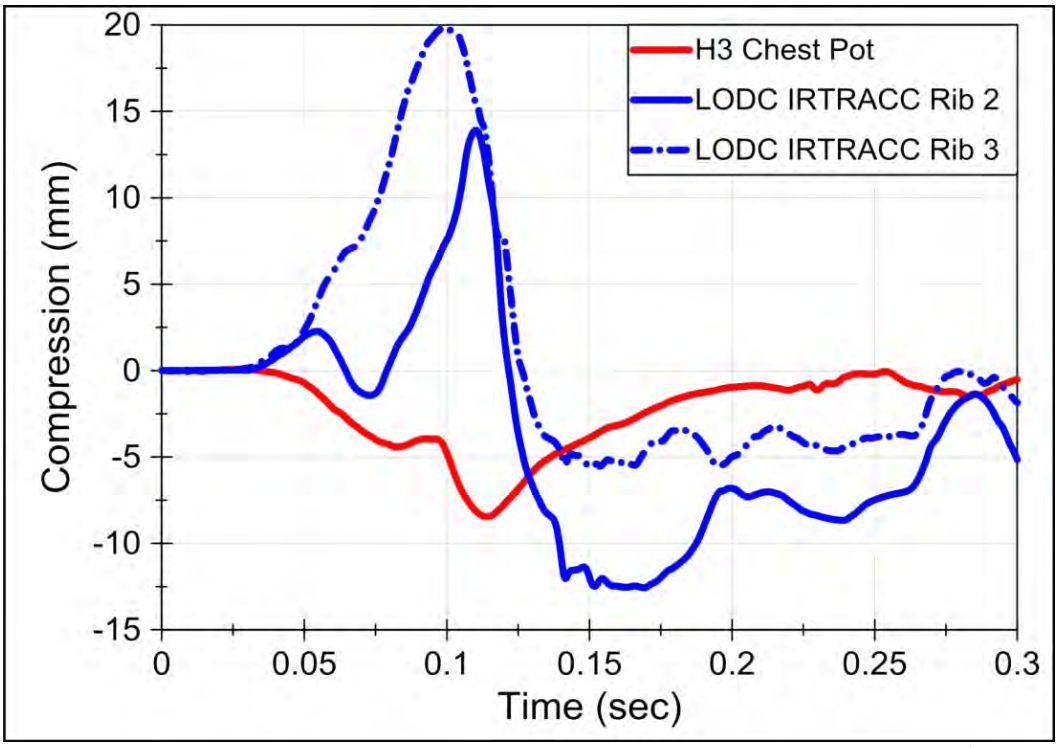

Figure 54. Chest compressions in the LODC and HIII-10C using a 5-point harness (40 km/h). A negative chest compression indicates that the sternum is moving towards the spine.

Figure 54 shows a significant amount of early chest expansion (positive value) in the 5pt harness case. There was actually about 15-20 mm of space between the sternum and vertical harness straps initially. It appears that as the torso flexes over, the superior portion of the abdomen pushes up on the mid/lower portion of the ribcage, which results in expansion prior to the harness engaging the ribcage. This initial expansion was not present in the booster seat cases because the belt is initially engaging the sternum.

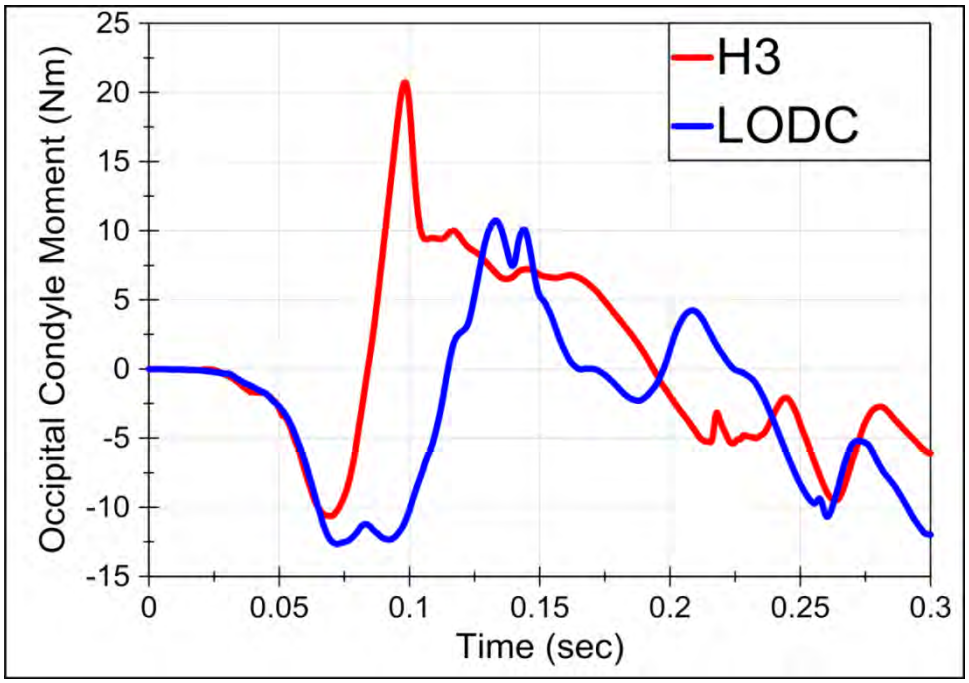

Figure 55. Occipital condyle moment in the LODC and HIII-10C using a 5-point harness (40 km/h)

Dummy kinematics were calculated for the head, neck (T1), mid-spine, and pelvis for both dummies using the corresponding accelerometers and angular rate sensors. For the HIII-10C dummy, the T1 kinematics were calculated using rigid body translations of the mid-spine transducers. The LODC kinematics are represented by the blue curves and the HIII-10C kinematics are represented by the red curves in Figure 56 below. Video screen captures correspond to the data point markers shown in the plots.

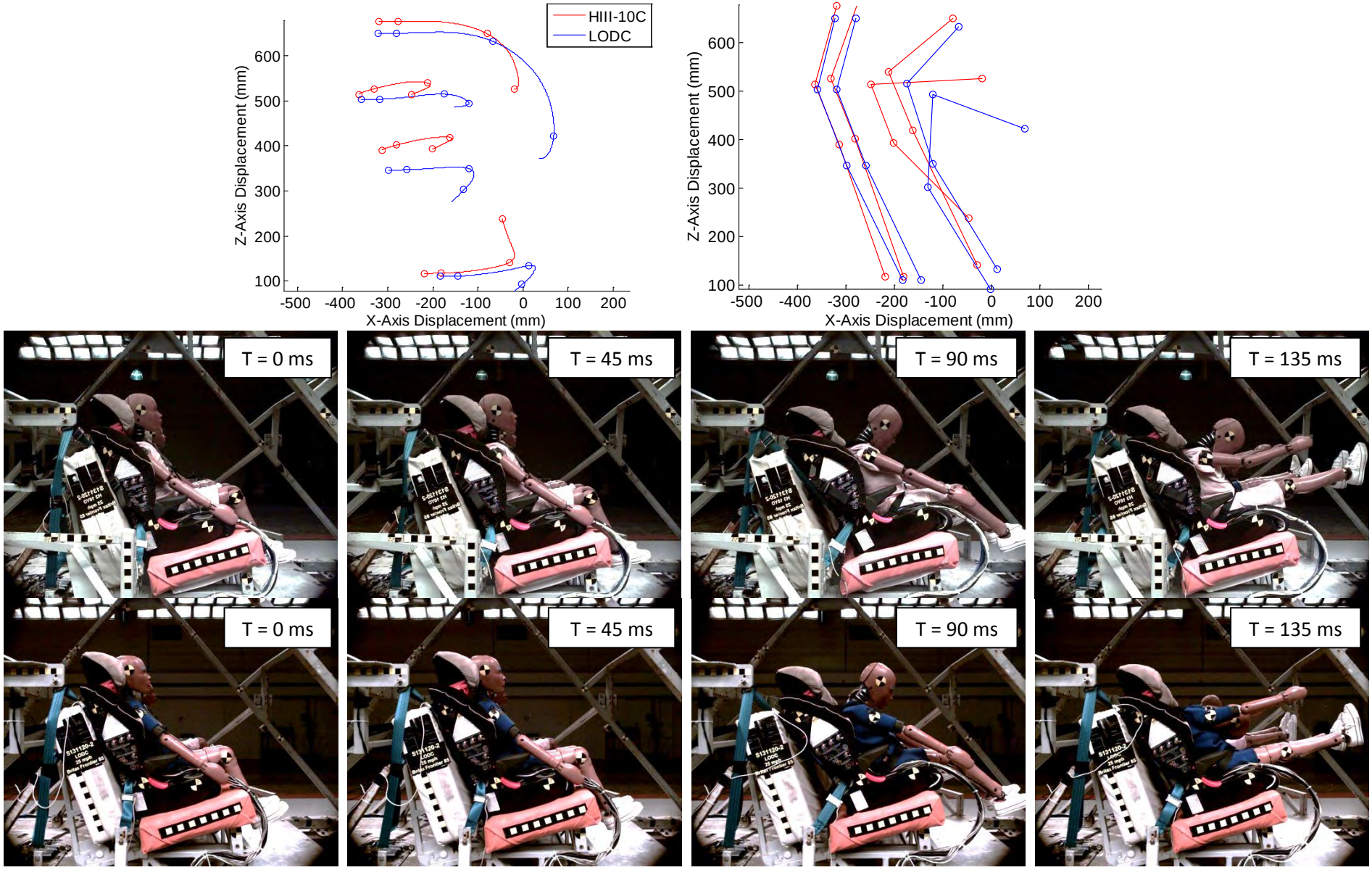

Figure 56. Kinematics of LODC and HIII-10C in 40 km/h test with 5 point harness CRS

High Back Booster (Graco TurboBooster)

Time histories for head acceleration, chest acceleration, chest compression, and occipital condyle moment are shown in Figures 57-60. Additional time history plots for the LODC and HIII-10C dummies seated in a highback BPB (Graco TurboBooster) are shown in Appendix B.

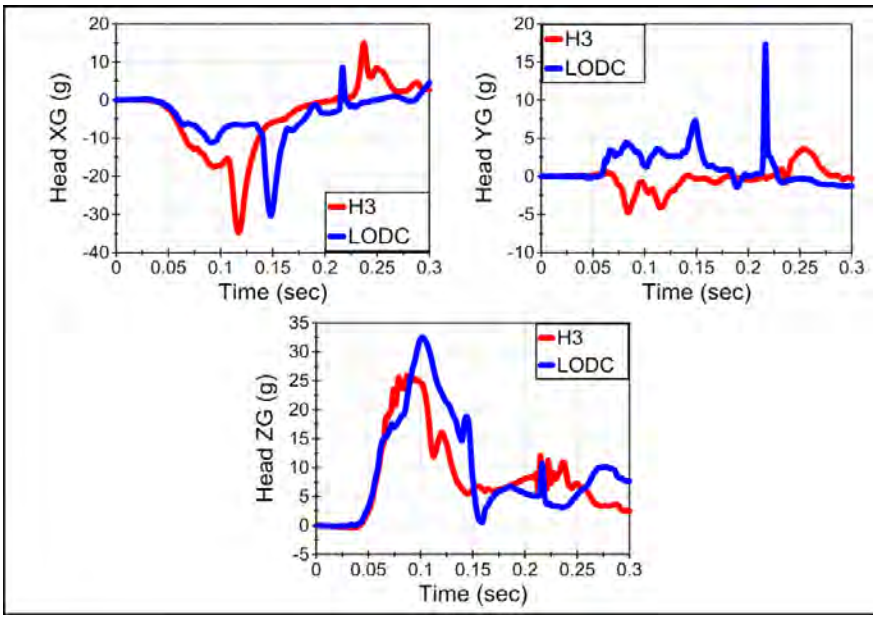

Figure 57. Head accelerations in the LODC and HIII-10C using a high back booster seat (40 km/h)

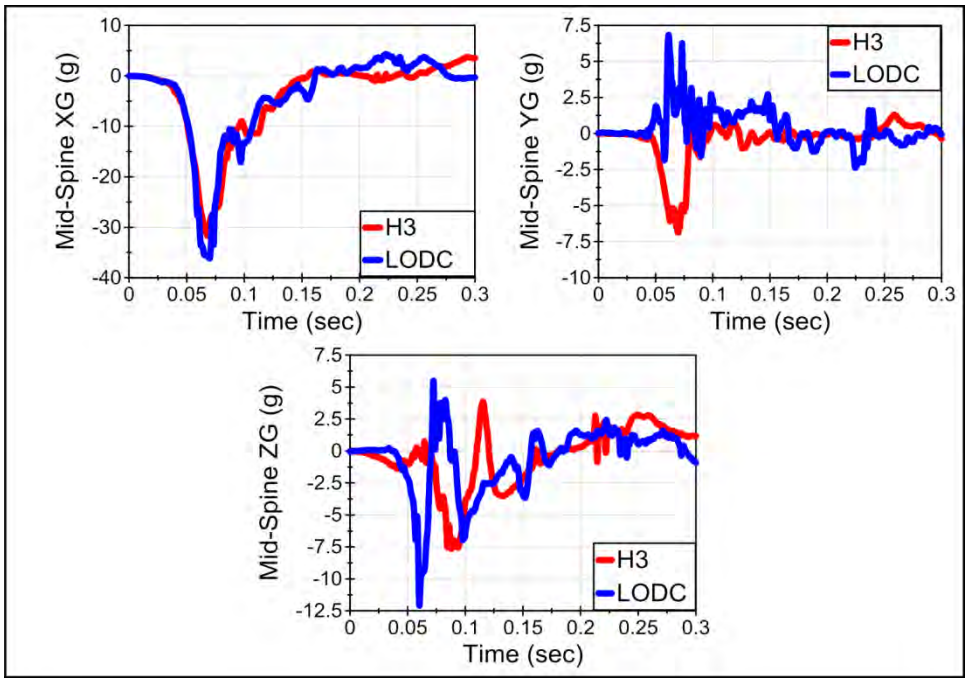

Figure 58. Mid-spine accelerations in the LODC and HIII-10C using a high back booster seat (40 km/h)

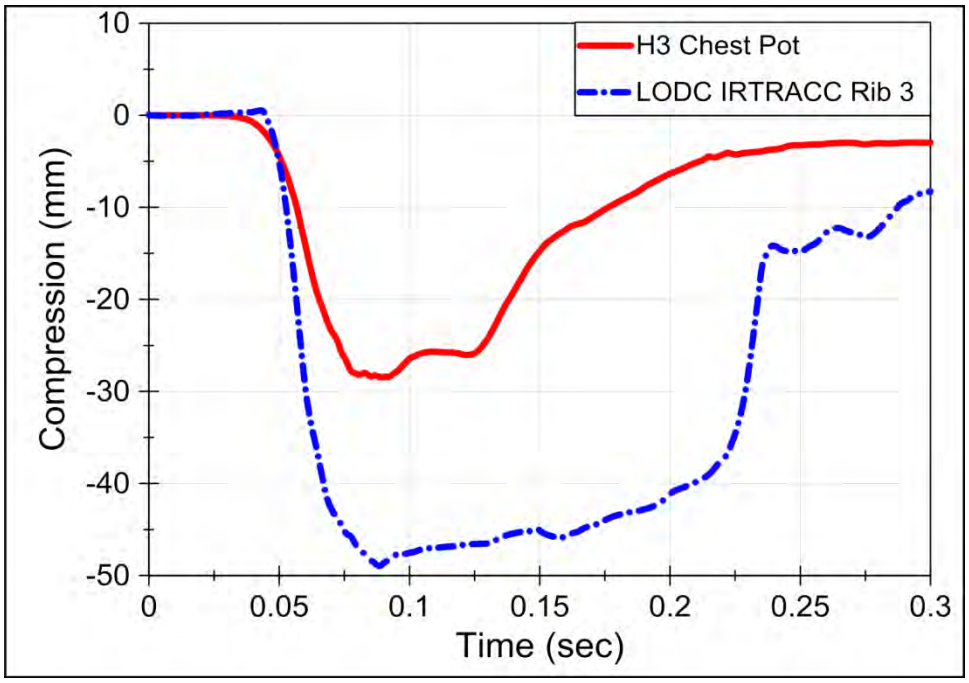

Figure 59. Chest compressions in the LODC and HIII-10C using a high back booster seat (40 km/h). A negative chest compression indicates that the sternum is moving towards the spine.

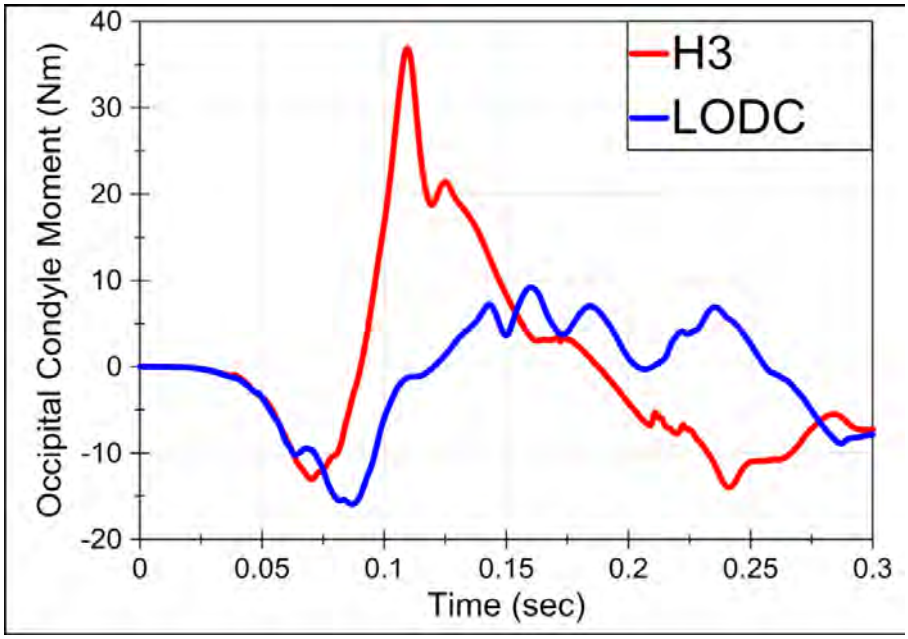

Figure 60. Occipital condyle moment in the LODC and HIII-10C in high back booster seat (40 km/h)

Dummy kinematics were calculated for the head, neck (T1), mid-spine, and pelvis for both dummies using the corresponding accelerometers and angular rate sensors. For the HIII-10C dummy, the T1 kinematics were calculated using rigid body translations of the mid-spine transducers. The LODC and HIII-10C kinematics are represented by the blue and red curves, respectively in Figure 61 below. Video screen captures correspond to the data point markers shown in the plots.

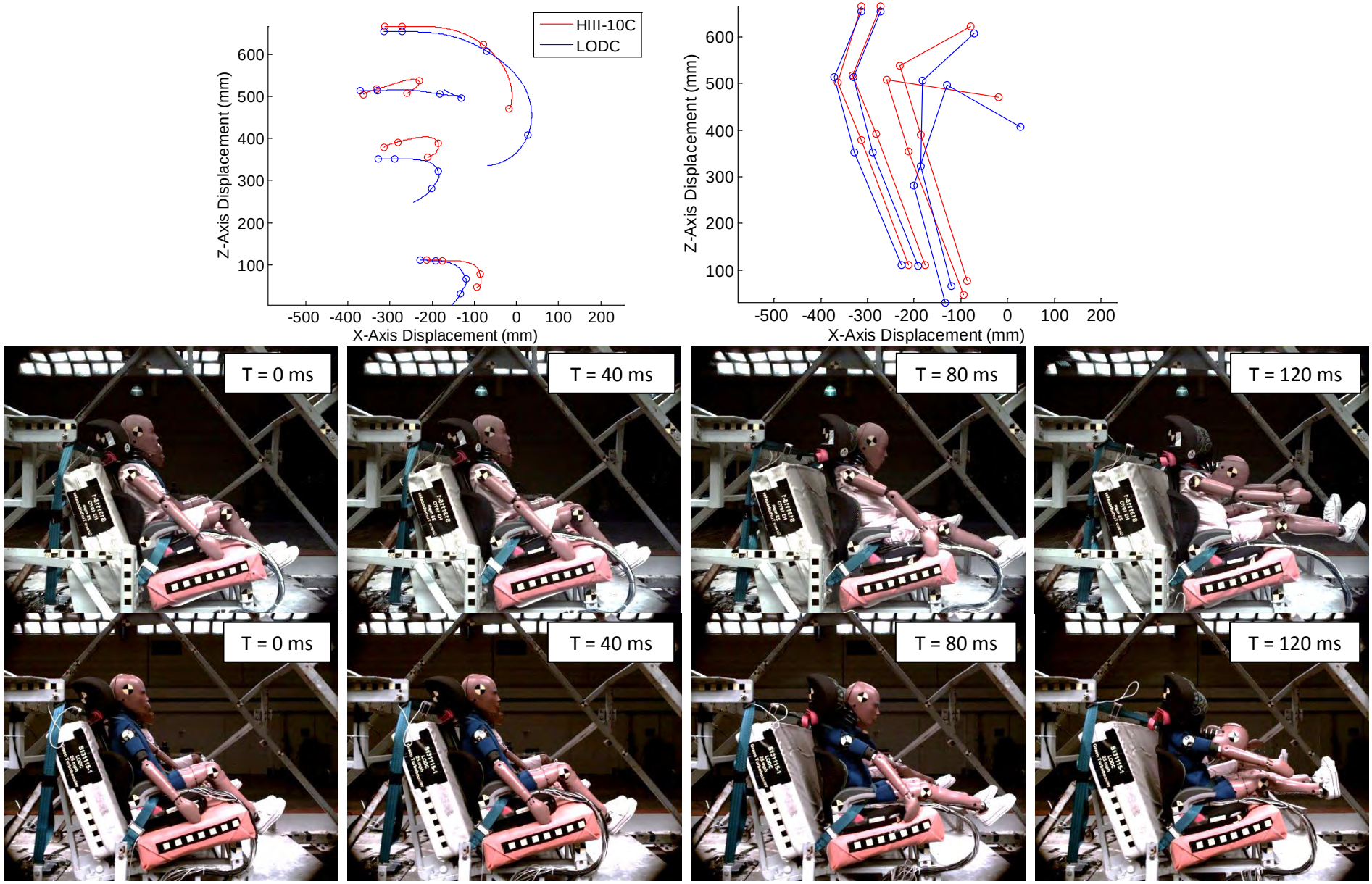

Figure 61. Kinematics of LODC and HIII-10C in 40 km/h test with highback booster

Backless Booster (Graco TurboBooster)

Time histories for head acceleration, chest acceleration, chest compression, and occipital condyle moment are shown in Figures 62-65. Additional time history plots for the LODC and HIII-10C dummies seated in a backless BPB (Graco TurboBooster) are shown in Appendix B.

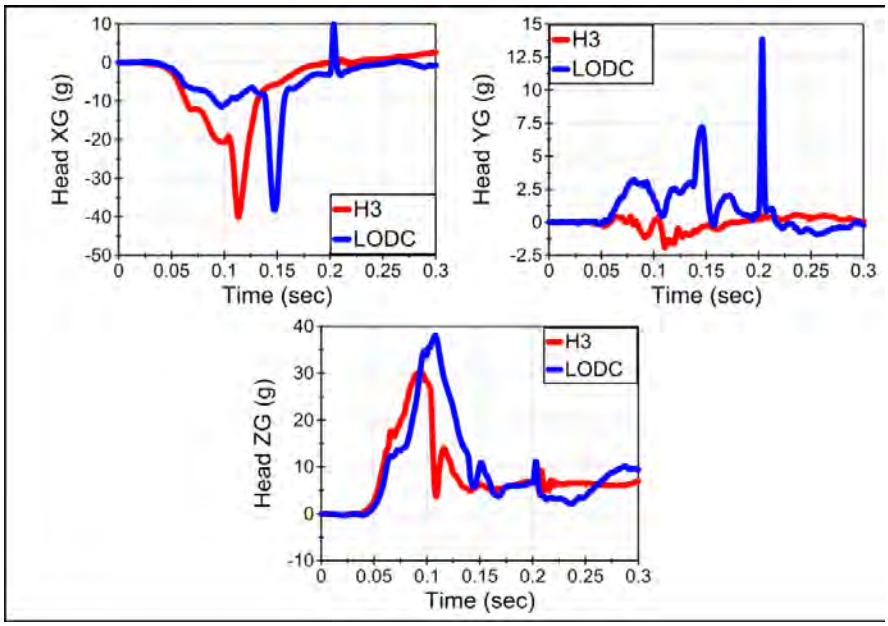

Figure 62. Head accelerations in the LODC and HIII-10C using a backless booster seat (40 km/h)

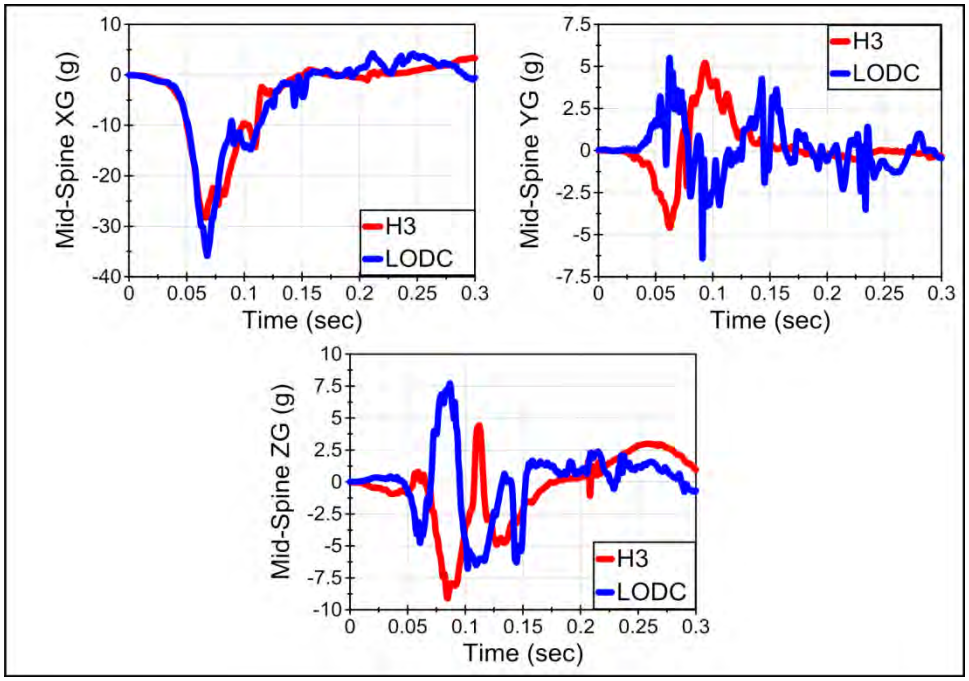

Figure 63. Mid-spine accelerations in the LODC and HIII-10C using a backless booster seat (40 km/h)

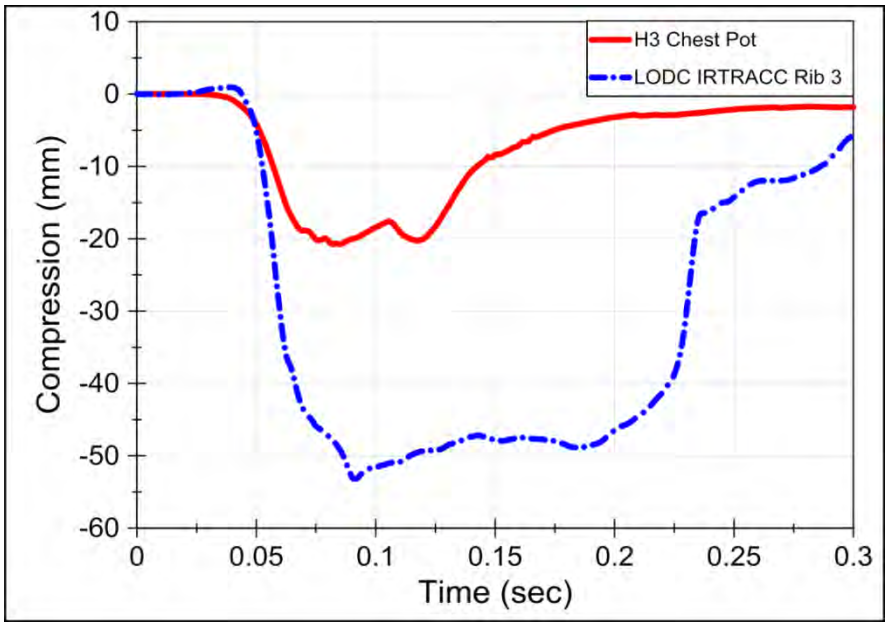

Figure 64. Chest compressions in the LODC and HIII-10C using a backless booster seat (40 km/h). A negative chest compression indicates that the sternum is moving towards the spine.

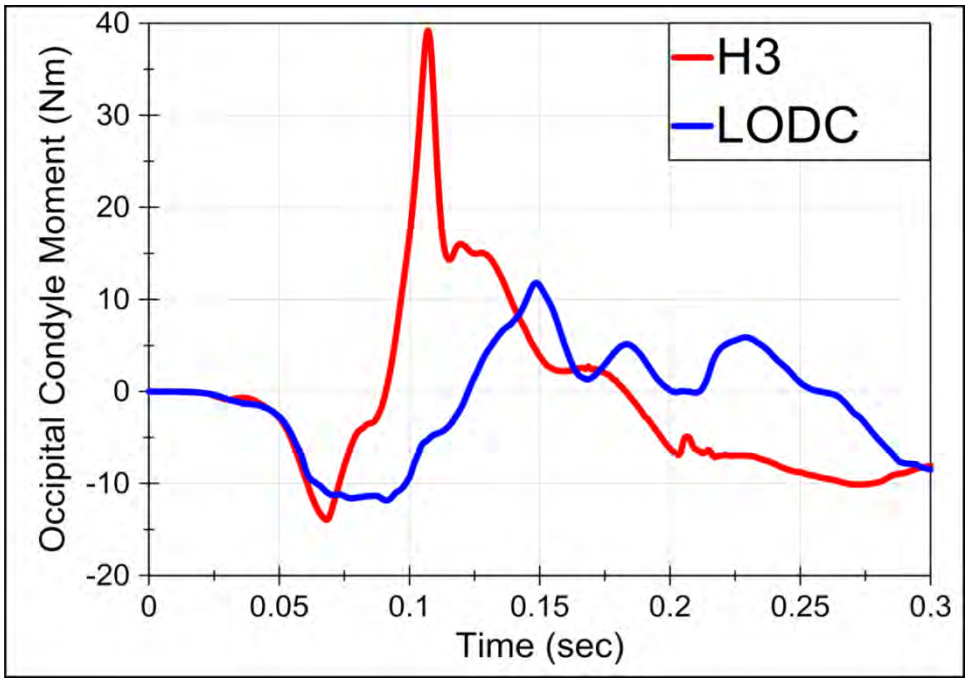

Figure 65. Occipital condyle moment in the LODC and HIII-10C in backless booster seat (40 km/h)

Dummy kinematics were calculated for the head, neck (T1), mid-spine, and pelvis for both dummies using the corresponding accelerometers and angular rate sensors. For the HIII-10C dummy, the T1 kinematics were calculated using rigid body translations of the mid-spine transducers. The LODC and HIII-10C kinematics are represented by the blue and red curves, respectively in Figure 66 below. Video screen captures correspond to the data point markers shown in the plots.

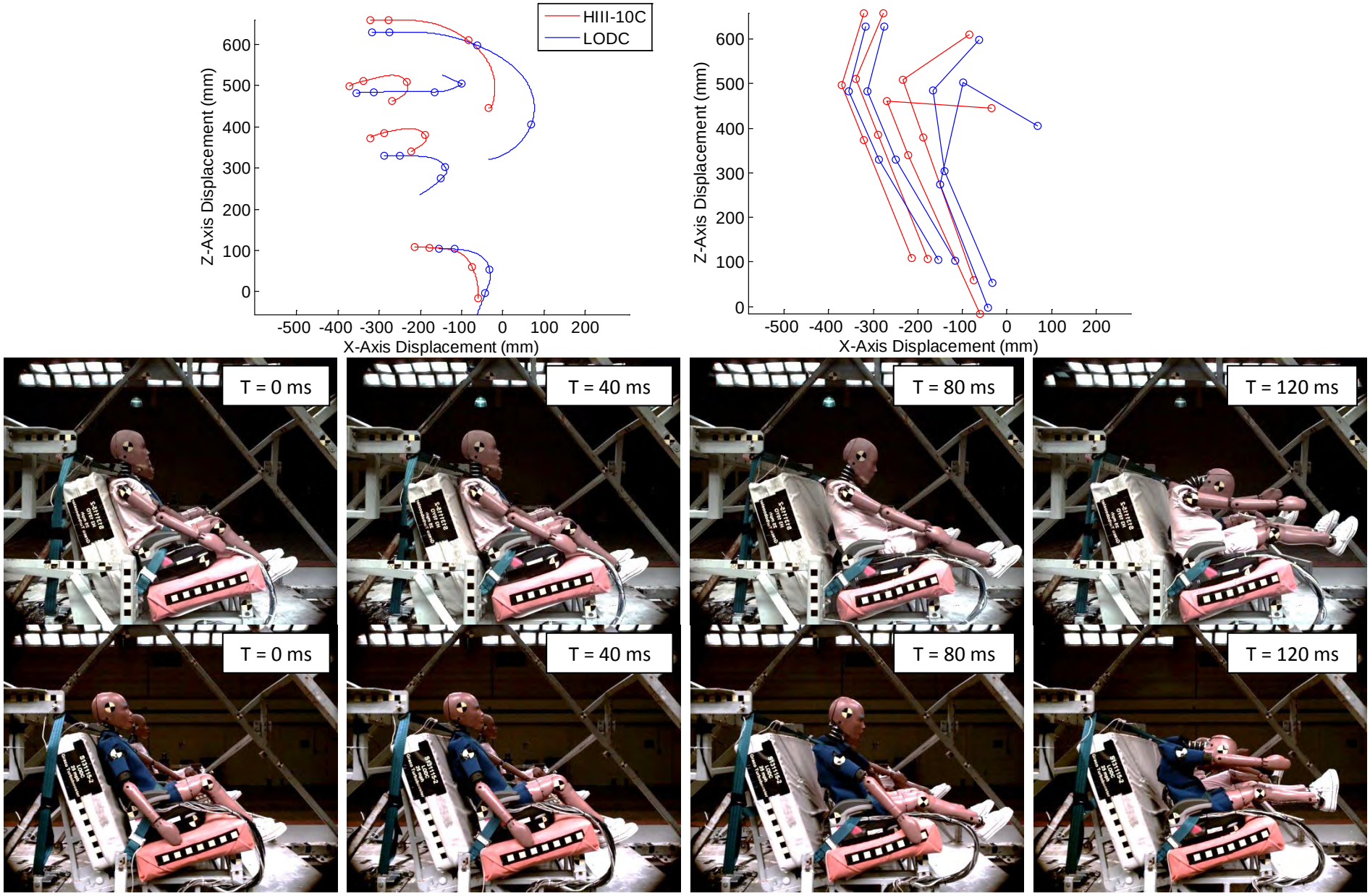

Figure 66. Kinematics of LODC and HIII-10C in 40 km/h test with backless booster

No Child Restraint System

Time histories for head acceleration, chest acceleration, chest compression, and occipital condyle moment are shown in Figures 67-70. Additional time history plots for the LODC and HIII-10C dummies seated in no CRS (3-point lap-shoulder belt) are shown in Appendix B.

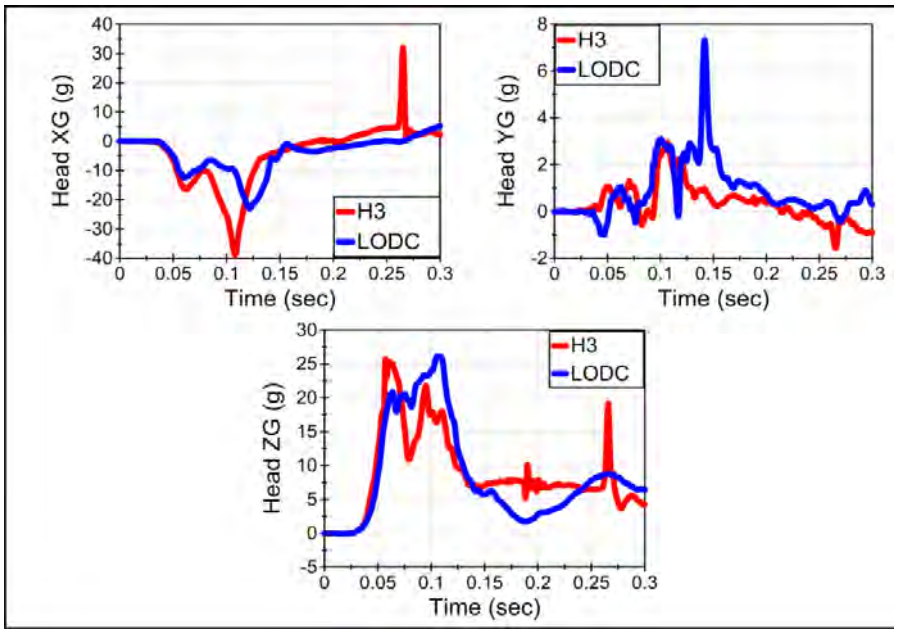

Figure 67. Head accelerations in the LODC and HIII-10C using no child restraint system (40 km/h)

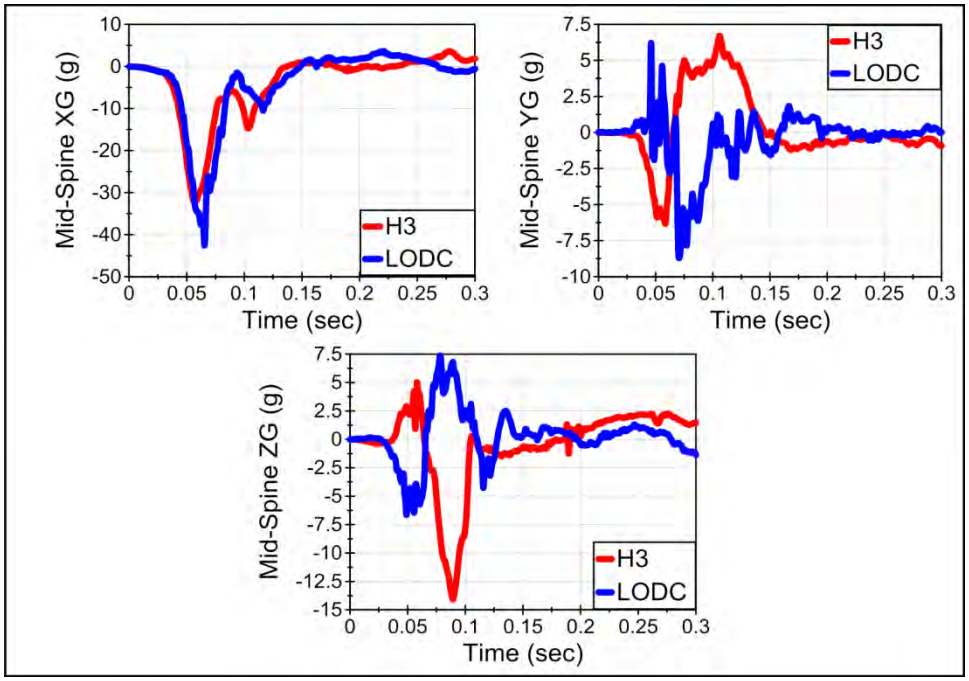

Figure 68. Mid-spine accelerations in the LODC and HIII-10C using no child restraint system (40 km/h)

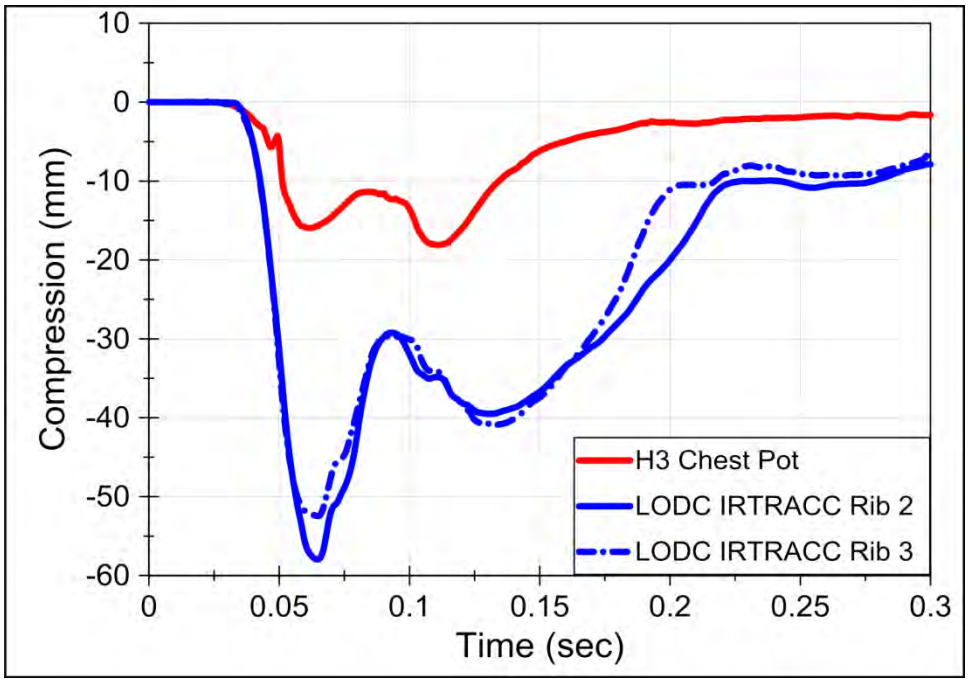

Figure 69. Mid-spine accelerations in the LODC and HIII-10C using no child restraint system (40 km/h). A negative chest compression indicates that the sternum is moving towards the spine.

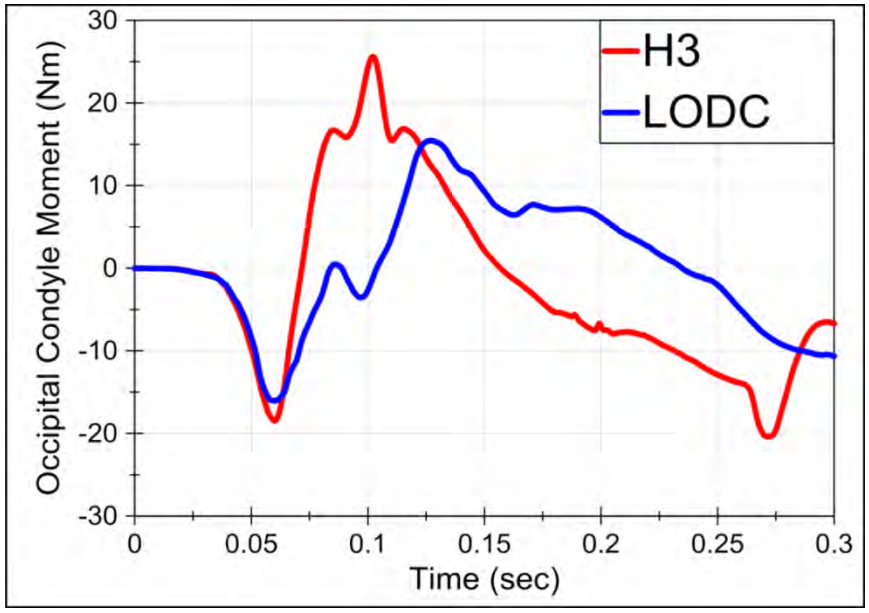

Figure 70. Occipital condyle moment in the LODC and HIII-10C in no CRS (40 km/h)

Dummy kinematics were calculated for the head, neck (T1), mid-spine, and pelvis for both dummies using the corresponding accelerometers and angular rate sensors. For the HIII-10C dummy, the T1 kinematics were calculated using rigid body translations of the mid-spine transducers. The LODC and HIII-10C kinematics are represented by the blue and red curves, respectively in Figure 71 below. Video screen captures correspond to the data point markers shown in the plots.

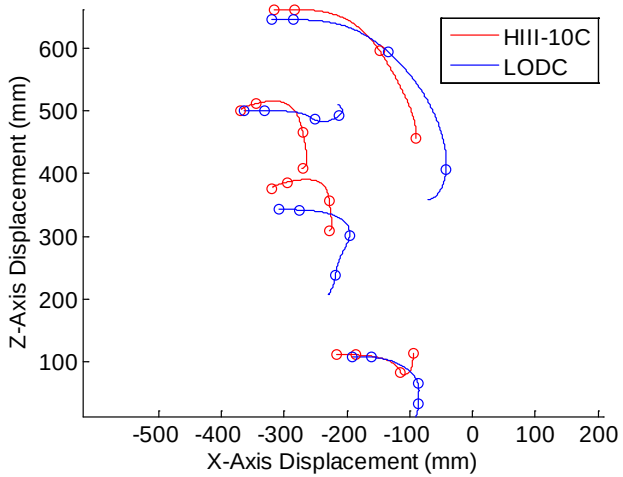

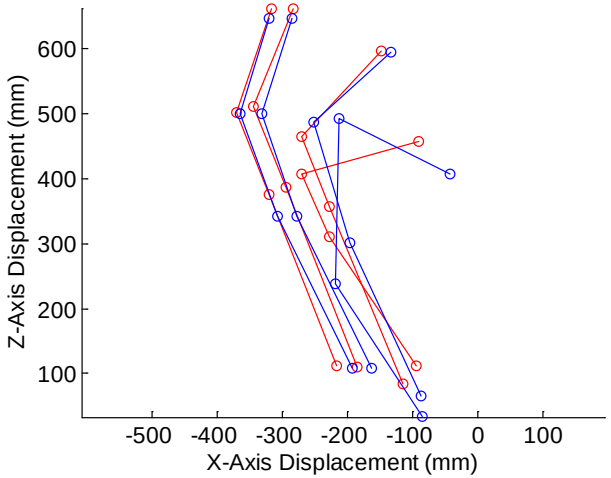

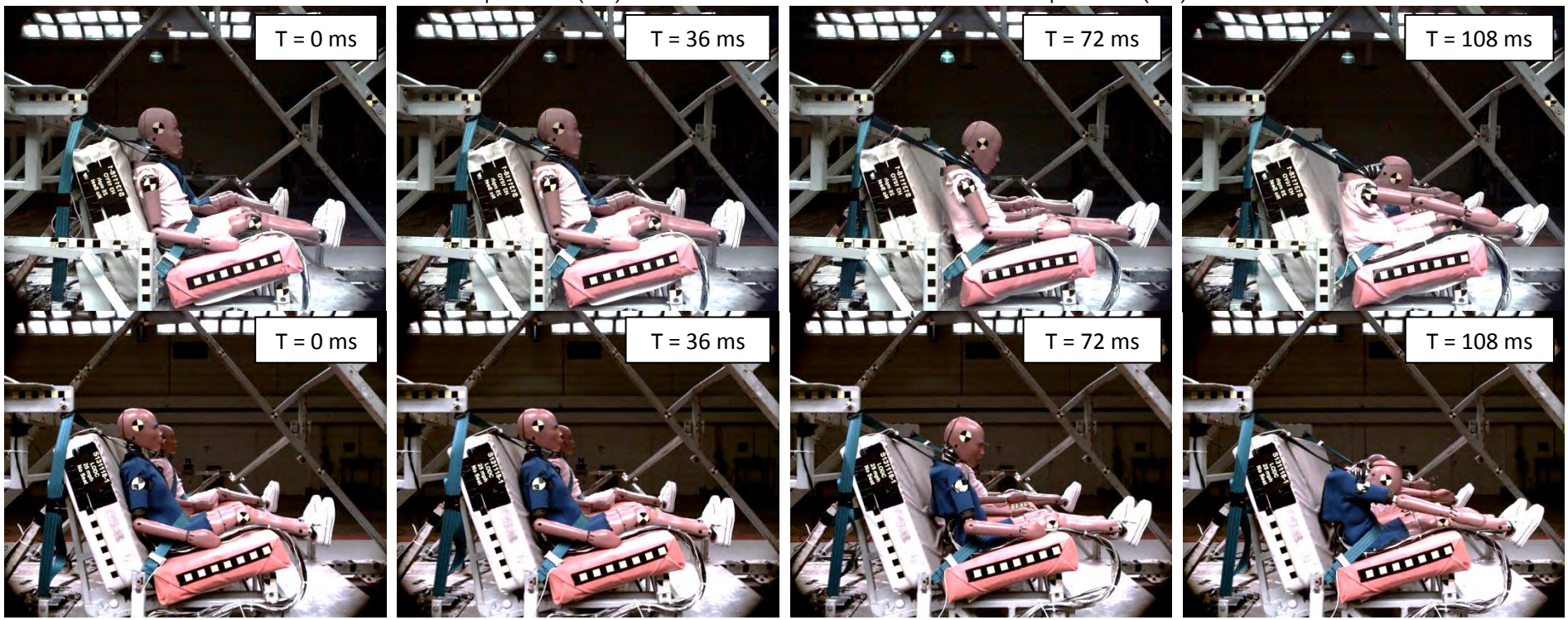

Figure 71. Kinematics of LODC and HIII-10C in 40 km/h test with three point belt only (no CRS)

Mid-Speed Summary

HIC, chest g, and maximum values for head and knee excursion, head-spine trajectories, chest compression, occipital condyle moment, and belt loads are tabulated in Table 5 for all child restraint conditions and for both the HIII-10C and LODC.

Table 5. Maximum value comparisons for the mid-speed (40 km/h) tests.

Description		5-Point Harness		High Back Booster		Backless Booster		No CRS	
		HIII-10C	LODC	HIII-10C	LODC	HIII-10C	LODC	HIII-10C	LODC
HIC 36		195	175	184	164	244	222	175	43
Chest G		28.5	29.6	31.1	36.1	28.0	34.3	31.3	37.2
Head Excursion (mm)		532	575	533	558	479	508	456	453
Knee Excursion (mm)		801	798	727	664	706	646	647	636
Head Displacement (mm)	X	309	391	302	350	301	394	227	278
	Z	150	278	195	317	213	308	206	286
T1 Displacement (mm)	X	158	238	134	241	141	256	106	157
	Z*	4.03	17.1	9.2	17	45.7	0	104	17.4
Mid-Spine Displacement (mm)	X	155	189	128	143	135	153	96.9	112
	Z*	1	135	31.5	169	42.1	165	79.5	236
Chest Compression (mm)		-8.5	-12.6	-28.5	-48.9	-20.7	-53.2	-18.1	-55.2
Moment About Occipital Condyle (Nm)		-10.6 20.7	-12.7 10.7	-13.0 36.9	-15.9 9.19	-13.9 39.2	-11.8 11.8	-18.5 25.6	-16.0 15.4
Peak Belt Tension (N)	Lap	3022	3918	3801	3500	3345	3518	4030	4053
	Shoulder	3440	3827	4907	4126	4230	3823	4005	3632

For all restraint conditions, the LODC has greater head and spine forward displacements, which reflects the relationship between spinal flexibility and head kinematics (Figure 72). Since the LODC's spine is more flexible than the HIII-10C, it is expected that the LODC would produce more head displacement. This increased flexibility has also been documented in children.

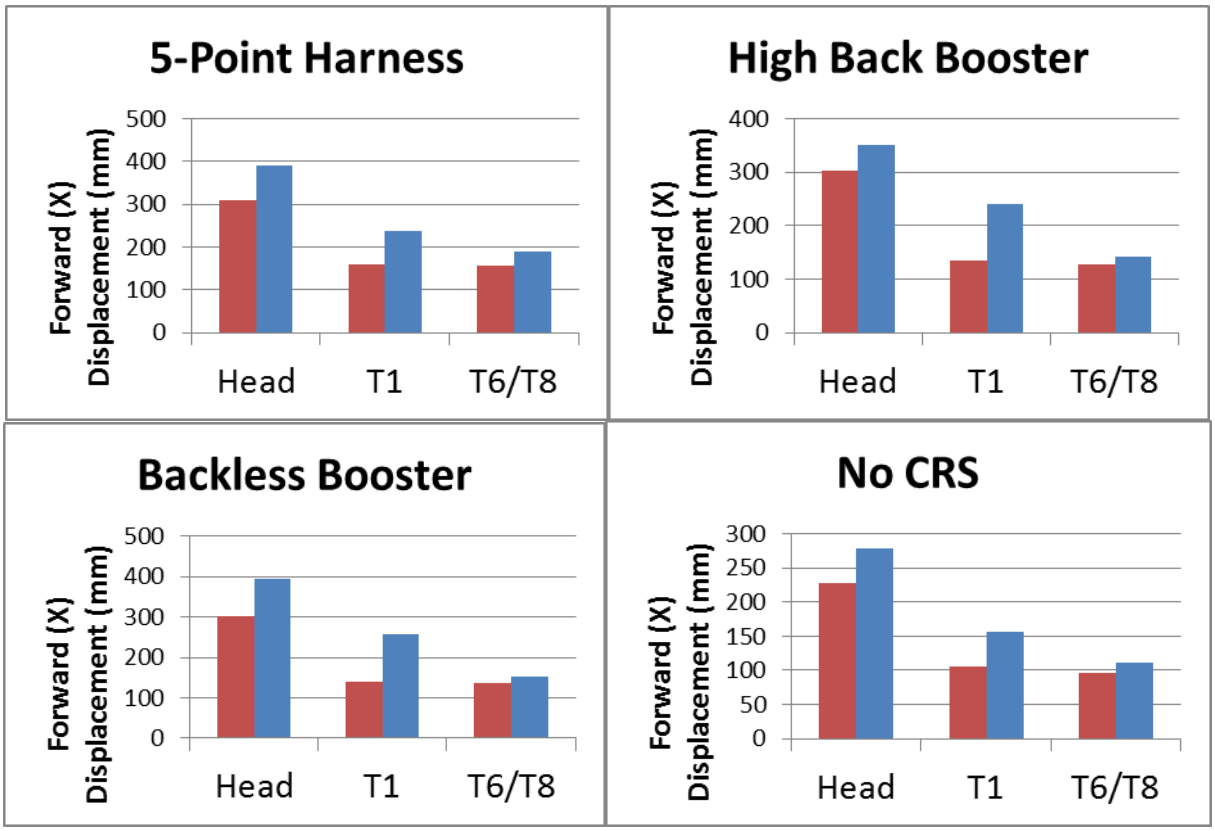

Figure 72. LODC (blue) and HIII-10C (red) head and spine displacements in various restraints (40 km/h)

In the medium-speed, 40 km/h pulse, the LODC had lower HIC values than the HIII-10C in all restraint conditions (Figure 73). However, all values, for both HIII-10C and LODC, were below 250. Head excursions were slightly higher for the LODC, reflecting its more flexible spine, but all values were below 600 mm.

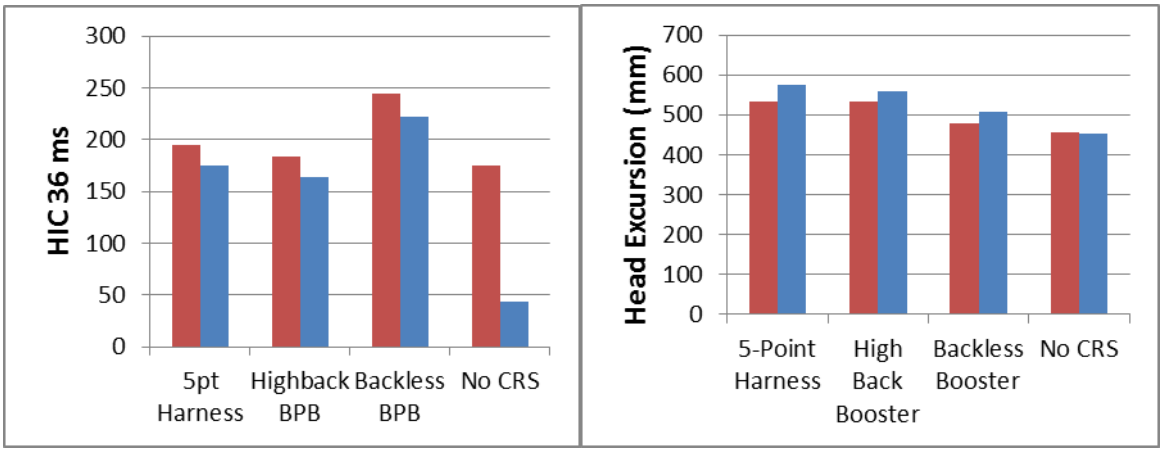

Figure 73. LODC (blue) and HIII-10C (red) HIC and head excursion in various restraints (40 km/h)

The LODC exhibited higher chest compressions and lower upper neck moments, which can be attributed to its softer thorax and more flexible neck and spine, respectively (Figure 74). The LODC was shown to have slightly lower knee excursions, but slightly higher chest accelerations than the HIII-10C. The

absolute values of peak compression were taken for the bar plot below so that positive compression means that the sternum is moving towards the spine.

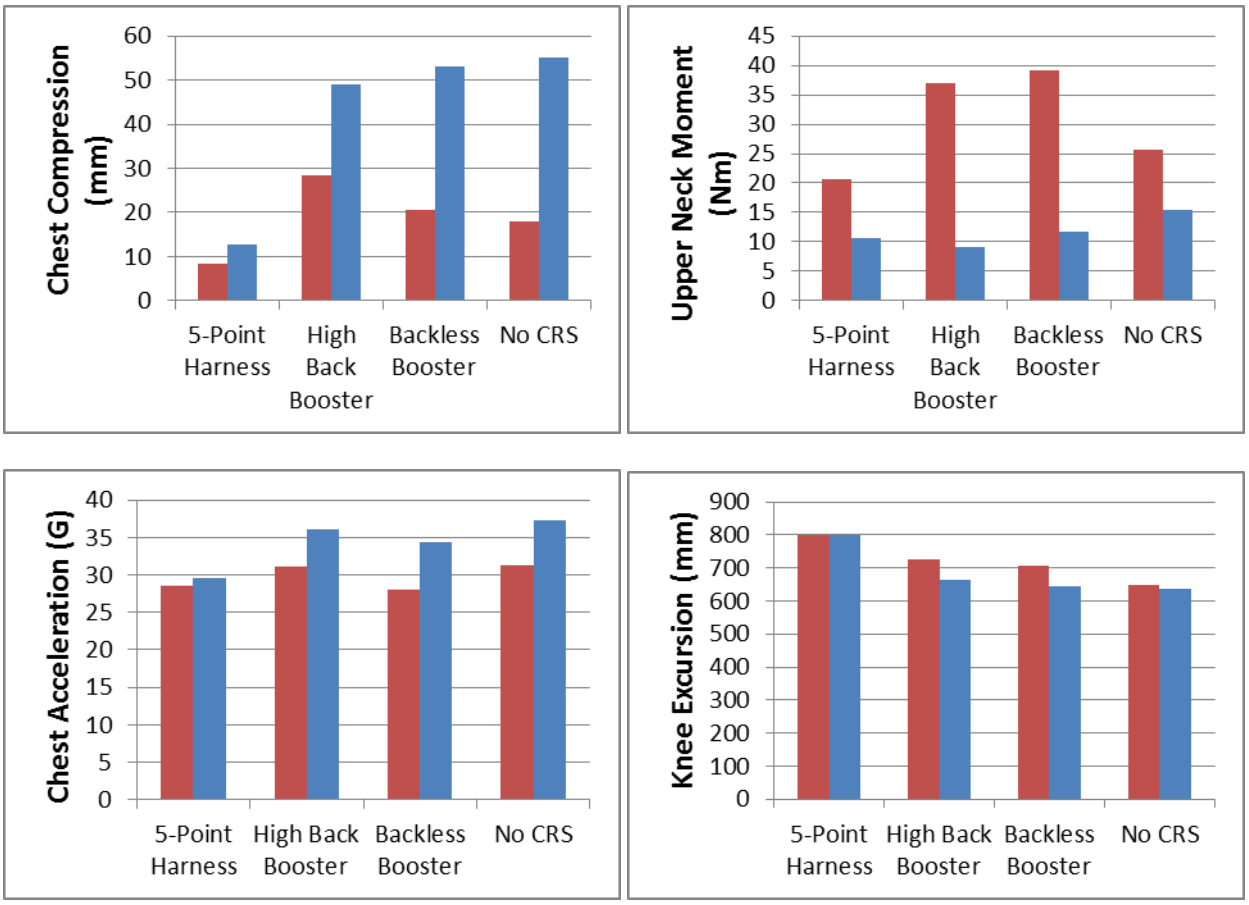

Figure 74. LODC (blue) and HIII-10C (red) chest/neck/knee peak values in various restraints (40 km/h)

3.3.2. High-Speed, 48 km/h Pulse (FMVSS 213)

5-Point Harness (Britax Frontier 85)

Time histories for head acceleration, chest acceleration, chest compression, and occipital condyle moment are shown in Figures 75-78. Additional time history plots for the LODC and HIII-10C dummies seated in a 5-point harness (Britax Frontier 85) are shown in Appendix C.

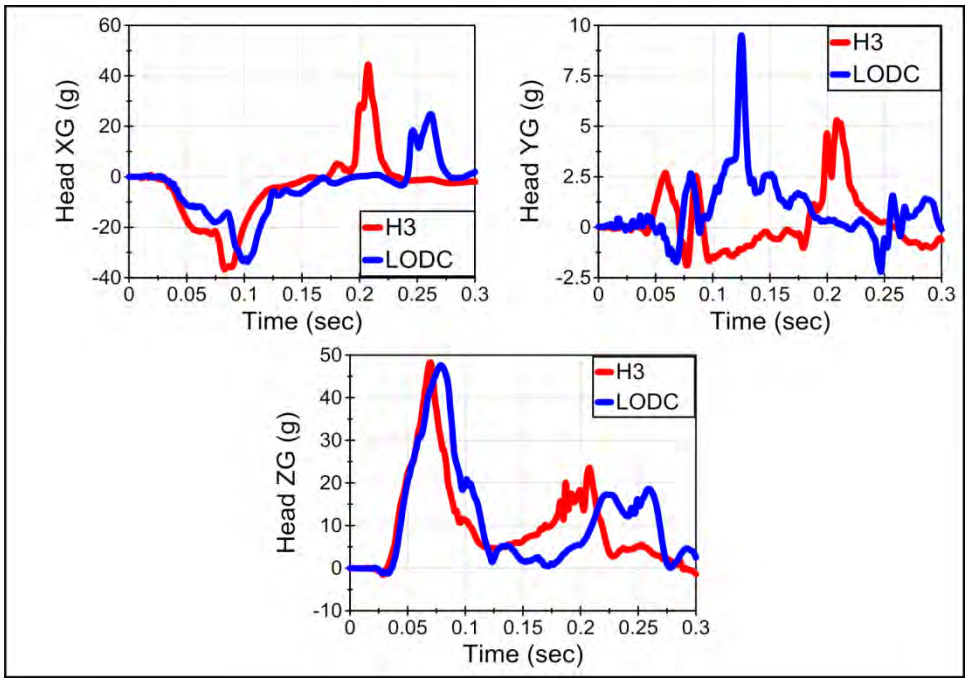

Figure 75. Head accelerations in the LODC and HIII-10C using a 5-point harness (48 km/h)

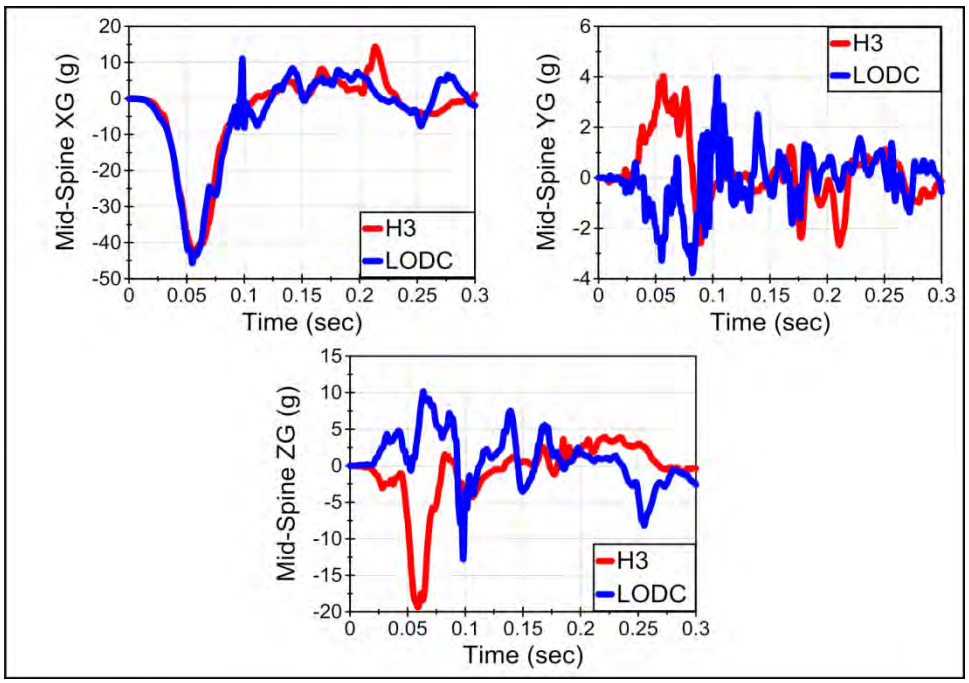

Figure 76. Mid-spine accelerations in the LODC and HIII-10C using a 5-point harness (48 km/h)

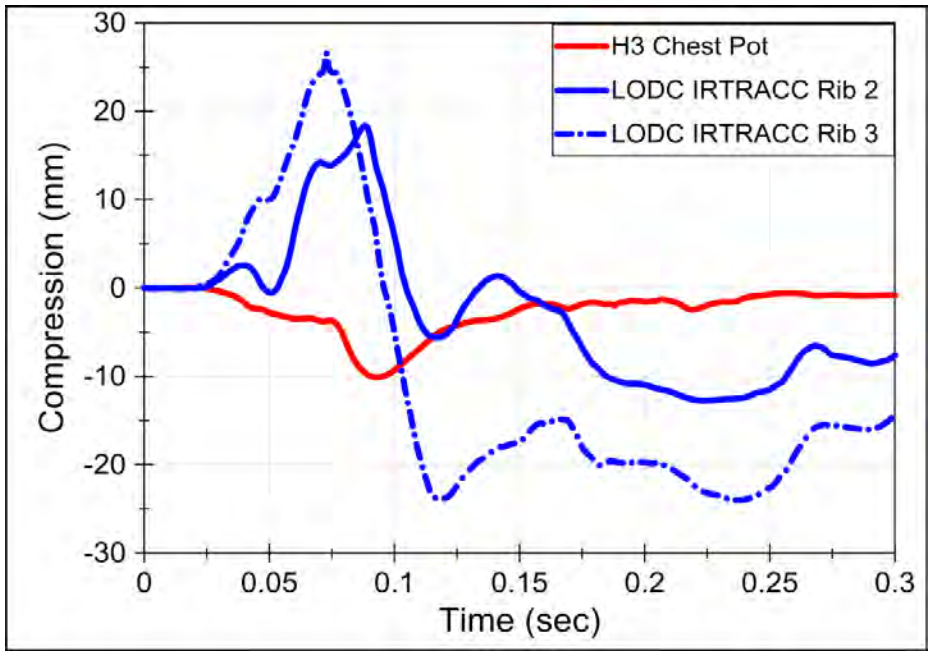

Figure 77. Chest compressions in the LODC and HIII-10C using a 5-point harness (48 km/h). A negative chest compression indicates that the sternum is moving towards the spine.

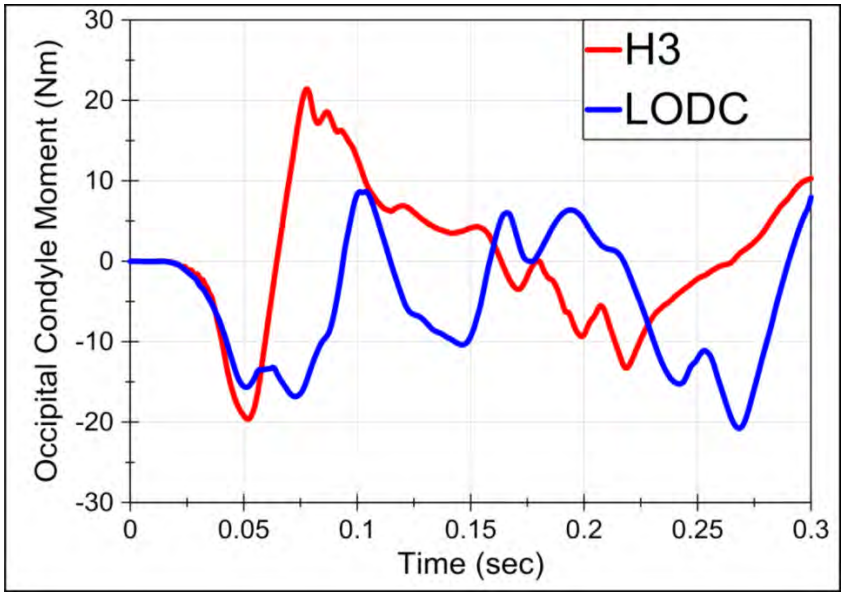

Figure 78. Occipital condyle moment in the LODC and HIII-10C in 5 point harness (48 km/h)

Similar to the mid-speed case (Figure 54), positive chest compression was observed early. Dummy kinematics were calculated for the head, neck (T1), mid-spine, and pelvis for both dummies using the corresponding accelerometers and angular rate sensors. For the HIII-10C dummy, the T1 kinematics were calculated using rigid body translations of the mid-spine transducers. The LODC kinematics are represented by the blue and red curves, respectively in Figure 79 below. Video screen captures correspond to the data point markers shown in the plots. There was integration error in the HIII-10C pelvis Z acceleration after motion had ceased; therefore, stick trajectories are only shown up to 66 ms.

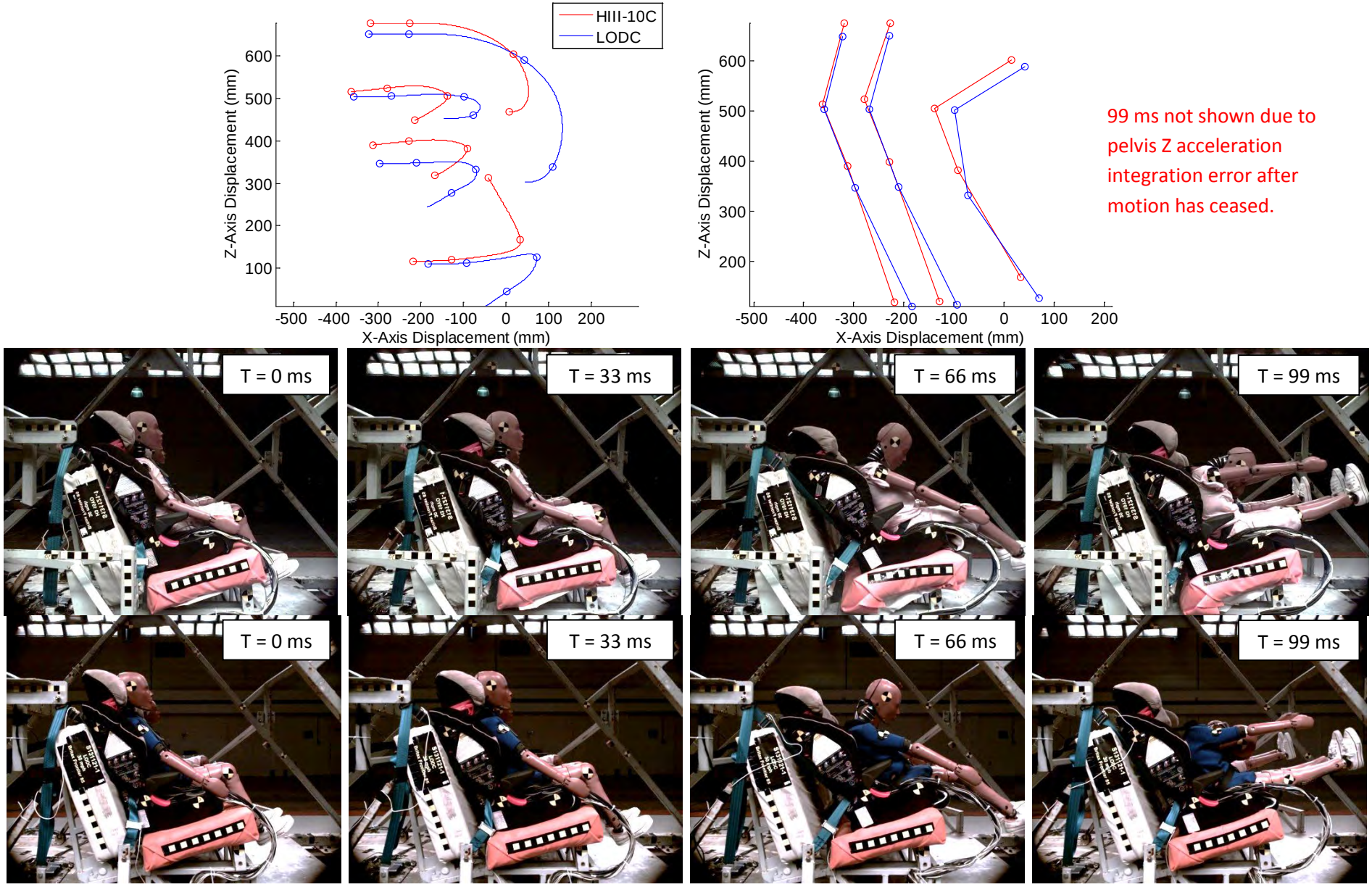

Figure 79. Kinematics of LODC and HIII-10C in 48 km/h test with 5 point harness CRS

High Back Booster (Graco TurboBooster)

Time histories for head acceleration, chest acceleration, chest compression, and occipital condyle moment are shown in Figures 80-83. Additional time history plots for the LODC and HIII-10C dummies seated in a highback BPB (Graco TurboBooster) are shown in Appendix C.

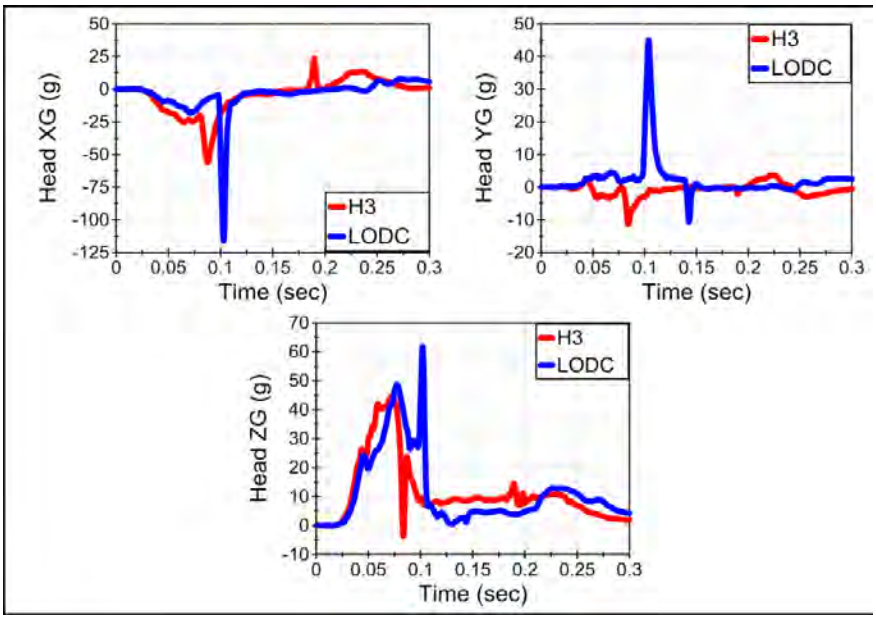

Figure 80. Head accelerations in the LODC and HIII-10C using a high back booster seat (48 km/h)

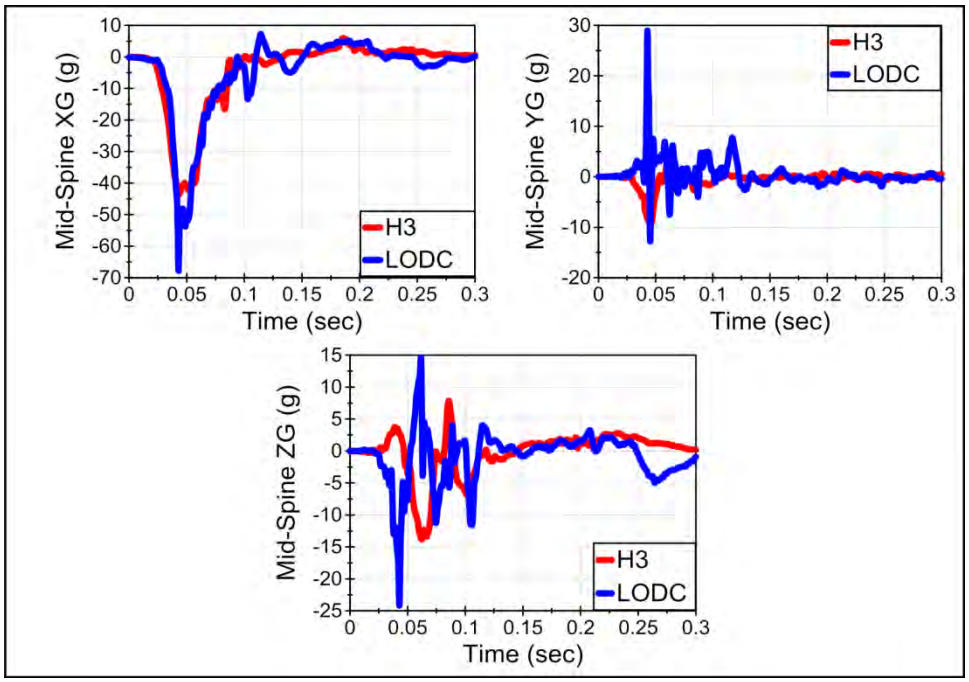

Figure 81. Mid-spine accelerations in the LODC and HIII-10C using a high back booster seat (48 km/h)

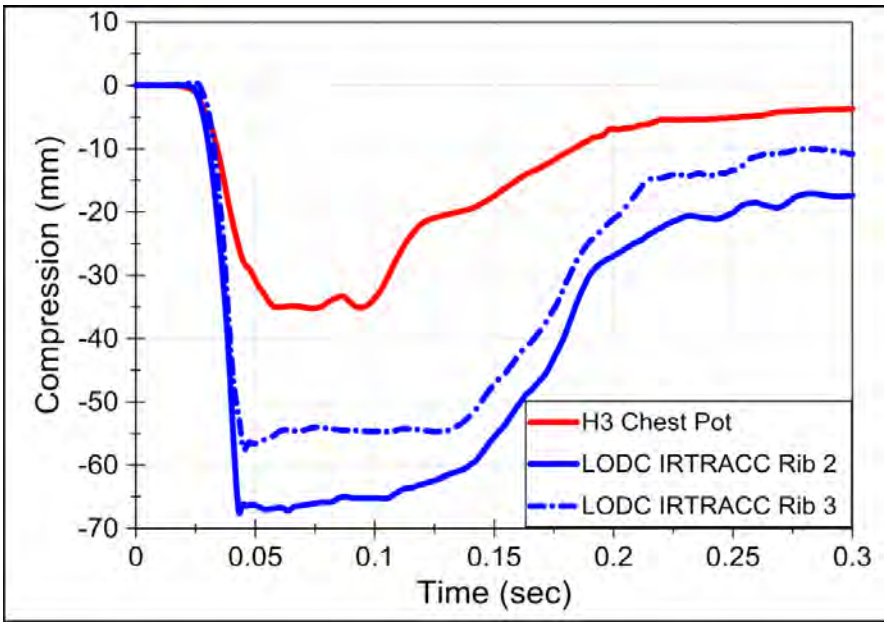

Figure 82. Chest compressions in the LODC and HIII-10C using a high back booster seat (48 km/h). A negative chest compression indicates that the sternum is moving towards the spine.

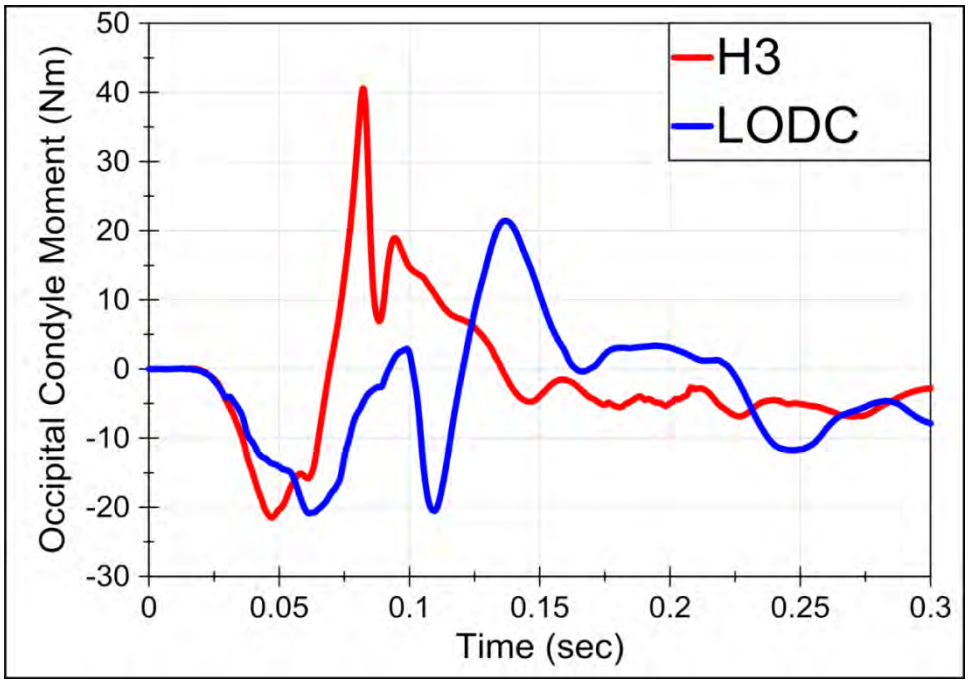

Figure 83. Occipital condyle moment in the LODC and HIII-10C in highback booster seat (48 km/h)

Dummy kinematics were calculated for the head, neck (T1), mid-spine, and pelvis for both dummies using the corresponding accelerometers and angular rate sensors. For the HIII-10C dummy, the T1 kinematics were calculated using rigid body translations of the mid-spine transducers. The LODC and HIII-10C kinematics are represented by the blue and red curves, respectively in Figure 84 below. Video screen captures correspond to the data point markers shown in the plots.

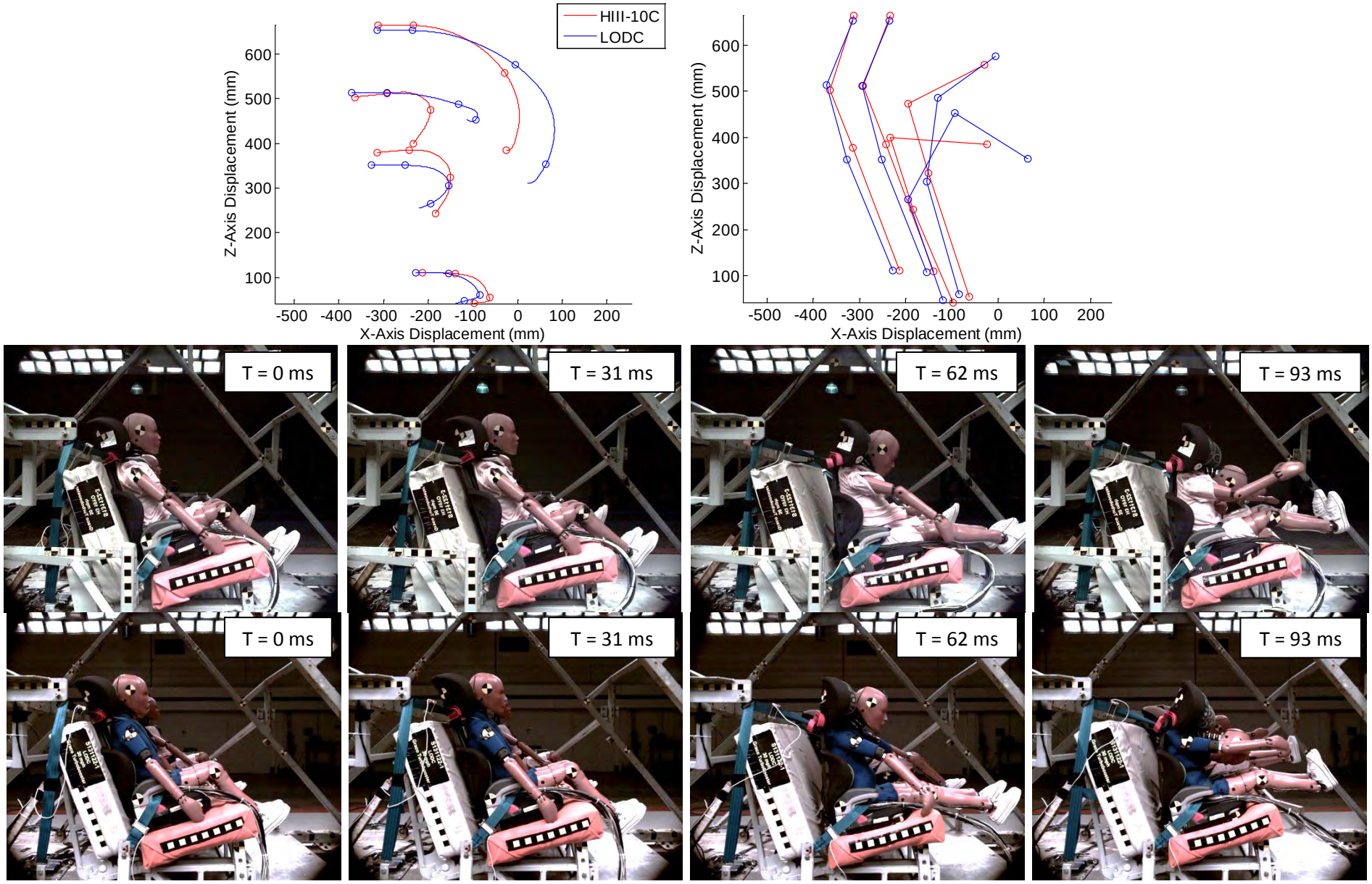

Figure 84. Kinematics of LODC and HIII-10C in 48 km/h test with highback booster

Backless Booster (Graco TurboBooster) and No Child Restraint System

Time histories for head acceleration, chest acceleration, chest compression, and occipital condyle moment are shown in Figures 85-88. Additional time history plots for the LODC seated in a backless BPB (Graco TurboBooster) and in no child restraint system are shown in Appendix D.

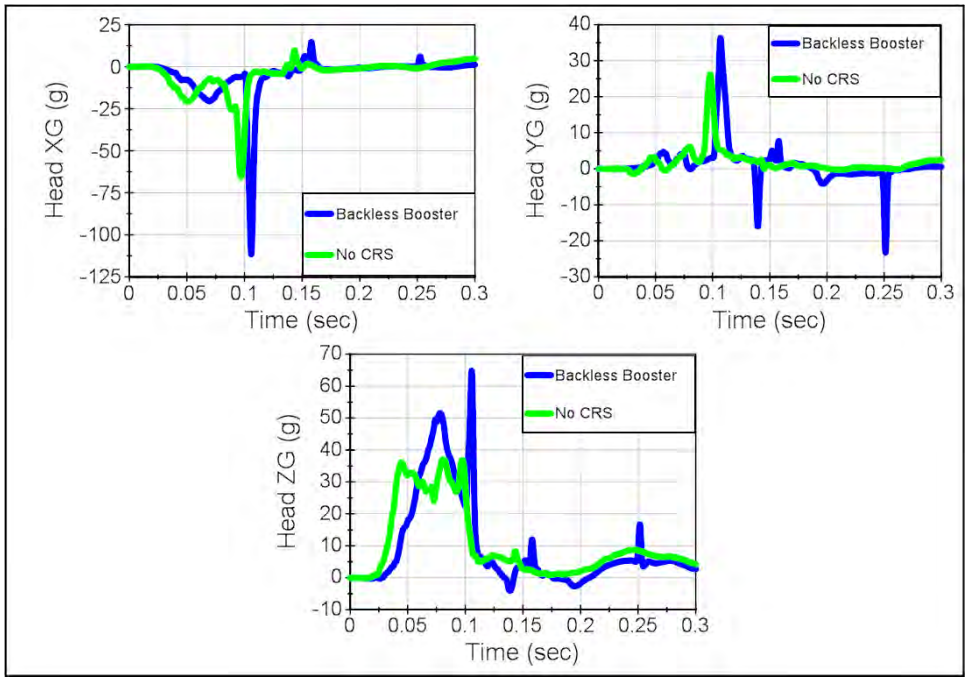

Figure 85. Head accelerations in the LODC using a backless booster seat and no CRS (48 km/h).

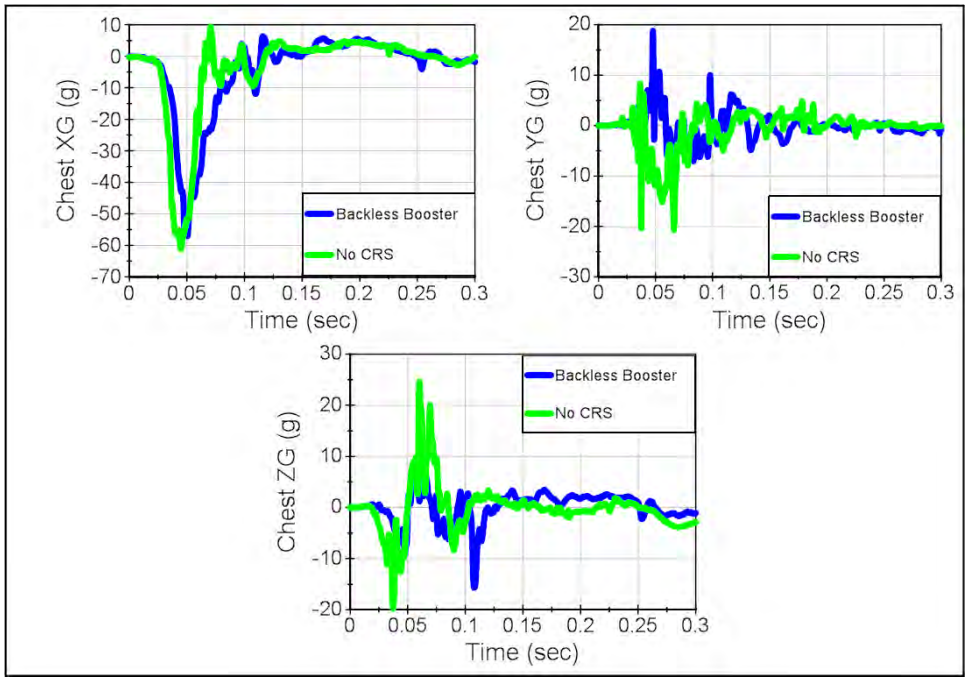

Figure 86. Chest accelerations in the LODC using a backless booster seat and no CRS (48 km/h).

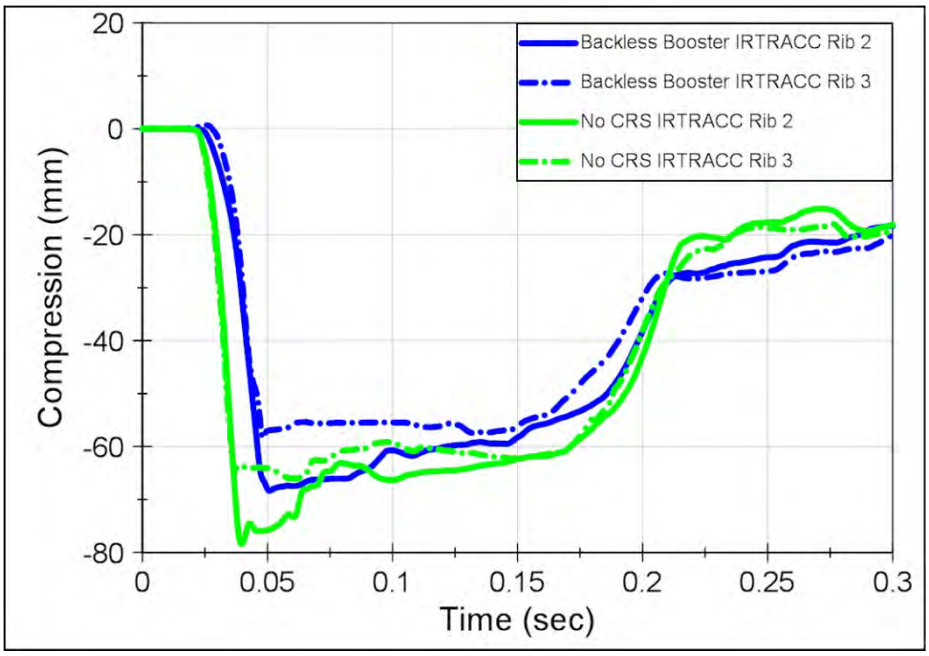

Figure 87. Chest compressions in the LODC using a backless booster seat and no CRS (48 km/h). A negative chest compression indicates that the sternum is moving towards the spine.

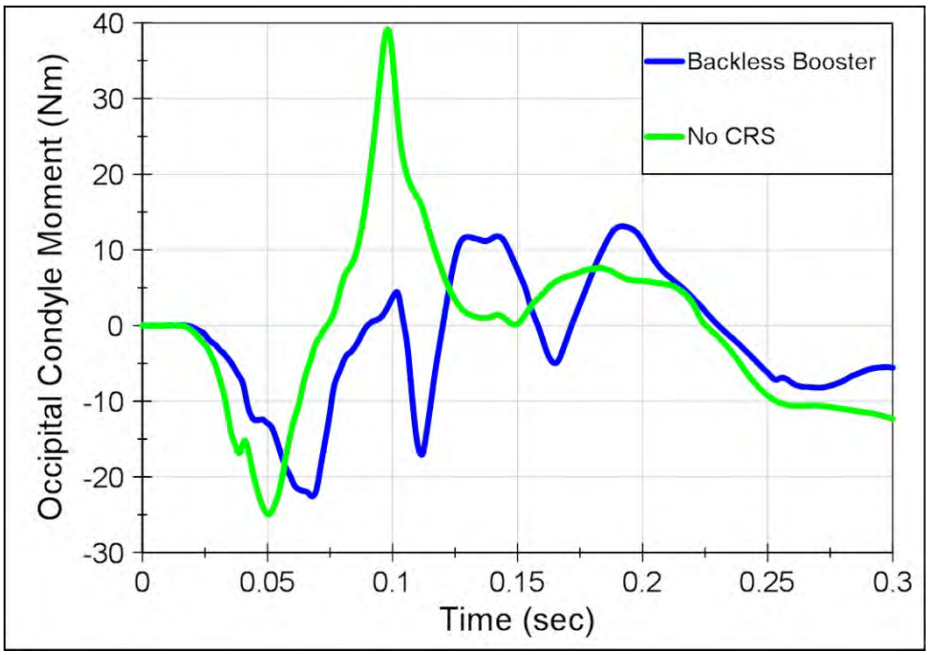

Figure 88. Occipital condyle moment in the LODC using a backless booster seat and no CRS (48 km/h).

Dummy kinematics were calculated for the head, neck (T1), mid-spine, and pelvis for the LODC using the corresponding accelerometers and angular rate sensors. The backless BPB condition is represented by the blue curves and the no child restraint condition is represented by the green curves in Figure 89 below. Video screen captures correspond to the data point markers shown in the plots. The LODC right shoulder became dislodged late in the event in the no CRS condition because of separation at both the scapula and clavicle causing the arm attachment to be overloaded (see section 3.6).

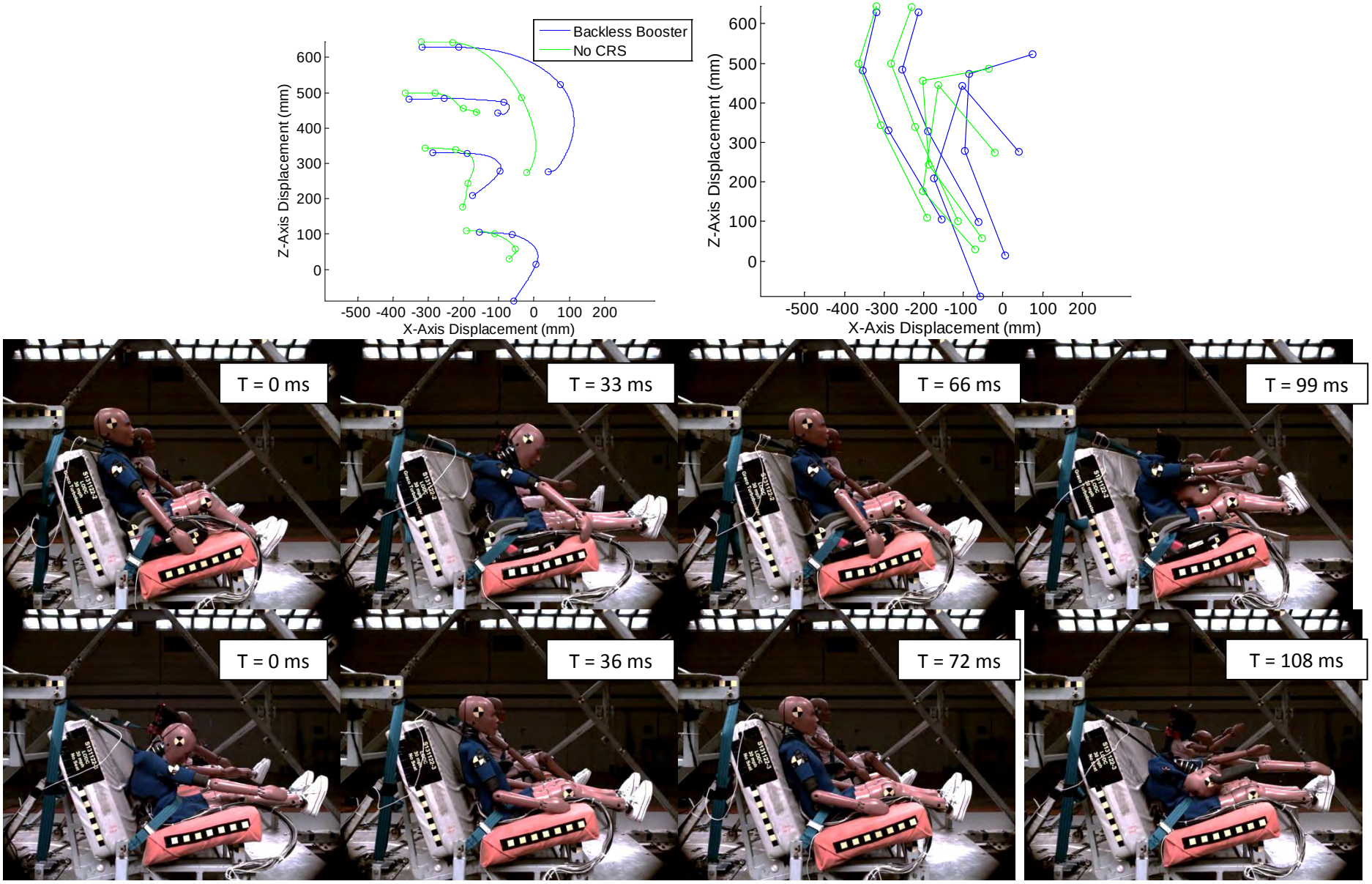

Figure 89. Kinematics of LODC in 48 km/h test with (top) backless booster and (bottom) no CRS

High-Speed Summary

HIC, chest g, and maximum values for head and knee excursion, head-spine trajectories, chest compression, occipital condyle moment, and belt loads are tabulated in Table 6 for the 5-point harness and high back booster conditions.

Table 6. Maximum value comparisons for the high-speed (48 km/h) tests.

Description		5-Point Harness		High Back Booster	
		HIII-10C	LODC	HIII-10C	LODC
HIC 36		439	439	536	651
Chest G		46.2	43.5	43.4	53.2
Head Excursion (mm)		604	639	538	588
Knee Excursion (mm)		867	861	723	694
Head Displacement (mm)	X	371	454	317	397
	Z	208	347	281	342
T1 Displacement (mm)	X	225	297	169	281
	Z*	102	51.3	195	63.7
Mid-Spine Displacement (mm)	X	222	228	164	174
	Z*	107	187	204	184
Chest Compression (mm)		-10.1	-23.8	-35.3	-61.9
Moment About Occipital Condyle (Nm)		-19.6 21.4	-16.8 8.64	-21.5 40.6	-20.9 21.4
Peak Belt Tension (N)	Lap	5245	5932	5513	5402
	Shoulder	4277	4768	6427	5569

For the 5-point harness and high back booster conditions, the LODC has greater head and spine forward displacements than the HIII-10C due to its more flexible spine (Figure 90).

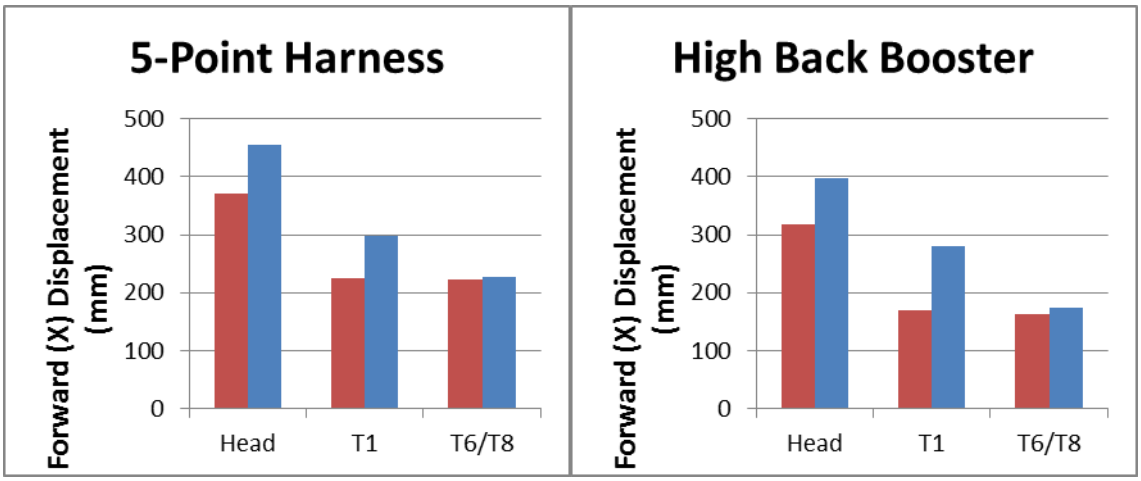

Figure 90. LODC (blue) and HIII-10C (red) head and spine displacements in various restraints (48 km/h)

The LODC exhibited higher chest compressions and lower upper neck moments (Figure 91), which again can be attributed to the softer thorax and a more flexible neck and spine, respectively. No big differences are observed, however, in knee excursion and chest acceleration.

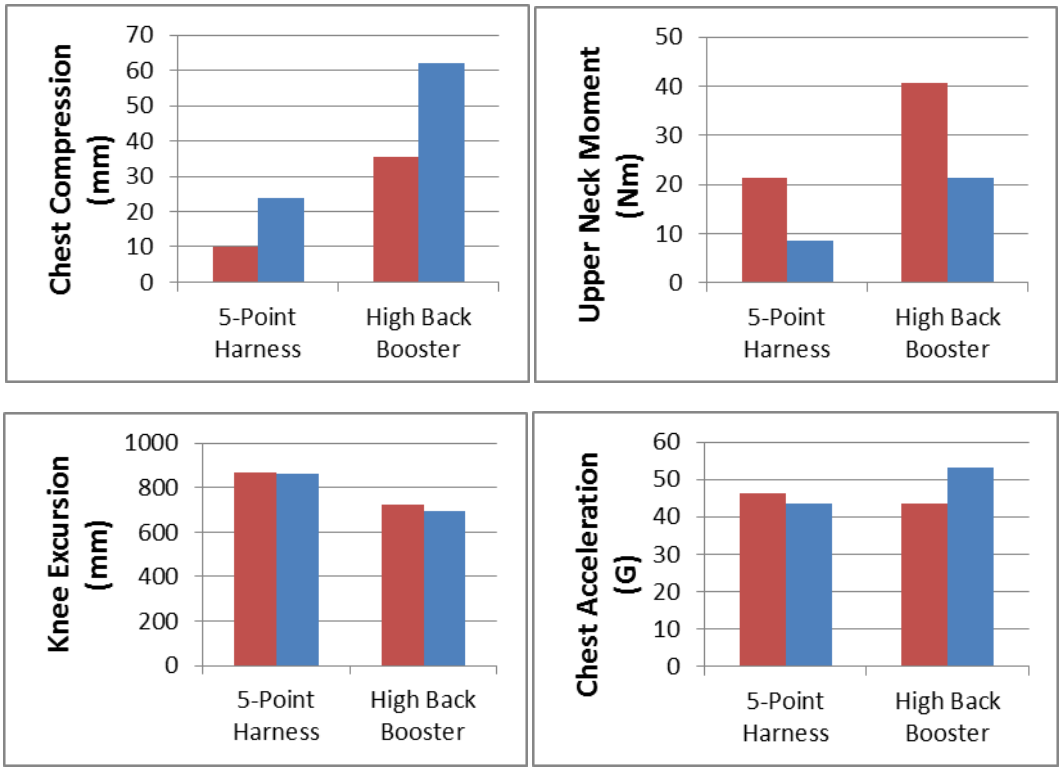

Figure 91. LODC (blue) and HIII-10C (red) chest/neck/knee peak values in various restraints (48 km/h)

Looking at HIC, it is observed that for the 5-point harness, the values are the same for the HIII-10C and LODC (Figure 92). This is very likely since hard chin-chest contact is not usually observed in 5-point harness cases. However, for the high back booster, a higher HIC is observed with the LODC. Looking at head excursions, the LODC is greater in both restraints, which can be attributed to the flexible spine. For both measures though, the observed values fall well below the injury reference limits of 1000 HIC and 813 mm of excursion.

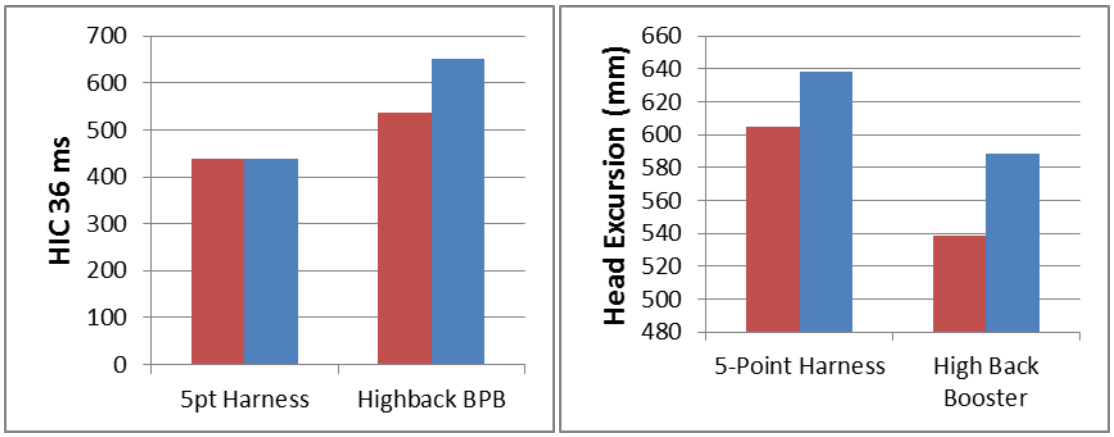

Figure 92. LODC (blue) and HIII-10C (red) HIC and head excursion in various restraints (48 km/h)

3.4. LODC Sensitivity to Restraint at 48 km/h

Key LODC measurements from the 48 km/h tests are tabulated and compared in Table 7 for all child restraint conditions.

Table 7. Maximum value comparisons for the LODC in high-speed (48 km/h) tests.

Description		5-Point Harness	High Back Booster	Backless Booster	No CRS
HIC 36		439	651	613	374
Chest G		43.5	53.2	51.2	58.6
Head Excursion (mm)		639	588	535	NA
Knee Excursion (mm)		861	694	669	668
Head Displacement (mm)	X	454	397	431	325
	Z	347	342	352	371
T1 Displacement (mm)	X	297	281	284	206
	Z*	51.3	63.7	43.0	56.2
Mid-Spine Displacement (mm)	X	228	174	194	137
	Z*	187	184	313	337
Chest Compression (mm)		-23.8	-61.9	-62.6	-71
Moment About Occipital Condyle (Nm)		-16.8 8.64	-20.9 21.4	-22.6 13.1	-24.9 39.1
Peak Belt Tension (N)	Lap	5932	5402	5565	5672
	Shoulder	4768	5569	5589	5780

The LODC exhibited the greatest amount of head and spine forward displacements in the 5-point harness case (Figure 93), likely because the large CRS mass is pulling everything forward. Conversely, the lowest forward displacements were in the no CRS case, which was likely a result of both the shoulder belt position being higher with respect to the dummy to restrict upper torso translation and separation of the right shoulder (Figure 89).

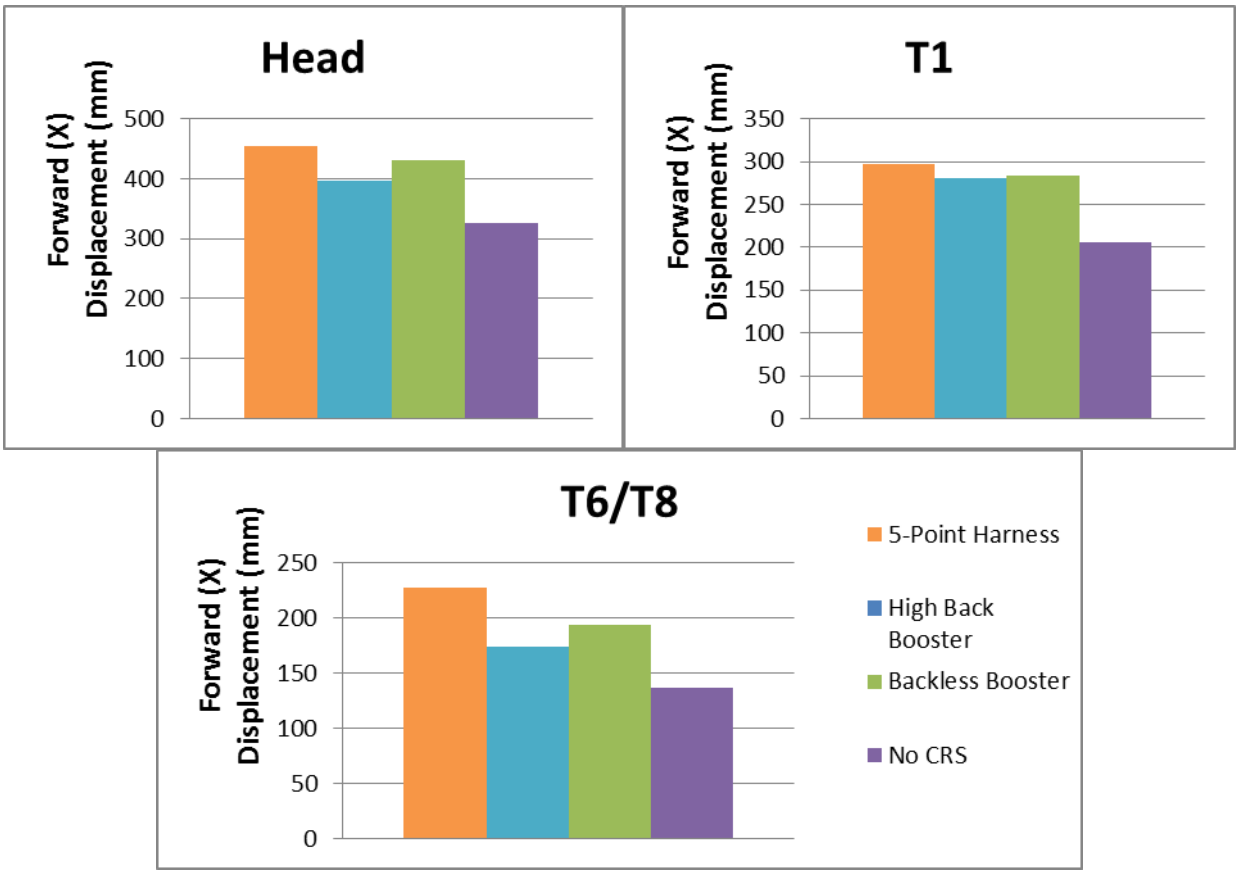

Figure 93. LODC head and spine displacements in various restraints (48 km/h).

HIC was highest in the case of the booster seats, due to head to upper leg contact late in the event, as described in Section 3.5 (Figure 94). The head excursion is greatest in the case of the 5 point harness, because the head and spine displacements are largest. This increase in head and spine displacement is a trade-off for less thoracic loading and lower upper neck loads, as shown in Figure 95. The 5 point harness case has by far the lowest chest acceleration, chest compression, and upper neck loads while the no CRS case has the highest of these values out of all the restraint conditions. Clearly, the 5 point harness is designed to distribute the overall loading of the thorax better than the vehicle belt alone. The greater absolute displacements of the head and spine are due in part to the mass of the booster and dummy combined in the case of the 5 point harness condition. The dummy and seat appear to move together over a larger distance without much thorax compression. Even though this distance is larger than the booster cases, the head excursions are still significantly lower than the FMVSS No. 213 criterion of 813 mm.

The highback and backless boosters provide a different type of protection according to the LODC measurements, by a more evenly distributed protection of the chest and neck, along with lower head/spine displacements to reduce the risk of contacts with the vehicle interior. The booster cases had more off-axis head displacement and reduced forward (x axis) displacement. The LODC appears to show that while both 5 point harness and booster provide benefit to the child occupant, they do so in different ways. The booster allows a slightly higher level of chest and upper neck loading but limits the risk of head contact with the vehicle interior, while the 5 point harness reduces the available occupant space but provides more protection to the chest and neck by efficiently distributing the load.

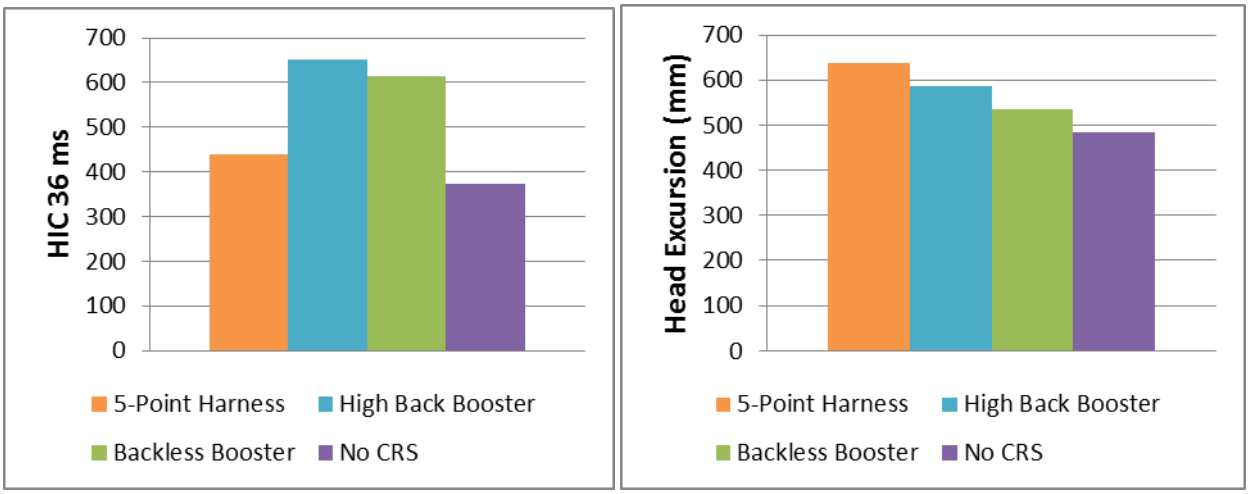

Figure 94. LODC HIC and head excursions in various restraints (48 km/h).

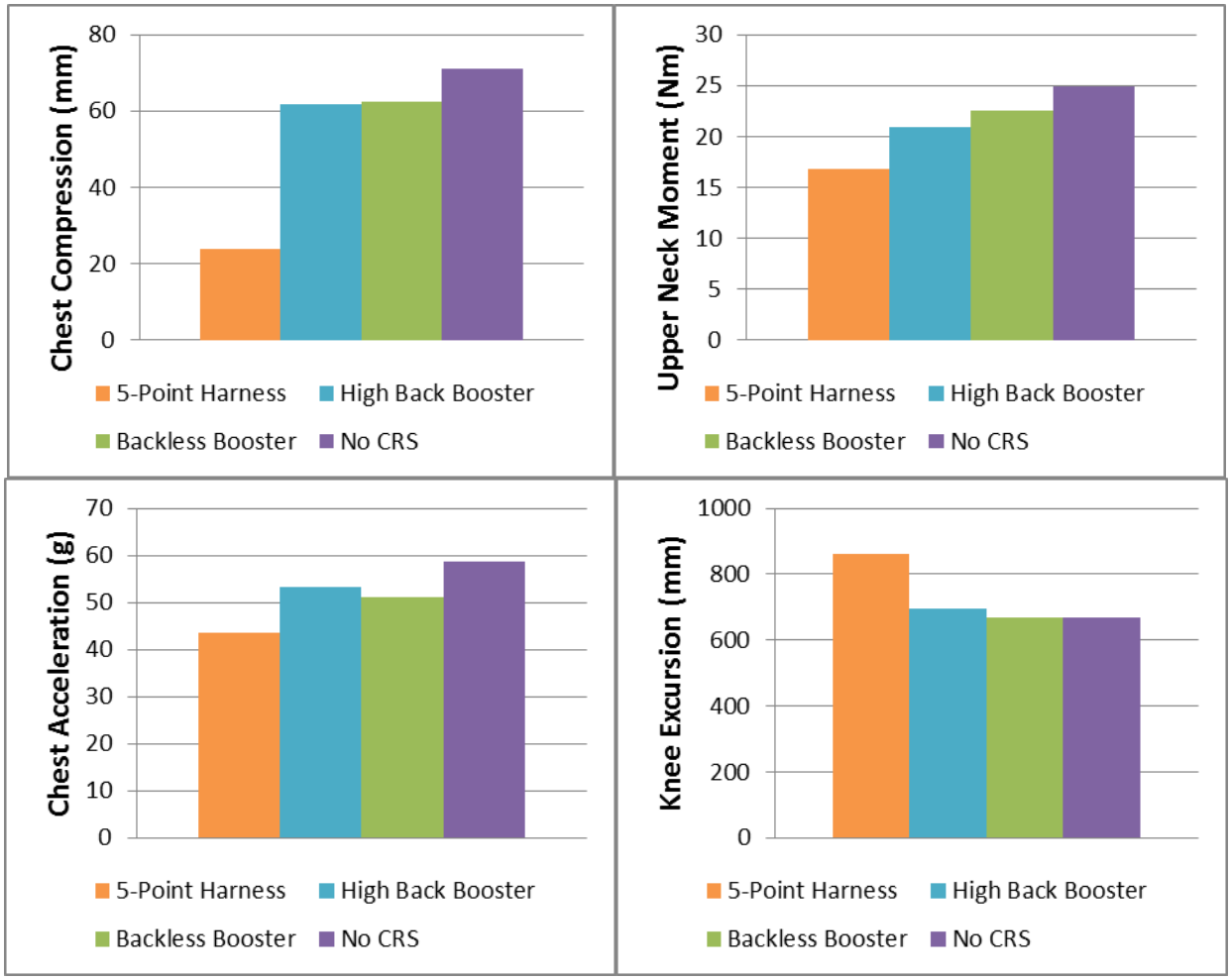

Figure 95. LODC chest/neck/knee peak values in various restraints (48 km/h).

3.5. HIC Analysis

Figure 96 shows head acceleration time histories in various restraints for the LODC and HIII-10C. The 5-point harness head accelerations appear to be very similar for both ATDs, which explains the similarity in HIC. There is no spike in the data in the 75 to 90 millisecond range, the typical range of chin-chest contact, for the 5-point harness case in either ATD. The high back booster head accelerations contain a spike for both ATDs. The spike occurs in the 75 to 90 millisecond range for the HIII-10C, but for the LODC, the spike occurs later in the event (90 to 110 ms).

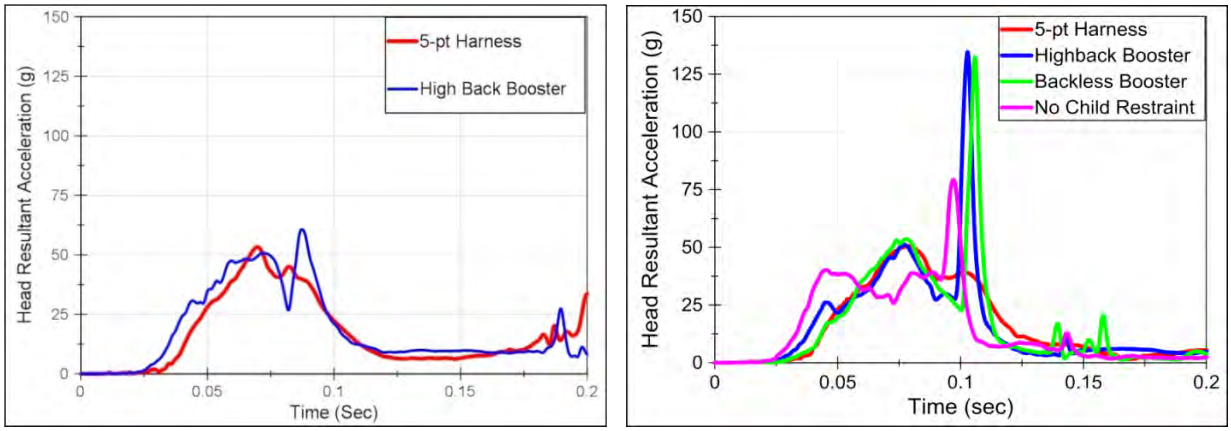

Figure 96. Head resultant acceleration versus time for (left) HIII-10C and (right) LODC at 48 km/h

It is known that the spike in the head acceleration for the HIII-10C is due to chin-chest contact. The spike in the LODC data is due to head to upper leg contact very late in the event. Figure 97 shows the LODC with the high back booster around the time of the LODC acceleration spike. The extreme downward motion of the head is likely due to a combination of a bi-modal thoracic spine response and a soft thorax reflecting a six-year-old stiffness. The bi-modal thoracic spine response is due in part to the T1 joint being very soft in bending - the neck itself does not bend significantly as the head moves downward.

Figure 97. Head-upper leg contact in LODC in highback BPB test (48 km/h)

In addition to differences in the thorax and thoracic spine, the component and low-speed tests appear to indicate that the shoulder may be too stiff. The combined effect of these discrepancies from human data targets result in too much upper torso flexion leading to excessive downward displacement in the LODC. There was no thoracic spine biofidelity target available at the time the LODC was designed and built. Therefore, the spine was designed to be tunable. The idea was to develop a spine that would

probably be more flexible than desired, and then it could be stiffened as needed depending on test results from this initial study. Using the results of these sled tests and a newly developed 10-year-old target, the LODC spine will be tuned and optimized, which should reduce the amount of upper torso bending and ultimately eliminate the head-leg contact that was observed in this test series.

The tests in this study indicate a correlation in HIC values between the LODC and HIII-10C, as shown below in Figure 98. It is likely that if the LODC were tested in the same conditions where the HIII-10C has exhibited artificially high HIC values, that the LODC would demonstrate more humanlike head accelerations than the HIII-10C. However, at this time, nothing can be definitively concluded about HIC until a wider range of test conditions can be evaluated with a revised LODC.

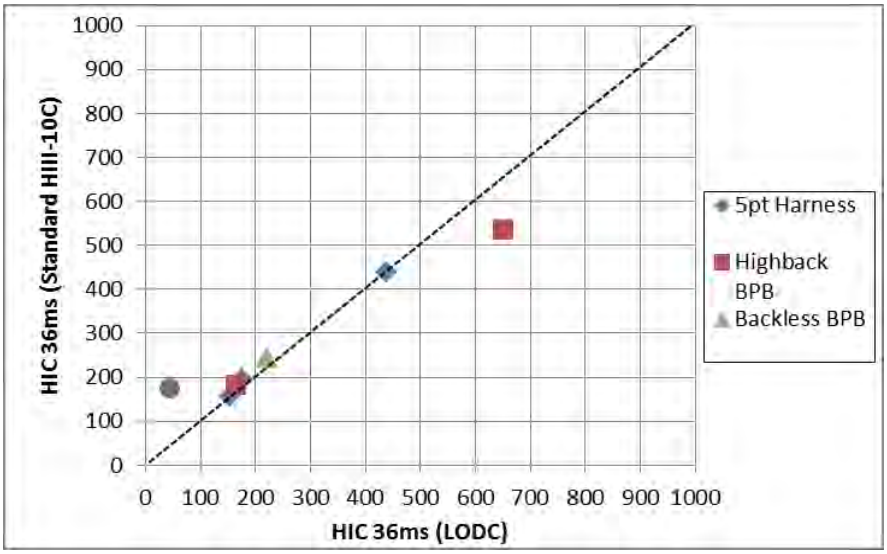

Figure 98. HIC correlation for LODC versus HIII-10C in same restraint conditions and pulse severities

In Table 8, the HIC values for the LODC were recalculated prior to head-leg contact. Originally, in the highback booster condition, the HIC was observed to be higher in the LODC than the HIII-10C. After recalculating, the HIC was reduced by 49 percent and is now lower than the HIII-10C. In the backless and no CRS conditions the HIC was also reduced by 30 percent and 36 percent, respectively. There was no reduction in HIC for the 5-point harness since head-leg contact was not observed in this restraint condition.

Table 8. Recalculated HIC prior to head-leg contact

CRS Type	HIC 36ms	HIC 36ms - Recalculated Prior to Head-Leg Contact	%Reduction
***5pt Harness**	439	--	--
Highback BPB	651	333	49%
Backless BPB	613	432	30%
No CRS	374	239	36%

*The 5pt Harness did not produce head-leg contact

3.6. Repeatability & Durability

Repeatability

In all component test conditions where repeat tests were conducted, the LODC displayed very good consistency in both overall time history response (Figures 35-41) and peak values. As described in Rhule, Rhule, and Donnelly (2005), NHTSA has assessed and categorized the repeatability of a regulatory test tool using percent coefficient of variance. To be classified as having "excellent" repeatability, the %CV value must be less than or equal to 5. For "good" and "marginal" repeatability, the %CV values must fall within $5 < \%CV \leq 8$ or $8 < \%CV \leq 10$, respectively. To be classified as having "poor" repeatability, the %CV must be greater than 10. Table 8 shows the consistency of LODC peak responses in repeated component tests. A majority of the %CV values were below 6 percent, indicating that the LODC has excellent to good repeatability. This will be an important consideration to monitor as the LODC prototype evolves. A more thorough and statistical analysis of repeatability will be conducted with the revised LODC.

Table 9. Repeatability Analysis

Test	Measurement	n	Peak Mean	Peak Standard Deviation	CV
Frontal Thorax	**Rib 2 X-Compression (mm)**	3	53.1	0.25	0.5%
	Rib 3 X-Compression (mm)		55.5	0.88	1.6%
	Pendulum Force (N)		1442	24.9	1.7%
Abdomen	**Penetration (mm)**	4	148	8.45	5.7%
	Belt Force (N)		2829	141	5.0%
Neck Flexion	**Head Rotation (Deg)**	3	96.2	2.34	2.4%
	Occipital Condyle Moment (Nm)		38.6	0.82	2.1%
Neck Extension	**Head Rotation (Deg)**	3	122	1.01	0.8%
	Occipital Condyle Moment (Nm)		25.6	0.32	1.3%
Thoracic Spine (3.8 m/s)	**T6 Force (N)**	3	1419	21.4	1.5%
	T1 X Displacement (mm)		77.5	3.20	4.1%
Thoracic Spine (5.0 m/s)*	**T6 Force (N)**	3	2262	136	6.0%
	T1 X Displacement (mm)		91.6	11.90	13.0%

*A tear in a spine rubber element was observed in one of the tests at this-speed which degraded the repeatability. See Figure 99b.

Durability

Component Testing

A couple of durability issues were observed during component testing. Several of the rubber elements within the LODC were showing signs of degradation (Figure 99). In addition, one of the spine rubber elements tore in the last high-speed (5.0 m/s) thoracic spine sled test, likely because the spine was immobilized there, which created a high load to be experienced by this closest rubber element.

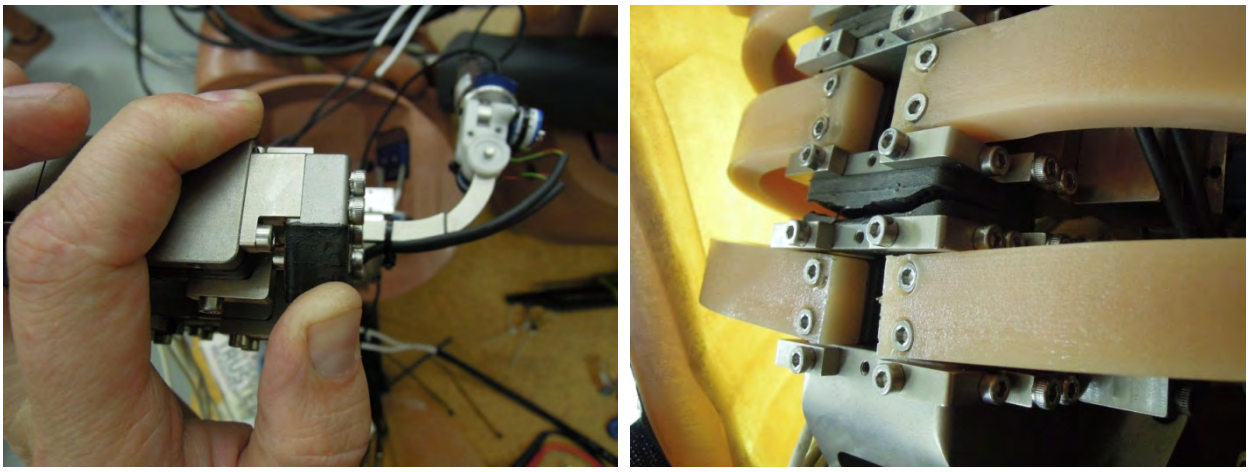

(a) (b)

Figure 99. (a) Degradation of rubber elements and (b) a spine element tear from thoracic spine testing

Sled Testing

Some durability issues also arose during sled testing. Each scapula is attached to the flexible spine at the rear by four elements. These elements are a series of plastic, rubber, and metal pieces. The plastic portion allows attachment to the scapula, the rubber portion allows for flexibility, and the metal portion is attached to the spine. During the sled tests, the weak plastic-rubber bond broke, allowing the scapula to separate from the spine (Figure 100). Because the thoracic spine can deform in multiple directions, these scapula attachments experience combined loading. In order to combat this issue, zip-ties were used to temporarily reinforce the scapula-spine attachment after replacing the rubber elements.

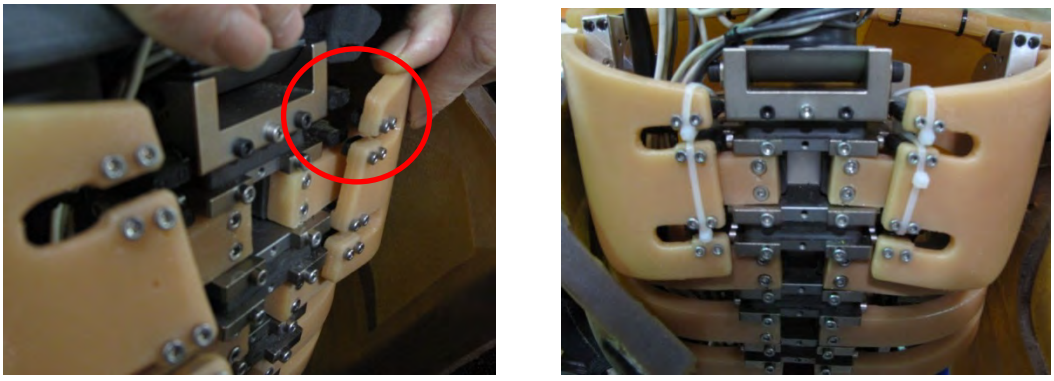

Figure 100. Separation of scapula from spine and reinforcement after replacing the rubber elements

Other structural durability issues that were observed included a tearing of the clavicle-sternum attachment (Figure 101a) and a loosening of the sternum within the bib material simulating rib cartilage (Figure 101b).

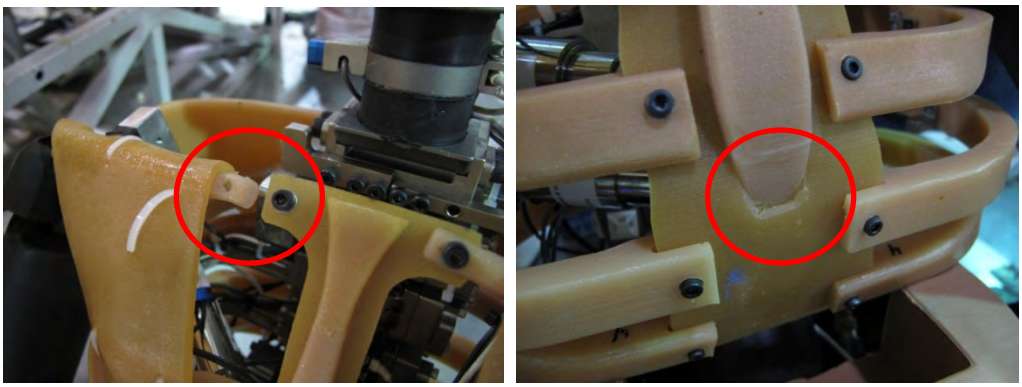

(a) (b)

Figure 101. (a) Separation of clavicle from sternum and (b) sternum embedded into rib cartilage

In the 48 km/h no CRS test, the LODC right arm dislodged from the shoulder structure (see Figure 84). This was due to both the scapula (Figure 100) and clavicle (Figure 101a) separating from the ATD. This condition overloaded the upper arm attachment to the shoulder structure and caused the two small screws to shear off (Figure 102).

Figure 102. Separation of upper arm from shoulder structure

Lastly, during one of the sled tests, an IR-TRACC rotary potentiometer was damaged when its wire got caught on a rib during a test. The potentiometer was re-wired between tests, but this damage can be easily prevented in the future with the addition of a protective sheath.

All damaged parts were easily fixed as the LODC is made up of multiple subassemblies. The spine consists of multiple vertebral bodies that can be replaced if damaged. The ribcage consists of a set of individual left and right thoracic ribs, each with their own, separate attachment to the spine and sternum. The left and right shoulder girdle consists of a separate scapula, clavicle, and shoulder joint, also with their own sets of attachments to the spine, sternum, and shoulder girdle. Therefore, if a structure or attachment point were to undergo any sort of damage during a test, parts and pieces can be easily replaced.

Modifications are currently being made to the LODC to eliminate the structural issues observed in this series of tests and also refine the overall response of the dummy to better reflect pediatric data targets. Testing on the next version of the LODC will begin in summer 2014.

3.7. Considerations for Lateral/Oblique Biofidelity

While the primary focus of this evaluation was on the assessment of the LODC thorax for use in FMVSS No. 213 frontal conditions, the LODC was also designed to have lateral biofidelity so that it could potentially be used in lateral test scenarios as well. In lateral shoulder and thorax tests, the LODC was shown to conform to ISO lateral biofidelity requirements for a 10-year-old ATD (see Figures 37-39). As the LODC design is improved to better match frontal biofidelity requirements, it may possibly degrade lateral biofidelity. Therefore, as the design evolves, lateral and oblique impact scenarios will continue to be conducted to monitor the effects of frontal-based upgrades on lateral biofidelity.

An omnidirectional neck design is currently under development to improve upon the neck biofidelity in not only frontal conditions but also lateral and torsion scenarios. With the majority of the durability issues occurring in the shoulder area and the importance of the shoulder for both belt interaction and impact in non-frontal applications, improvements to the shoulder design will likely have an effect on its response in multiple loading directions. Given the lack of direct pediatric shoulder data, shoulder range of motion as well as additional scaled lateral/oblique shoulder data scenarios may be necessary to evaluate as the LODC evolves. The abdomen and pelvis will also likely undergo some changes to address the interaction between the inferior ribcage and superior abdomen surfaces, a condition shown to affect chest compression in this study (see Figures 54 and 77). The lateral response of the pelvis may need to be revised if the dummy is used in lateral crash scenarios. In addition, while the LODC abdomen was shown to be biofidelic in the frontal belt loading condition, its geometry may need to be streamlined to fit better with the thorax.

4. Conclusions

A new 10-year-old size thorax, referred to as the large omnidirectional child (LODC), has been developed by the NHTSA VRTC to improve the overall response of the Hybrid III 10-year-old ATD (HIII-10C). In this study, the LODC was compared to both the HIII-10C and pediatric data in component and sled tests.

- The LODC displayed improved biofidelity over the HIII-10C in component and low-speed sled test conditions:
    - In frontal thorax testing, the LODC met a 6 year old-based pediatric response corridor that it was designed to represent.
    - In lateral thorax and shoulder tests, the LODC met scaled 10-year-old response requirements, which is encouraging for testing where oblique loading is present.
    - In quasi-static posteromedial shoulder compressions, the LODC was significantly more stiff than pediatric volunteers but considerably softer than the HIII-10C.
    - In abdomen belt pull tests, the LODC met the pediatric corridor.
    - The LODC thoracic spine was stiffer than the scaled human biofidelity target data (10 year old), but appeared to approach the human data at higher test-speeds.
    - In neck tests, the LODC peak moment was closer to pediatric data in flexion than the HIII-10C. In extension, the LODC rotation was increased from the HIII-10C due to the soft T1 joint. The overall response will be improved by a new omnidirectional neck design.
    - The response of the LODC in repeated testing was very consistent.
    - In low-speed testing, the LODC was closer to the pediatric volunteer response than the HIII-10C, but still too stiff. The high shoulder belt forces reflect the difference in shoulder stiffness between the LODC and volunteer data in the quasi-static compression tests. The greater downward displacement component in the LODC may indicate the effect of active neck musculature in the volunteers.

- In medium and high-speed sled tests, the LODC displayed higher head/spine displacements, chest compressions, and head excursions but lower neck loads than the HIII-10C. The LODC was sensitive to restraint condition, with its measurements identifying differences in protection strategies between a 5 point harness and booster seat.

- There was correlation in HIC for the LODC and HIII-10C in the same restraint condition/pulse combination, but only a small set of the CRS fleet was tested, which did not include seats known to produce high HIC values in the HIII-10C. However, it is likely that if the LODC were tested in the same conditions where the HIII-10C has exhibited artificially high HIC values, that the LODC would demonstrate more humanlike head accelerations than the HIII-10C. However, at this time, nothing can be definitively concluded about HIC until a wider range of test conditions can be evaluated with a revised LODC.

- The combined effects of a stiff shoulder, soft thorax, and soft thoracic spine resulted in the LODC head contacting the upper leg in some tests. Addressing these individual body components in the next version of the LODC while improving the durability of the shoulder connection to the thorax should result in improved kinematics.

In summary, the LODC shows promise as a potential enhancement to the HIII-10C. Testing beginning in summer 2014 on a revised and improved LODC will include: testing the revised LODC and HIII-10C in conditions known to produce high HIC values in the HIII-10C; a quantitative biofidelity assessment to prove that the LODC is more humanlike; a thorough repeatability and reproducibility assessment; FMVSS No. 213-type testing on a larger range of child restraints that are currently on the market in order to assess the fleet and to explore IARV efficacy; testing of the revised LODC in rear seat crash tests; testing on the same sled as pediatric volunteers; and comparing the revised LODC to the Q10 dummy that is under development in Europe.

5. References

1. 49 CFR Part 571, FMVSS No. 213 Final Rule.

2. CFR 49 Part 572, Anthropomorphic Test Devices.

3. 76 FR 55825 under 49 CFR 571, Agency Docket No. NHTSA-2011-0139, RIN 2127-AJ44, Docket No. 2011-23047, available at https://federalregister.gov/a/2011-23047

4. Irwin, A. L., Mertz, H. J., Elhagediab, A. M., & Moss, S. (2002). Guidelines for assessing the biofidelity of side impact dummies of various sizes and ages. *Stapp Car Crash Journal, 46*; 297-319.

5. Parent, D. P., Crandall, J. R., Bolton, J. R., Bass, C. R., Ouyang, J., & Lau, S. H. (2010, August). Comparison of Hybrid III child test dummies to pediatric PMHS in blunt thoracic impact response. *Traffic Injury Prevention;11*(4):399-410. doi: 10.1080/15389588.2010.486430.

6. Suntay, B., Moorhouse, K., & Bolte IV, J. (2011), Characterization of the pediatric shoulder's resistance to lateral loading . In: *Proccedings of the 22nd International Technical Conference on the Enhanced Safety of Vehicles*, June 13-16, Washington, DC. Available at www-esv.nhtsa.dot.gov/Proceedings/22/files/22ESV-000038.pdf

7. Kent, R., Stacey, S., Mattice, J., Kindig, M., Forman, J., Woods, W. J. & Evans, J. (2006). Assessment of abdominal injury criteria for use with pediatric seatbelt loading. In: *Proceedings of the 5th World Congress of Biomechanics*, Munich, Germany, July 29-August 4, 2006.

8. Kent, R. W., Lopez-Valdes, F. J., Lamp, J., Lau, S. H., Parent, D. P., Kerrigan, J. R., Lessley, D. J., & Salzar, R. S.. (2011), Characterization of the pediatric chest and abdomen using three post-mortem human subjects. (Paper Number 11-0394). In: *Proceedings of the 22nd International Conference on the Enhanced Safety of Vehicles*, Washington, DC, June 13-16, 2011.

9. Stammen, J. A., Herriott, R., Kang, Y.-S., Bolte, J., & Dupaix, R. (2012, October), Sequential biomechanics of the human upper thoracic spine and pectoral girdle. *Ann Adv Automot Med. 56*:151-62.

10. Stammen, J. A., Herriott, R., Kang, Y.-S., Dupaix, R., & Bolte, J. (2012, Octob er 1), Dynamic properties of the upper thoracic spine-pectoral girdle (UTS-PG) system and corresponding kinematics in PMHS sled tests. (Paper presented at 56th Stapp Car Crash Conference, Savannah, GA, October 29-31, 2012). In: *Stapp Car Crash Journal, 56*:65-104.

11. Stammen, J. A., Donnelly, B. R., Suntay, B., & Moorhouse, K. M. (2014), Dynamic response criteria for a large child ATD thoracic spine. (Report No. IRC-14-36). In: *2014 IRCOBI Conference Proceedings*, September 10-12, 2014, Berlin.

12. Donnelly, B., Moorhouse, K., Stammen, J., & Rhule H. (2013). A methodology for creating PMHS targets with a two-dimensional standard deviation ellipse tolerance for quantitatively assessing dummy biofidelity. (Report No. IRC-13-102). In: *2013 IRCOBI Conference Proceedings*, September 11-13, 2013, Gothenburg, Sweden.

13. Donnelly, B. R., Moorhouse, K. M., Rhule, H. H., & Stammen, J. A.. (2014). A deformation energy approach to normalizing PMHS response data and developing biofidelity targets for dummy design. (Report No. IRC-14-37). In: *2014 IRCOBI Conference Proceedings*, September 10-12, 2014, Berlin.

14. Lopez-Valdes, F. J., Seacrist, T., Balasubramanian, S., Maltese, M. R., Arbogast, K. B., Tanji, H., & Kent, R. (2011) Comparing the kinematics of the head and spine between volunteers and PMHS: A methodology to estimate the kinematics of pediatric occupants in a frontal impact. In: *2014 IRCOBI Conference Proceedings*, September 14-16, 2011, Krakow, Poland.

15. Arbogast, K. B., Balasubramanian, S., Seacrist, T., Maltese, M. R., García-España, J. F., Hopely, T., & Higuchi, K. (2009, November) Comparison of the kinematic responses of the head and spine for children and adults in low-speed frontal sled tests. *Stapp Car Crash Journal, 53*:329-72.

16. Shaw, J. M., Herriott, R. G., McFadden, J. D., Donnelly, B. R., & Bolte 4th, J.H. (2006, November), Oblique and lateral impact response of the PMHS thorax. *Stapp Car Crash Journal, 50*:147-67.

17. Dibb, A. T., Cutcliffe, H. C., Luck, J. F., Cox, C. A.,Myers, B. S., Bass, C. R., & Nightingale, R. W. (2013). Pediatric head and neck dynamics in frontal impact: analysis of important mechanical factors and proposed neck performance corridors for 6- and 10- year-old ATDs. *Traffic Inj Prev;15(4)*:386-94. Also in: *Proceedings of the 23rd International Technical Conference on the Enhanced Safety of Vehicles*, Seoul, Republic of Korea, May 27-30, 2013, Paper Number 13-0207.

18. Maltese, M. R., Arbogast, K. B., Nadkarni, V., Berg, R., Balasubramanian, S., Seacrist, T., & Ridella, S. A. (2010). Incorporation of CPR data into ATD chest impact response requirements. *Annals of Advances in Automotive Medicine (AAAM) 54: 79-88.*

19. Ouyang, J., Zhao, W., Xu, Y., Chen, W., & Zhong, S. (2006, December). Thoracic impact testing of pediatric cadaveric subjects. *Journal of Trauma, 61*:6 pg 1492-500.

20. Irwin, A. L., & Mertz, H. J. (1997). Biomechanical bases for the CRABI and HIII-10C child dummies. (SAE Technical Paper 973317). In: *Proceedings, 41st Stapp Car Crash Conference.* Warrendale, PA: Society of Automotive Engineers.

21. Lopez-Valdes, F. J., Lau, A. G., Lamp, J., Riley, P.O., Lessley, D.J., Damon, A.M., & Tanji, H. (2010). Analysis of spinal motion during frontal impacts. Comparison between PMHS and ATD. *Annals of Advances in Automotive Medicine, 54*: 61-78.

22. Hardy, W. N., Schneider, L. W., & Rouhana, S. W. (2001) Abdominal impact response to rigid-bar, seatbelt, and airbag loading. (SAE Technical Paper 973317). In: *Proceedings, 41st Stapp Car Crash Conference.* Warrendale, PA: Society of Automotive Engineers. Also in: *Stapp Car Crash Journal; 45*:1-32.

23. Reed, M. P., Ebert-Hamilton, S. M., Klinich, K. D., Manary, M. A., & Rupp, J. D. (2008, September). *Assessing child belt fit, Volume I: Effects of vehicle seat and belt geometry on belt fit for children with and without belt positioning booster seats*. (Report No. UMTRI-2008-49-1). Washington, DC: National Highway Traffic Safety Administration. Available at http://mreed.umtri.umich.edu/mreed/pubs/UMTRI-2008-49-1.pdf

24. Rhule, D., Rhule, H., & Donnelly, B.,. (2005, June). The process of evaluation and documentation of crash test dummies for Part 572 of the Code of Federal Regulations. (Paper No. 05-0284). In: *Proceedings of the 19th International Technical Conference on the Enhanced Safety of Vehicles.* Washington, DC: National Highway Traffic Safety Administration.

25. Reed, M. P., Ebert, S. M., & Rupp, J. D. (2010). *Pediatric thoracic and shoulder skeletal geometry*. (UMTRI Technical Report 2010–40). Ann Arbor, MI: University of Michigan Transportation Research Institute.

Appendix A: Low-Speed Time History Data

Time history comparisons of head, mid-spine, and pelvis accelerations and angular rates; upper neck and lumbar forces and moments; iliac and seatbelt forces; and chest compressions for the LODC and HIII-10C dummies seated without a child restraint system are shown in Figures 103-141 below. The LODC time histories are represented by the blue curves. The HIII-10C time histories are represented by the red curves.

Test 1

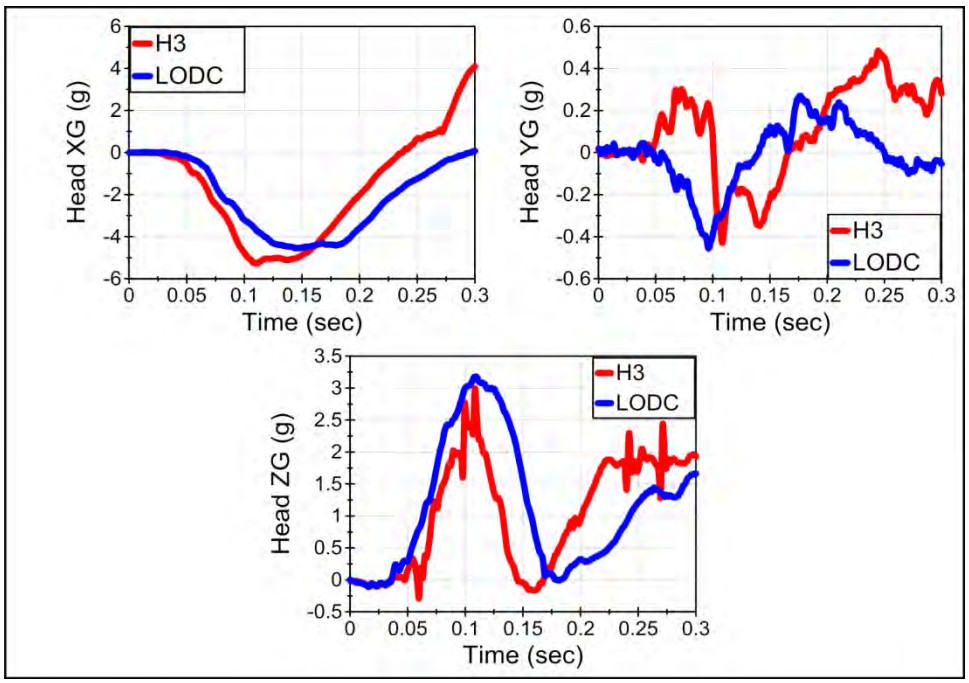

Figure 103. Head accelerations in the LODC and HIII-10C in low-speed bumper car pulse (Test 1).

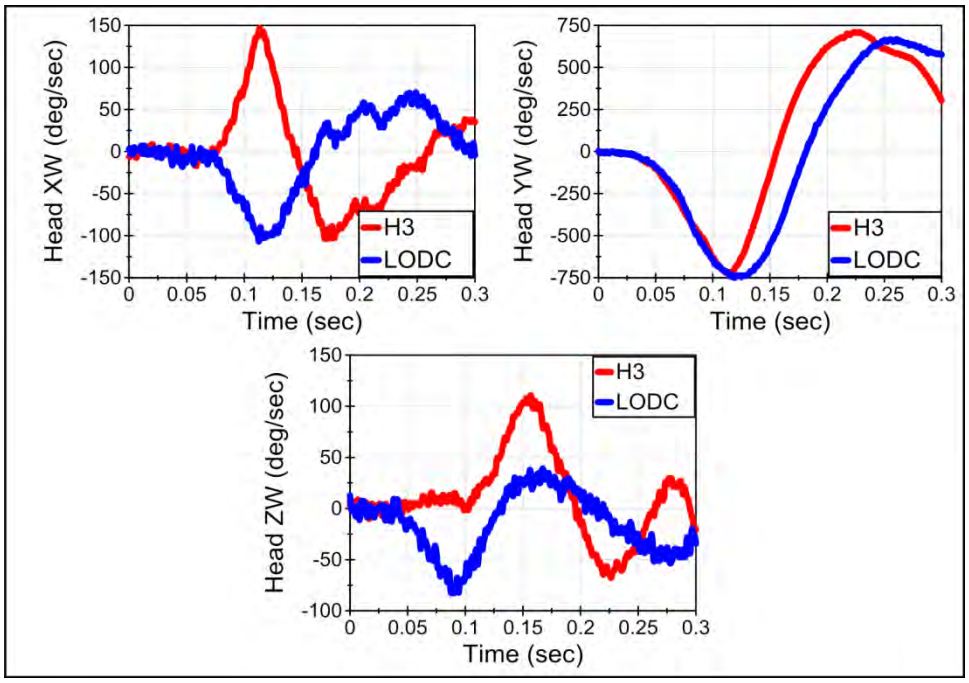

Figure 104. Head angular rates in the LODC and HIII-10C under the low-speed bumper car pulse (Test 1).

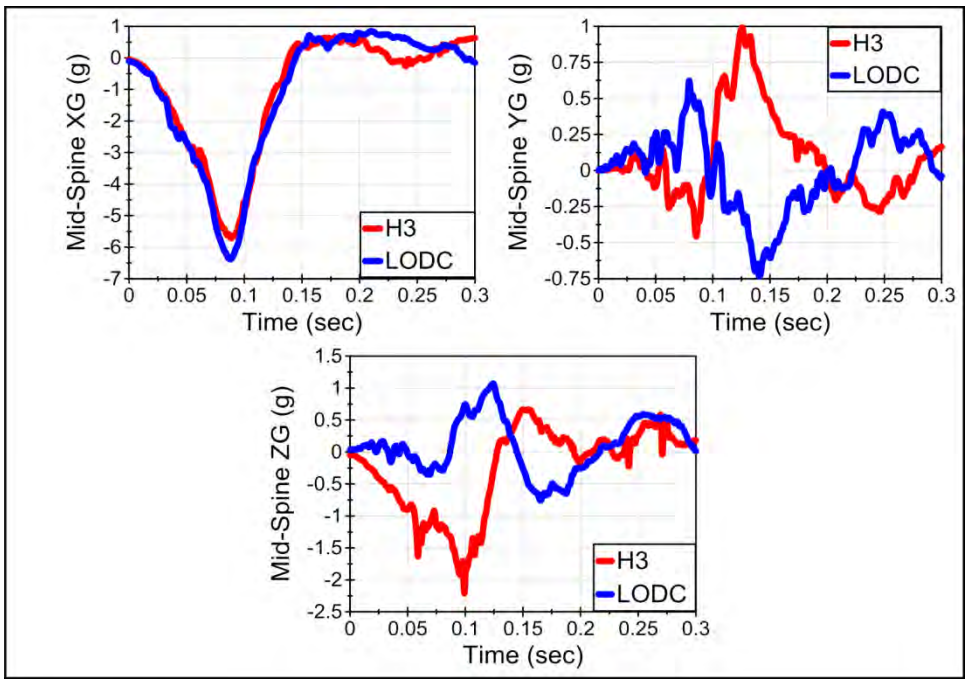

Figure 105. Mid-spine accelerations in the LODC and HIII-10C under the low-speed bumper car pulse (Test 1).

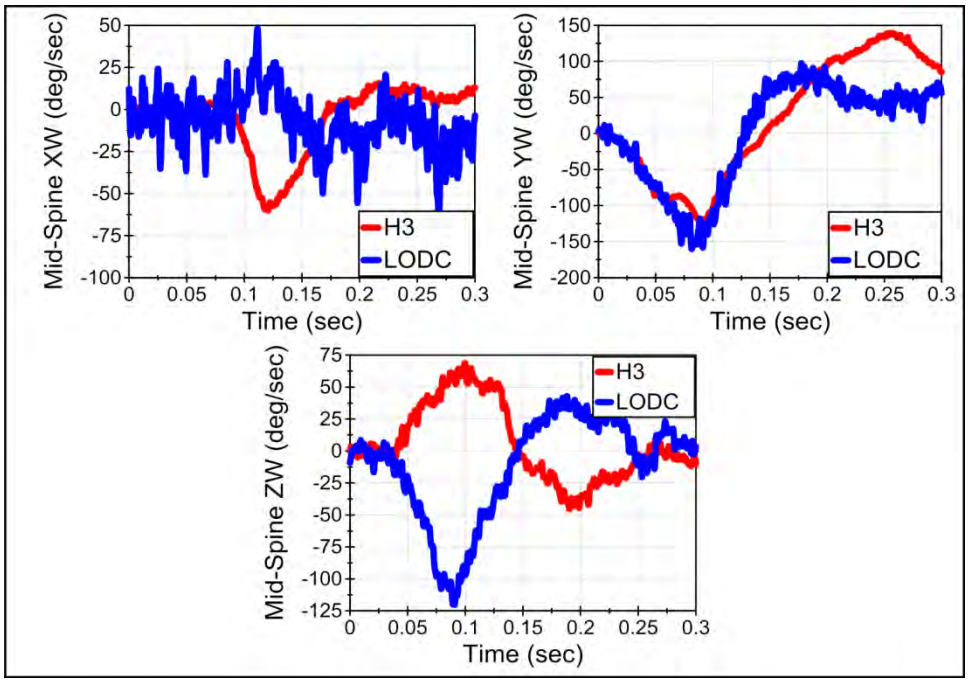

Figure 106. Mid-spine angular rates in the LODC and HIII-10C under the low-speed bumper car pulse (Test 1).

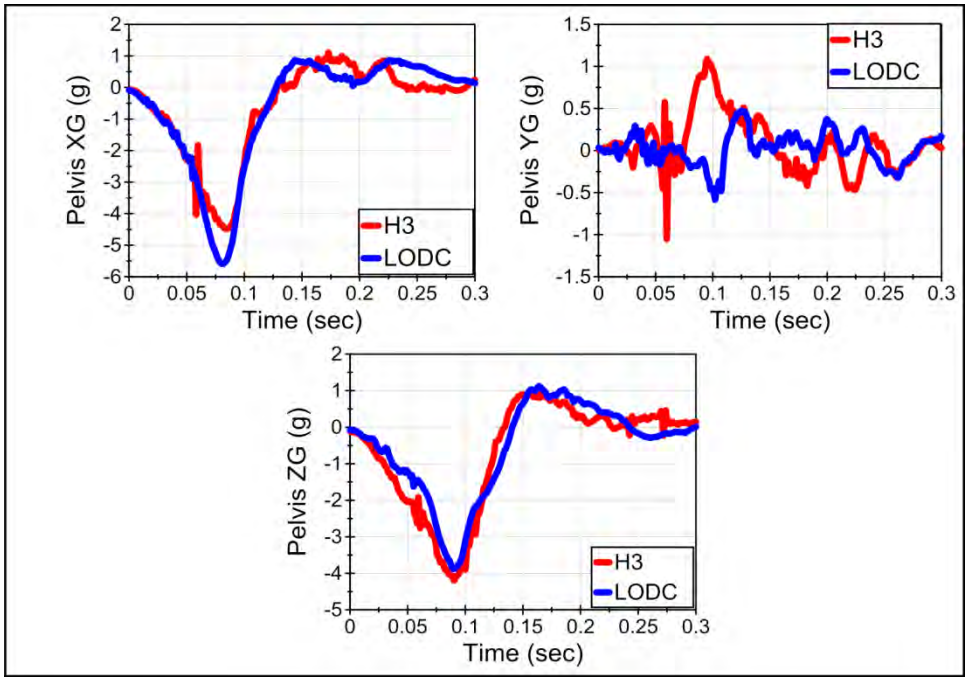

Figure 107. Pelvis accelerations in the LODC and HIII-10C under the low-speed bumper car pulse (Test 1).

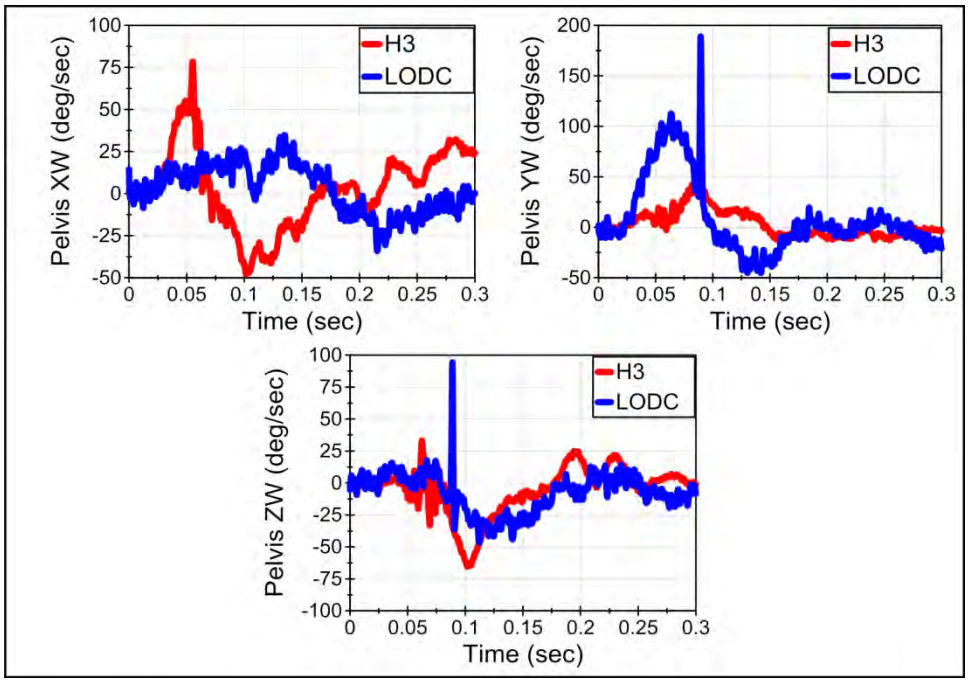

Figure 108. Pelvis angular rates in the LODC and HIII-10C under the low-speed bumper car pulse (Test 1).

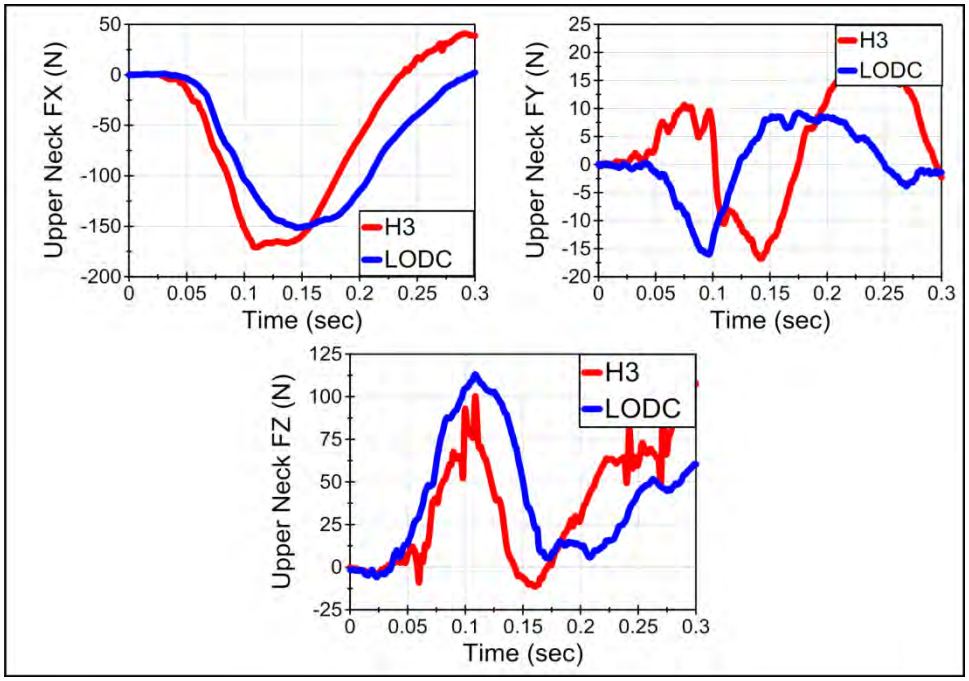

Figure 109. Upper neck forces in the LODC and HIII-10C under the low-speed bumper car pulse (Test 1).

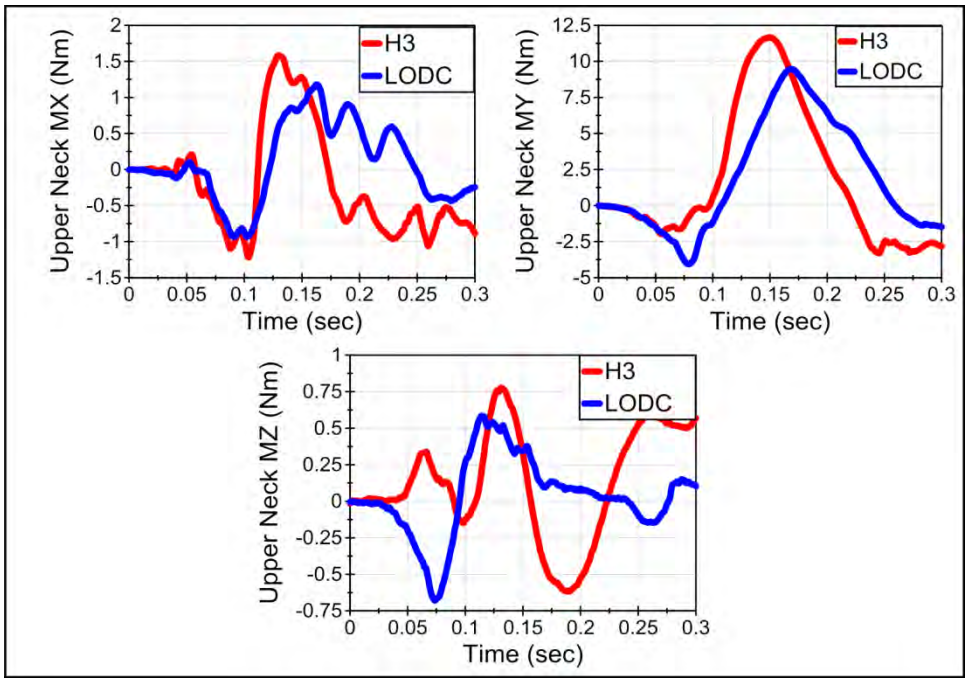

Figure 110. Upper neck moments in the LODC and HIII-10C under the low-speed bumper car pulse (Test 1).

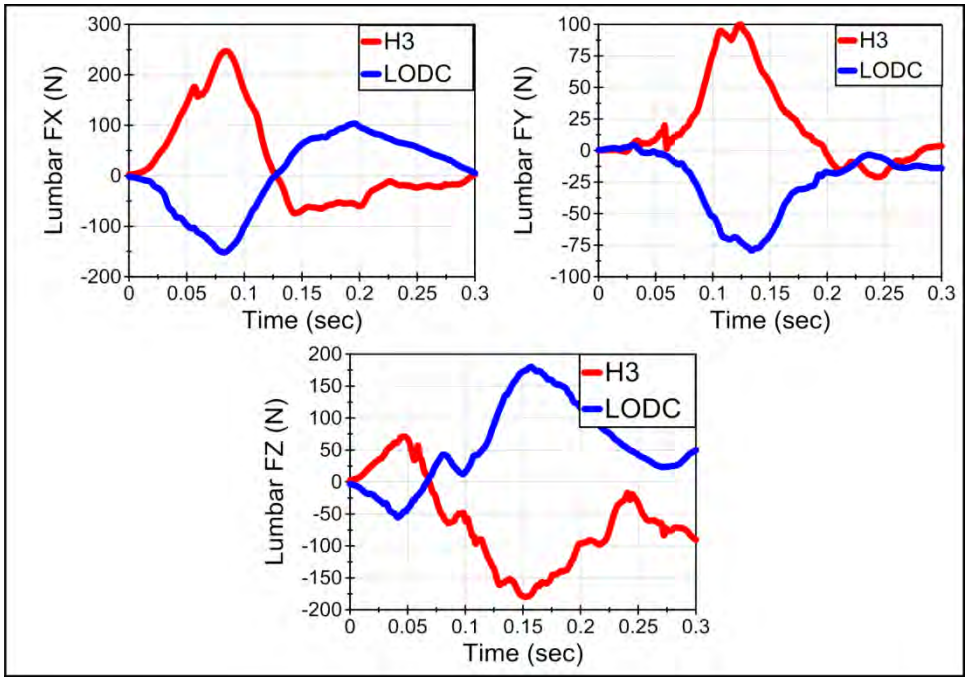

Figure 111. Lumbar forces in the LODC and HIII-10C under the low-speed bumper car pulse (Test 1).

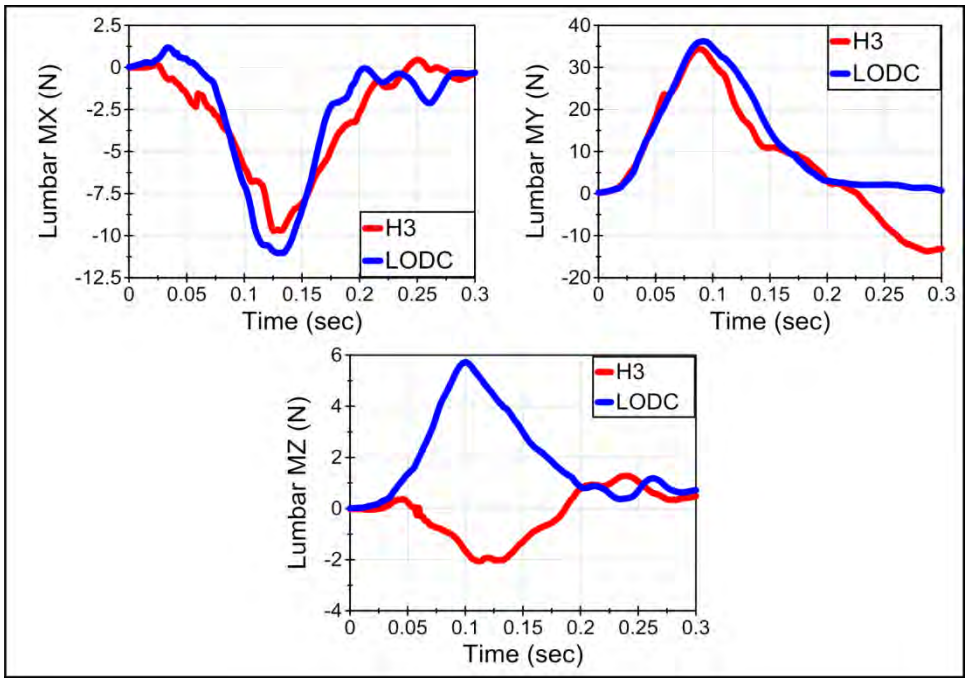

Figure 112. Lumbar moments in the LODC and HIII-10C under the low-speed bumper car pulse (Test 1).

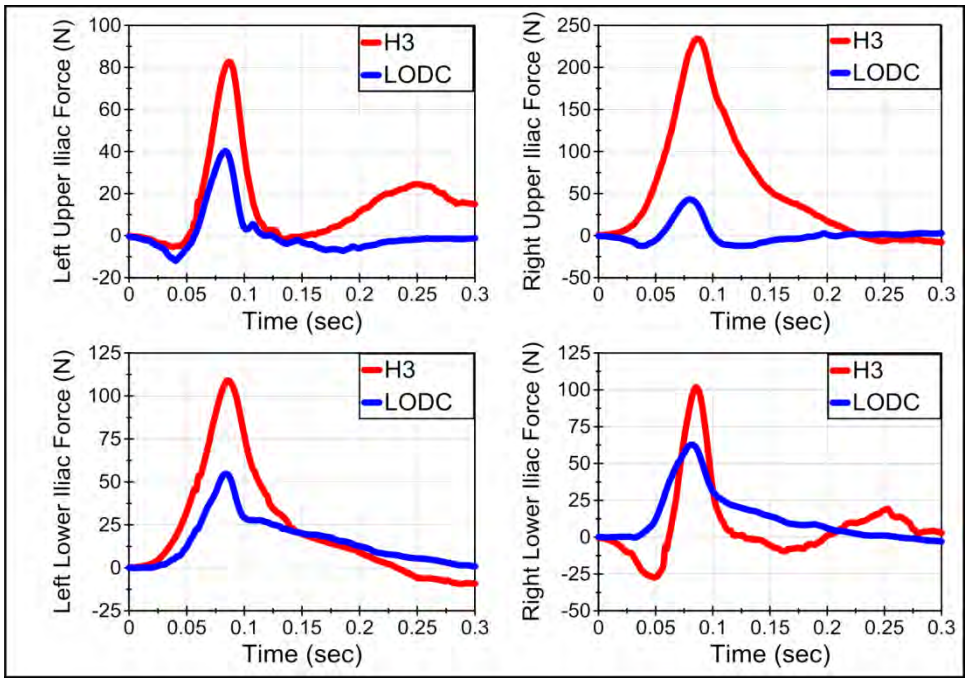

Figure 113. Iliac forces in the LODC and HIII-10C under the low-speed bumper car pulse (Test 1).

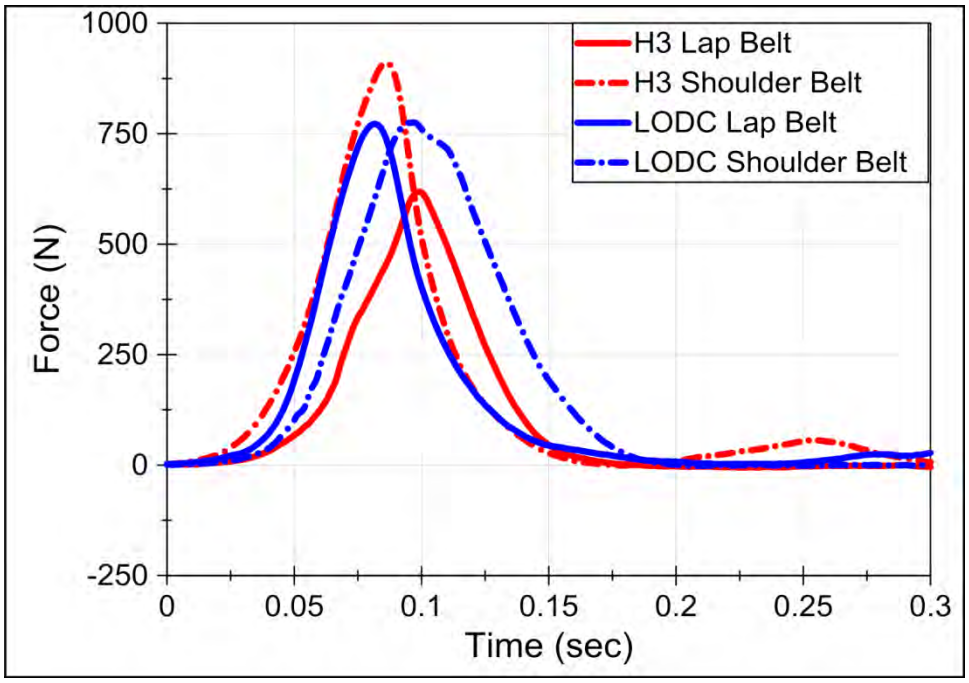

Figure 114. Seatbelt loads in the LODC and HIII-10C under the low-speed bumper car pulse (Test 1).

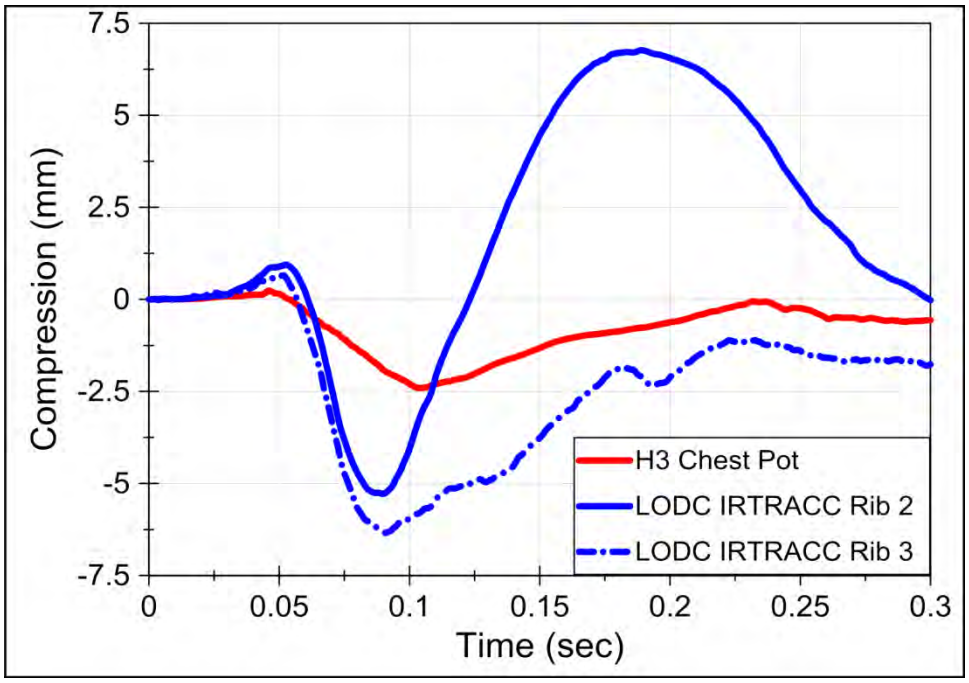

Figure 115. Chest compressions in the LODC and HIII-10C under the low-speed bumper car pulse (Test 1).

Test 2

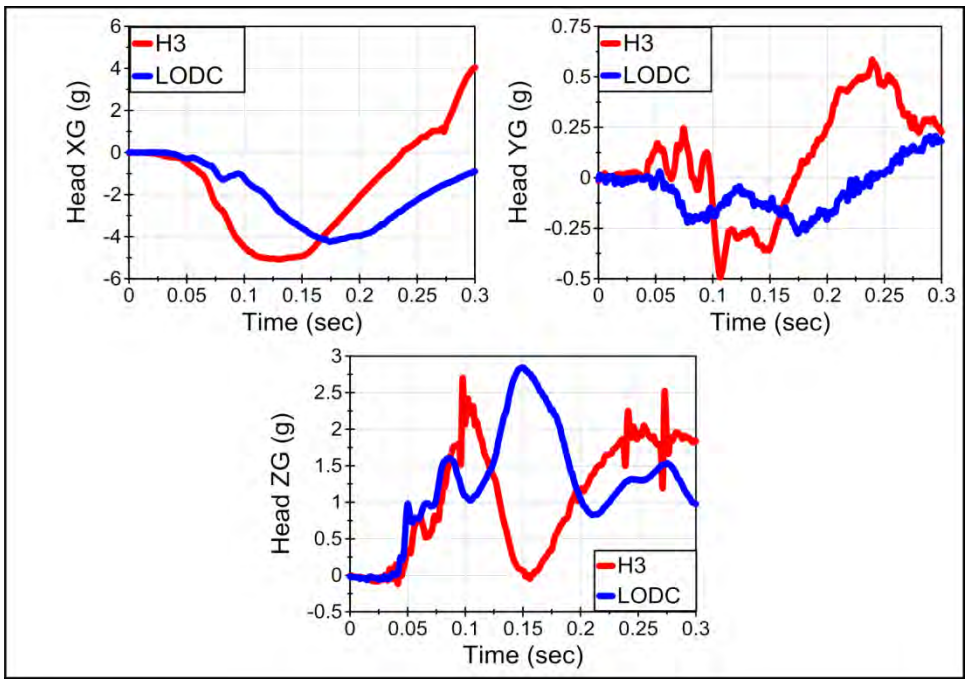

Figure 116. Head accelerations in the LODC and HIII-10C under the low-speed bumper car pulse (Test 2).

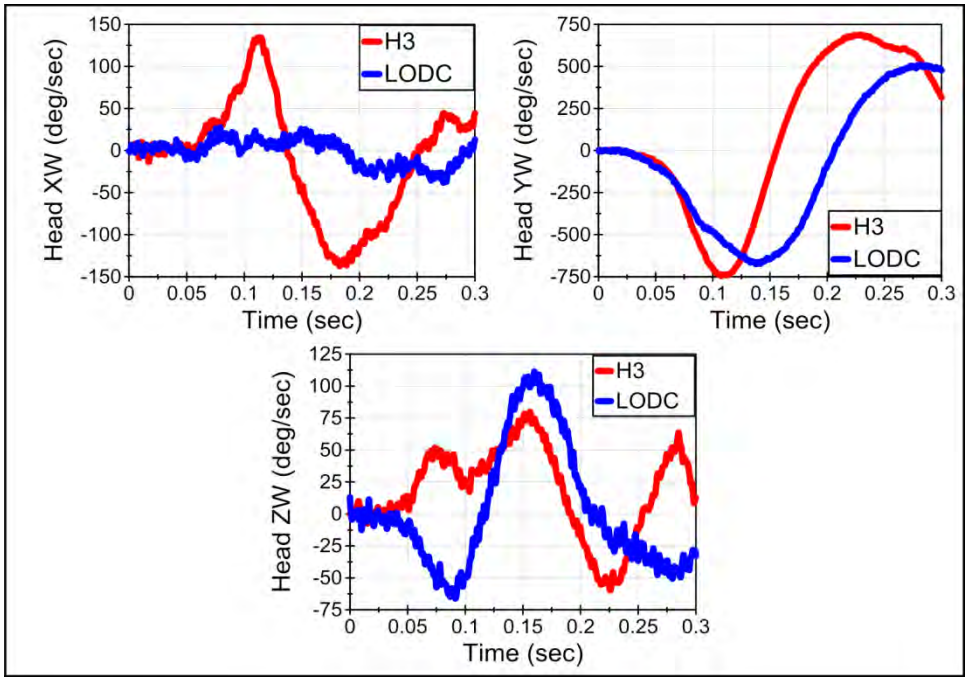

Figure 117. Head angular rates in the LODC and HIII-10C under the low-speed bumper car pulse (Test 2).

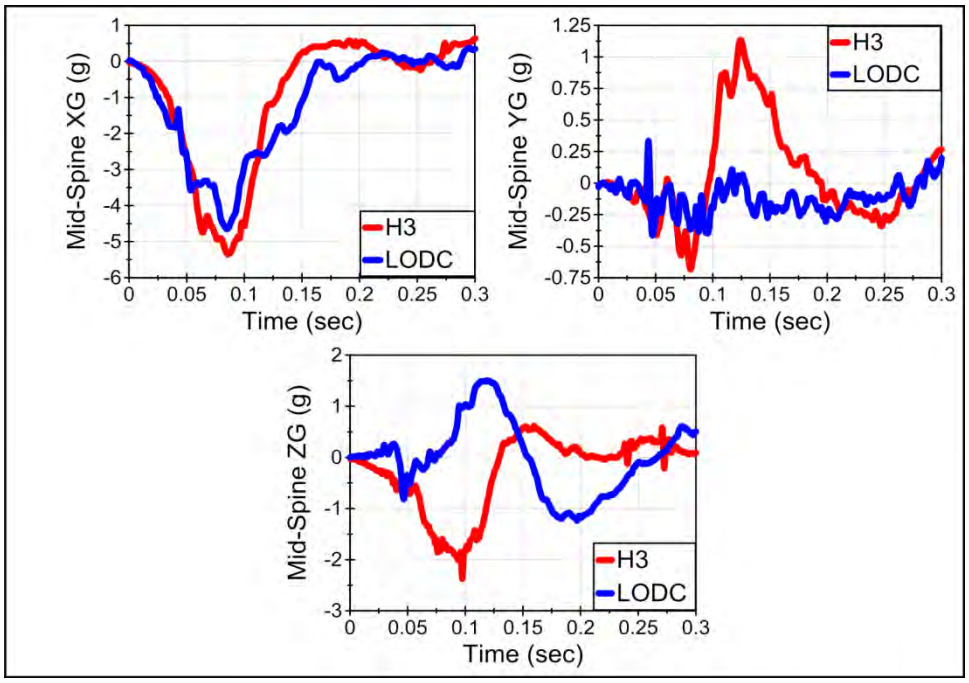

Figure 118. Mid-spine accelerations in the LODC and HIII-10C under the low-speed bumper car pulse (Test 2).

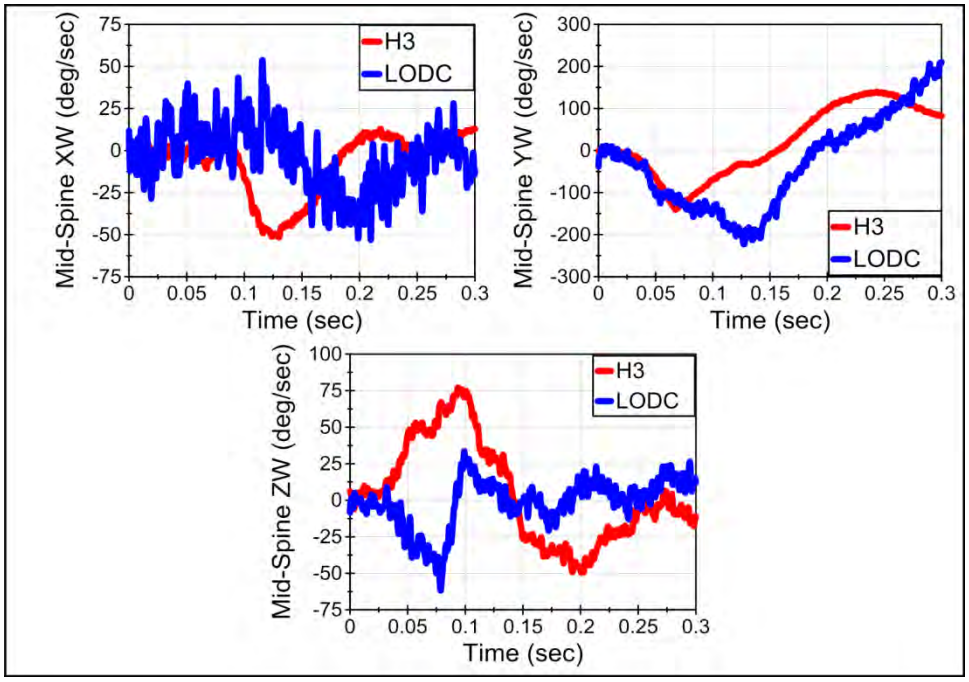

Figure 119. Mid-spine angular rates in the LODC and HIII-10C under the low-speed bumper car pulse (Test 2).

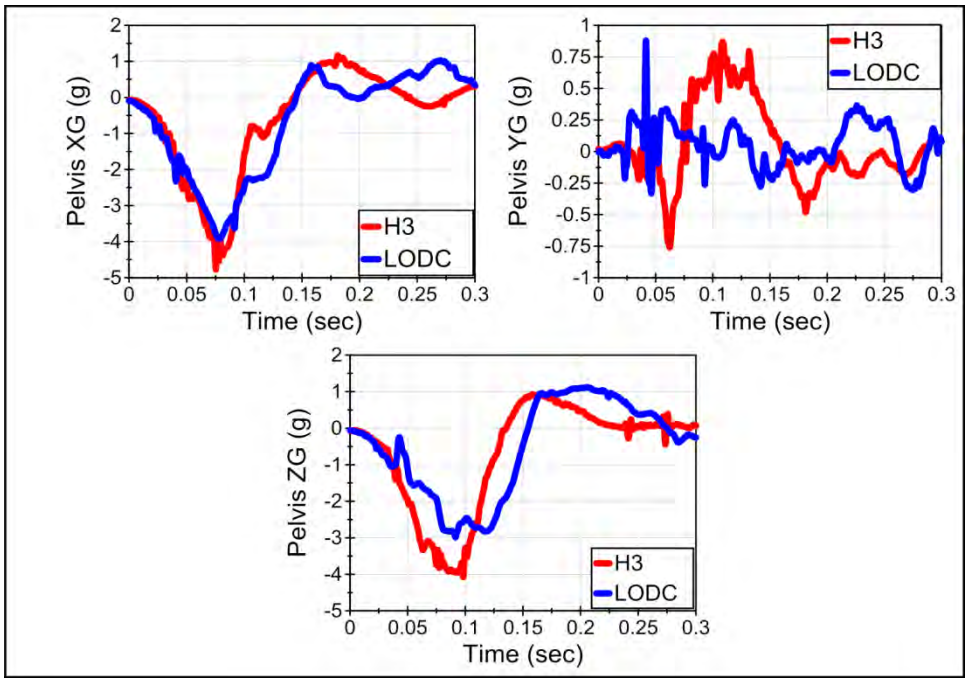

Figure 120. Pelvis accelerations in the LODC and HIII-10C under the low-speed bumper car pulse (Test 2).

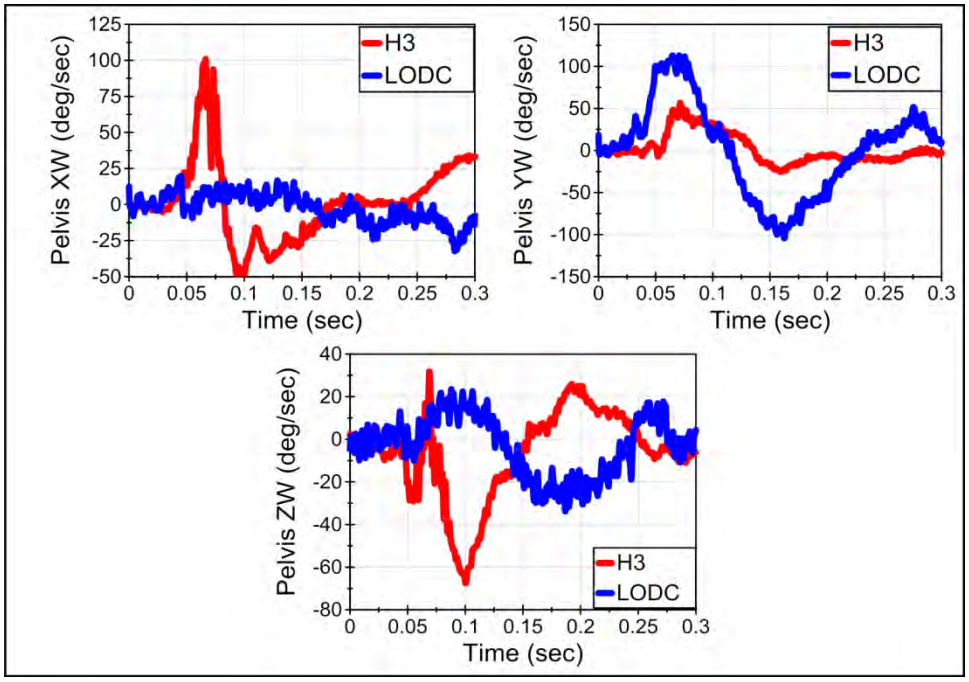

Figure 121. Pelvis angular rates in the LODC and HIII-10C under the low-speed bumper car pulse (Test 2).

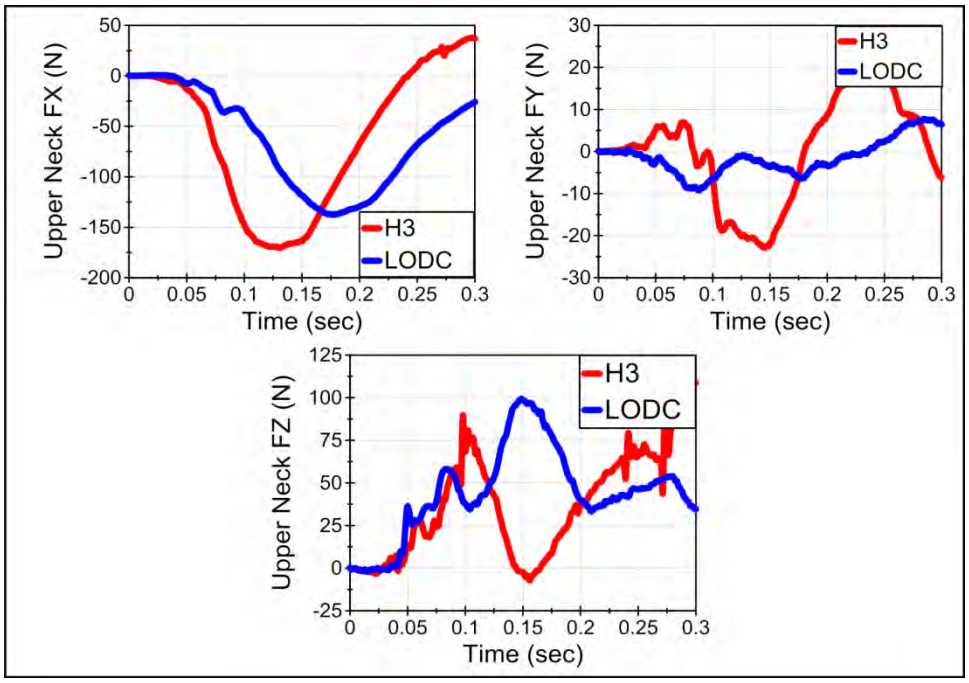

Figure 122. Upper neck forces in the LODC and HIII-10C under the low-speed bumper car pulse (Test 2).

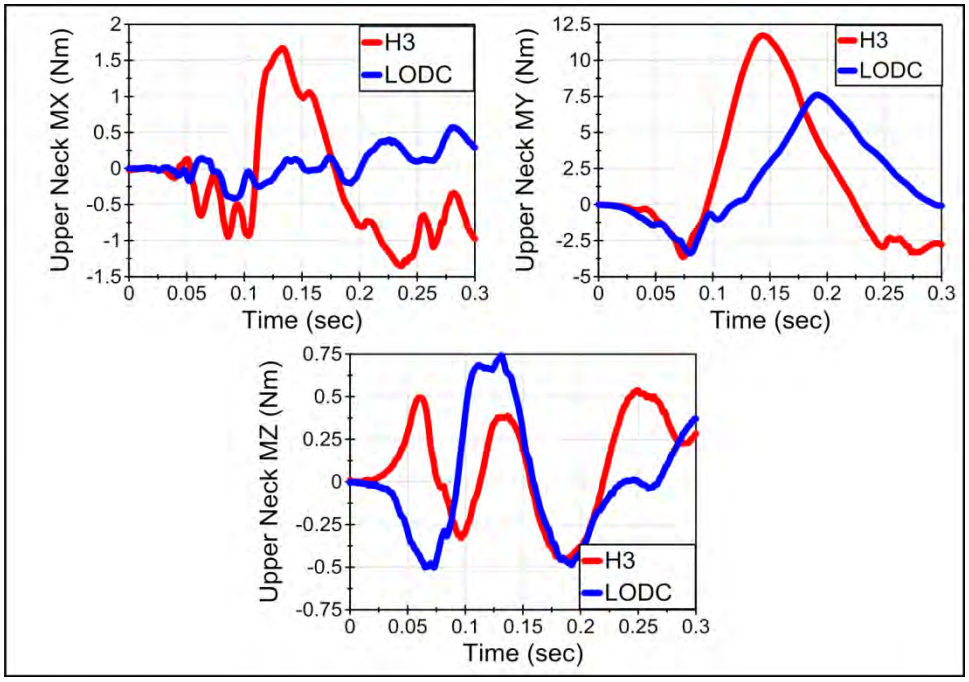

Figure 123. Upper neck moments in the LODC and HIII-10C under the low-speed bumper car pulse (Test 2).

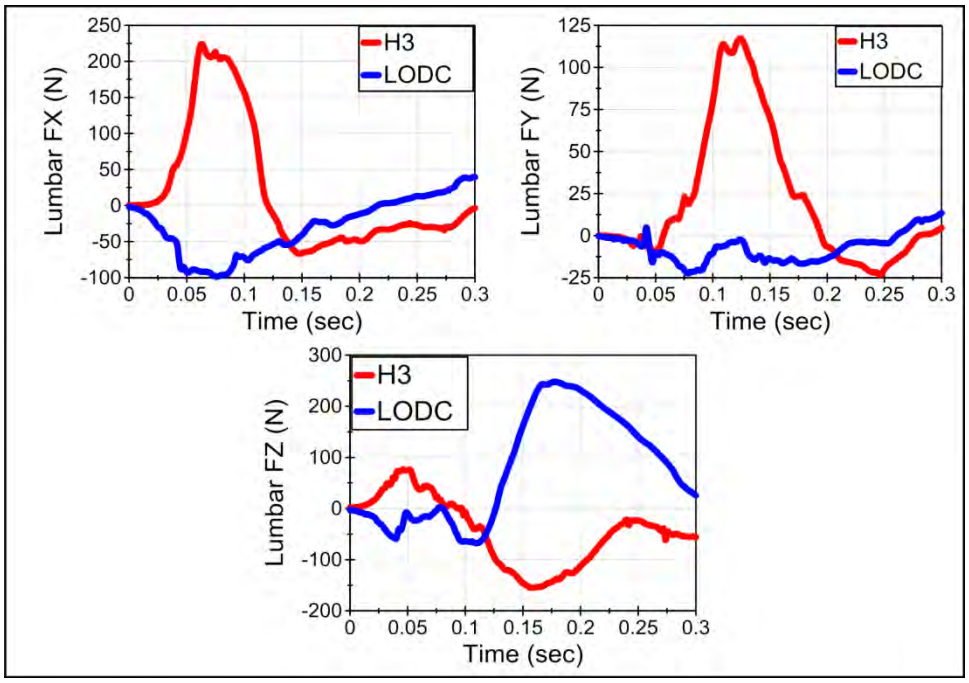

Figure 124. Lumbar forces in the LODC and HIII-10C under the low-speed bumper car pulse (Test 2).

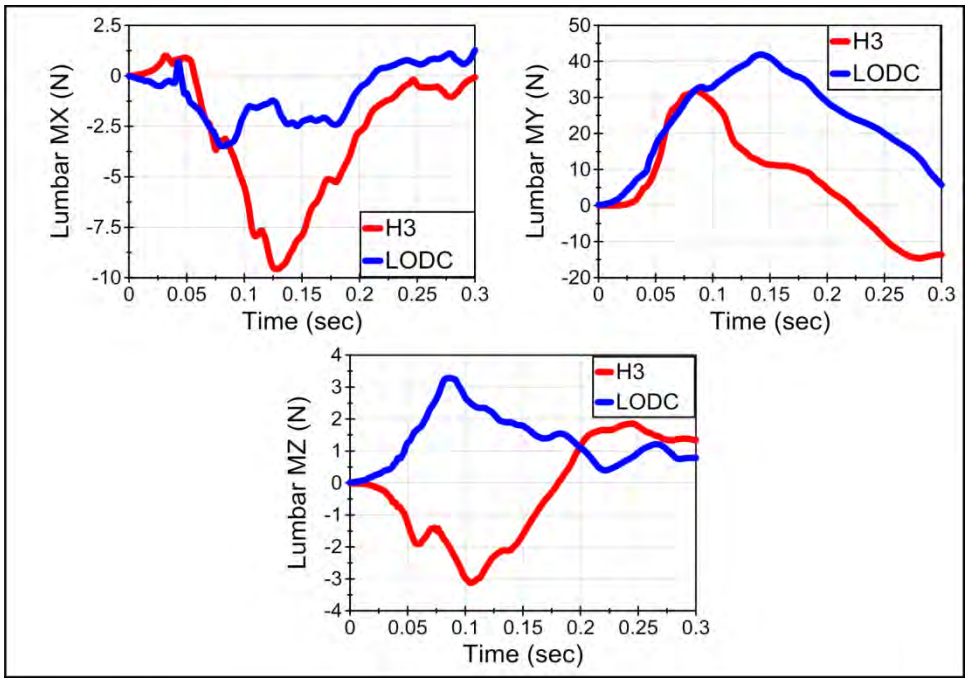

Figure 125. Lumbar moments in the LODC and HIII-10C under the low-speed bumper car pulse (Test 2).

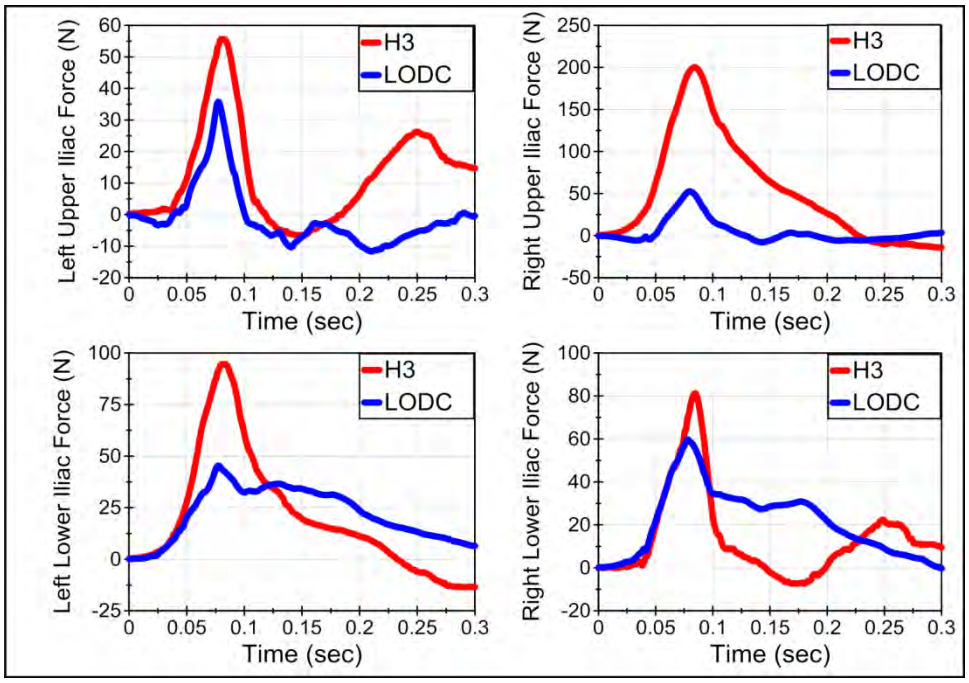

Figure 126. Iliac forces in the LODC and HIII-10C under the low-speed bumper car pulse (Test 2).

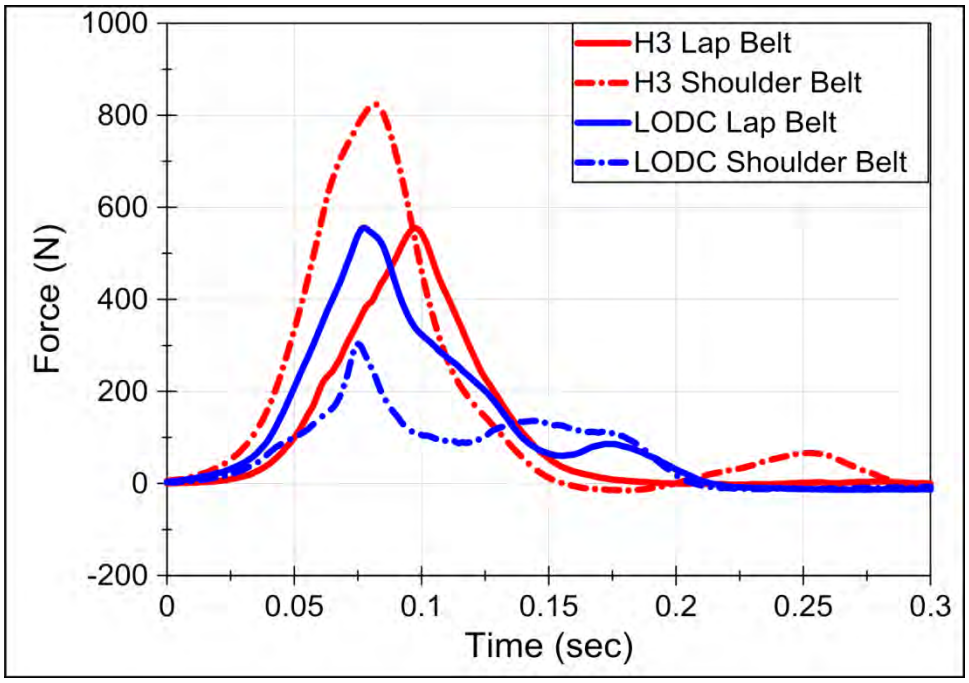

Figure 127. Seatbelt loads in the LODC and HIII-10C under the low-speed bumper car pulse (Test 2).

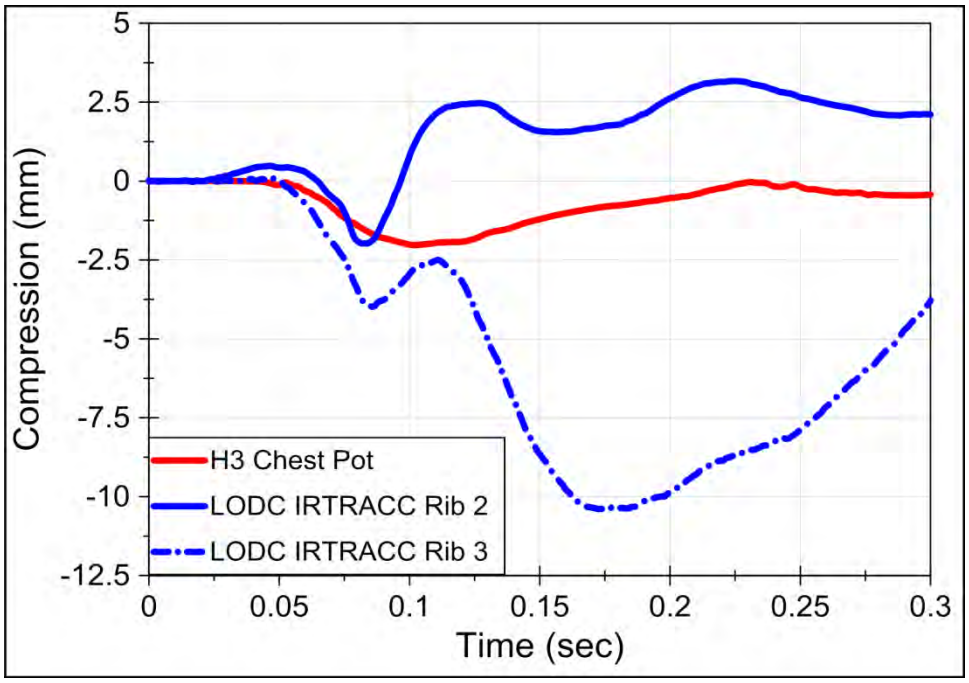

Figure 128. Chest compressions in the LODC and HIII-10C under the low-speed bumper car pulse (Test 2).

Test 3

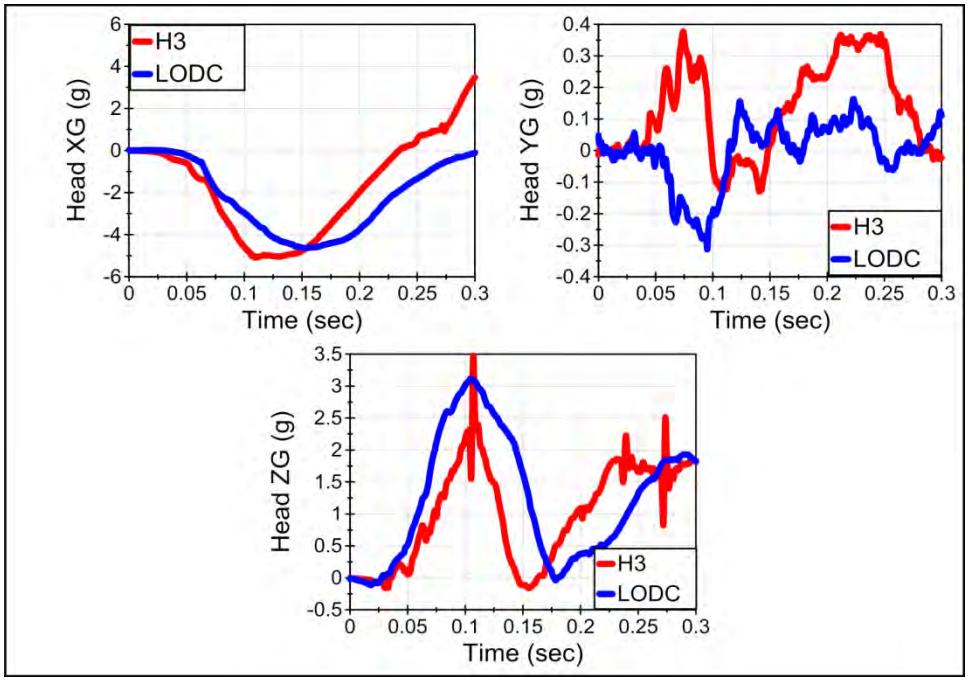

Figure 129. Head accelerations in the LODC and HIII-10C under the low-speed bumper car pulse (Test 3).

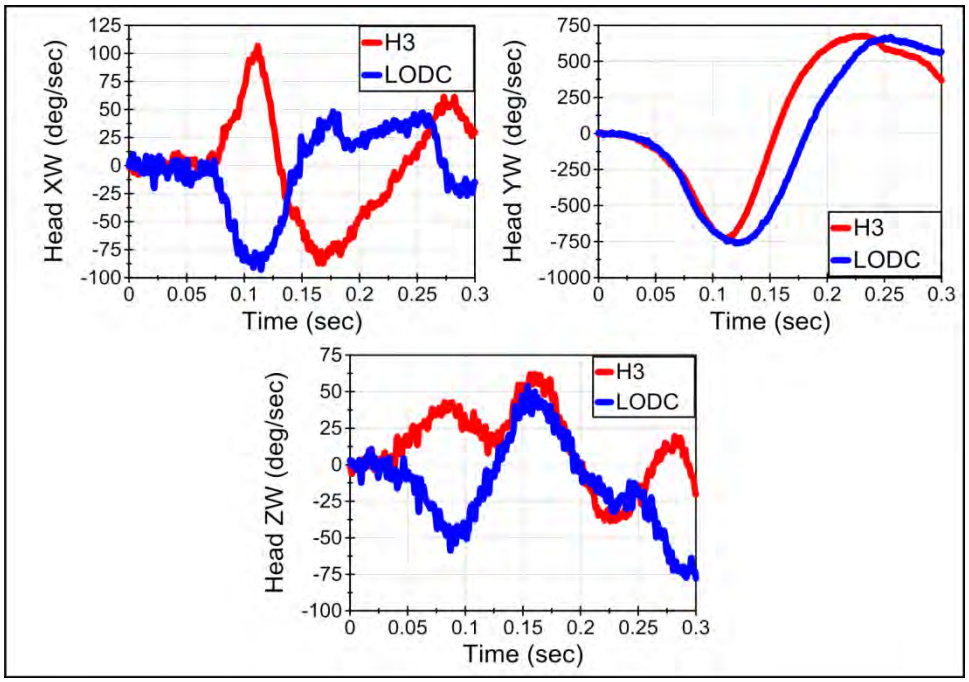

Figure 130. Head angular rates in the LODC and HIII-10C under the low-speed bumper car pulse (Test 3).

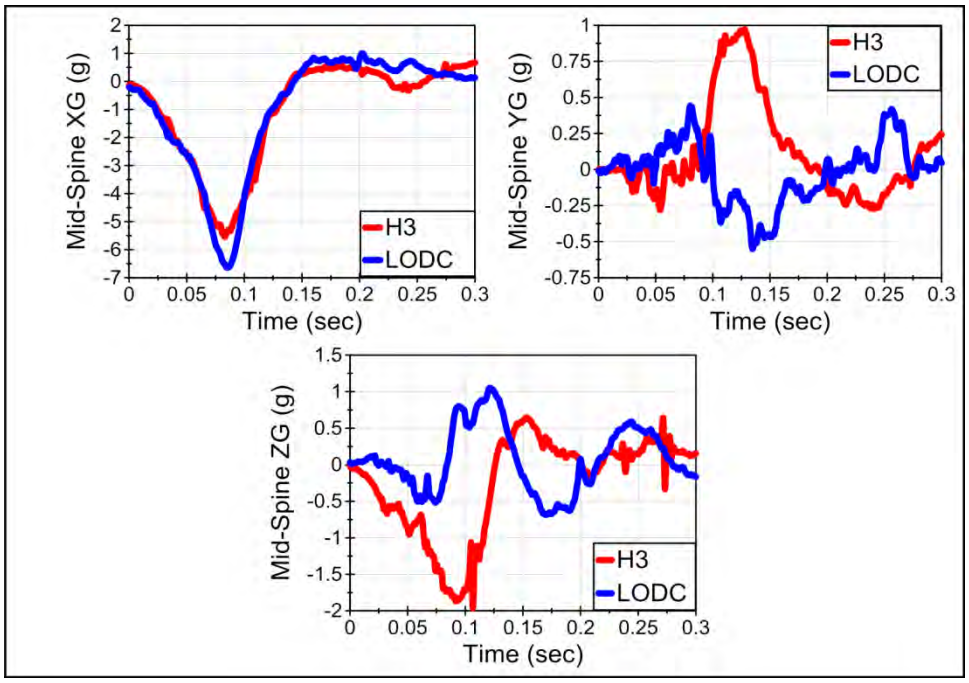

Figure 131. Mid-spine accelerations in the LODC and HIII-10C under the low-speed bumper car pulse (Test 3).

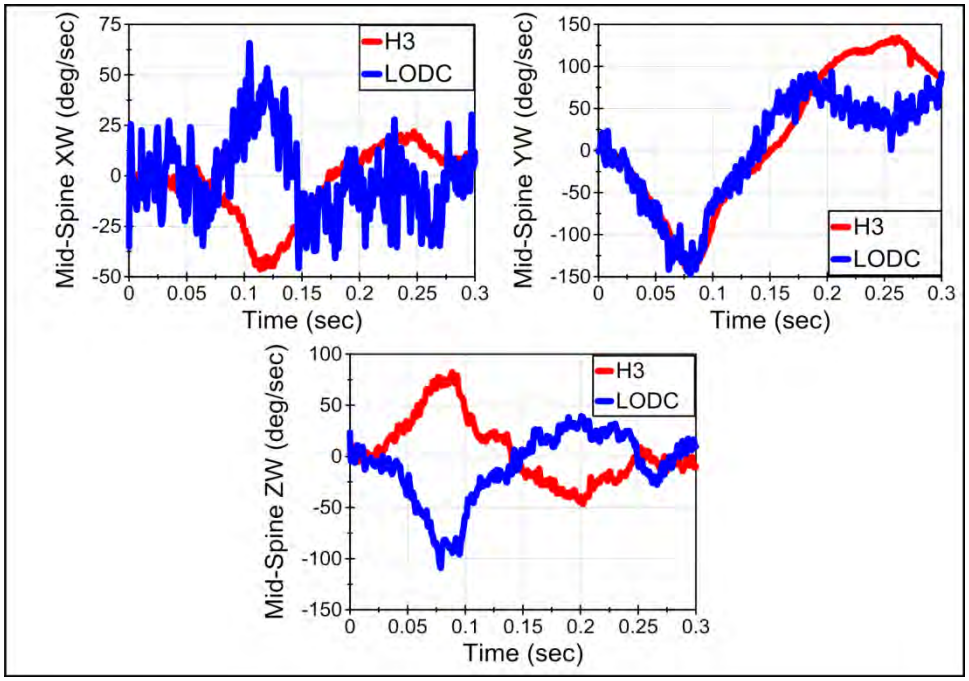

Figure 132. Mid-spine angular rates in the LODC and HIII-10C under the low-speed bumper car pulse (Test 3).

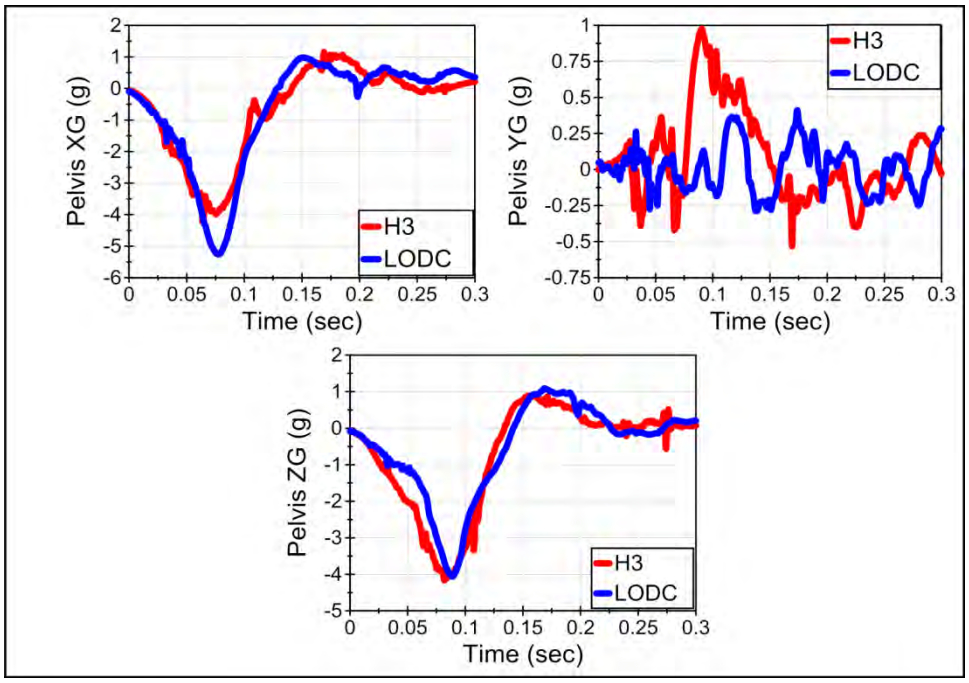

Figure 133. Pelvis accelerations in the LODC and HIII-10C under the low-speed bumper car pulse (Test 3).

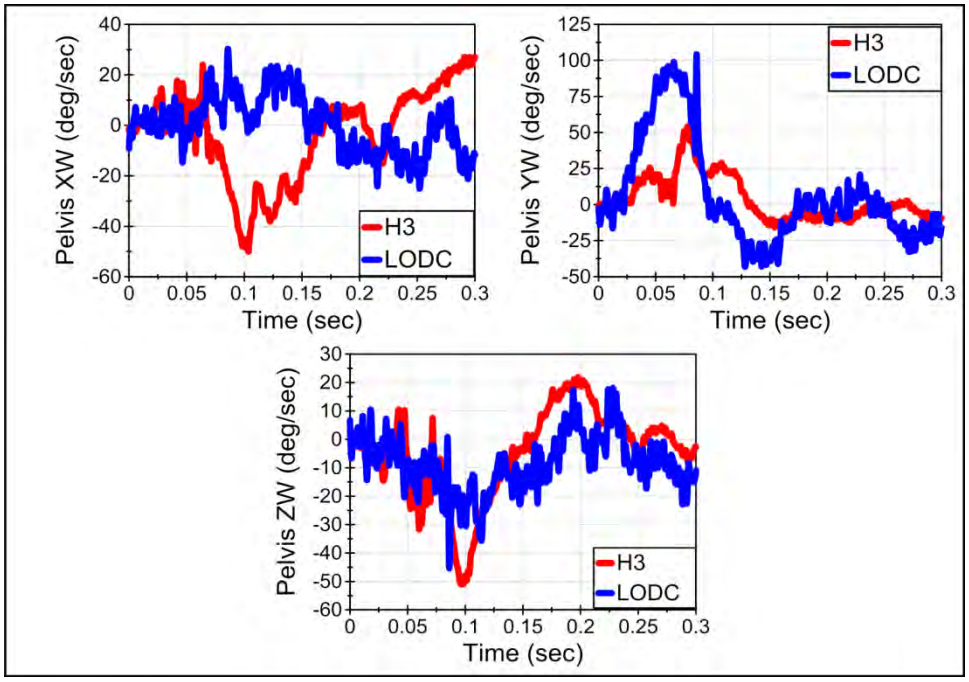

Figure 134. Pelvis angular rates in the LODC and HIII-10C under the low-speed bumper car pulse (Test 3).

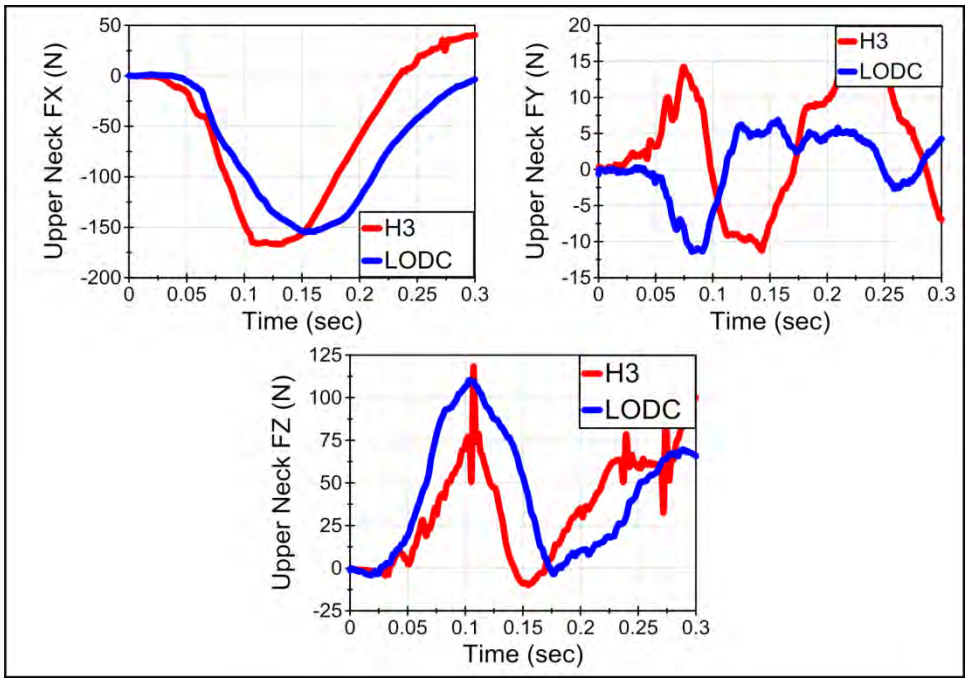

Figure 135. Upper neck forces in the LODC and HIII-10C under the low-speed bumper car pulse (Test 3).

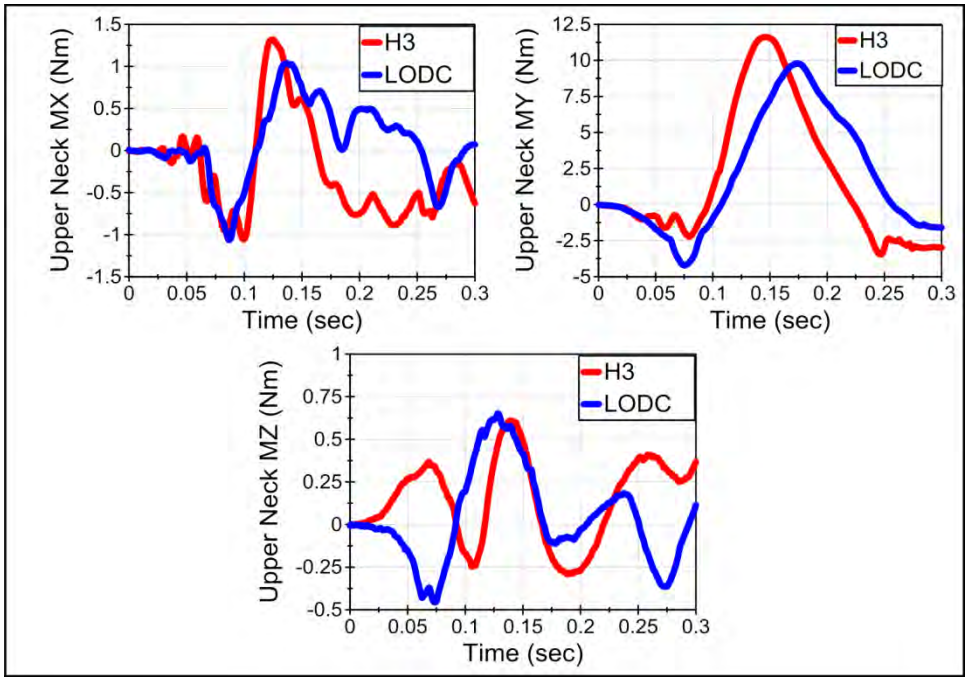

Figure 136. Upper neck moments in the LODC and HIII-10C under the low-speed bumper car pulse (Test 3).

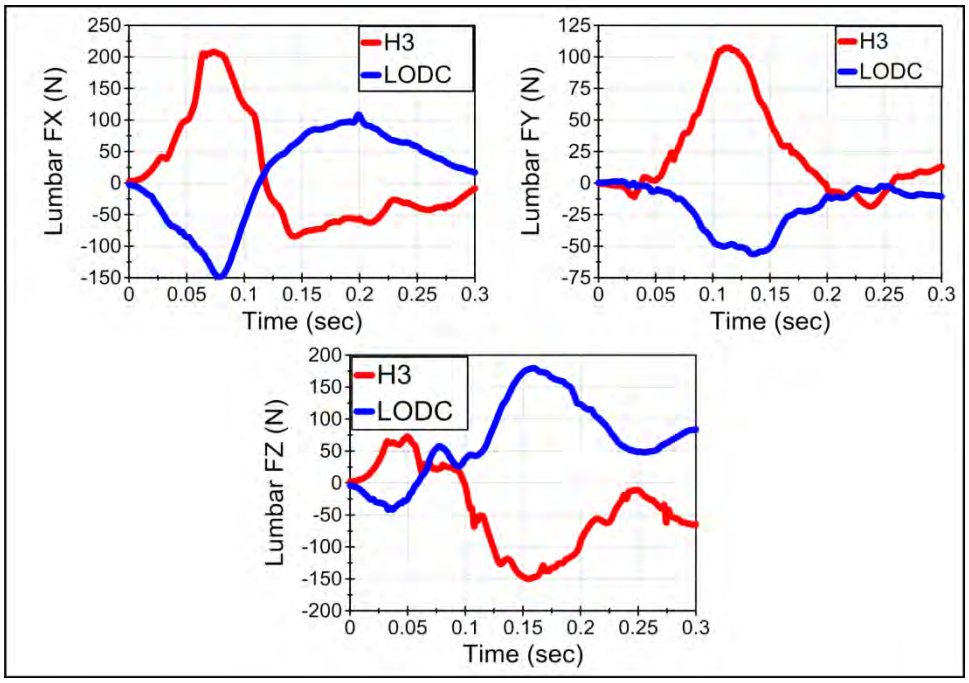

Figure 137. Lumbar forces in the LODC and HIII-10C under the low-speed bumper car pulse (Test 3).

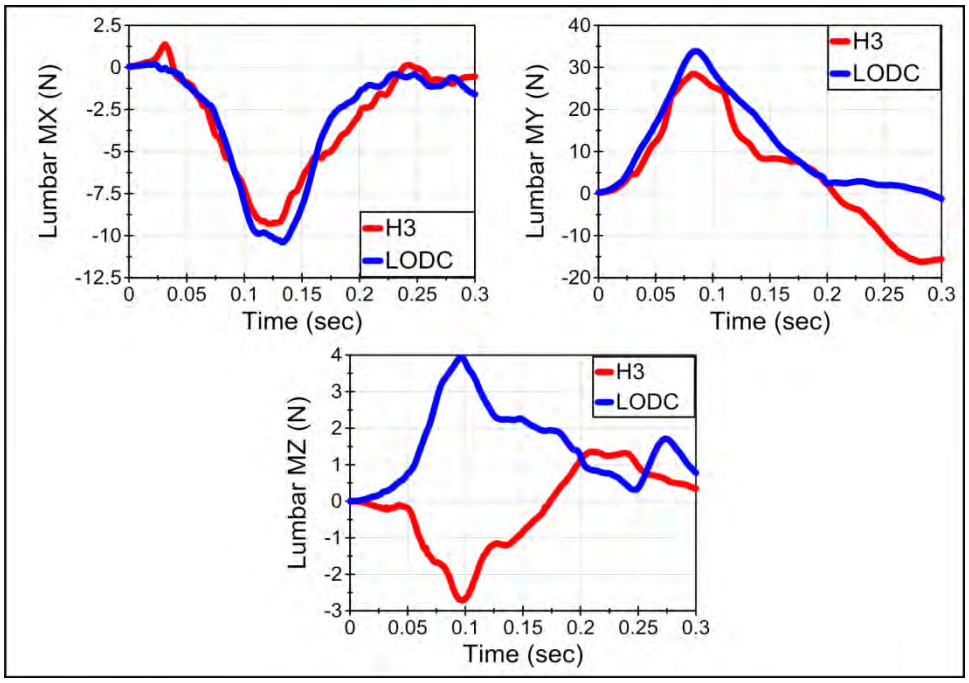

Figure 138. Lumbar moments in the LODC and HIII-10C under the low-speed bumper car pulse (Test 3).

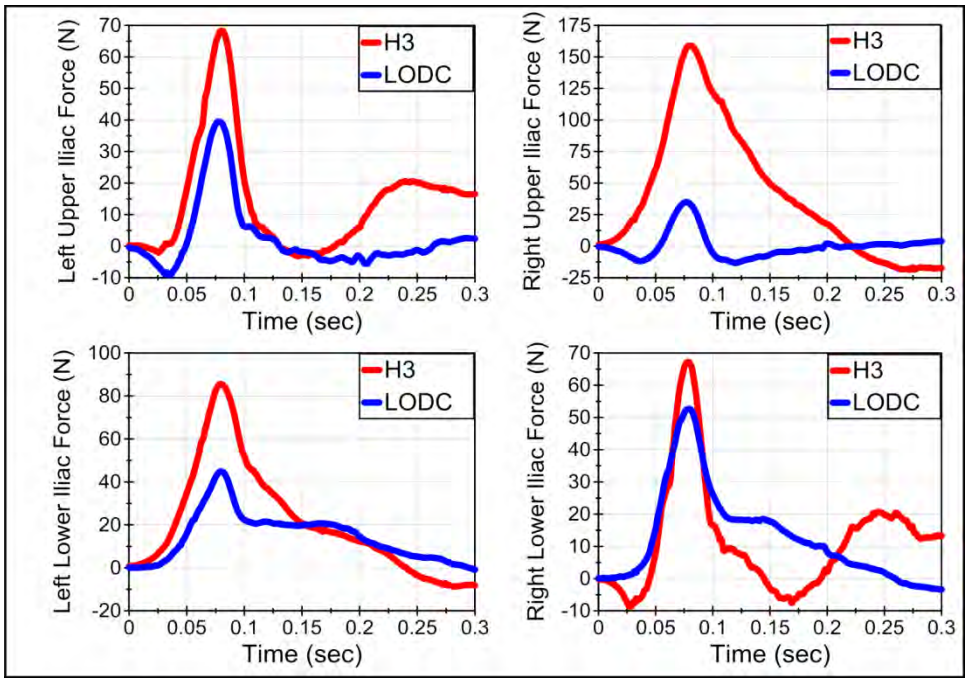

Figure 139. Iliac forces in the LODC and HIII-10C under the low-speed bumper car pulse (Test 3).

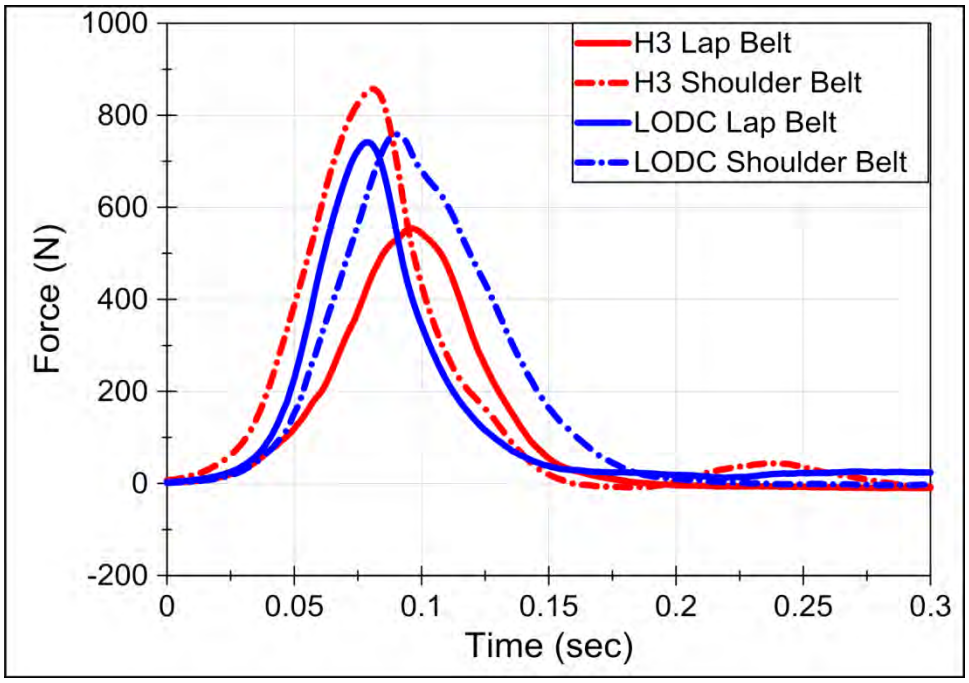

Figure 140. Seatbelt loads in the LODC and HIII-10C under the low-speed bumper car pulse (Test 3).

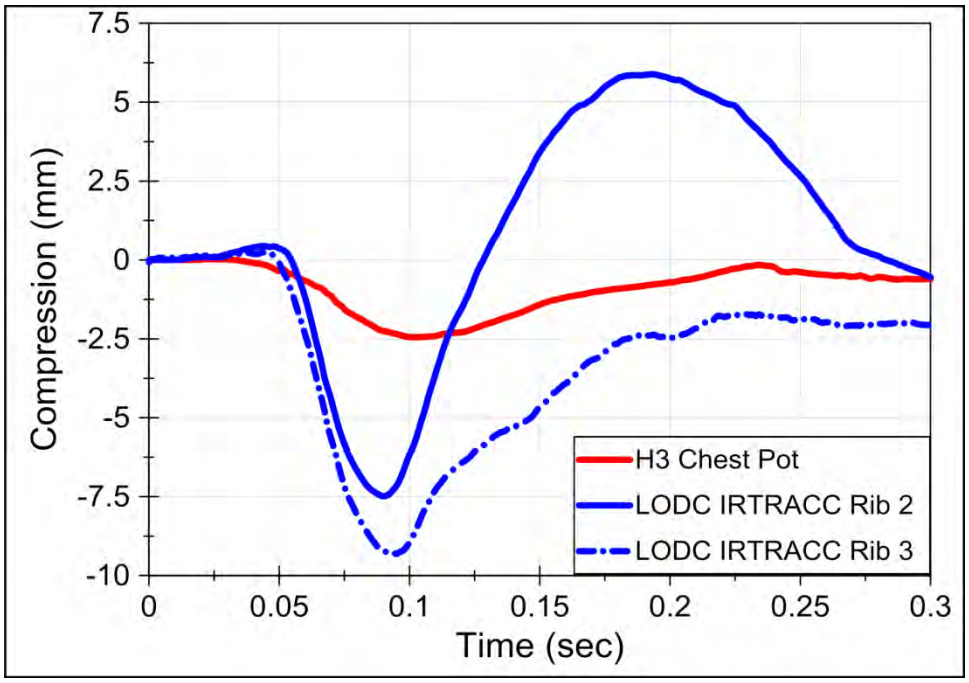

Figure 141. Chest compressions in the LODC and HIII-10C under the low-speed bumper car pulse (Test 3).

Appendix B: Mid-Speed (40 km/h) Time Histories

5-Point Harness (Britax Frontier 85)

Time history comparisons of head, mid-spine, and pelvis accelerations and angular rates; upper neck and lumbar forces and moments; iliac and seatbelt forces; and chest compressions for the LODC and HIII-10C dummies seated in a 5-point harness (Britax Frontier 85) are shown in Figures 142-151 below. The LODC time histories are represented by the blue curves. The HIII-10C time histories are represented by the red curves.

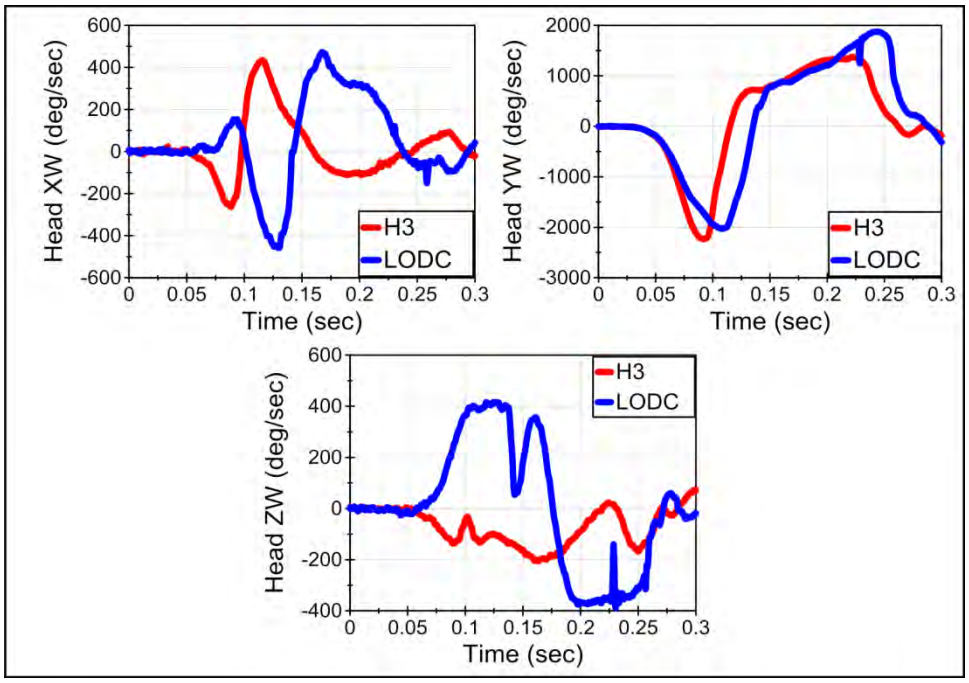

Figure 142. Head angular rates in the LODC and HIII-10C using a 5-point harness in 40 km/h test.

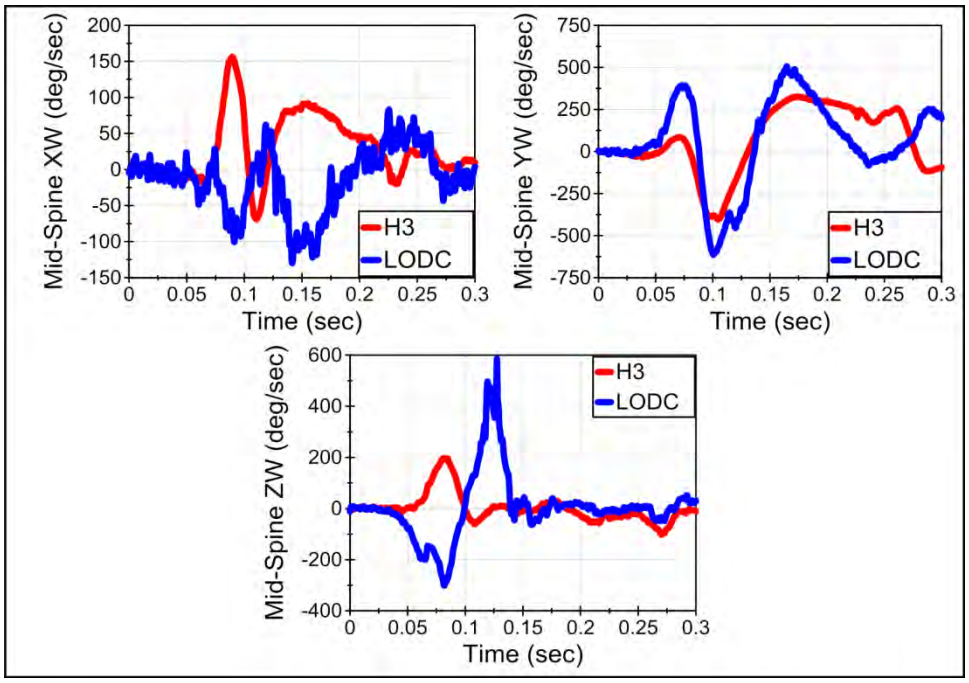

Figure 143. Mid-spine angular rates in the LODC and HIII-10C using a 5-point harness in 40 km/h test.

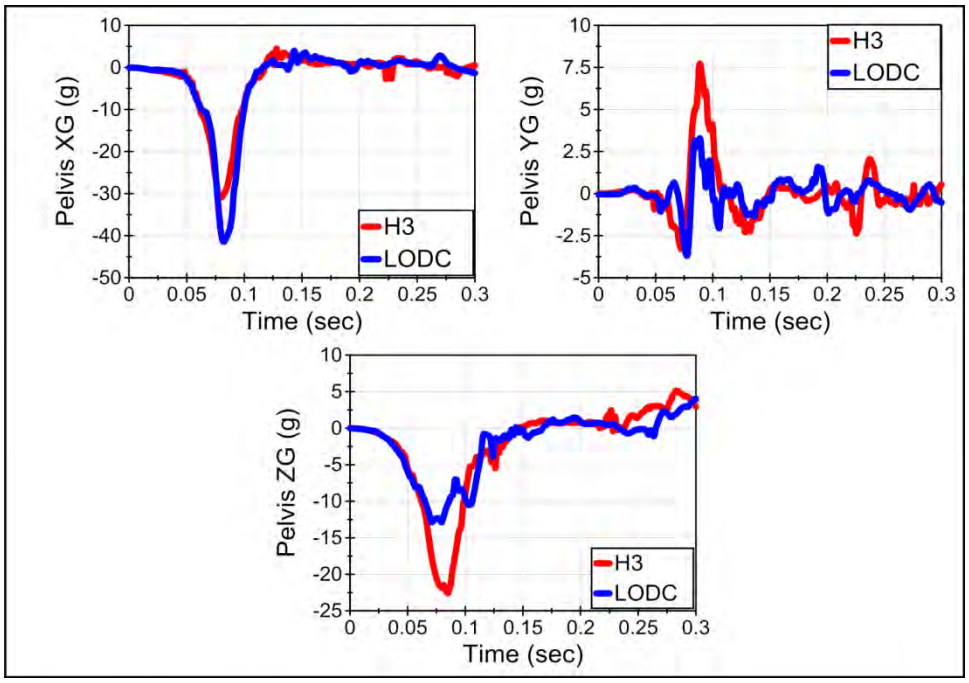

Figure 144. Pelvis accelerations in the LODC and HIII-10C using a 5-point harness in 40 km/h test.

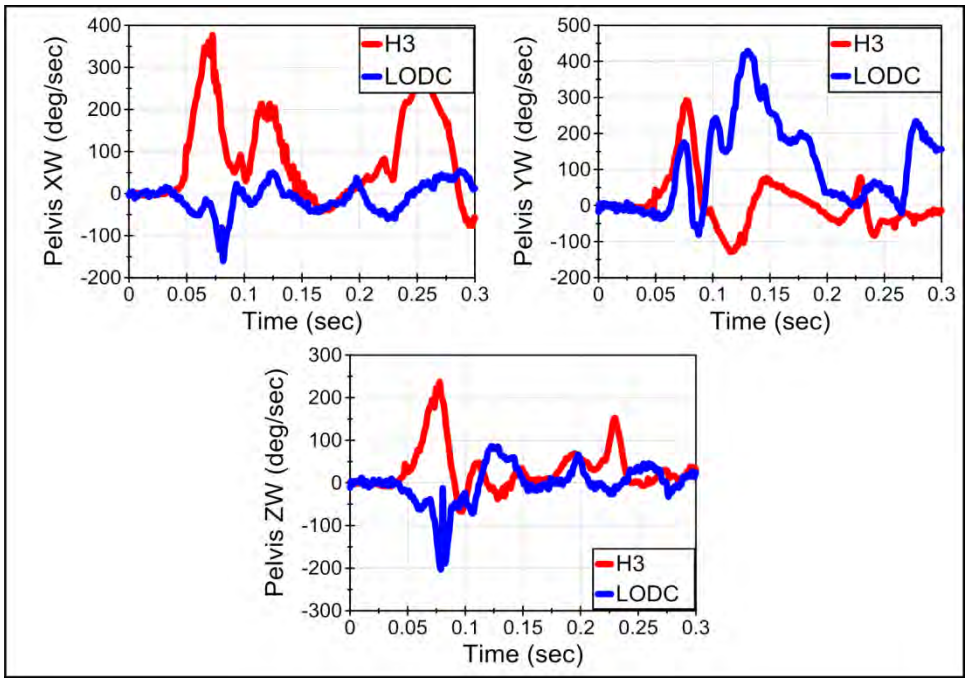

Figure 145. Pelvis angular rates in the LODC and HIII-10C using a 5-point harness in 40 km/h test.

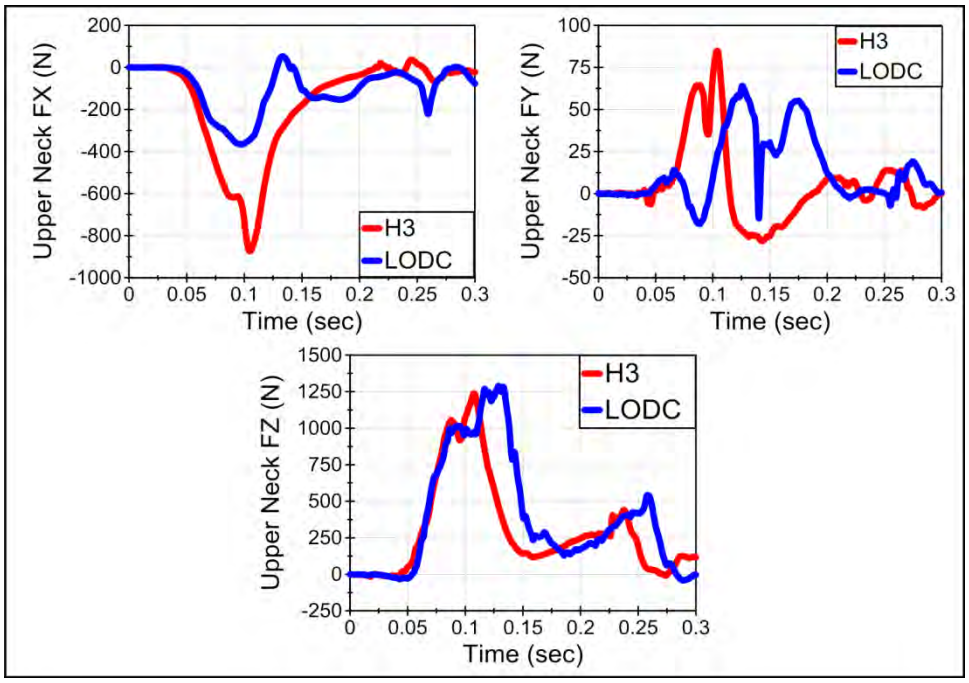

Figure 146. Upper neck forces in the LODC and HIII-10C using a 5-point harness in 40 km/h test.

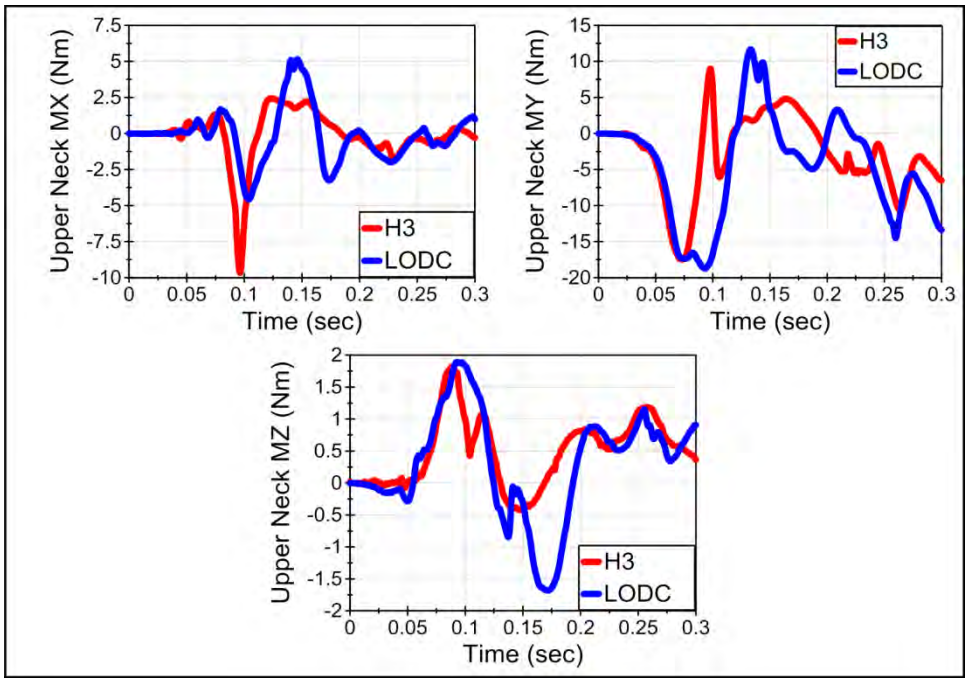

Figure 147. Upper neck moments in the LODC and HIII-10C using a 5-point harness in 40 km/h test.

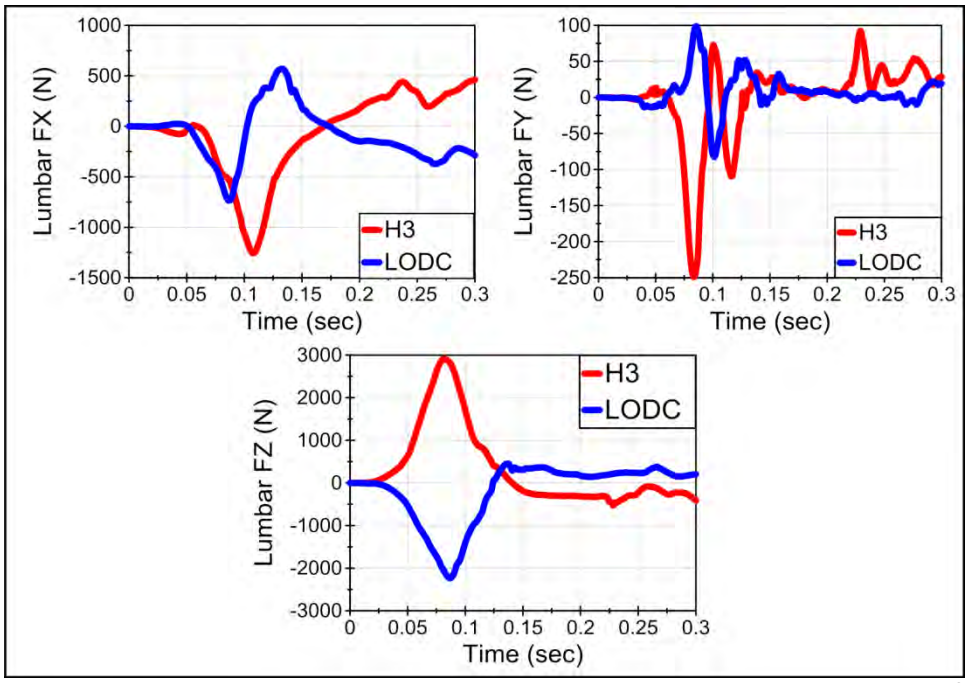

Figure 148. Lumbar forces in the LODC and HIII-10C using a 5-point harness in 40 km/h test.

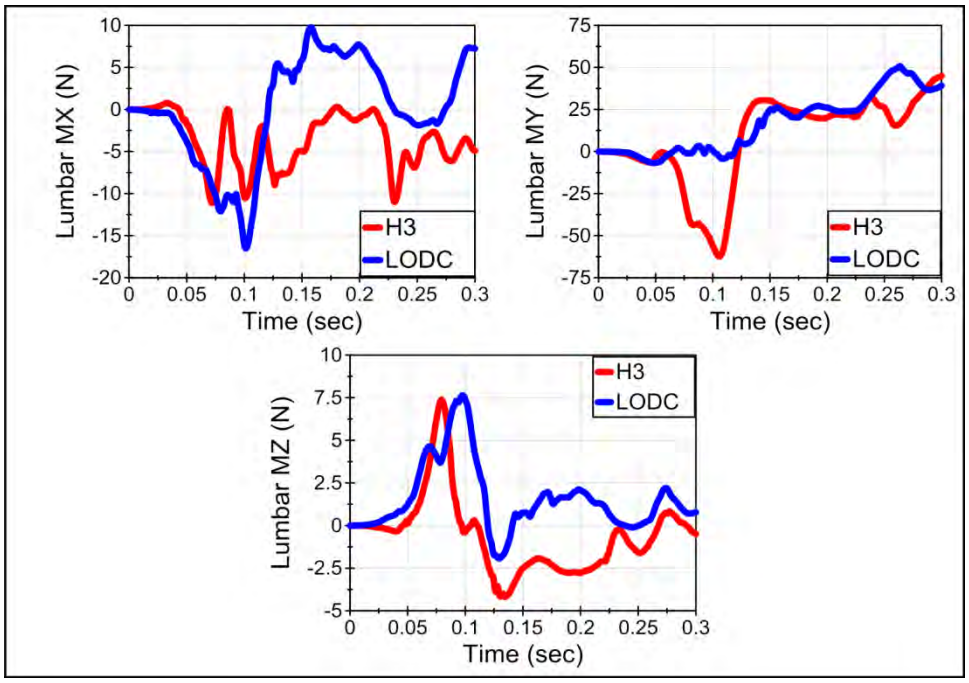

Figure 149. Lumbar moments in the LODC and HIII-10C using a 5-point harness in 40 km/h test.

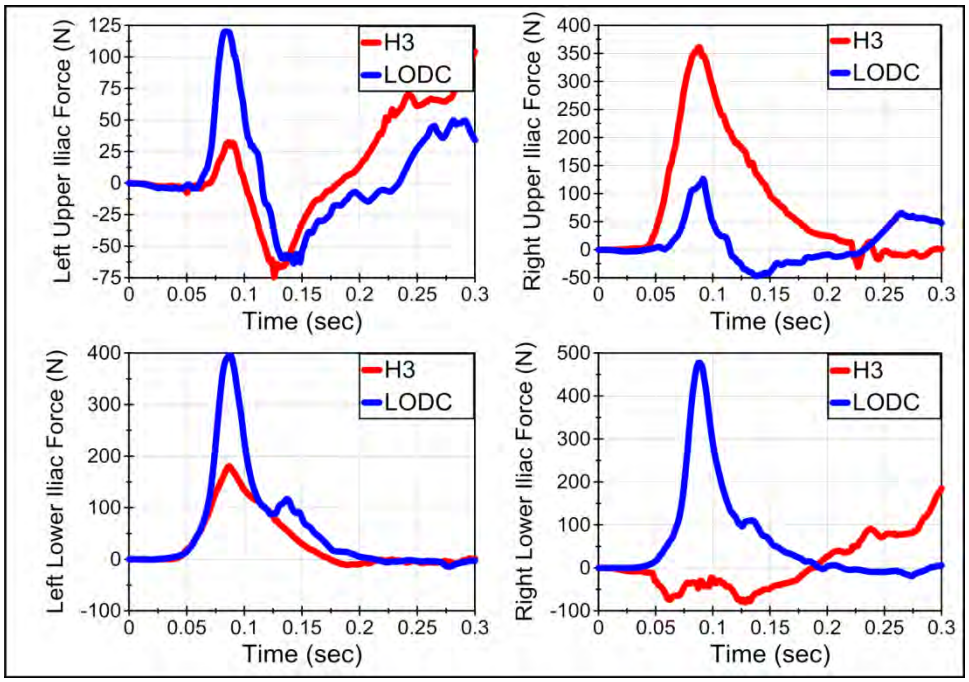

Figure 150. Iliac forces in the LODC and HIII-10C using a 5-point harness in 40 km/h test.

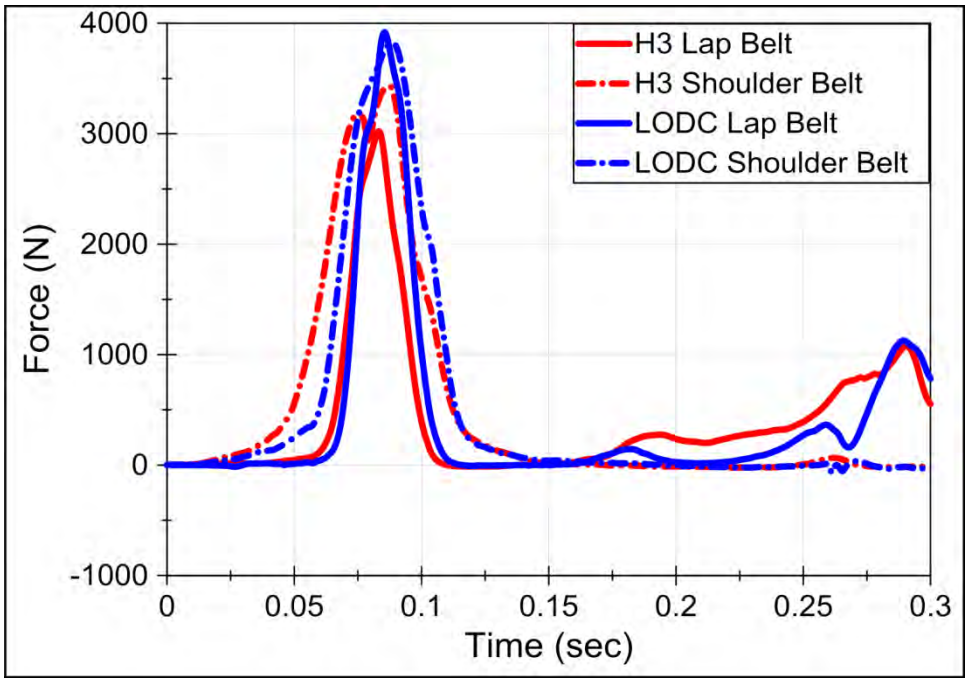

Figure 151. Seatbelt loads in the LODC and HIII-10C using a 5-point harness in 40 km/h test.

High Back Booster (Graco TurboBooster)

Time history comparisons of head, mid-spine, and pelvis accelerations and angular rates; upper neck and lumbar forces and moments; iliac and seatbelt forces; and chest compressions for the LODC and HIII-10C dummies seated in a high back booster seat (Graco TurboBooster) are shown in Figures 152-161 below. The LODC time histories are represented by the blue curves. The HIII-10C time histories are represented by the red curves.

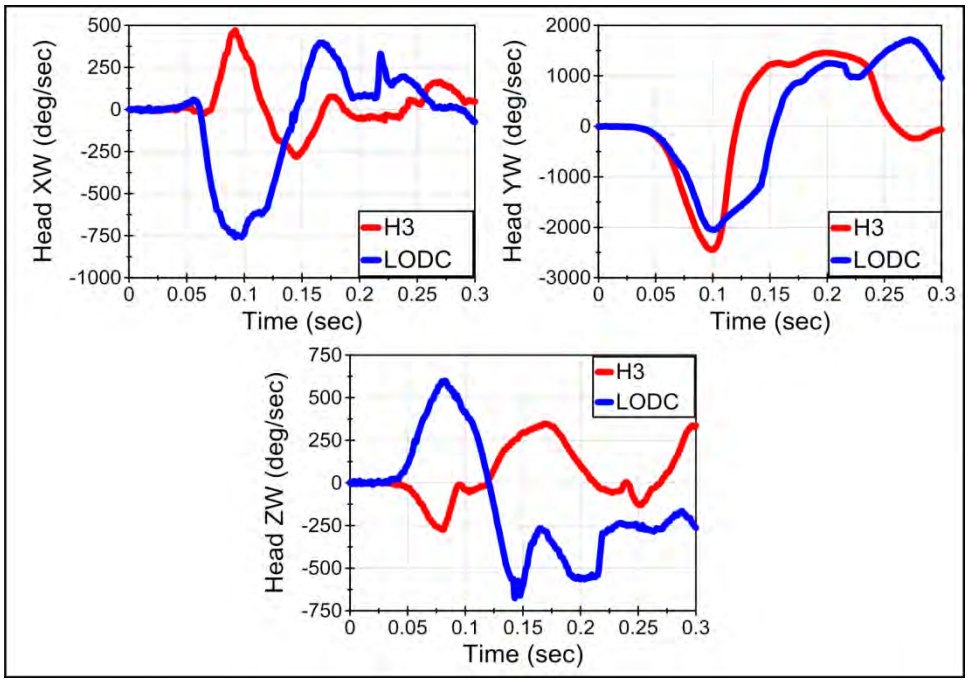

Figure 152. Head angular rates in the LODC and HIII-10C using a high back booster seat in 40 km/h test.

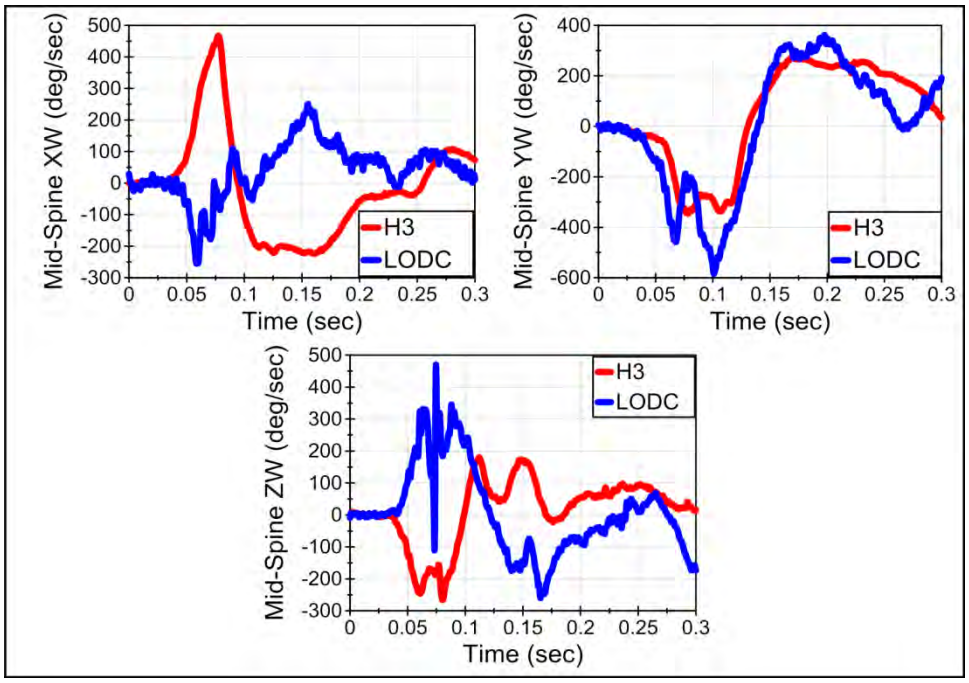

Figure 153. Mid-spine angular rates in the LODC and HIII-10C using a high back booster seat in 40 km/h test.

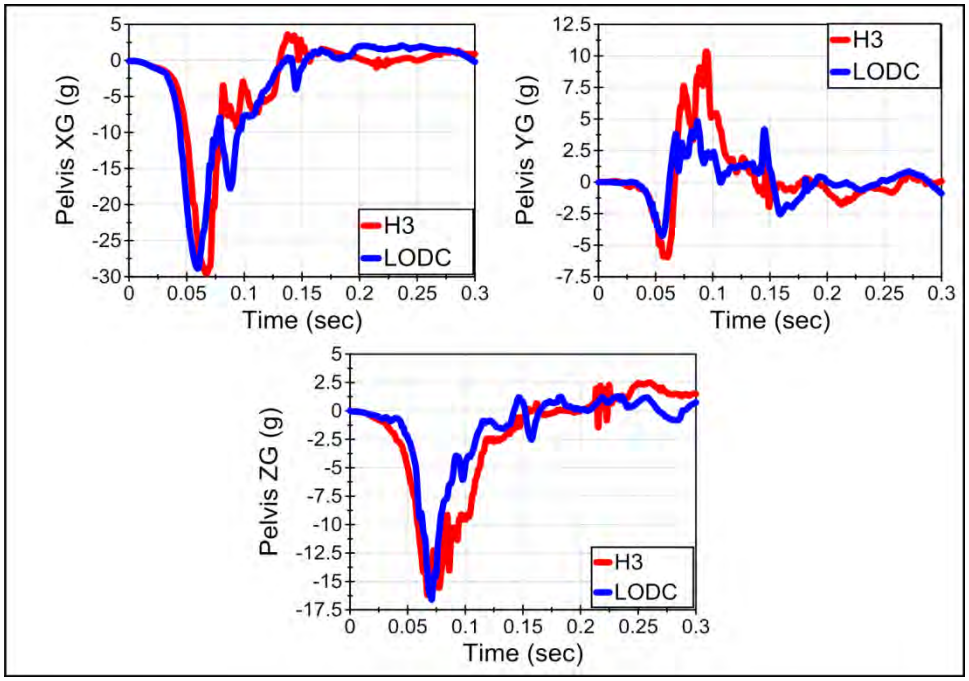

Figure 154. Pelvis accelerations in the LODC and HIII-10C using a high back booster seat in 40 km/h test.

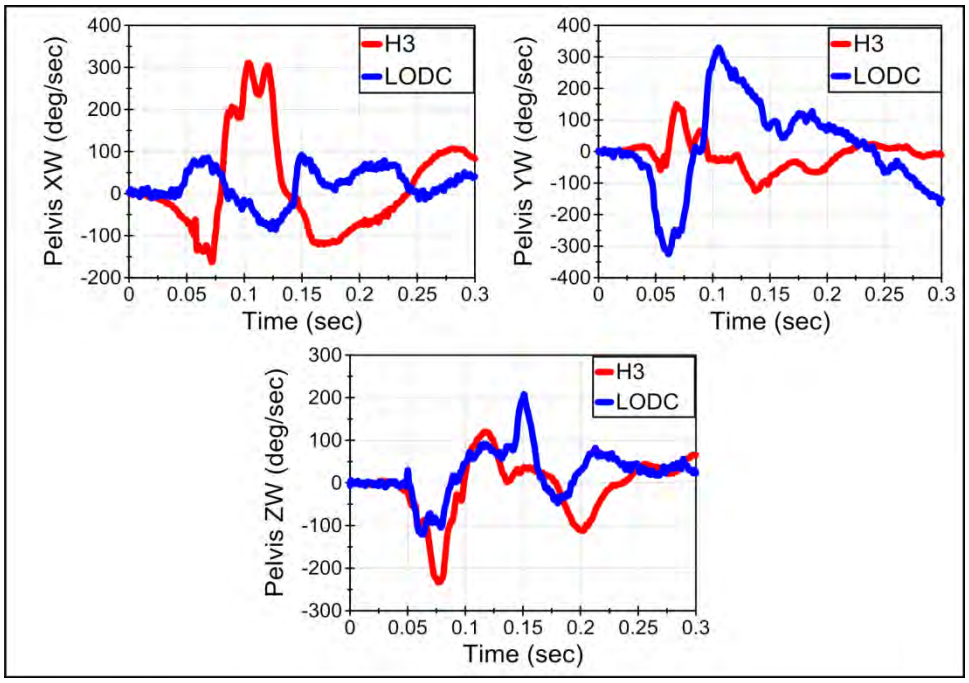

Figure 155. Pelvis angular rates in the LODC and HIII-10C using a high back booster seat in 40 km/h test.

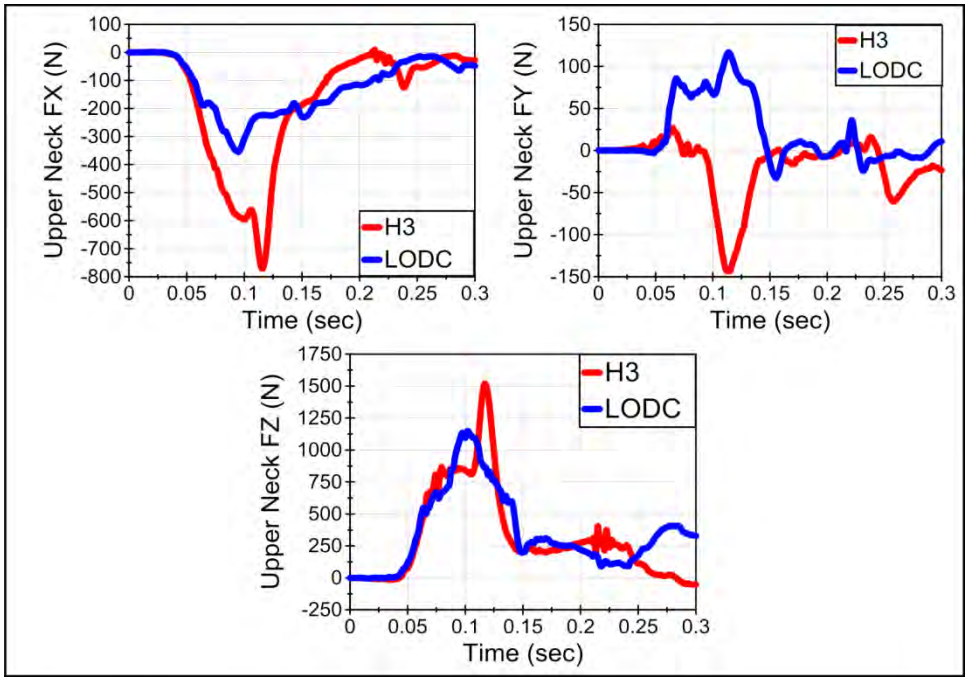

Figure 156. Upper neck forces in the LODC and HIII-10C using a high back booster seat in 40 km/h test.

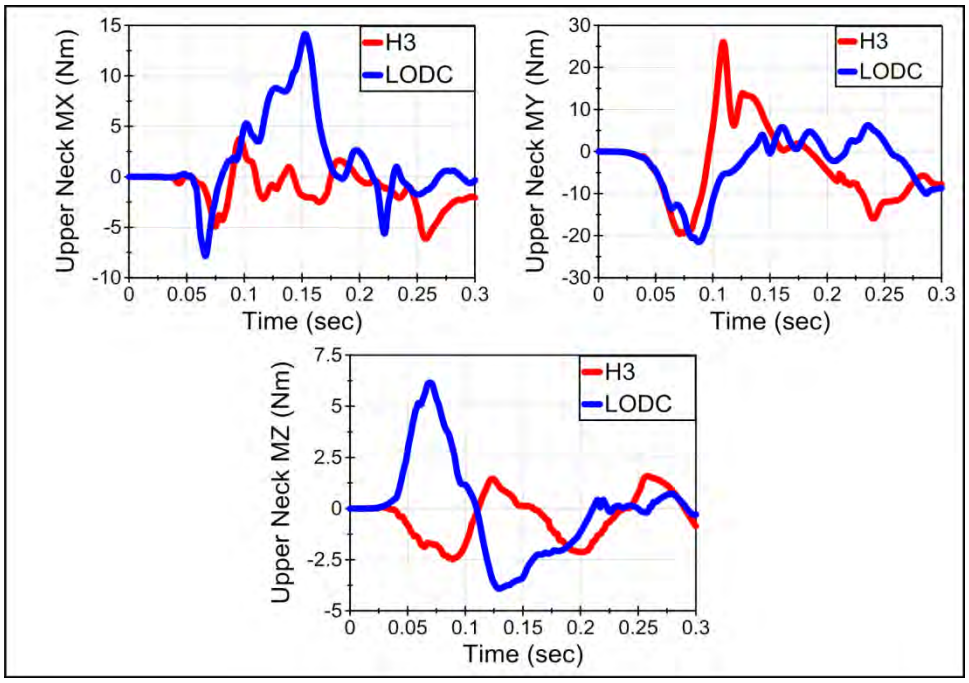

Figure 157. Upper neck moments in the LODC and HIII-10C using a high back booster seat in 40 km/h test.

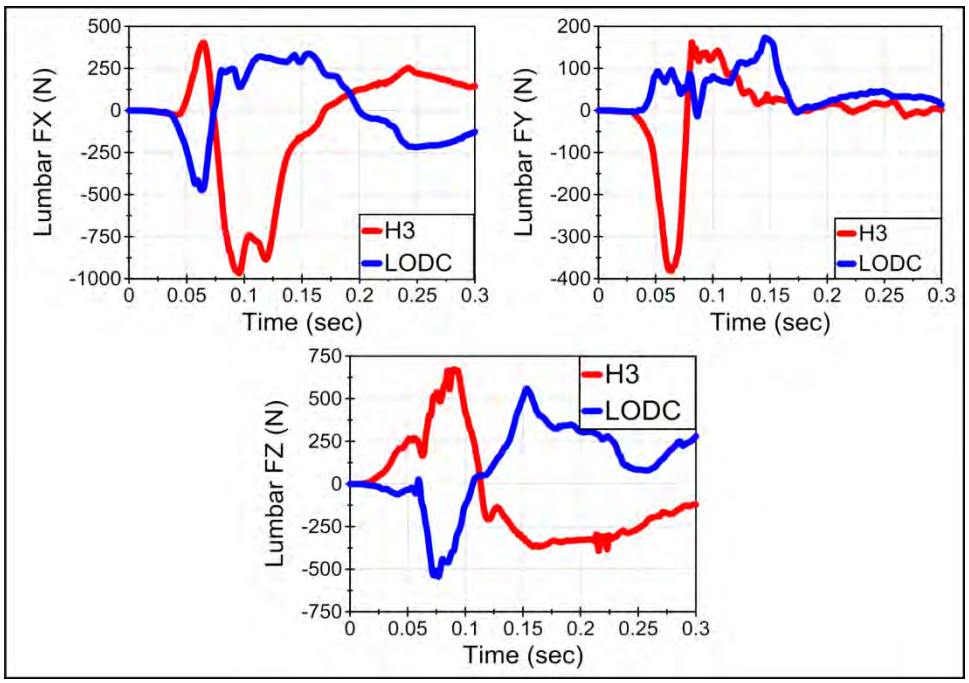

Figure 158. Lumbar forces in the LODC and HIII-10C using a high back booster seat in 40 km/h test.

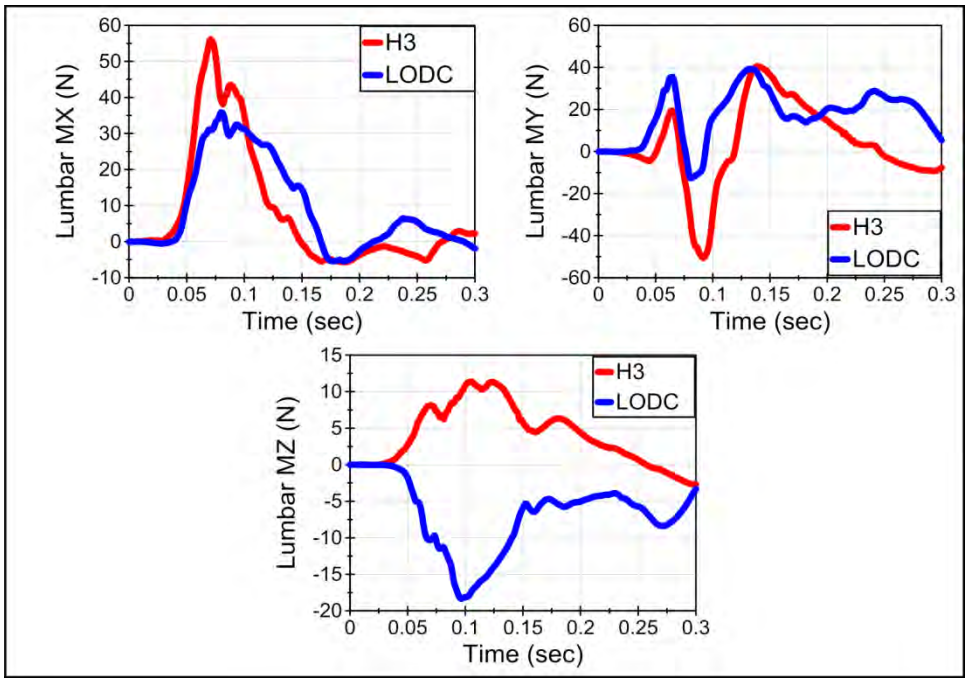

Figure 159. Lumbar moments in the LODC and HIII-10C using a high back booster seat in 40 km/h test.

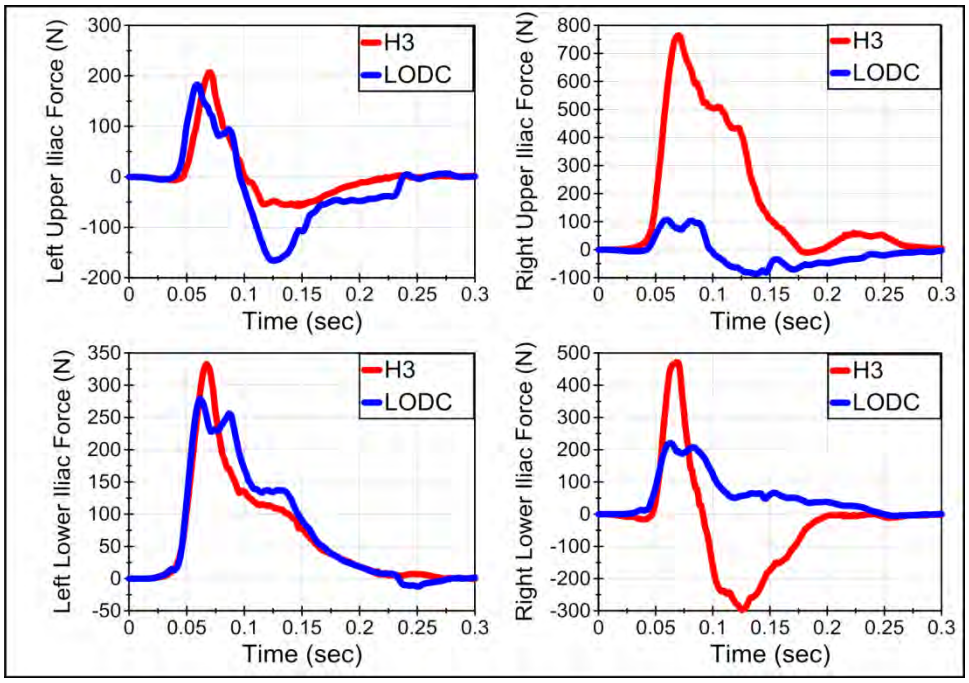

Figure 160. Iliac forces in the LODC and HIII-10C using a high back booster seat in 40 km/h test.

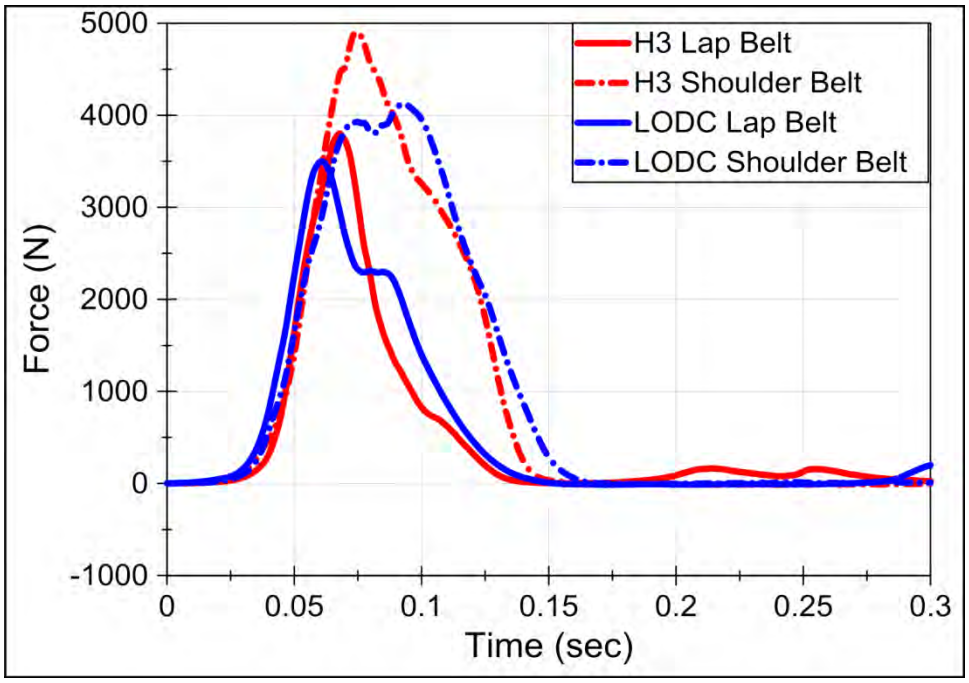

Figure 161. Seatbelt loads in the LODC and HIII-10C using a high back booster seat in 40 km/h test.

Backless Booster (Graco TurboBooster)

Time history comparisons of head, mid-spine, and pelvis accelerations and angular rates; upper neck and lumbar forces and moments; iliac and seatbelt forces; and chest compressions for the LODC and HIII-10C dummies seated in a backless booster seat (Graco TurboBooster) are shown in Figures 162-171 below. The LODC time histories are represented by the blue curves. The HIII-10C time histories are represented by the red curves.

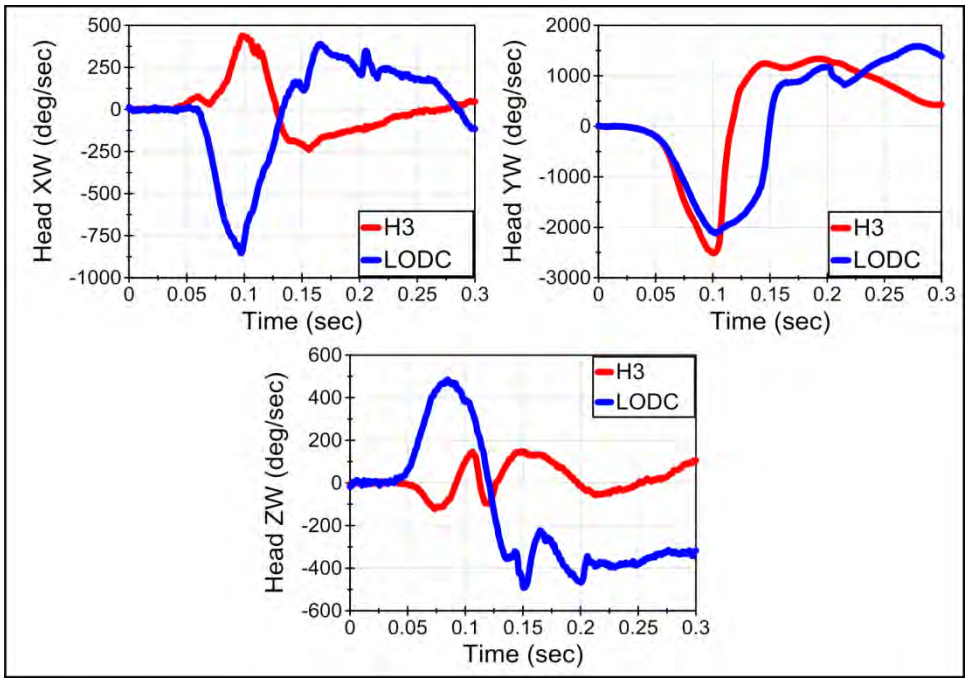

Figure 162. Head angular rates in the LODC and HIII-10C using a backless booster seat in 40 km/h test.

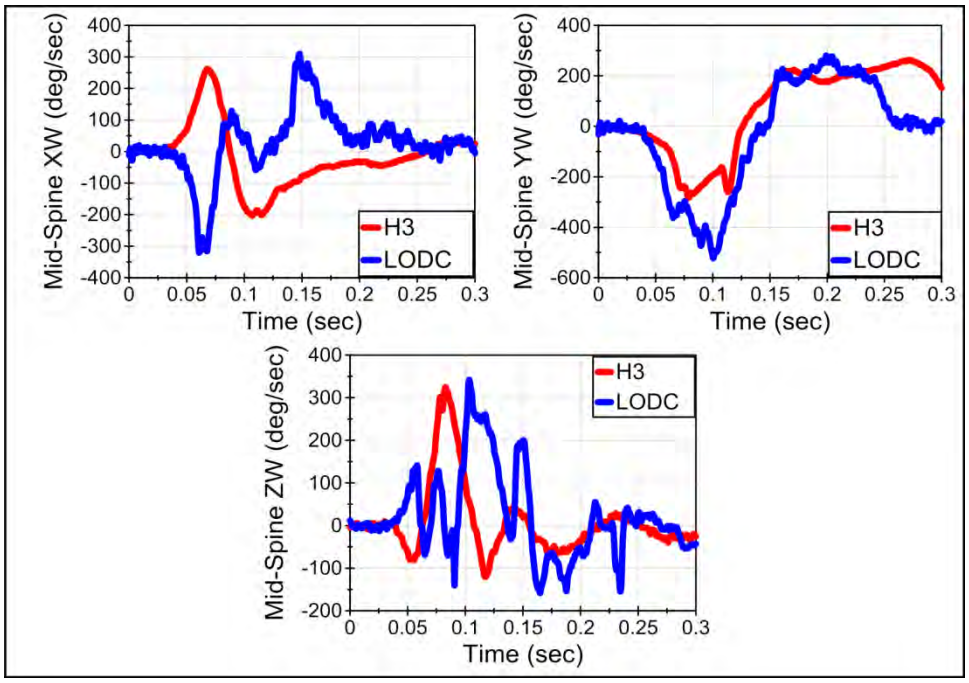

Figure 163. Mid-spine angular rates in the LODC and HIII-10C using a backless booster seat in 40 km/h test.

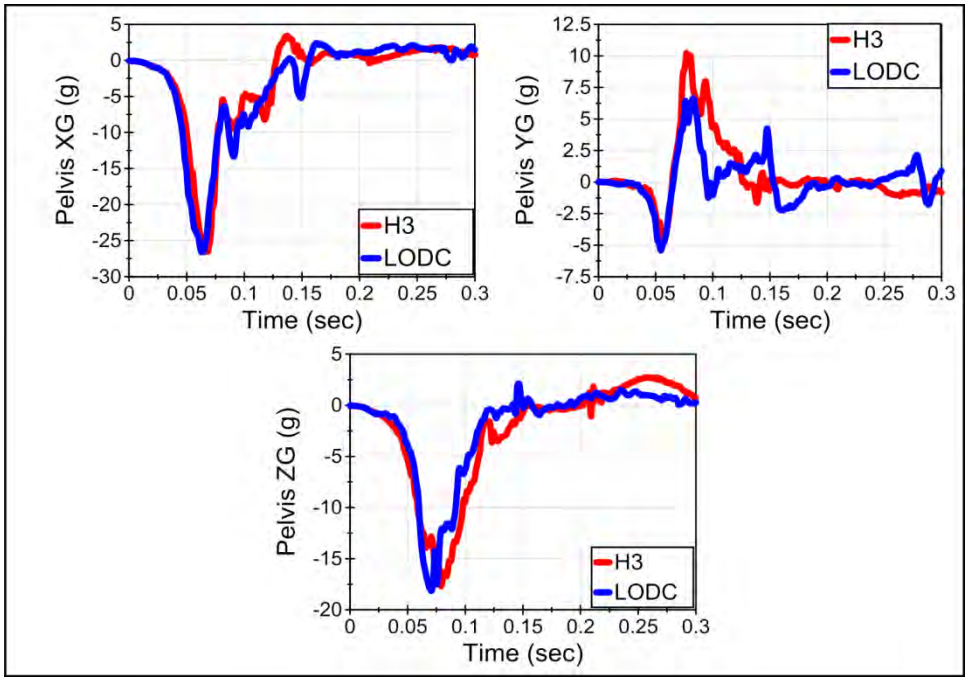

Figure 164. Pelvis accelerations in the LODC and HIII-10C using a backless booster seat in 40 km/h test.

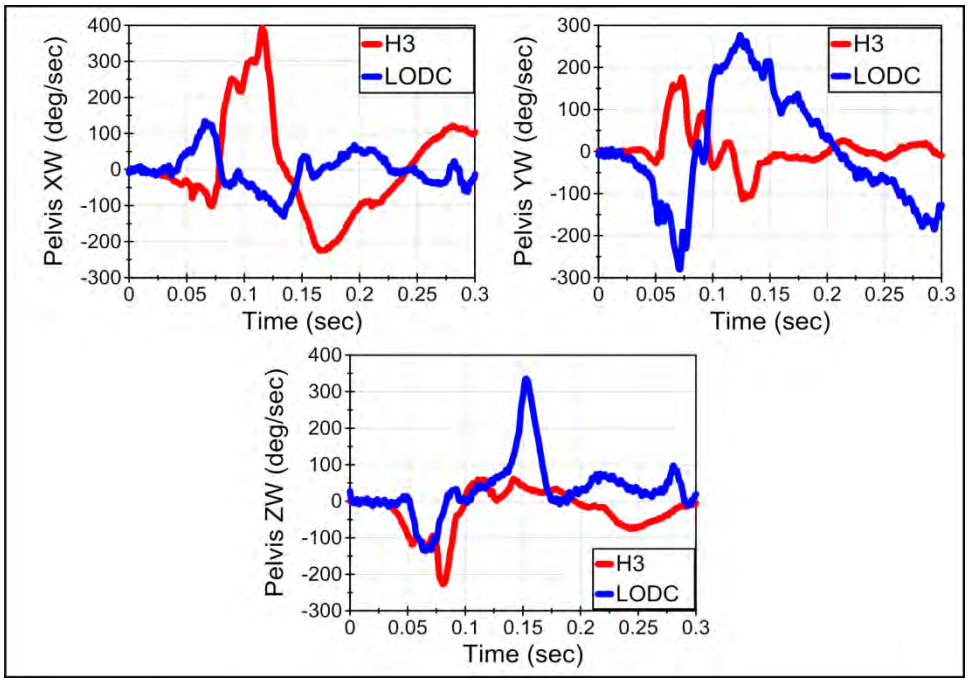

Figure 165. Pelvis angular rates in the LODC and HIII-10C using a backless booster seat in 40 km/h test.

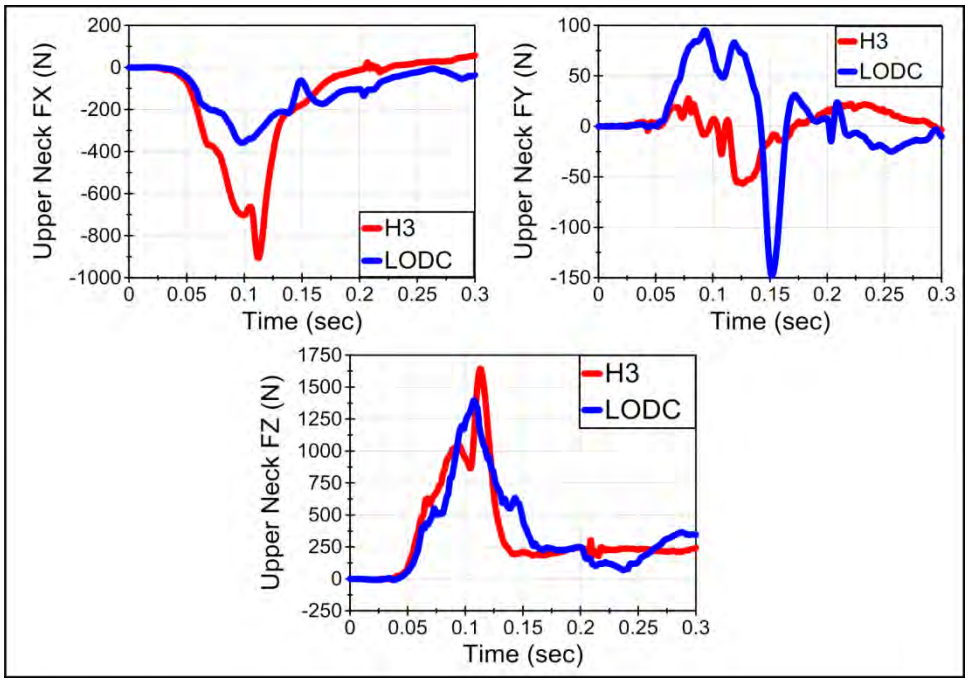

Figure 166. Upper neck forces in the LODC and HIII-10C using a backless booster seat in 40 km/h test.

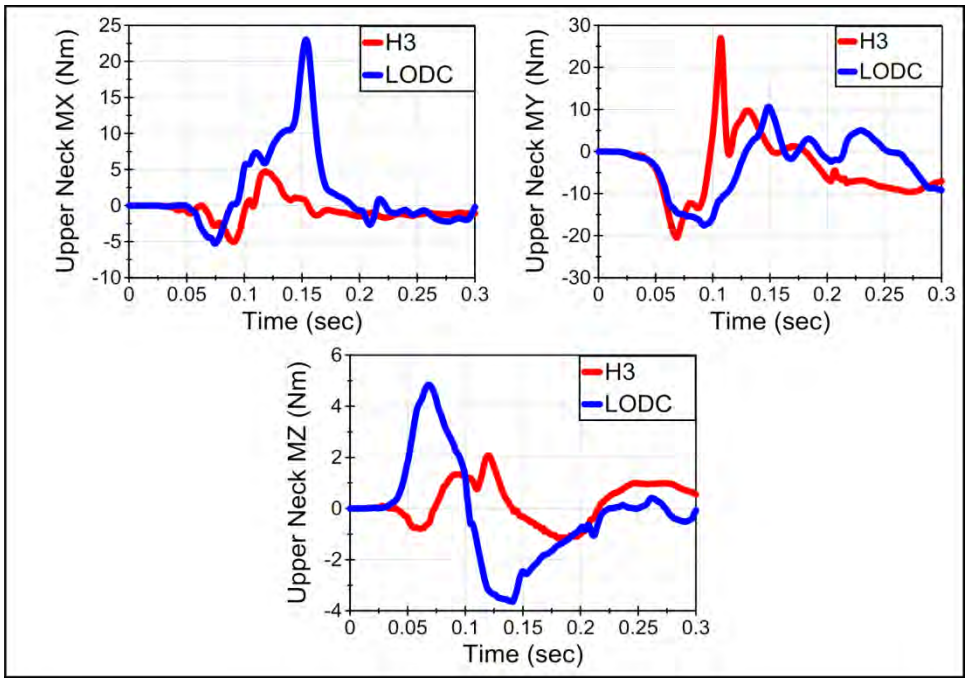

Figure 167. Upper neck moments in the LODC and HIII-10C using a backless booster seat in 40 km/h test.

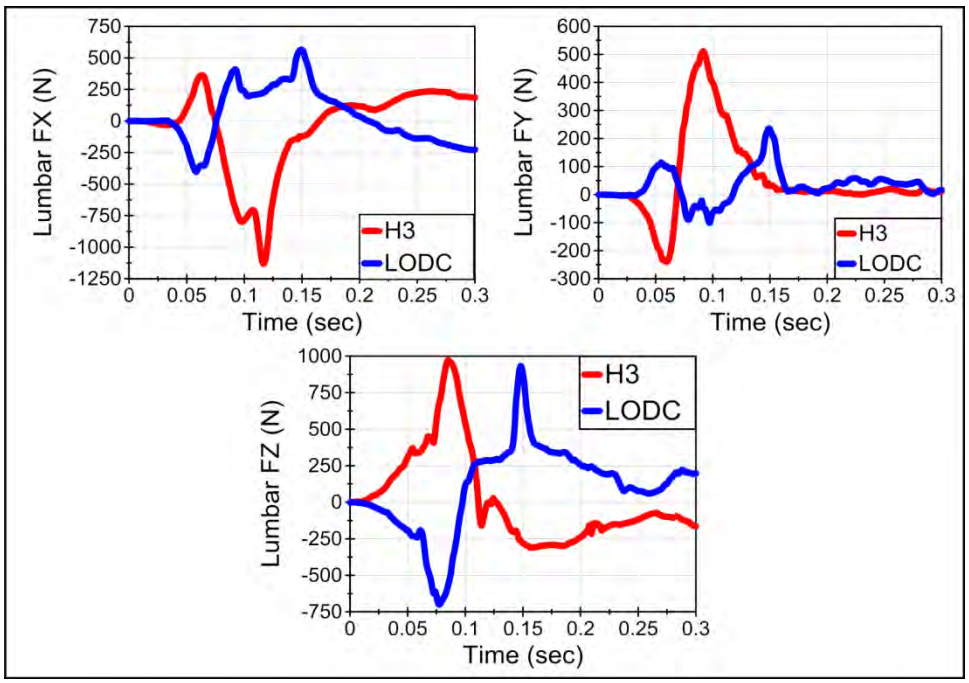

Figure 168. Lumbar forces in the LODC and HIII-10C using a backless booster seat in 40 km/h test.

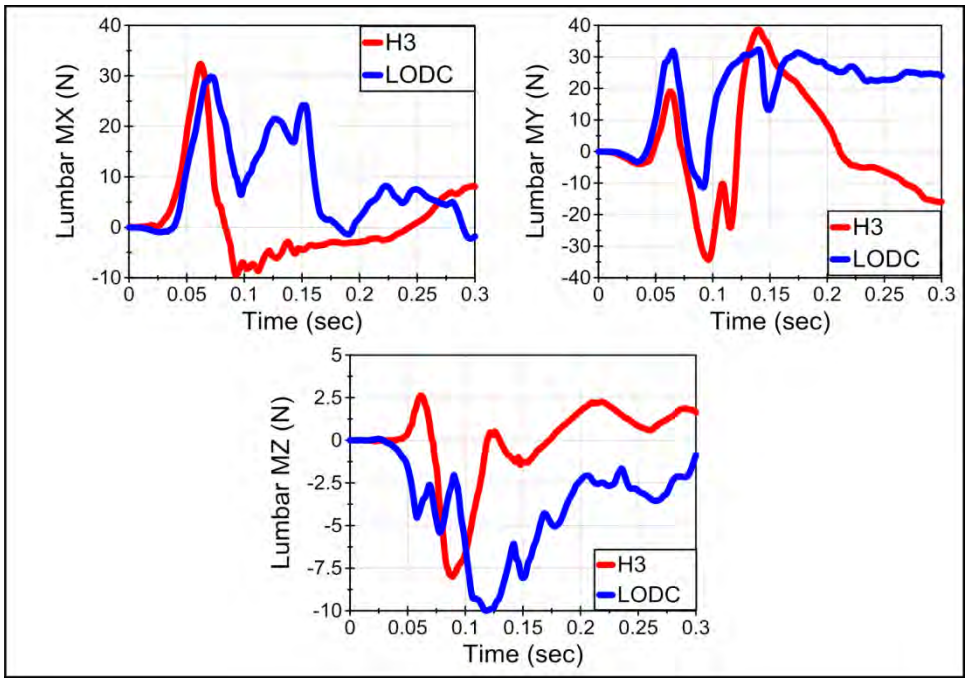

Figure 169. Lumbar moments in the LODC and HIII-10C using a backless booster seat in 40 km/h test.

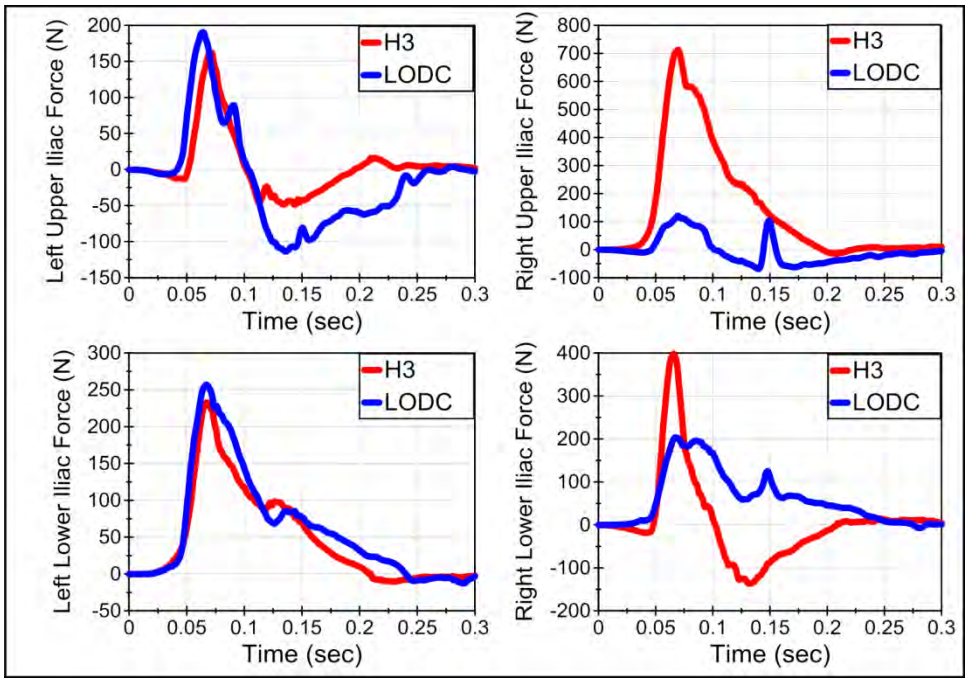

Figure 170. Iliac forces in the LODC and HIII-10C using a backless booster seat in 40 km/h test.

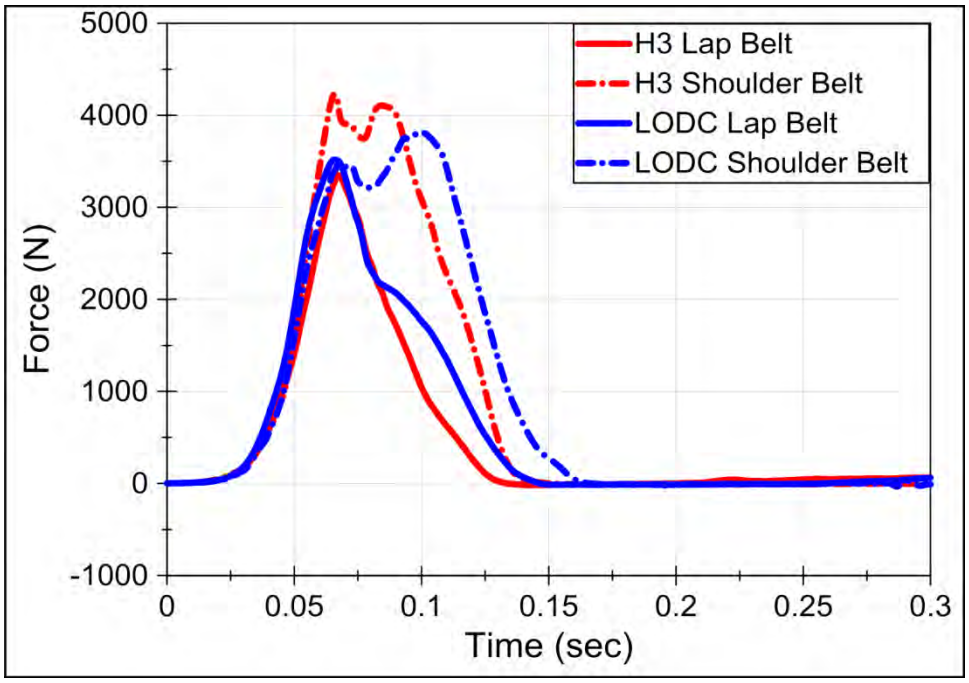

Figure 171. Seatbelt loads in the LODC and HIII-10C using a backless booster seat in 40 km/h test.

No Child Restraint (3-Point Belt)

Time history comparisons of head, mid-spine, and pelvis accelerations and angular rates; upper neck and lumbar forces and moments; iliac and seatbelt forces; and chest compressions for the LODC and HIII-10C seated without a child restraint system are shown in Figures 172-181 below. The LODC time histories are represented by the blue curves. The HIII-10C time histories are represented by the red curves.

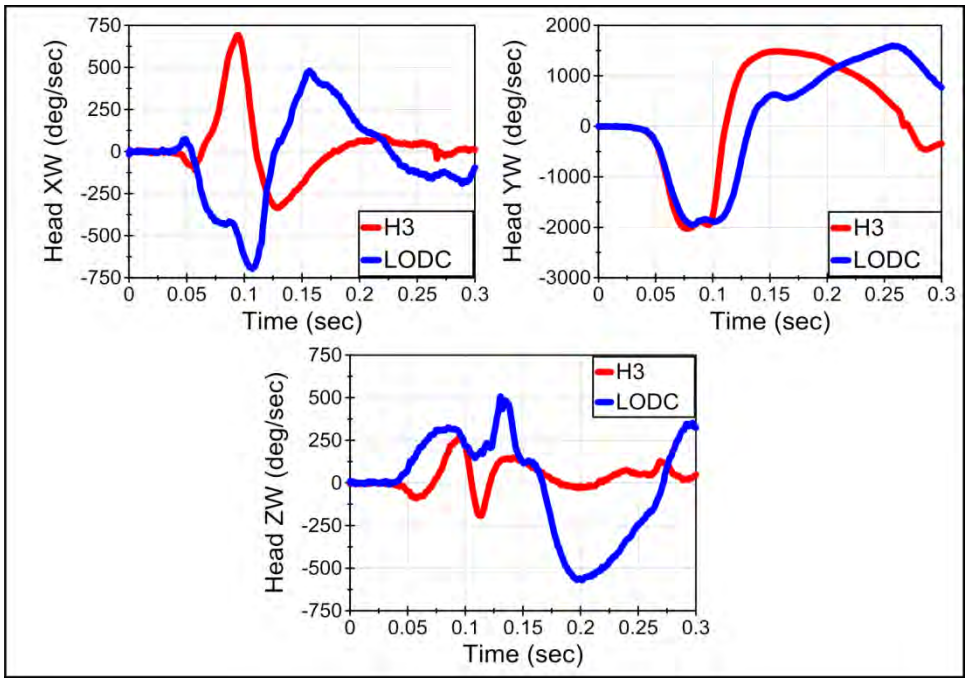

Figure 172. Head angular rates in the LODC and HIII-10C using no child restraint system in 40 km/h test.

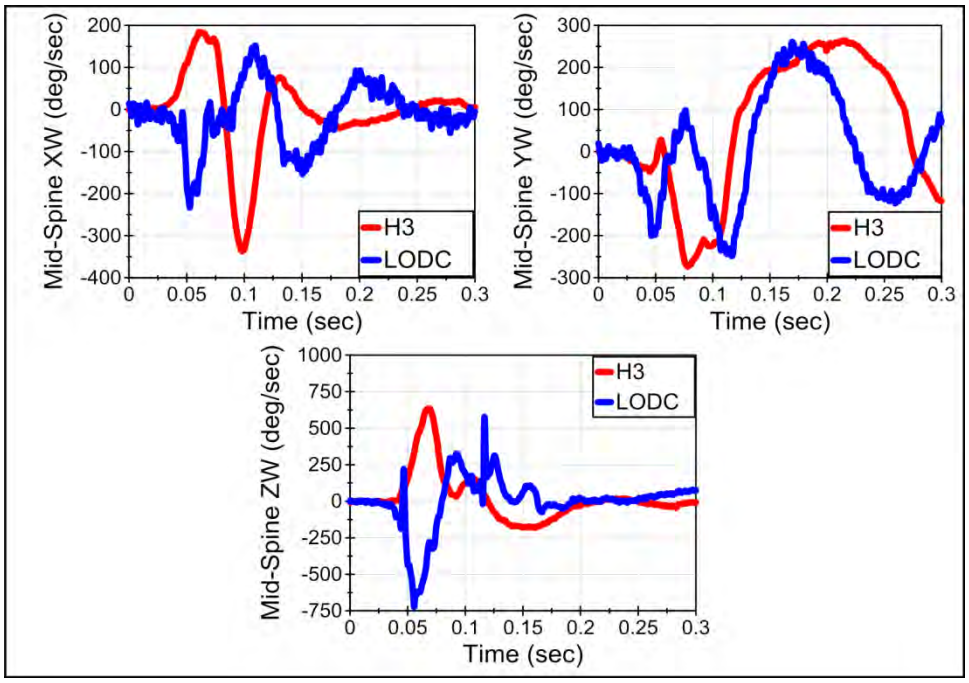

Figure 173. Mid-spine angular rates in the LODC and HIII-10C using no child restraint system in 40 km/h test.

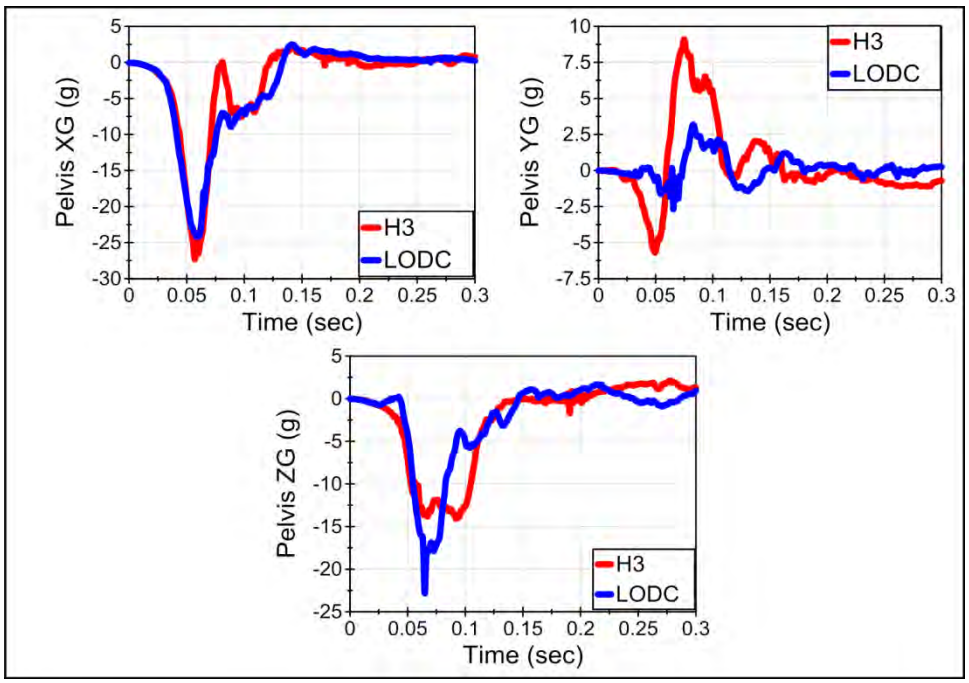

Figure 174. Pelvis accelerations in the LODC and HIII-10C using no child restraint system in 40 km/h test.

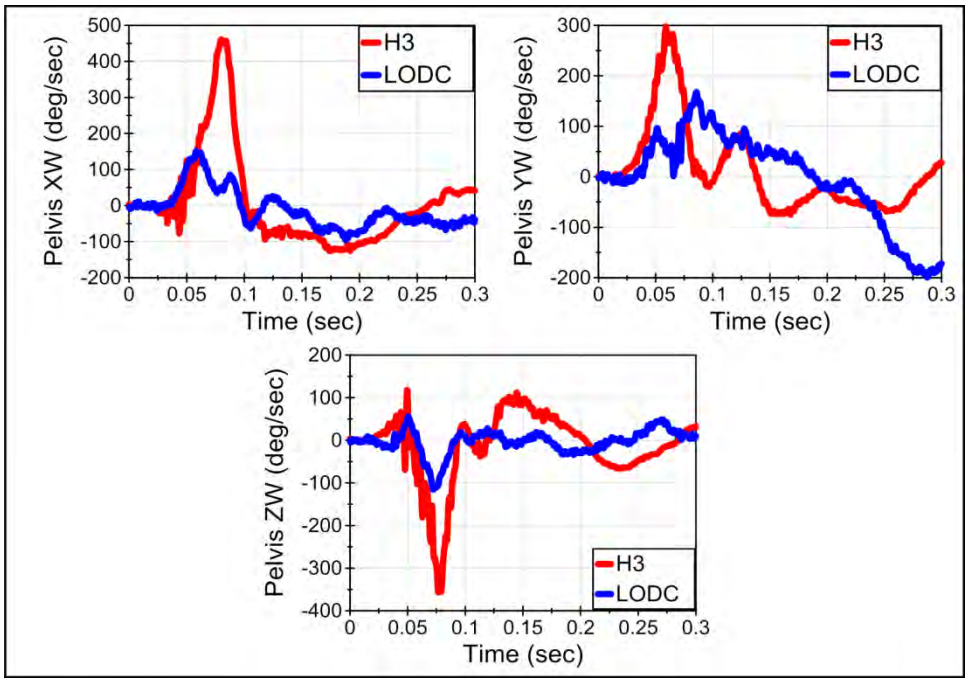

Figure 175. Pelvis angular rates in the LODC and HIII-10C using no child restraint system in 40 km/h test.

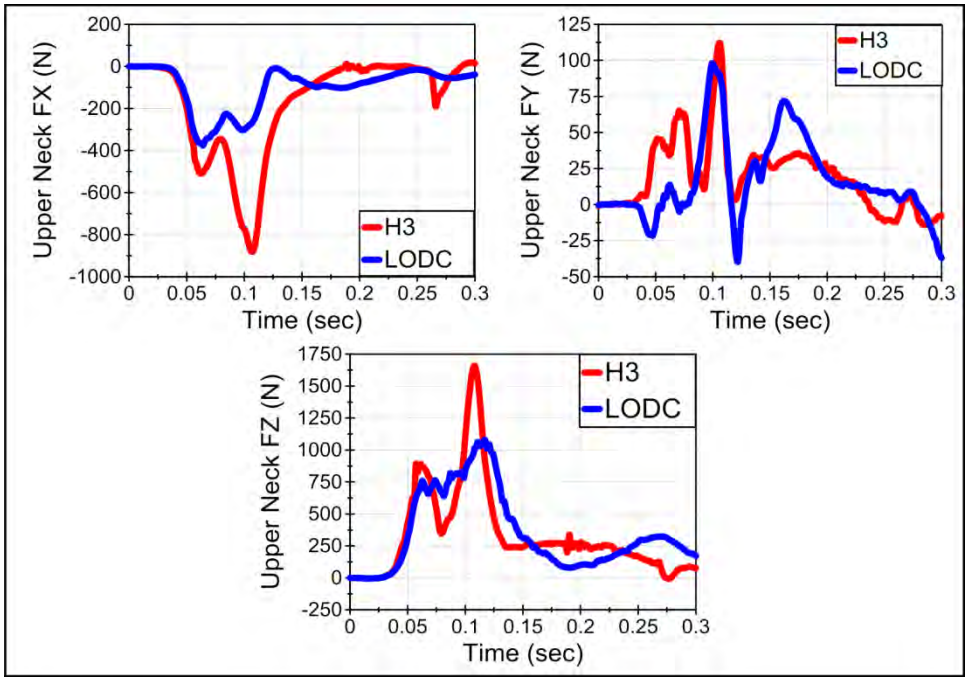

Figure 176. Upper neck forces in the LODC and HIII-10C using no child restraint system in 40 km/h test.

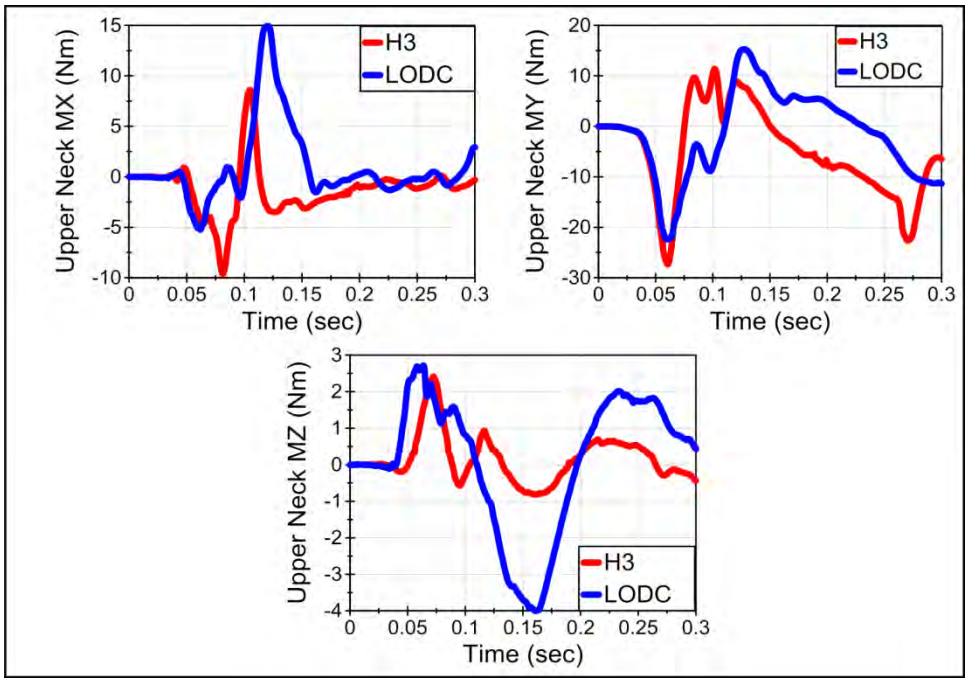

Figure 177. Upper neck moments in the LODC and HIII-10C using no child restraint system in 40 km/h test.

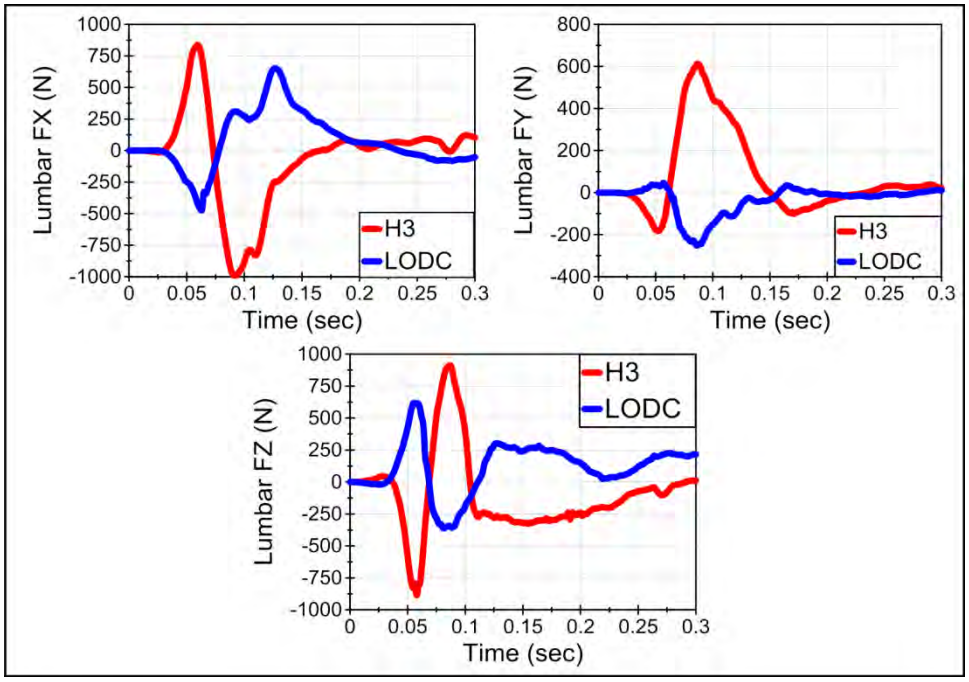

Figure 178. Lumbar forces in the LODC and HIII-10C using no child restraint system in 40 km/h test.

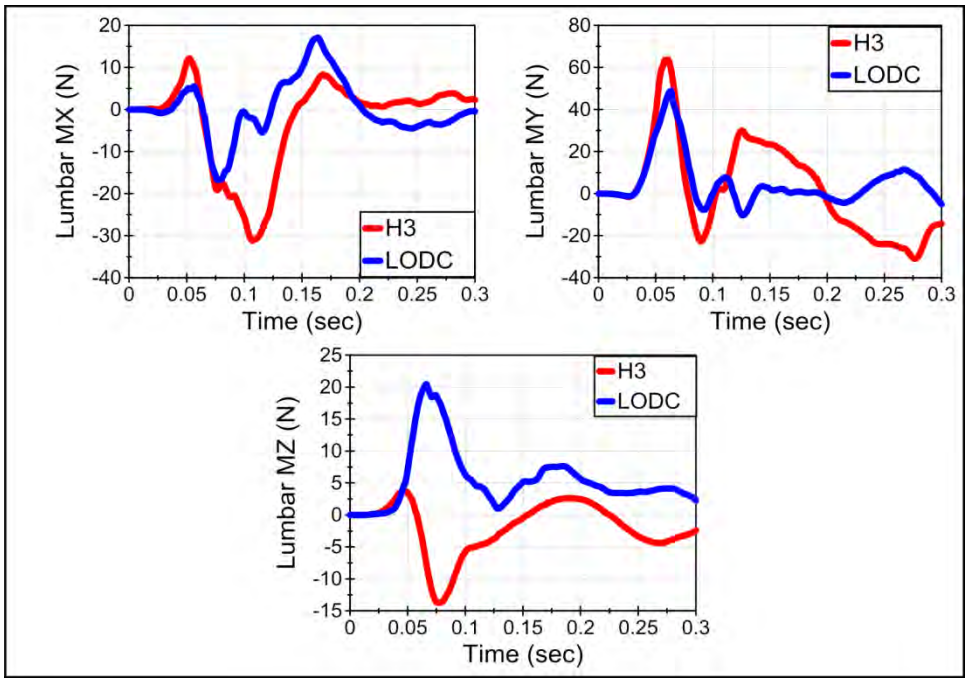

Figure 179. Lumbar moments in the LODC and HIII-10C using no child restraint system in 40 km/h test.

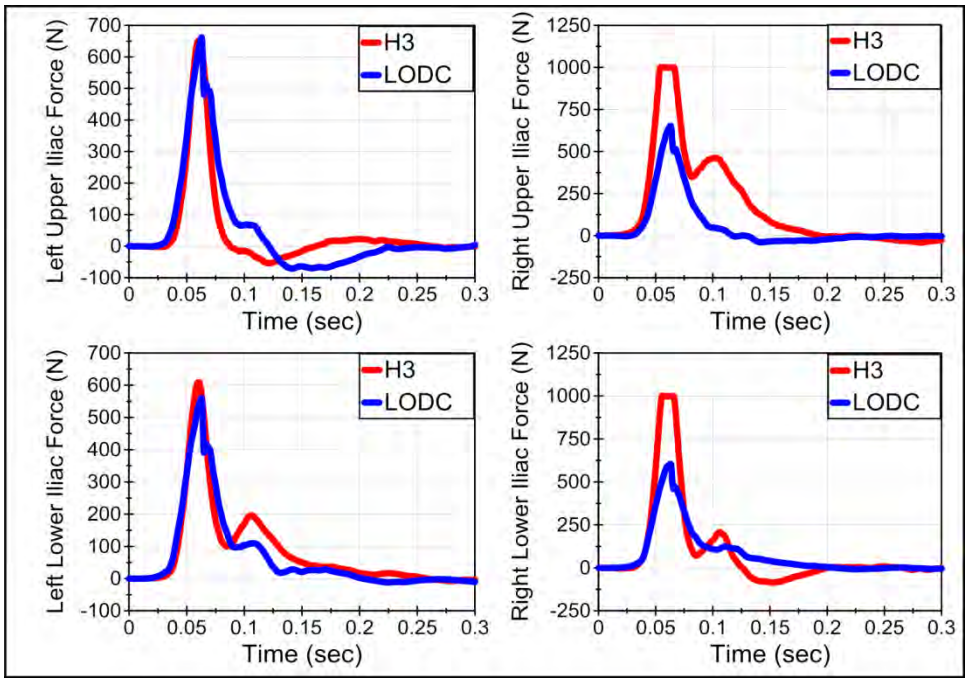

Figure 180. Iliac forces in the LODC and HIII-10C using no child restraint system in 40 km/h test.

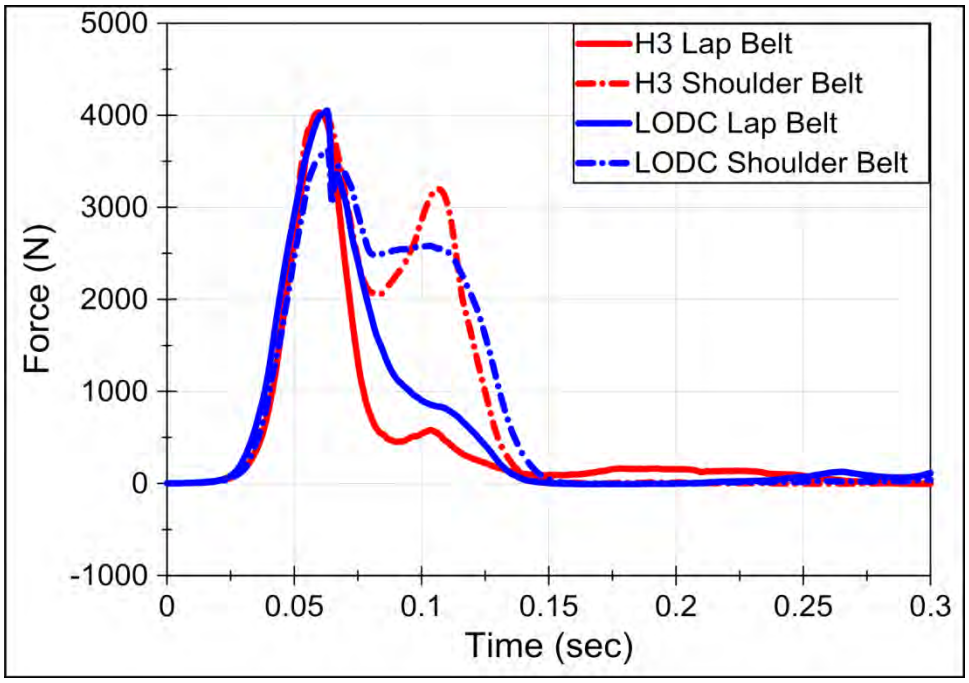

Figure 181. Seatbelt loads in the LODC and HIII-10C using no child restraint system in 40 km/h test.

Appendix C: High-Speed (48 km/h) Time Histories

5-Point Harness (Britax Frontier 85)

Time history comparisons of head, mid-spine, and pelvis accelerations and angular rates; upper neck and lumbar forces and moments; iliac and seatbelt forces; and chest compressions for the LODC and HIII-10C dummies seated in a 5-point harness (Britax Frontier 85) are shown in Figures 182-191 below. The LODC time histories are represented by the blue curves. The HIII-10C time histories are represented by the red curves.

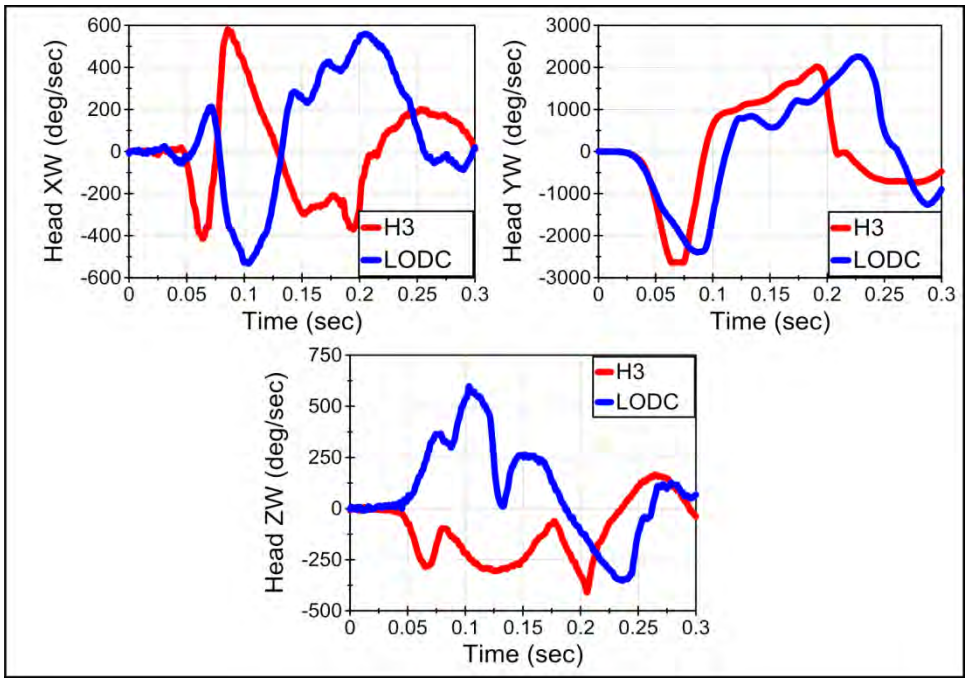

Figure 182. Head angular rates in the LODC and HIII-10C using a 5-point harness in 48 km/h (FMVSS No. 213) test.

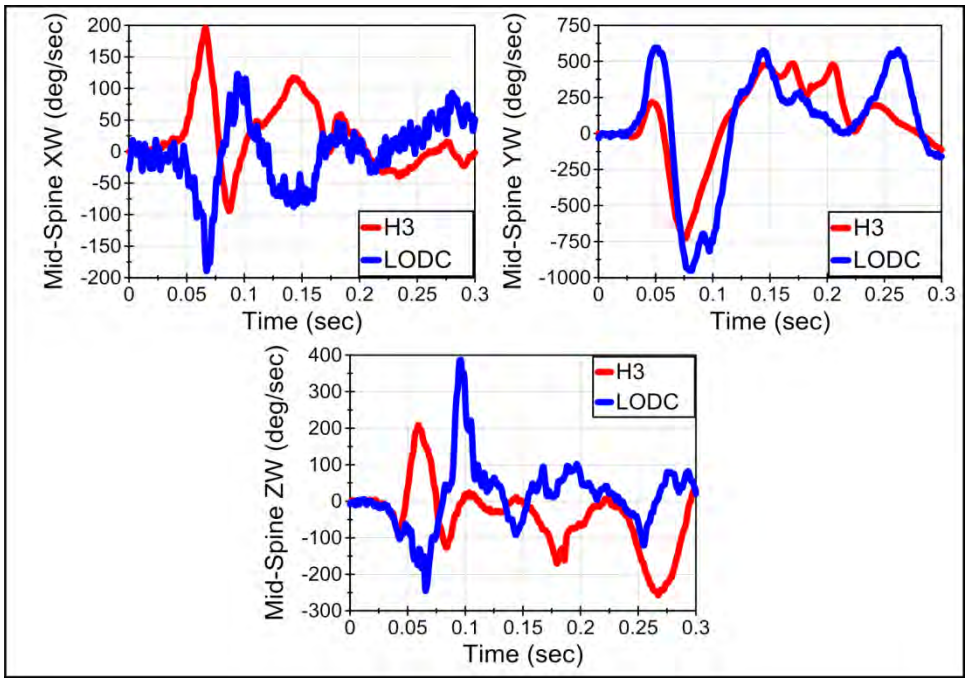

Figure 183. Mid-spine angular rates in the LODC and HIII-10C using a 5-point harness in 48 km/h (FMVSS No. 213) test.

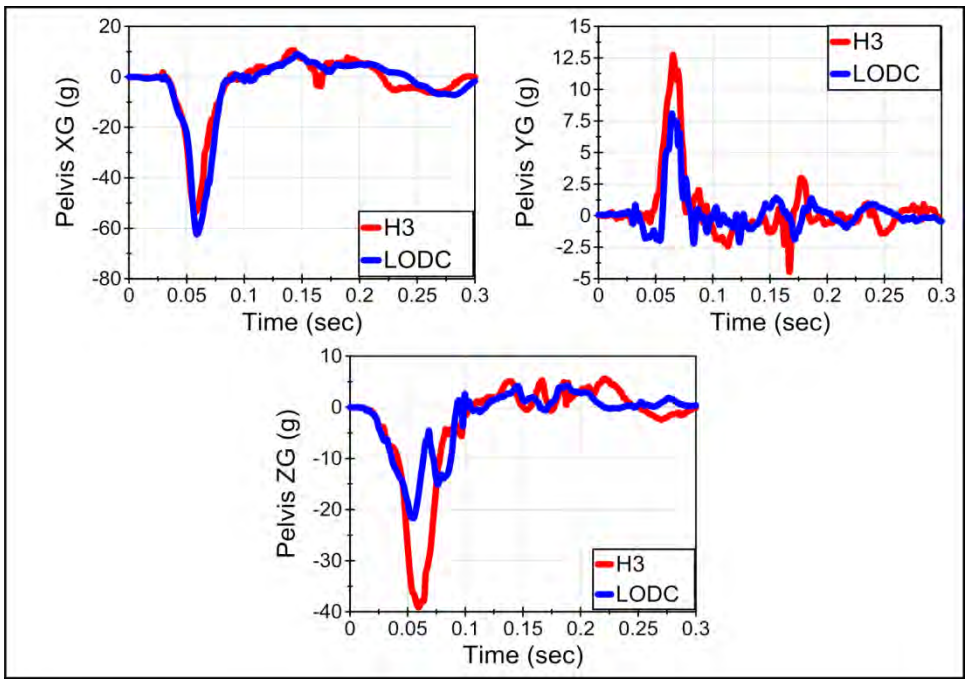

Figure 184. Pelvis accelerations in the LODC and HIII-10C using a 5-point harness in 48 km/h (FMVSS No. 213) test.

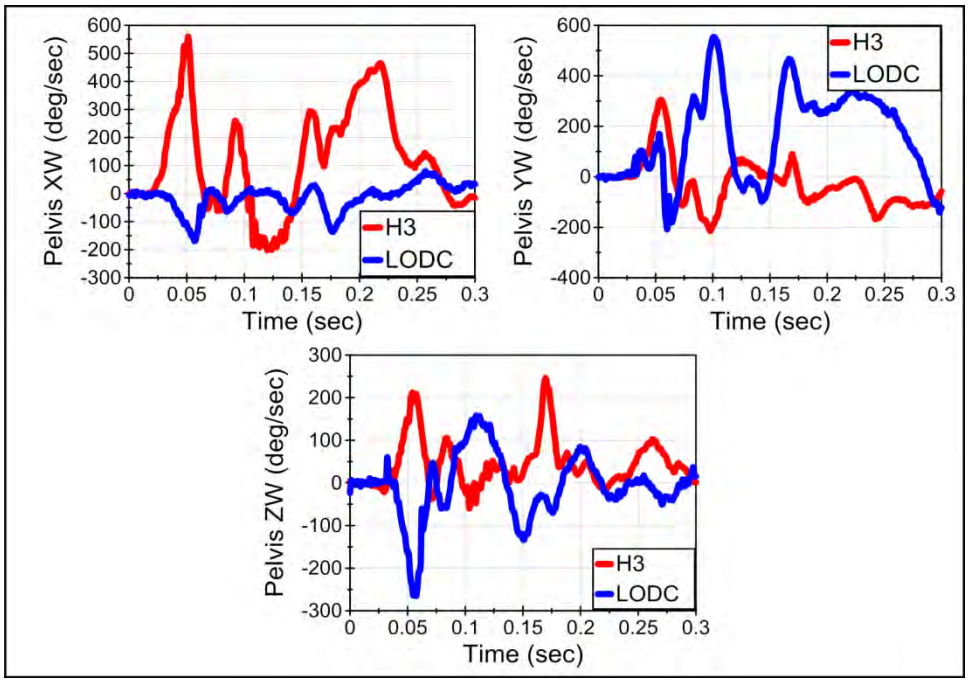

Figure 185. Pelvis angular rates in the LODC and HIII-10C using a 5-point harness in 48 km/h (FMVSS No. 213) test.

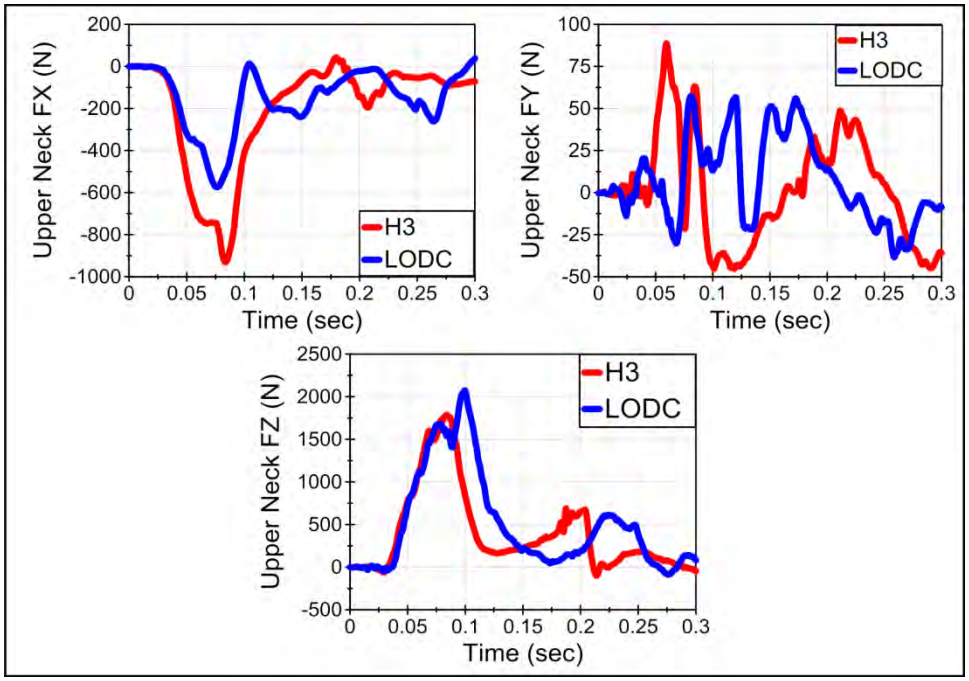

Figure 186. Upper neck forces in the LODC and HIII-10C using a 5-point harness in 48 km/h (FMVSS No. 213) test.

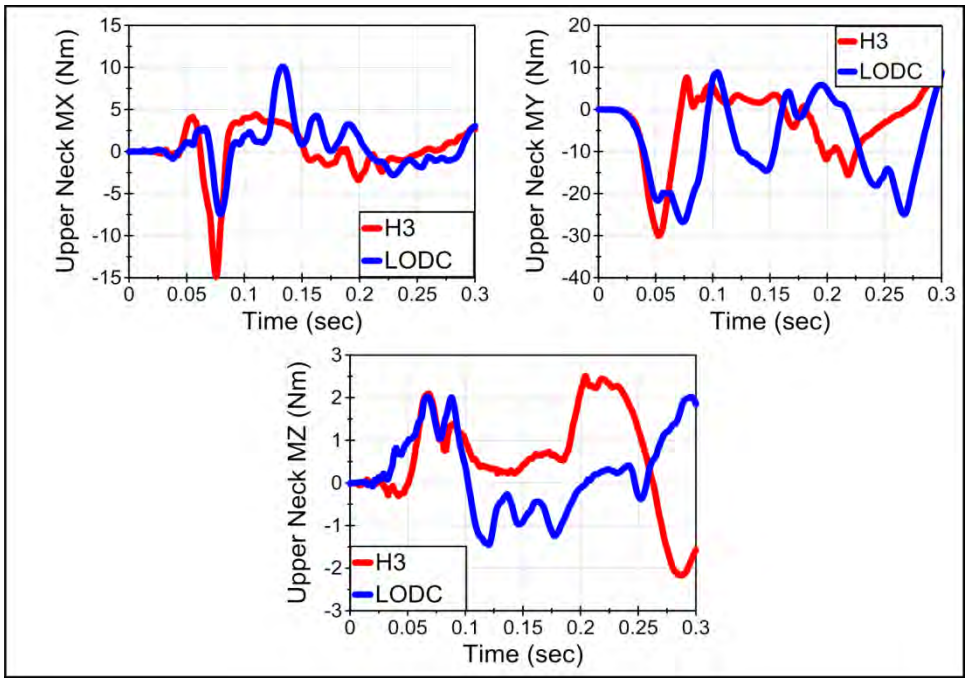

Figure 187. Upper neck moments in the LODC and HIII-10C using a 5-point harness in 48 km/h (FMVSS No. 213) test.

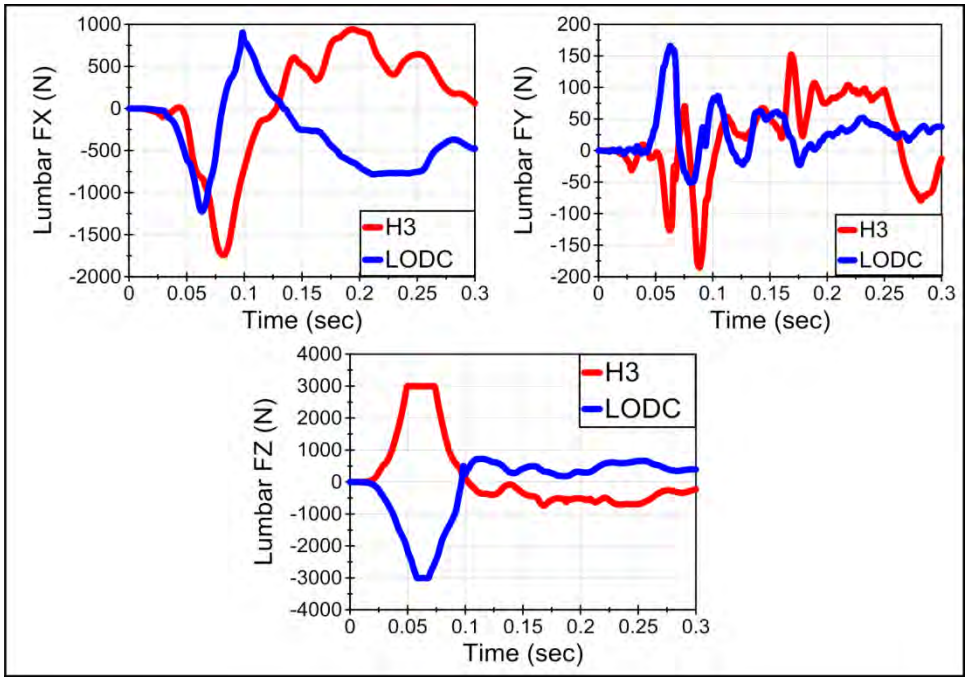

Figure 188. Lumbar forces in the LODC and HIII-10C using a 5-point harness in 48 km/h (FMVSS No. 213) test.

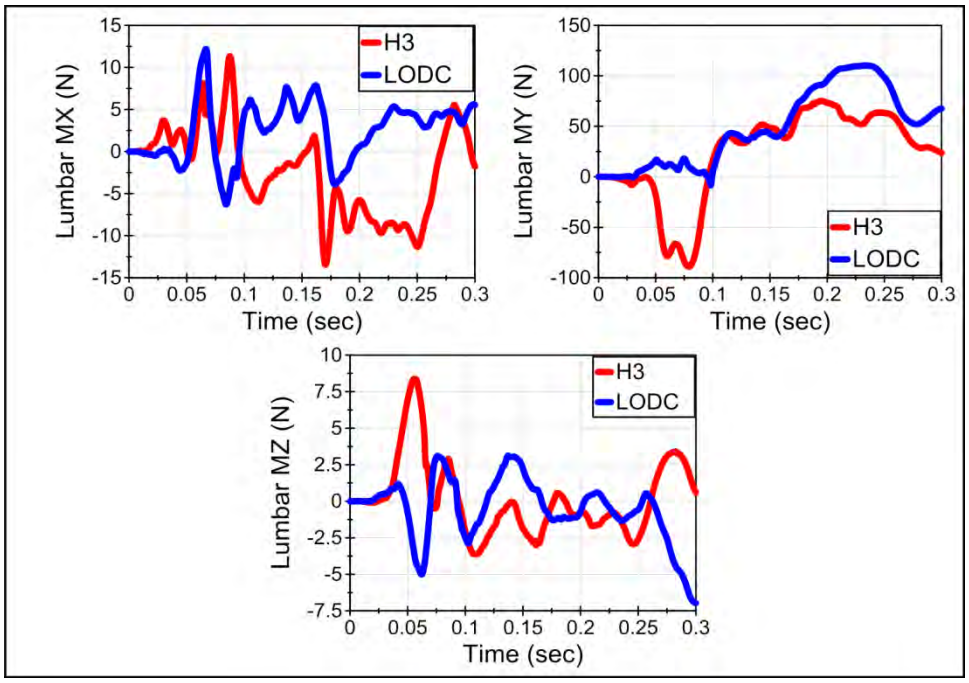

Figure 189. Lumbar moments in the LODC and HIII-10C using a 5-point harness in 48 km/h (FMVSS No. 213) test.

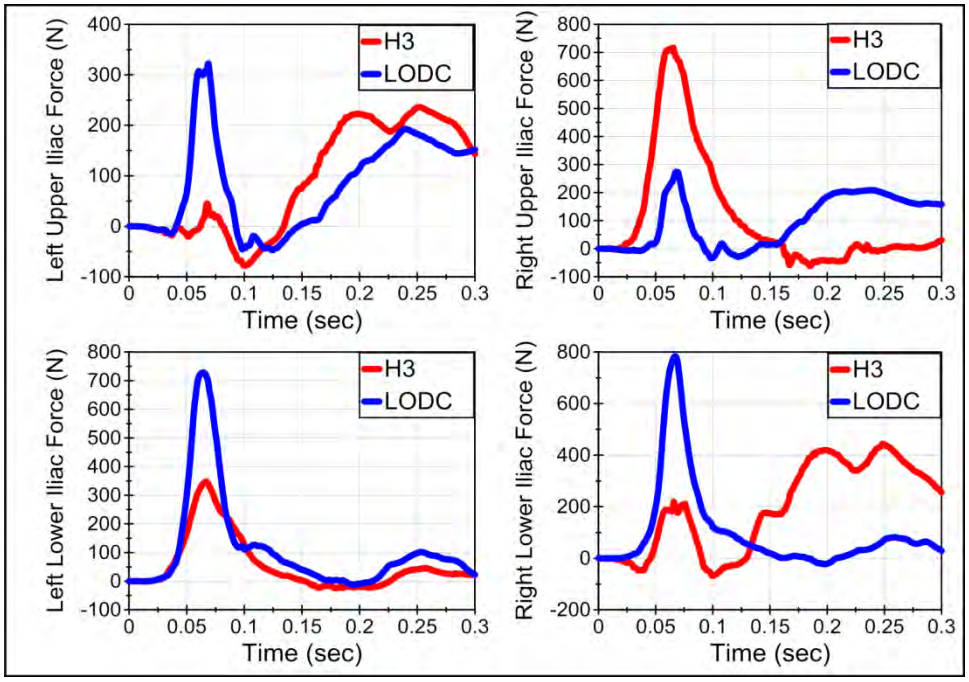

Figure 190. Iliac forces in the LODC and HIII-10C using a 5-point harness in 48 km/h (FMVSS No. 213) test.

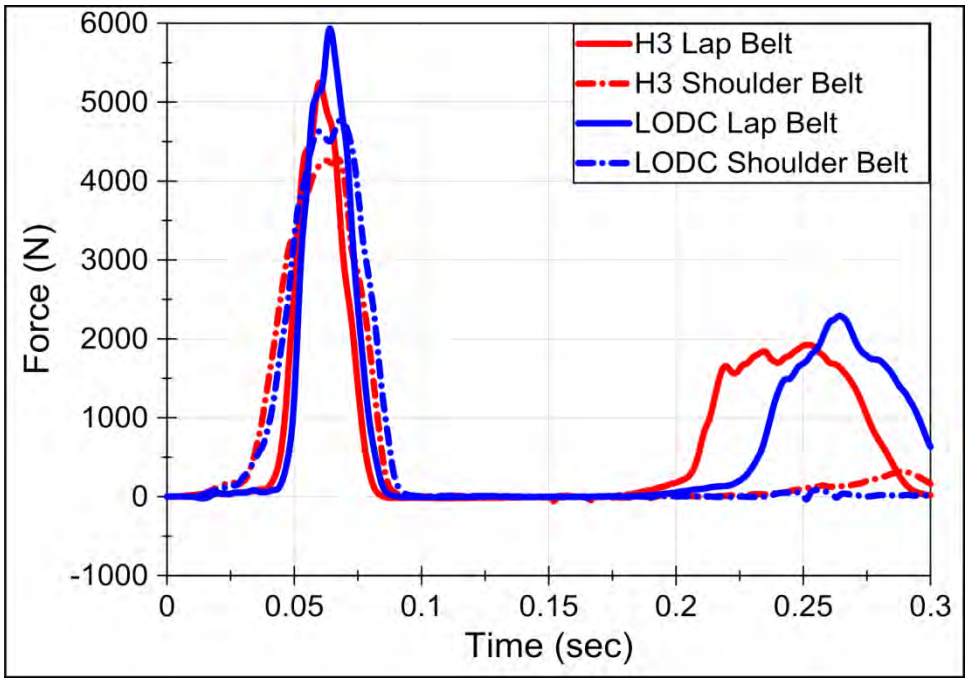

Figure 191. Seatbelt loads in the LODC and HIII-10C using a 5-point harness in 48 km/h (FMVSS No. 213) test.

High Back Booster (Graco TurboBooster)

Time history comparisons of head, mid-spine, and pelvis accelerations and angular rates; upper neck and lumbar forces and moments; iliac and seatbelt forces; and chest compressions for the LODC and HIII-10C dummies seated in a 5-point harness (Britax Frontier 85) are shown in Figures 192-201 below. The LODC time histories are represented by the blue curves. The HIII-10C time histories are represented by the red curves.

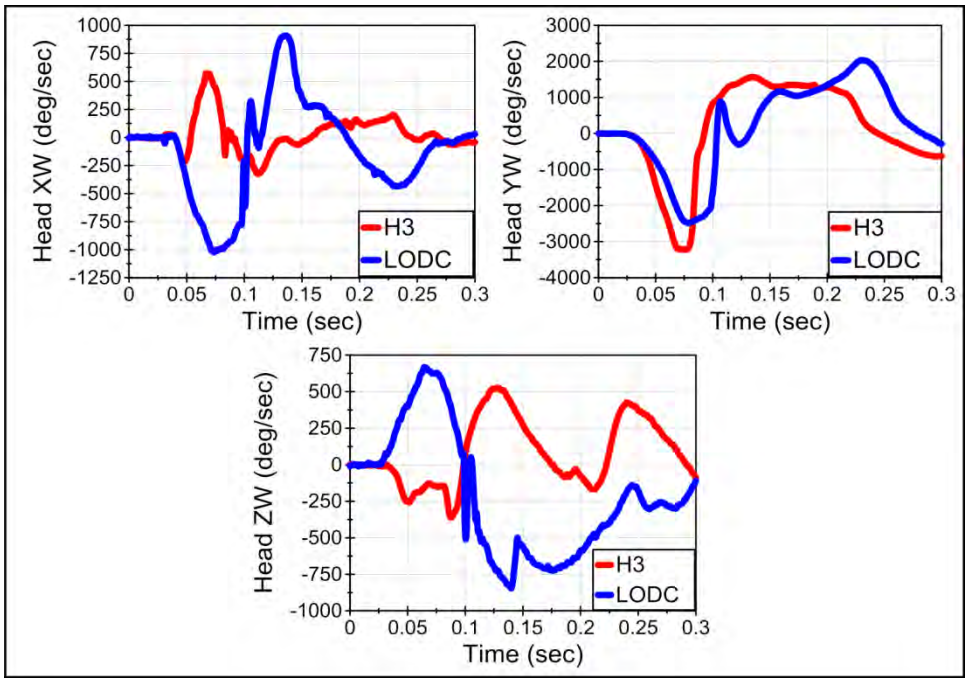

Figure 192. Head angular rates in the LODC and HIII-10C using a high back booster seat in 48 km/h (FMVSS No. 213) test.

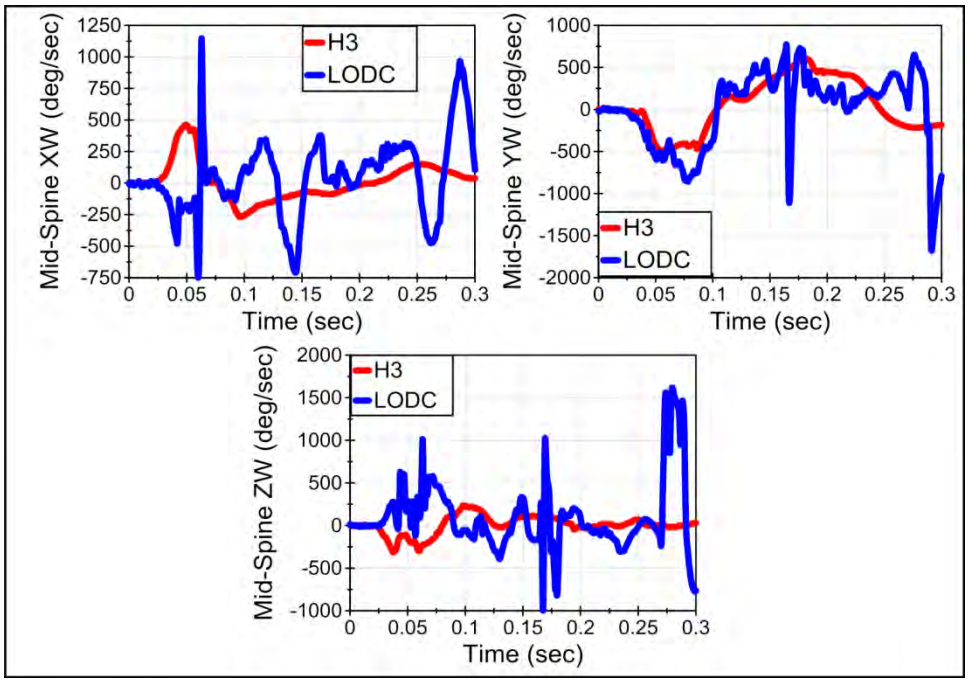

Figure 193. Mid-spine angular rates in the LODC and HIII-10C using a high back booster seat in 48 km/h (FMVSS No. 213) test.

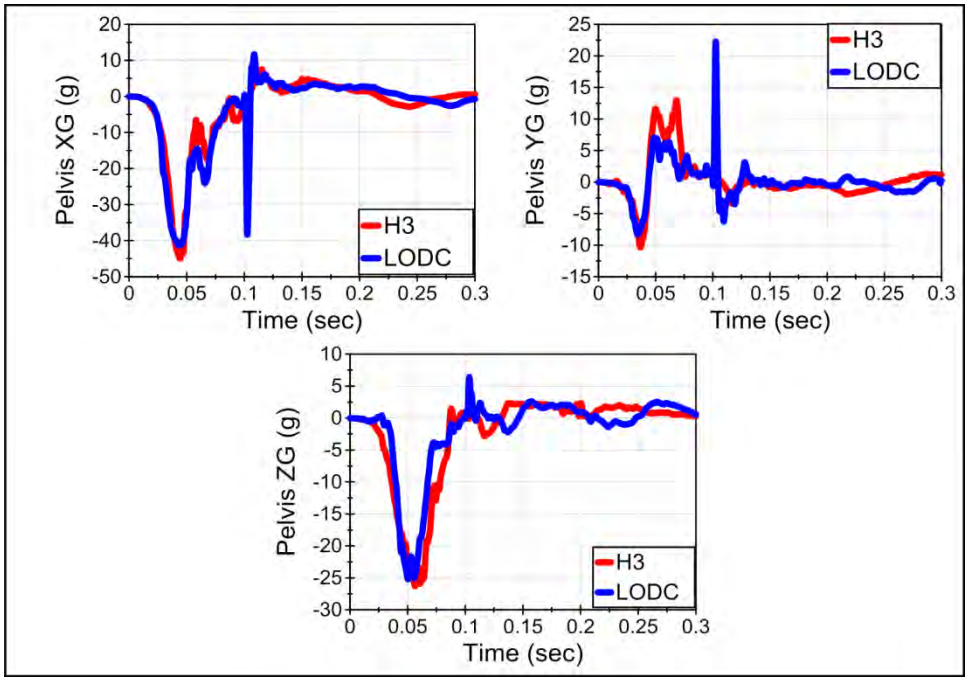

Figure 194. Pelvis accelerations in the LODC and HIII-10C using a high back booster seat in 48 km/h (FMVSS No. 213) test.

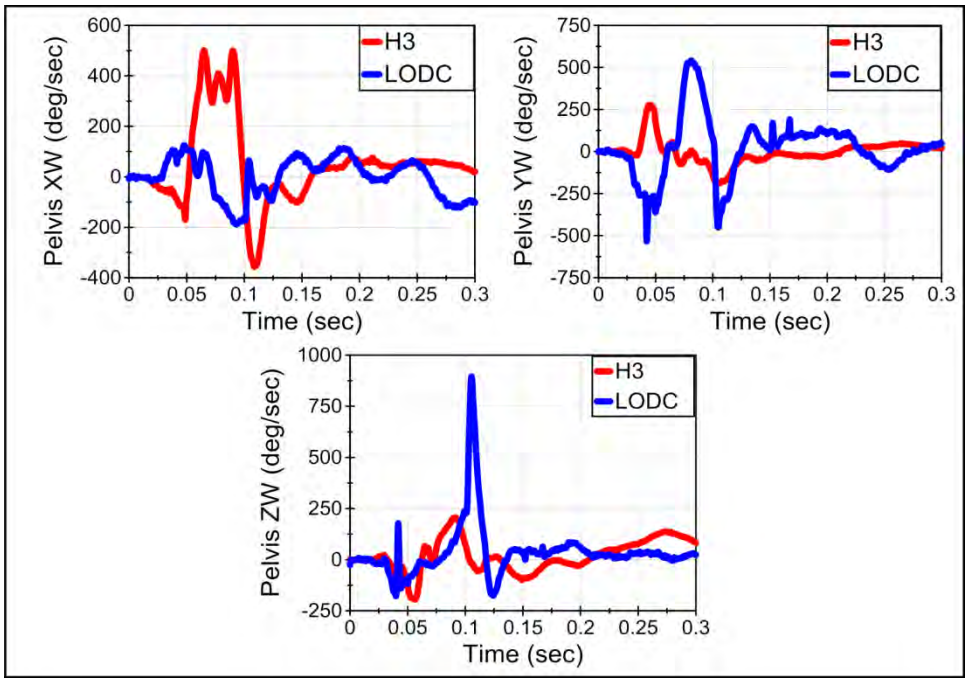

Figure 195. Pelvis angular rates in the LODC and HIII-10C using a high back booster seat in 48 km/h (FMVSS No. 213) test.

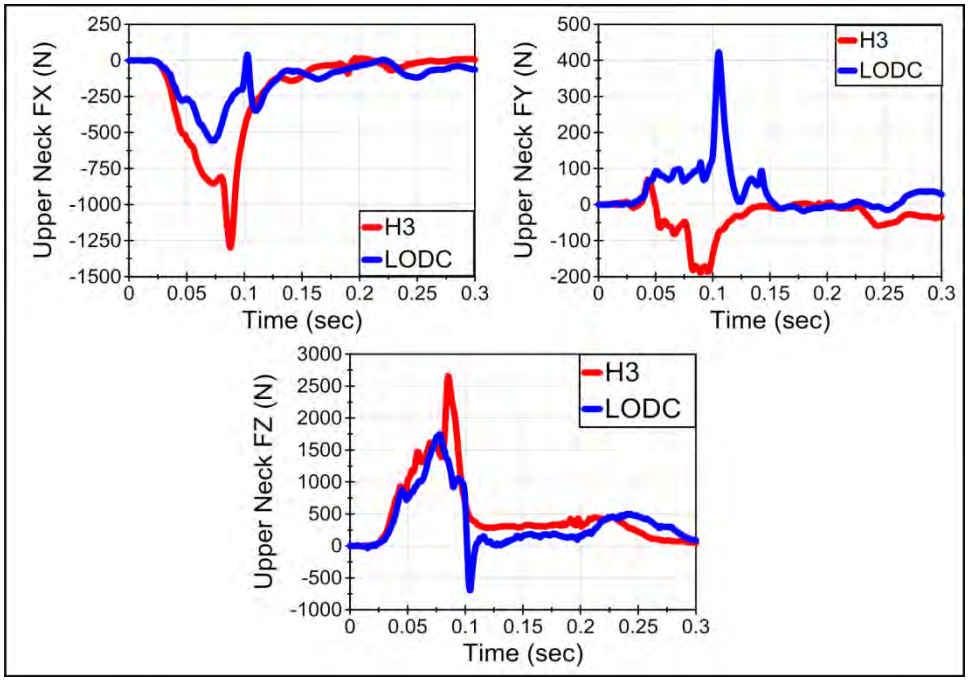

Figure 196. Upper neck forces in the LODC and HIII-10C using a high back booster seat in 48 km/h (FMVSS No. 213) test.

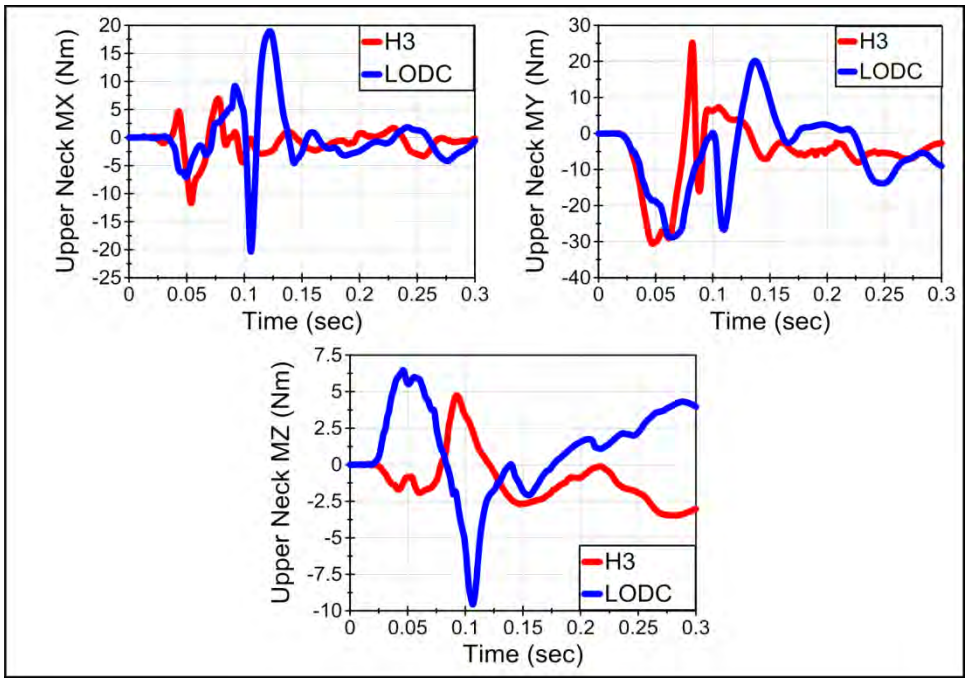

Figure 197. Upper neck moments in the LODC and HIII-10C using a high back booster seat in 48 km/h (FMVSS No. 213) test.

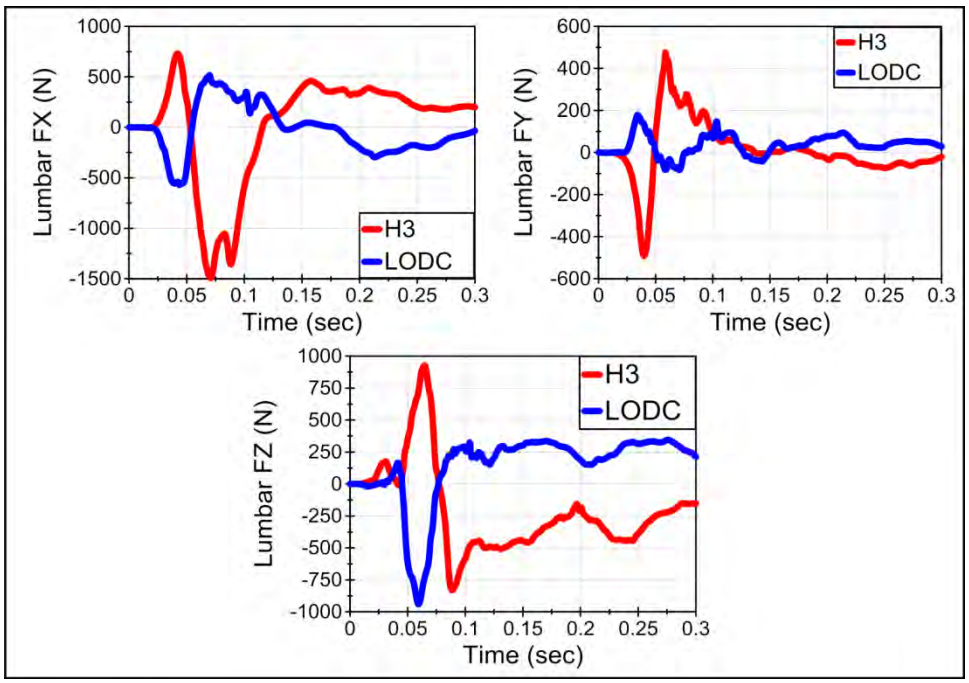

Figure 198. Lumbar forces in the LODC and HIII-10C using a high back booster seat in 48 km/h (FMVSS No. 213) test.

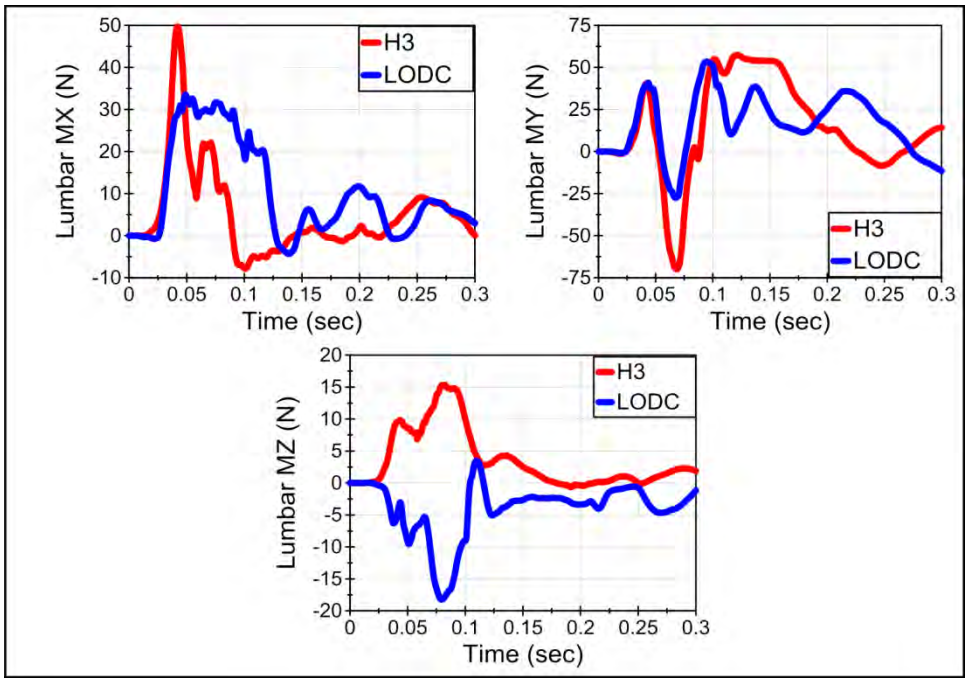

Figure 199. Lumbar moments in the LODC and HIII-10C using a high back booster seat in 48 km/h (FMVSS No. 213) test.

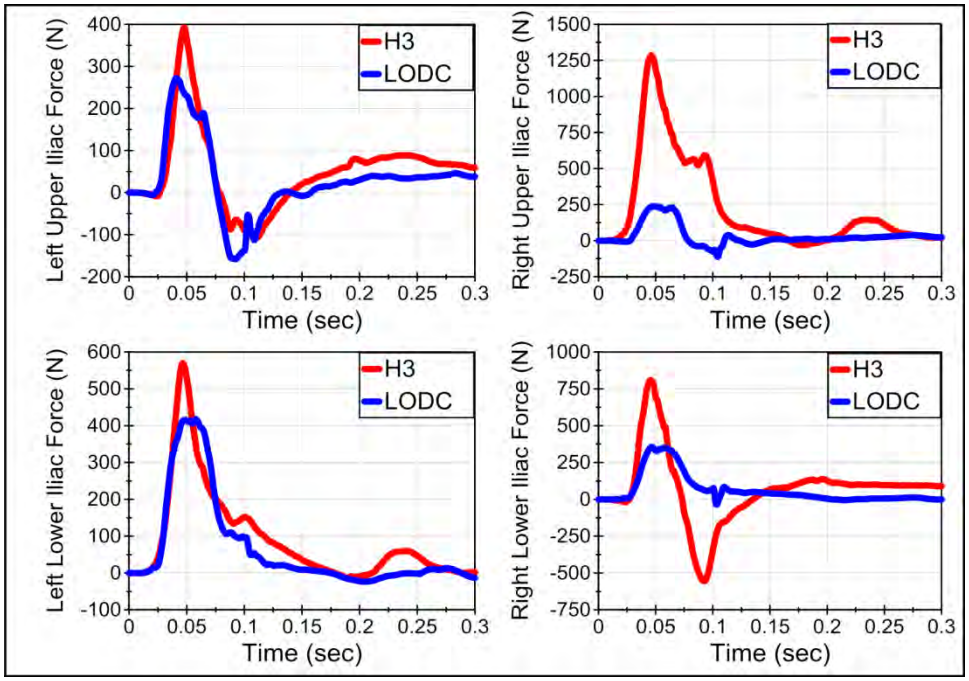

Figure 200. Iliac forces in the LODC and HIII-10C using a high back booster seat in 48 km/h (FMVSS No. 213) test.

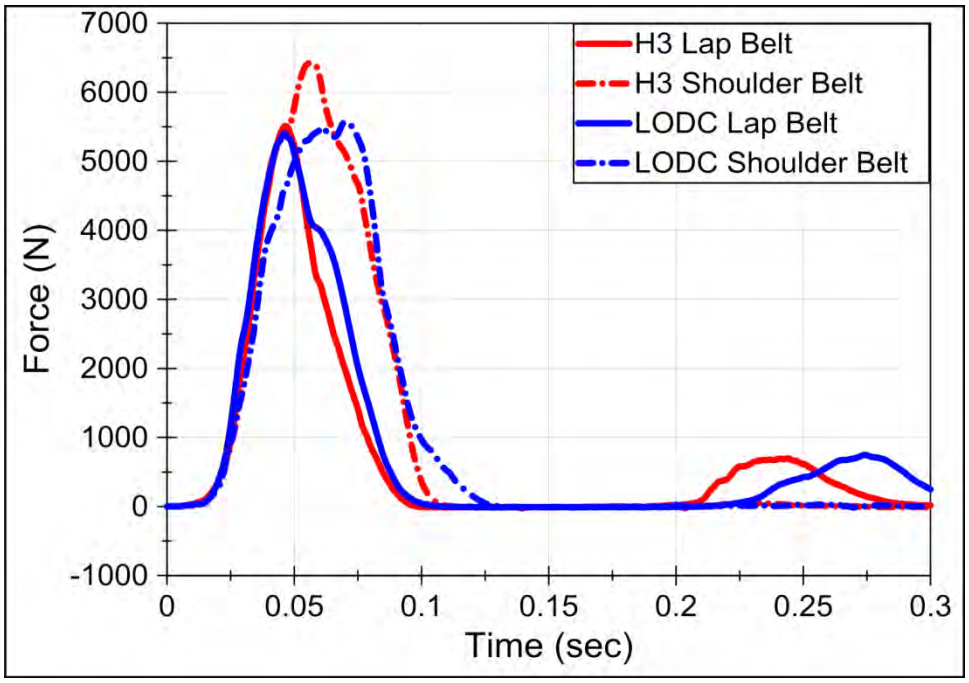

Figure 201. Seatbelt loads in the LODC and HIII-10C using a high back booster seat in 48 km/h (FMVSS No. 213) test.

Appendix D: LODC Comparison

Figures 202-235 compare the responses of the LODC in each of the four child restraint configurations tested for all data channels.

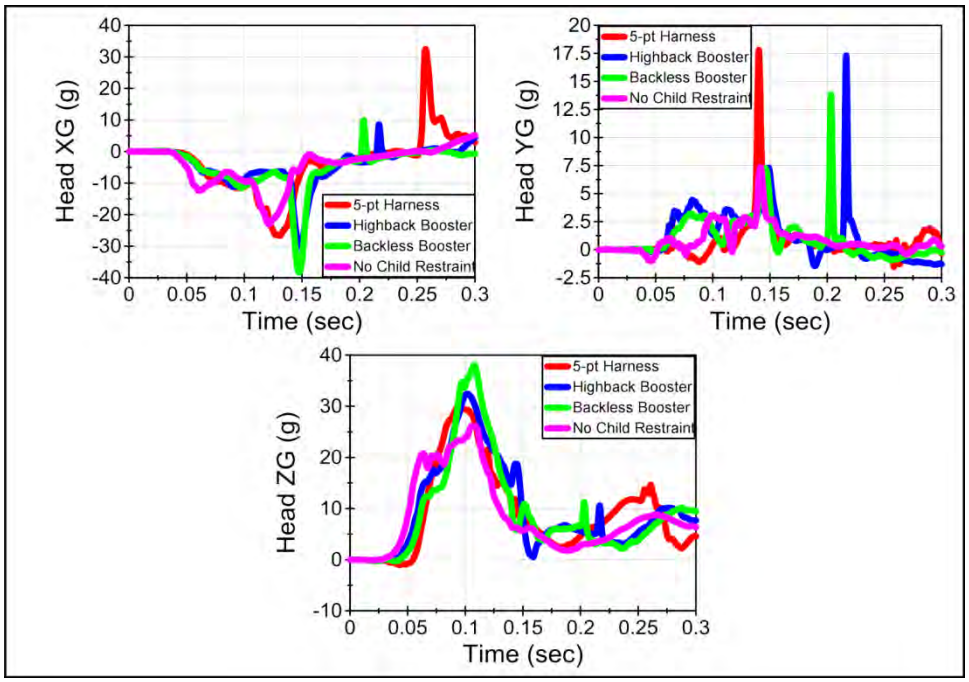

Figure 202. A comparison of head accelerations in the LODC for all CRS configurations in 40 km/h test.

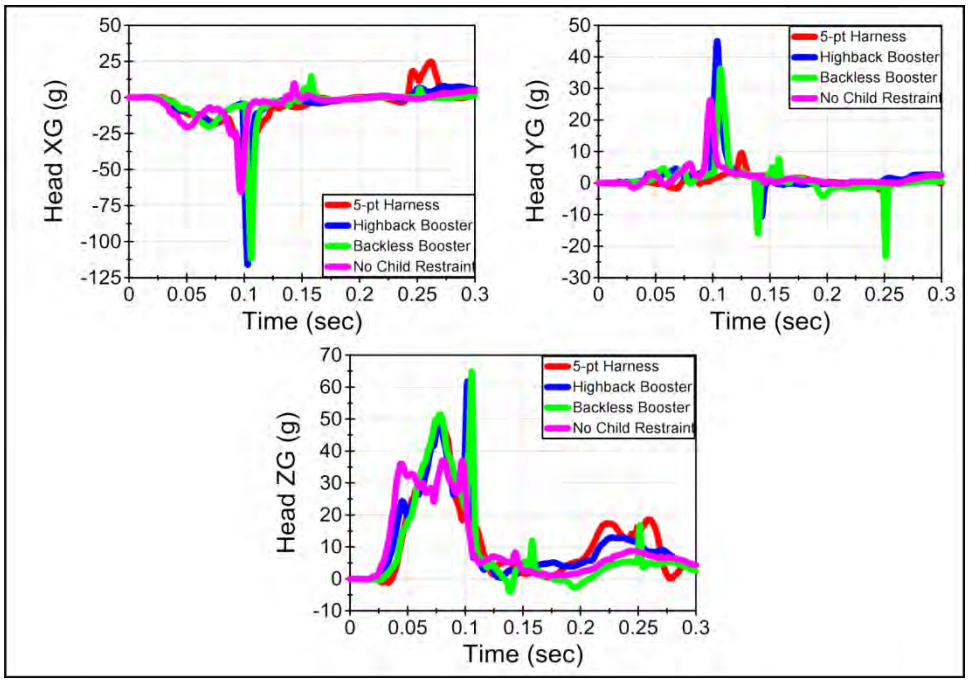

Figure 203. A comparison of head accelerations in the LODC for all CRS configurations in 48 km/h (FMVSS No. 213) test.

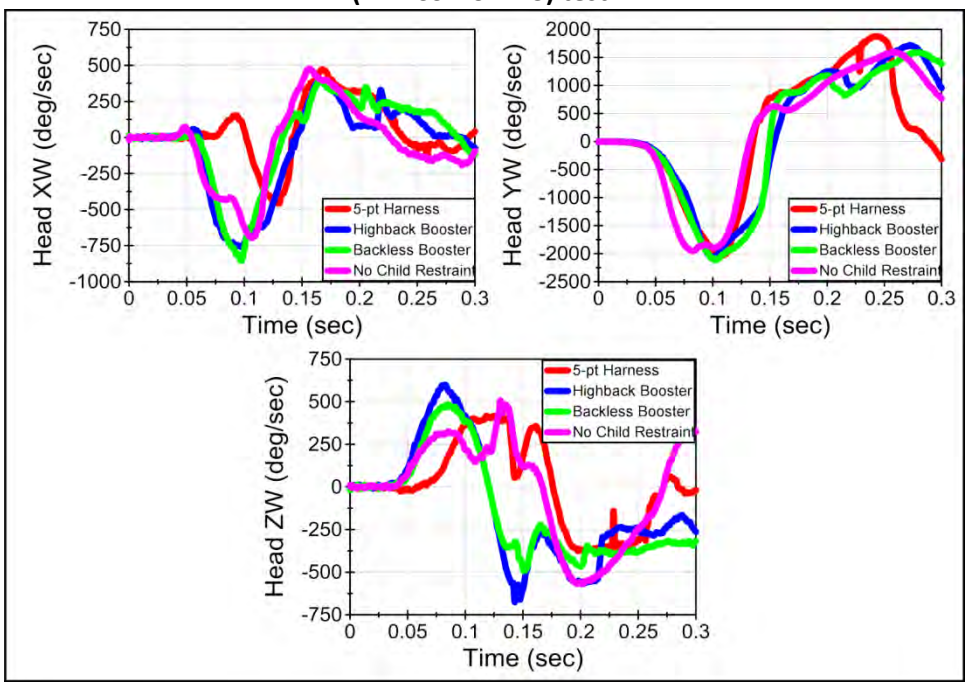

Figure 204. A comparison of head angular rates in the LODC for all CRS configurations in 40 km/h test.

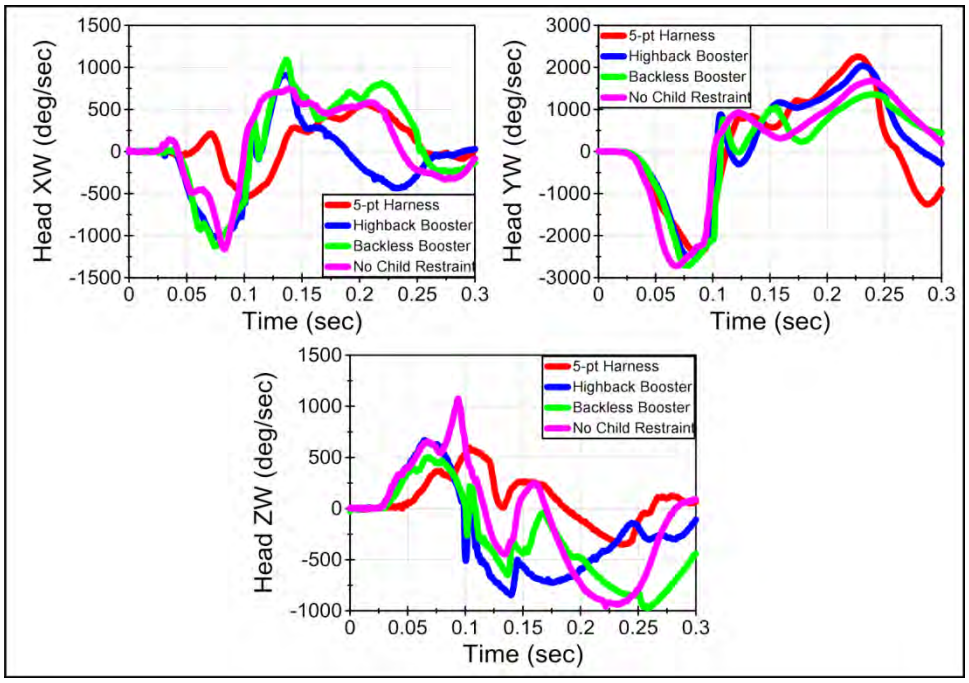

Figure 205. A comparison of head angular rates in the LODC for all CRS configurations in 48 km/h (FMVSS No. 213) test.

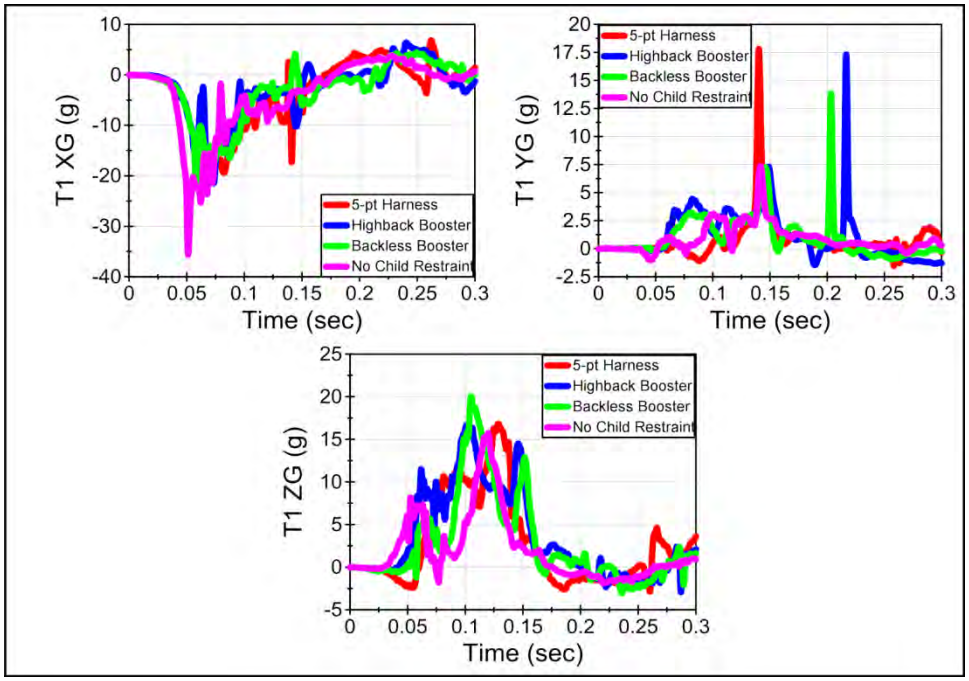

Figure 206. A comparison of T1 (neck) accelerations in the LODC for all CRS configurations in 40 km/h test.

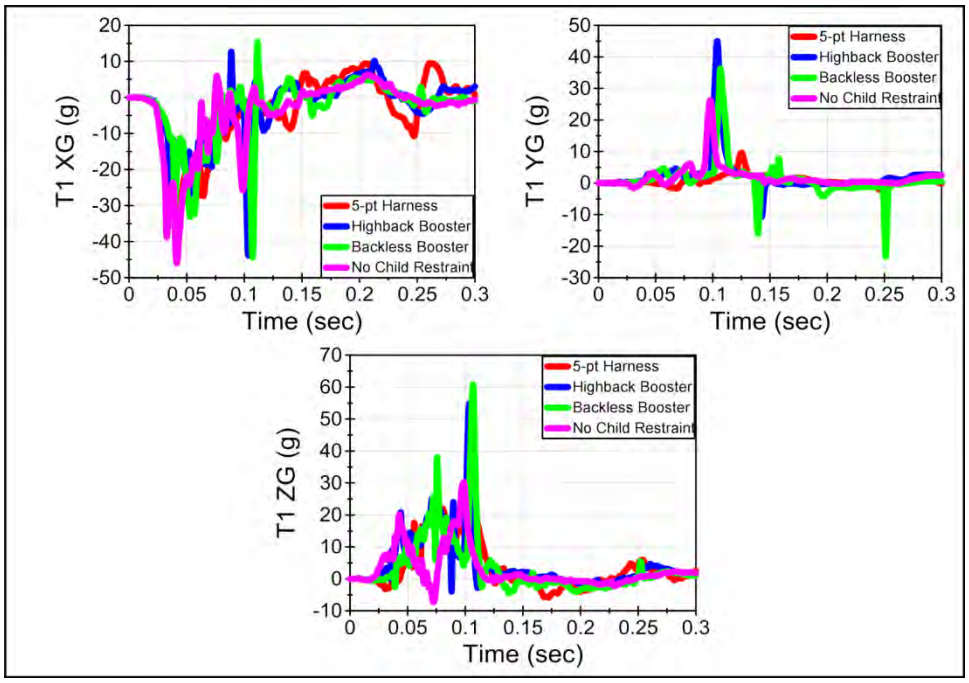

Figure 207. A comparison of T1 (neck) accelerations in the LODC for all CRS configurations in 48 km/h (FMVSS No. 213) test.

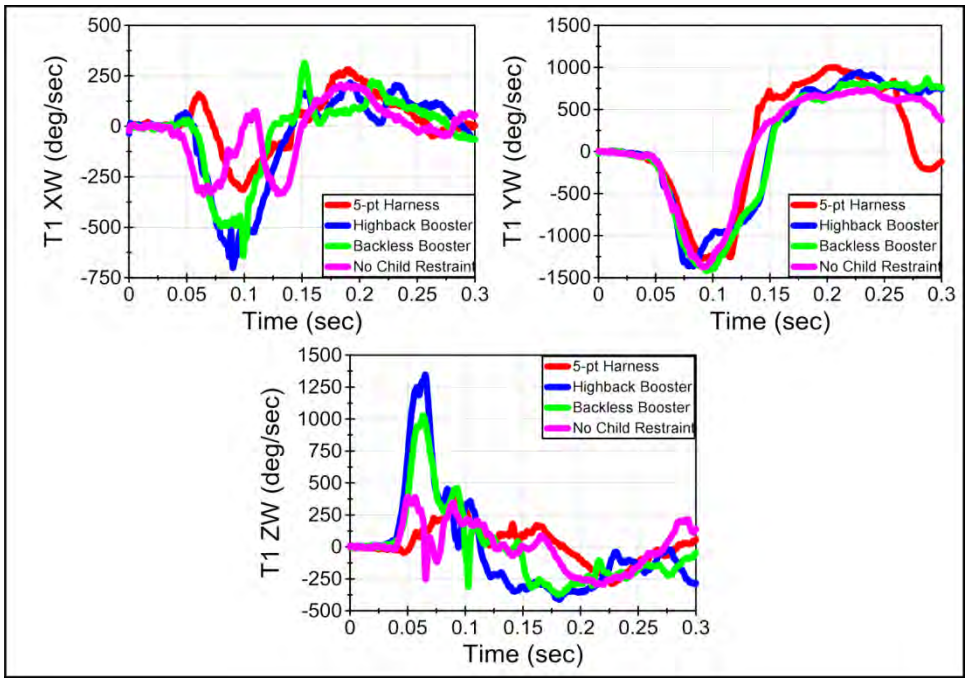

Figure 208. A comparison of T1 (neck) angular rates in the LODC for all CRS configurations in 40 km/h test.

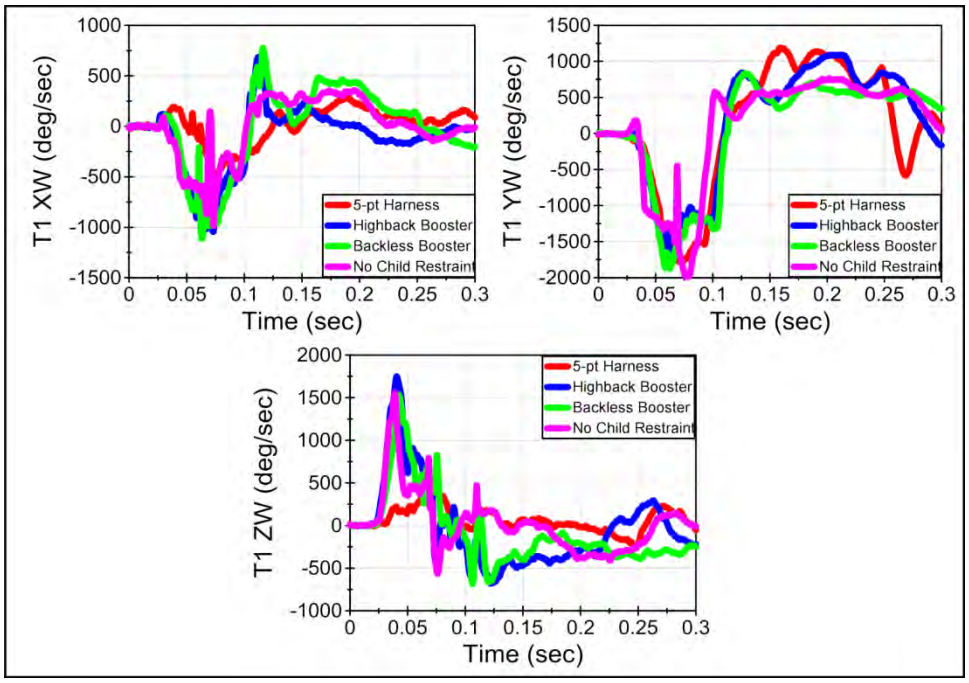

Figure 209. A comparison of T1 (neck) angular rates in the LODC for all CRS configurations in 48 km/h (FMVSS No. 213) test.

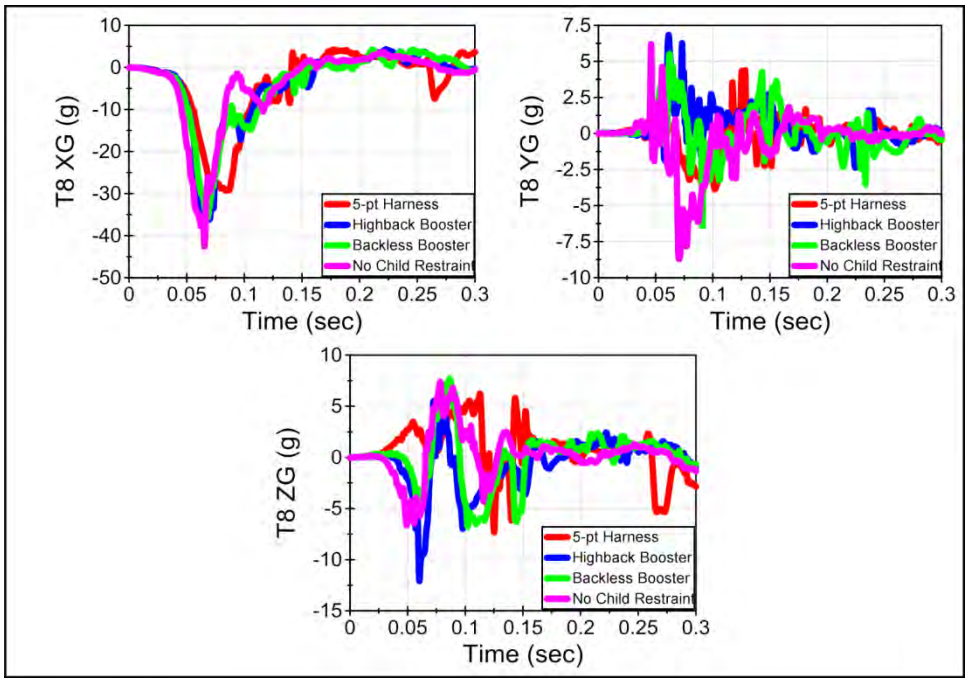

Figure 210. A comparison of T8 (mid-spine) accelerations in the LODC for all CRS configurations in 40 km/h test.

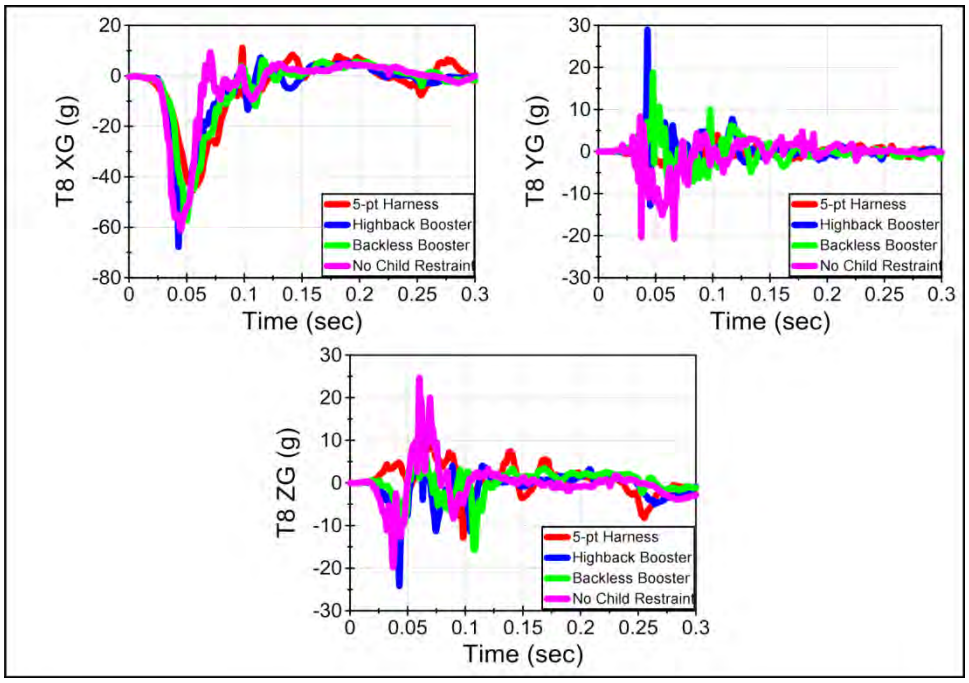

Figure 211. A comparison of T8 (mid-spine) accelerations in the LODC for all CRS configurations in 48 km/h (FMVSS No. 213) test.

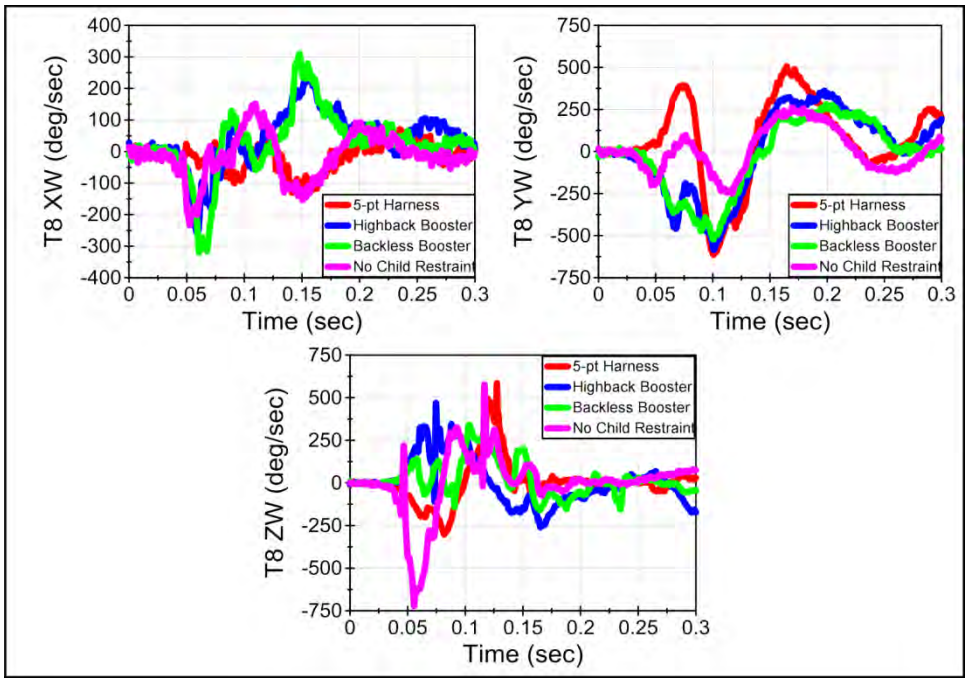

Figure 212. A comparison of T8 (mid-spine) angular rates in the LODC for all CRS configurations in 40 km/h test.

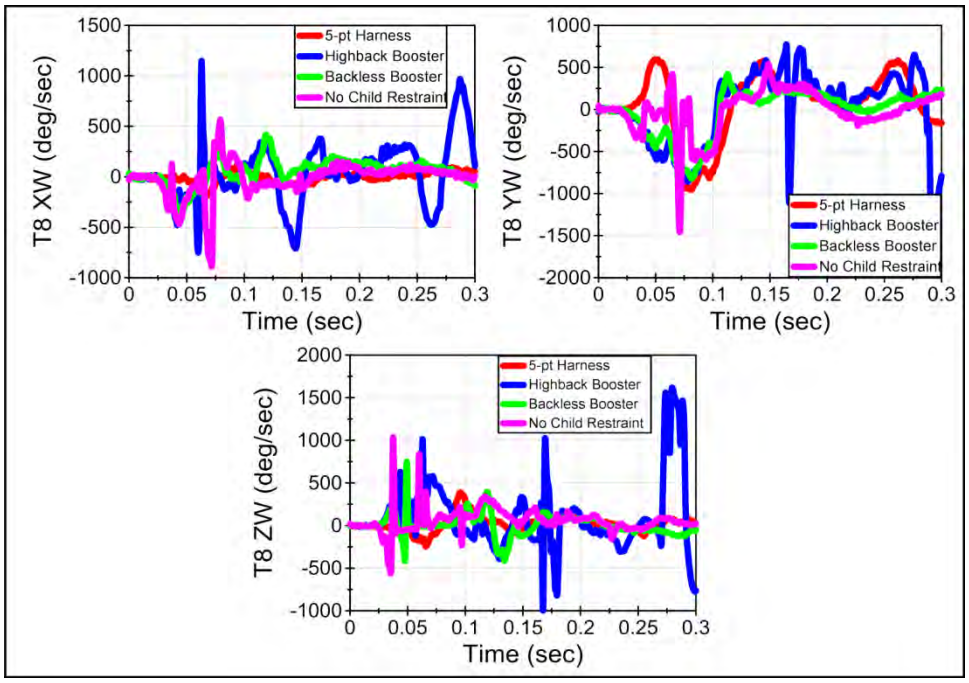

Figure 213. A comparison of T8 (mid-spine) angular rates in the LODC for all CRS configurations in 48 km/h (FMVSS No. 213) test.

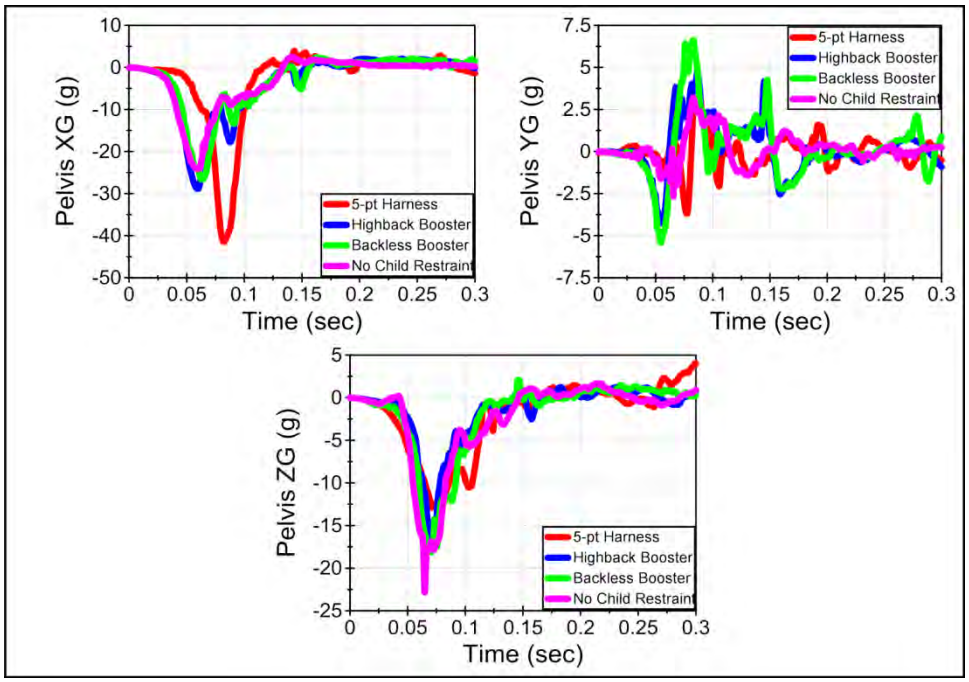

Figure 214. A comparison of pelvis accelerations in the LODC for all CRS configurations in 40 km/h test.

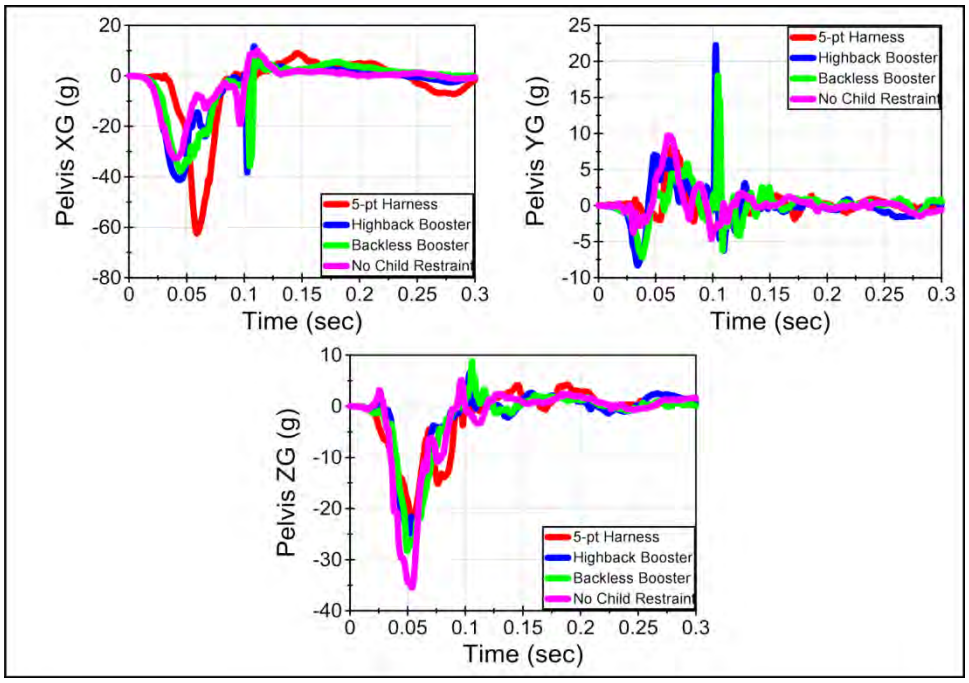

Figure 215. A comparison of pelvis accelerations in the LODC for all CRS configurations in 48 km/h (FMVSS No. 213) test.

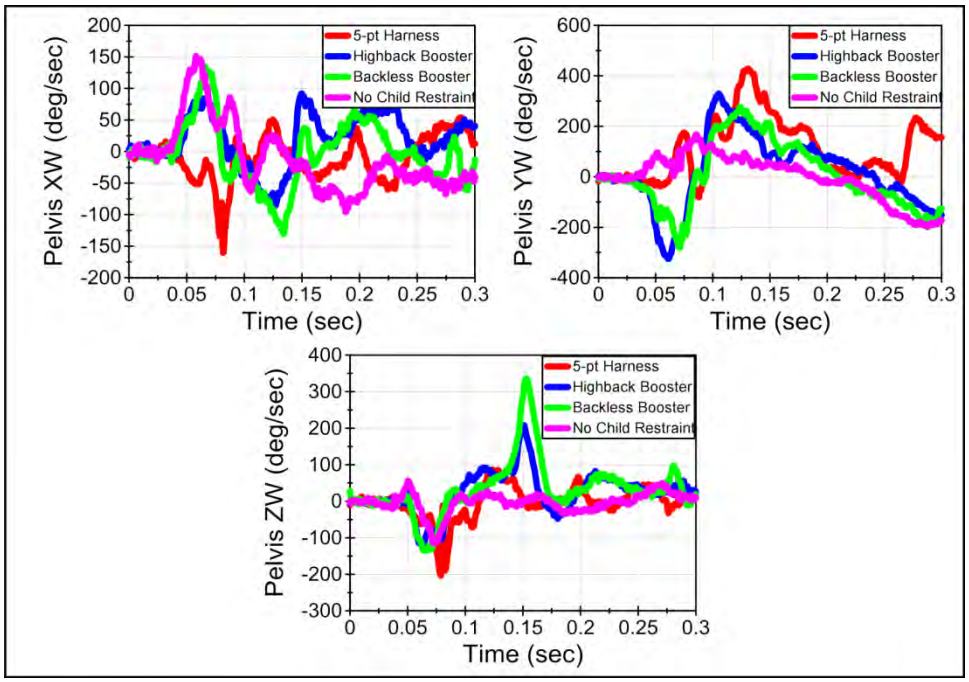

Figure 216. A comparison of pelvis angular rates in the LODC for all CRS configurations in 40 km/h test.

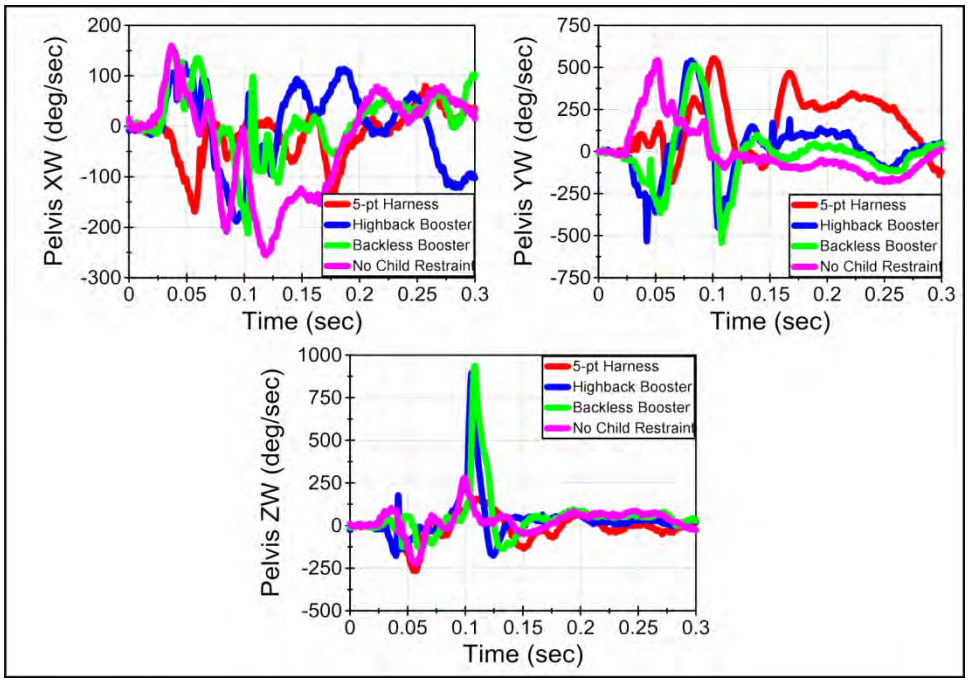

Figure 217. A comparison of pelvis angular rates in the LODC for all CRS configurations in 48 km/h (FMVSS No. 213) test.

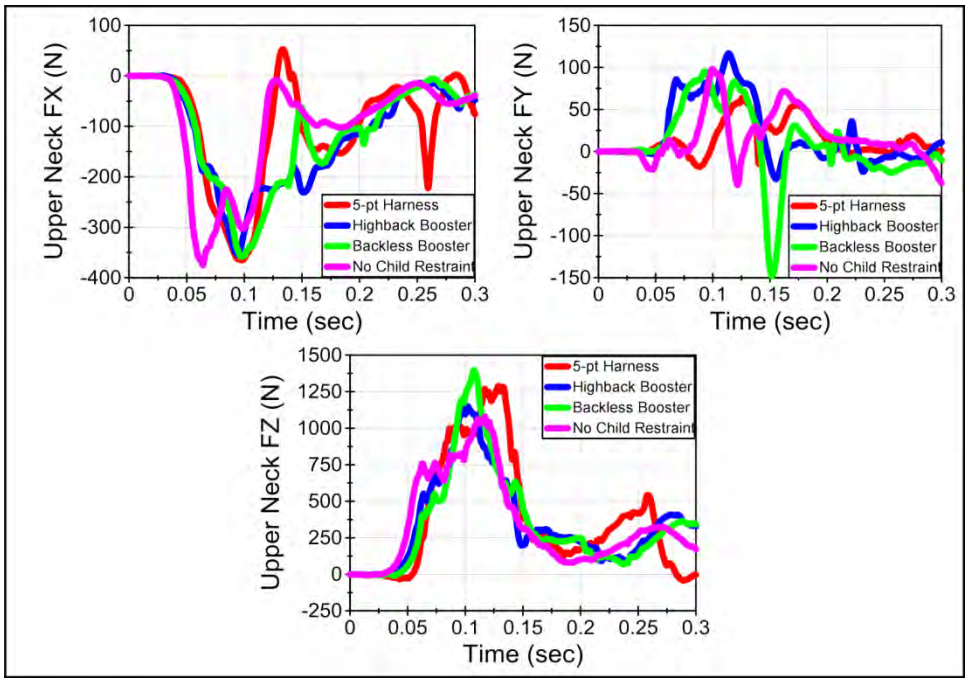

Figure 218. A comparison of upper neck forces in the LODC for all CRS configurations in 40 km/h test.

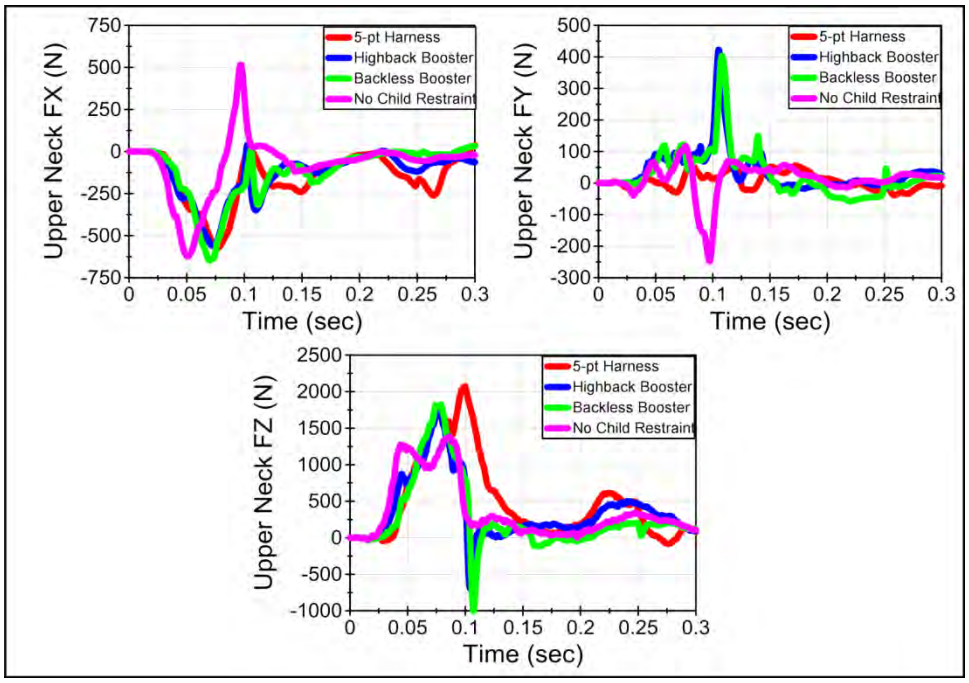

Figure 219. A comparison of upper neck forces in the LODC for all CRS configurations in 48 km/h (FMVSS No. 213) test.

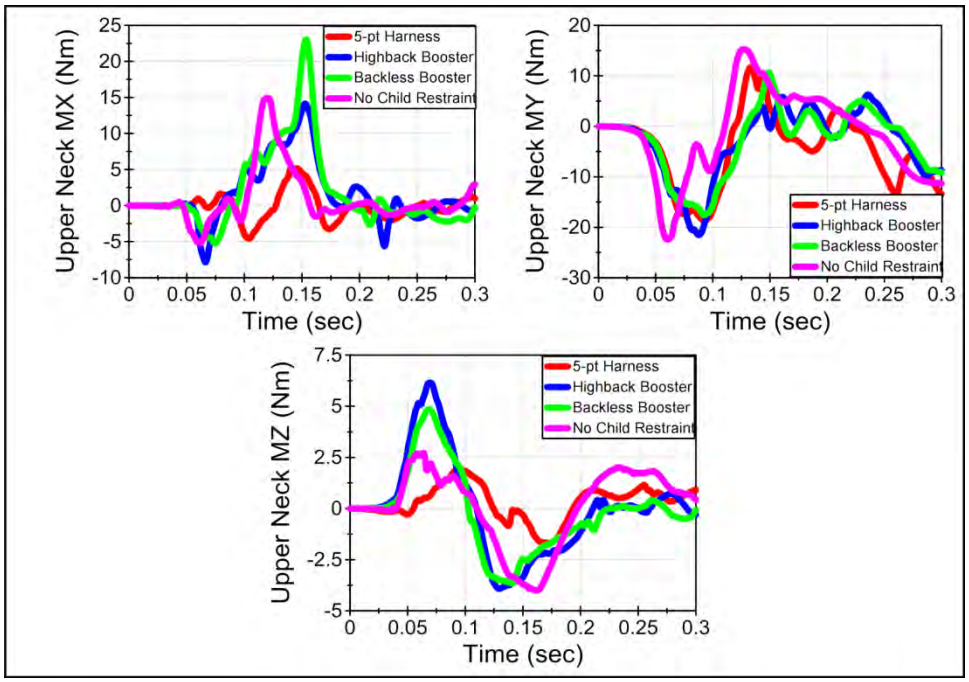

Figure 220. A comparison of upper neck moments in the LODC for all CRS configurations in 40 km/h test.

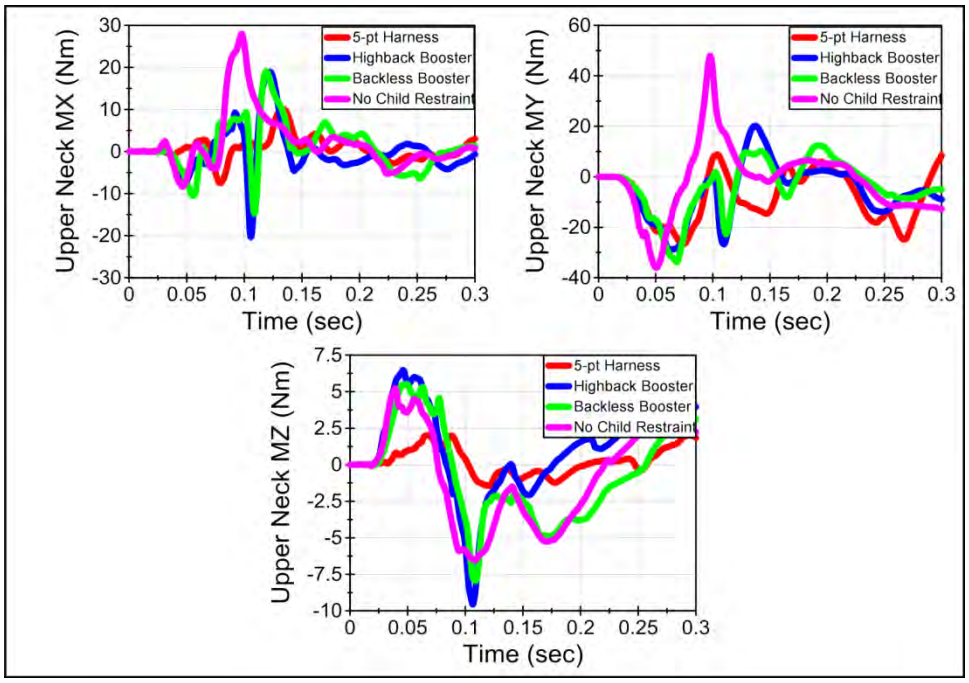

Figure 221. A comparison of upper neck moments in the LODC for all CRS configurations in 48 km/h (FMVSS No. 213) test.

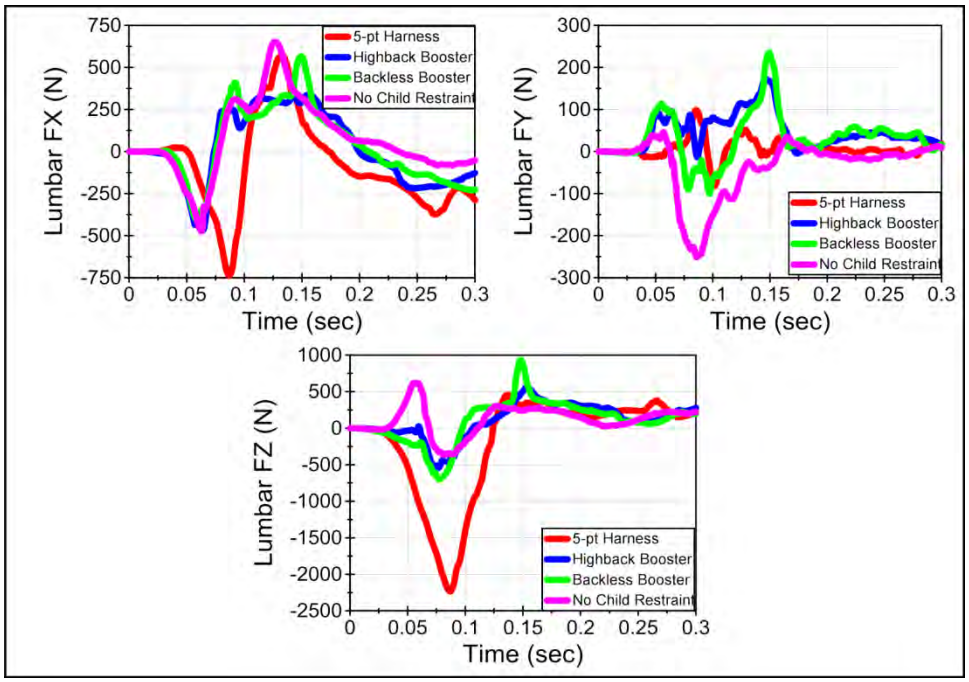

Figure 222. A comparison of lumbar forces in the LODC for all CRS configurations in 40 km/h test.

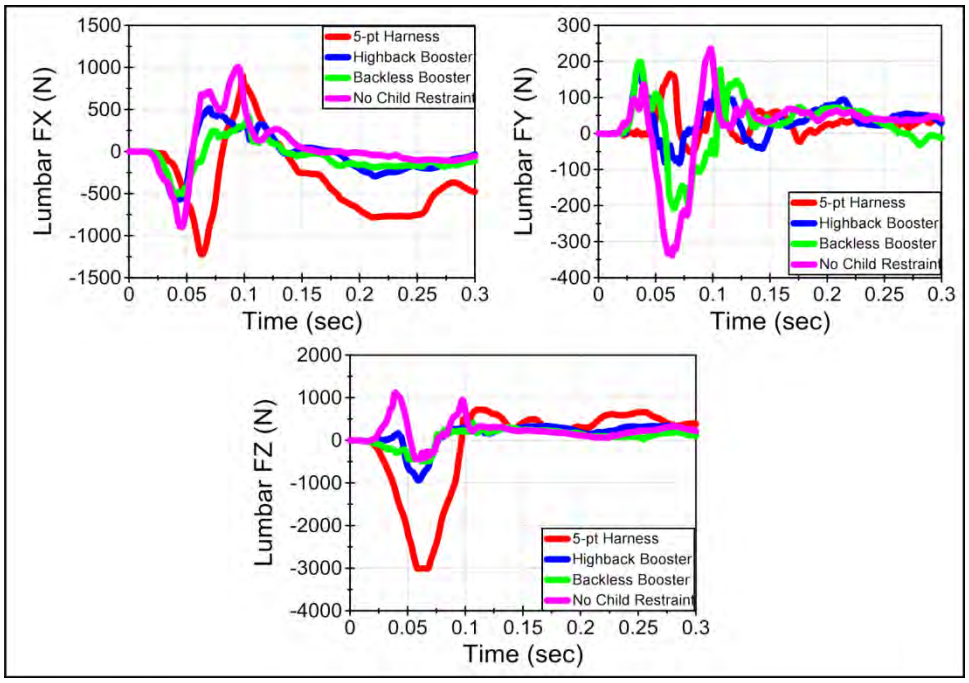

Figure 223. A comparison of lumbar forces in the LODC for all CRS configurations in 48 km/h (FMVSS No. 213) test.

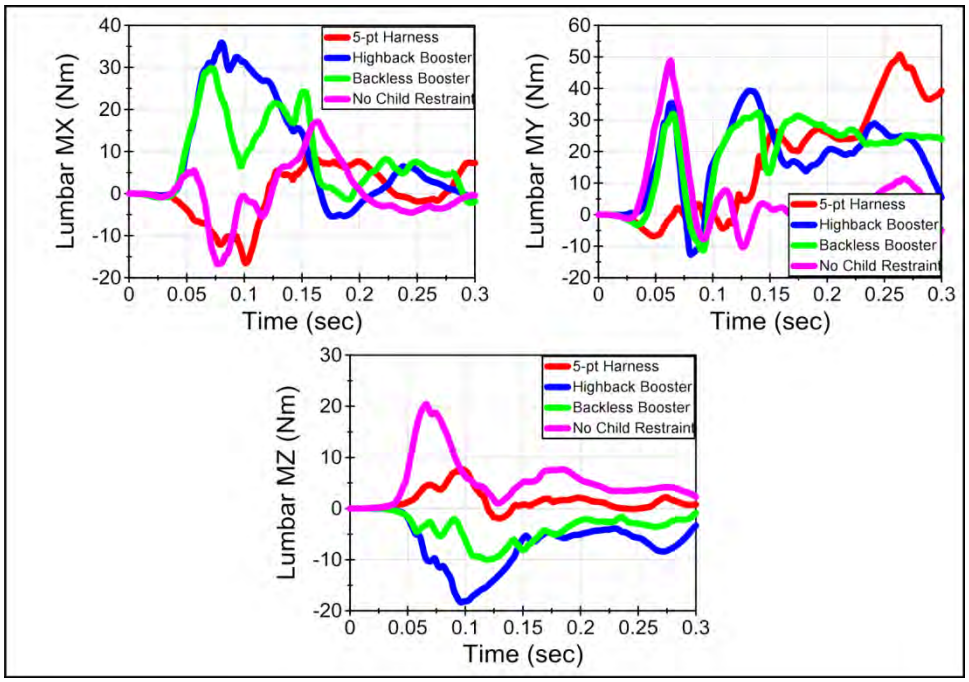

Figure 224. A comparison of lumbar moments in the LODC for all CRS configurations in 40 km/h test.

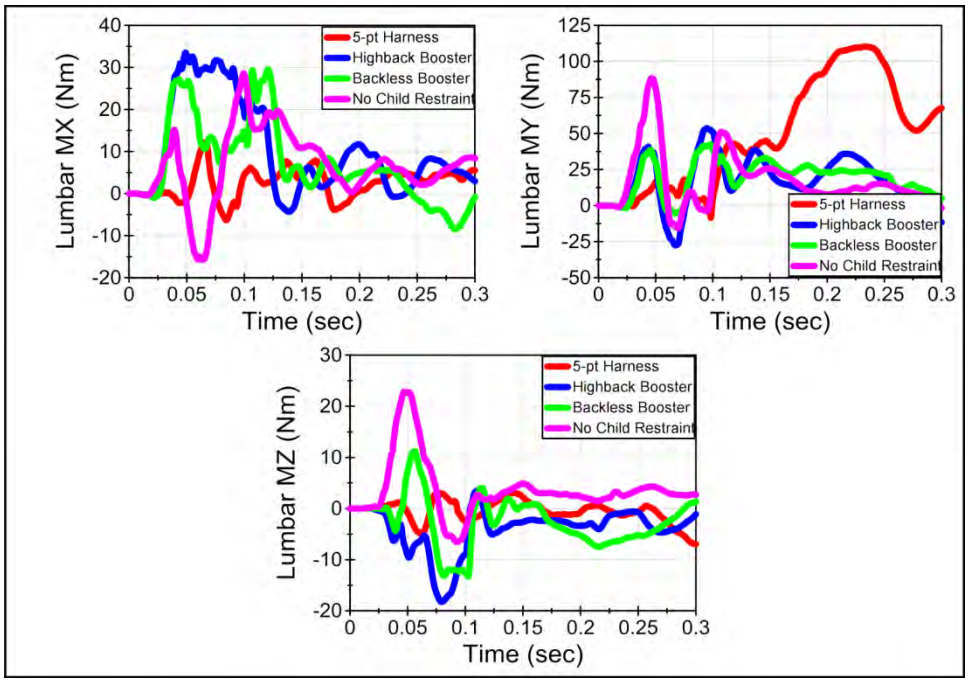

Figure 225. A comparison of lumbar moments in the LODC for all CRS configurations in 48 km/h (FMVSS No. 213) test.

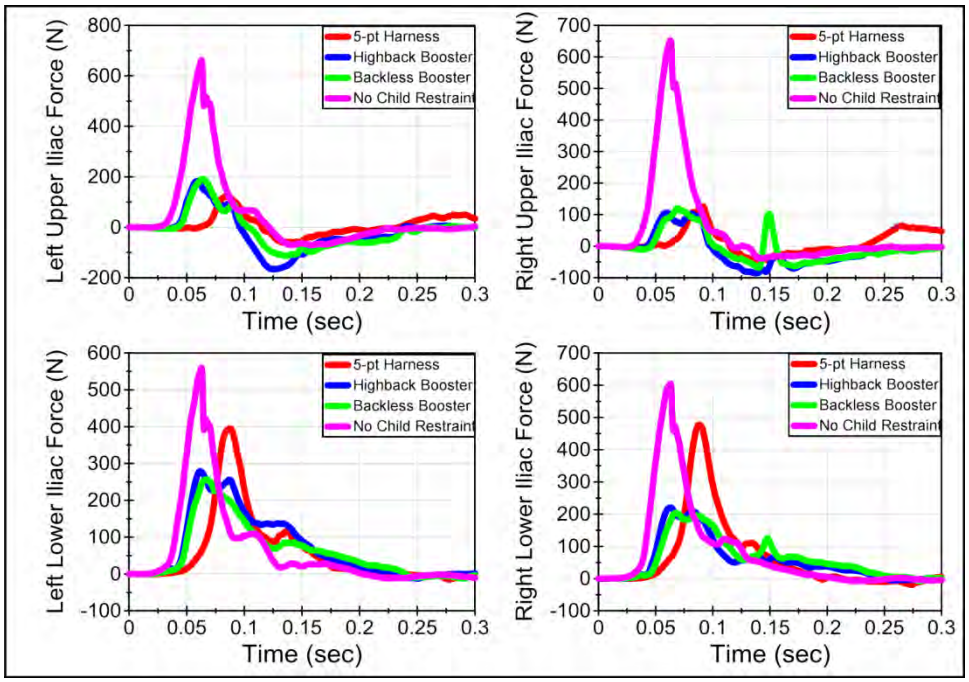

Figure 226. A comparison of iliac forces in the LODC for all CRS configurations in 40 km/h test.

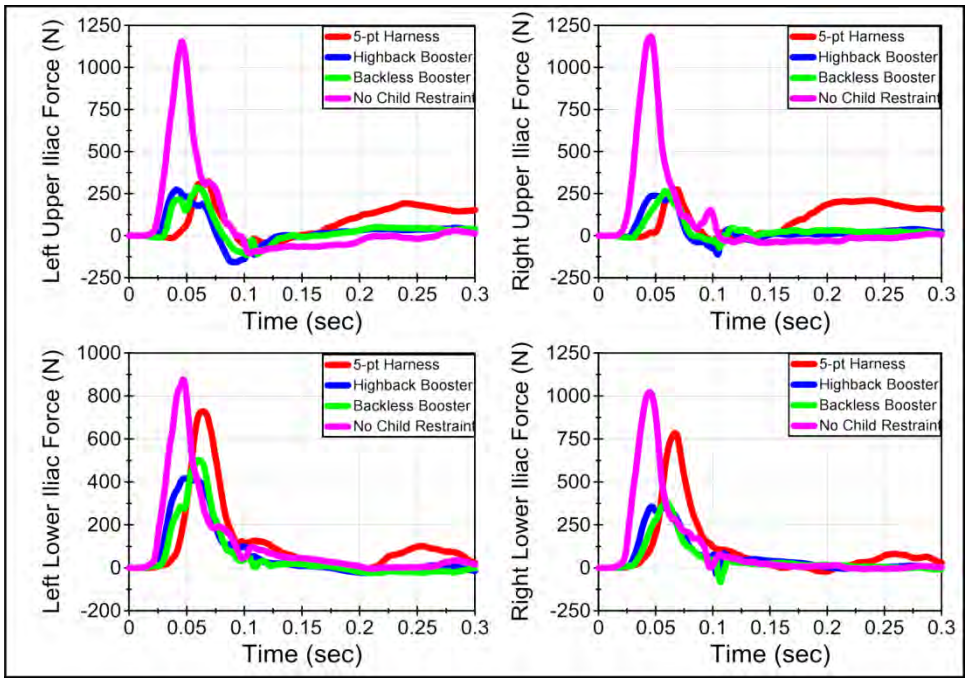

Figure 227. A comparison of iliac forces in the LODC for all CRS configurations in 48 km/h (FMVSS No. 213) test.

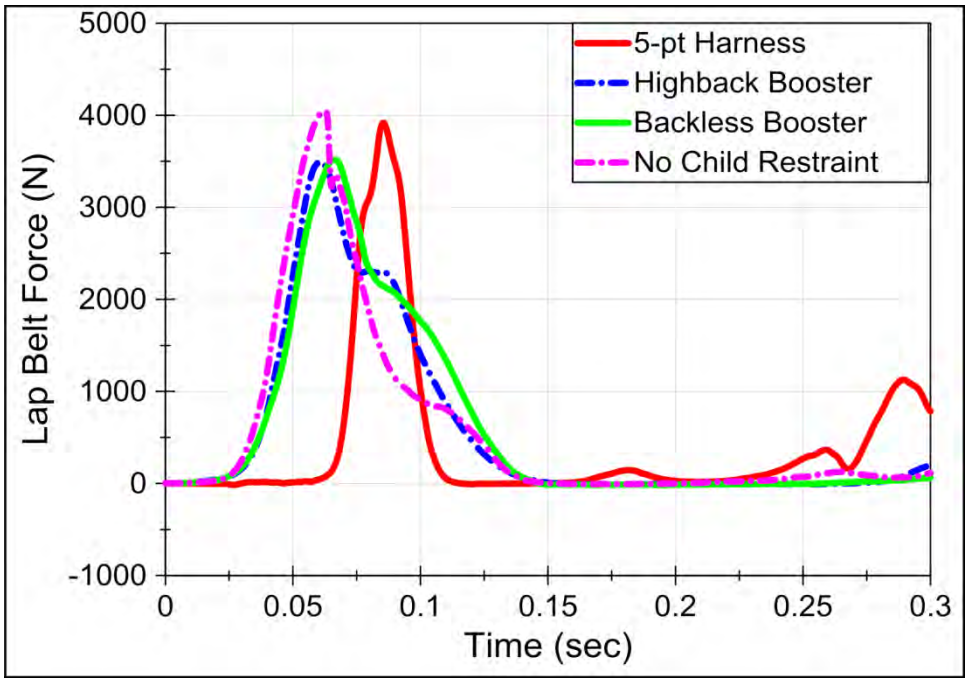

Figure 228. A comparison of lap belt forces in the LODC for all CRS configurations in 40 km/h test.

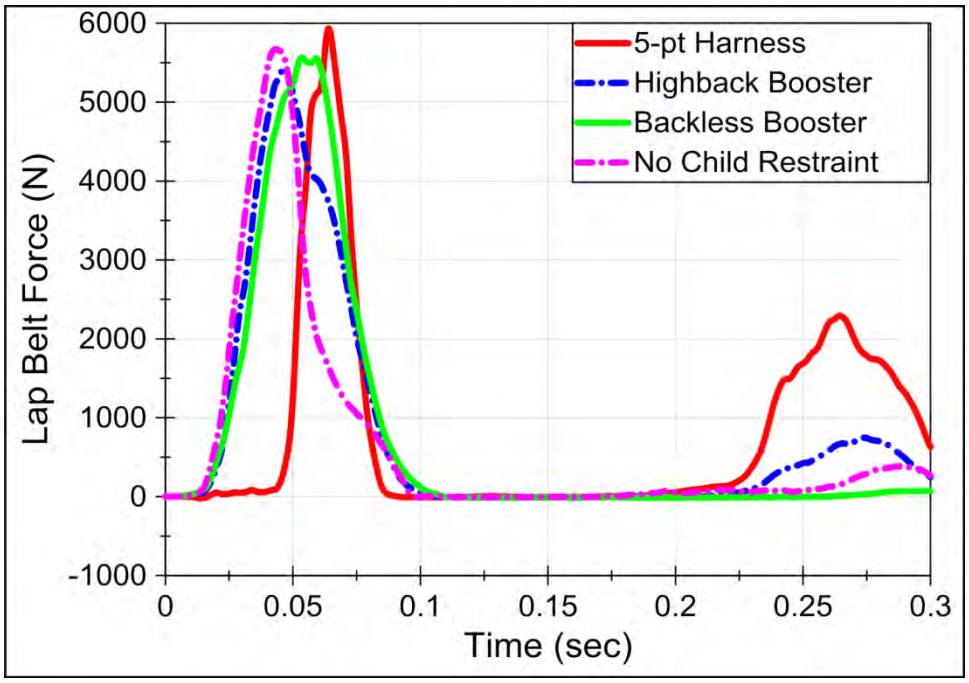

Figure 229. A comparison of lap belt forces in the LODC for all CRS configurations in 48 km/h (FMVSS No. 213) test.

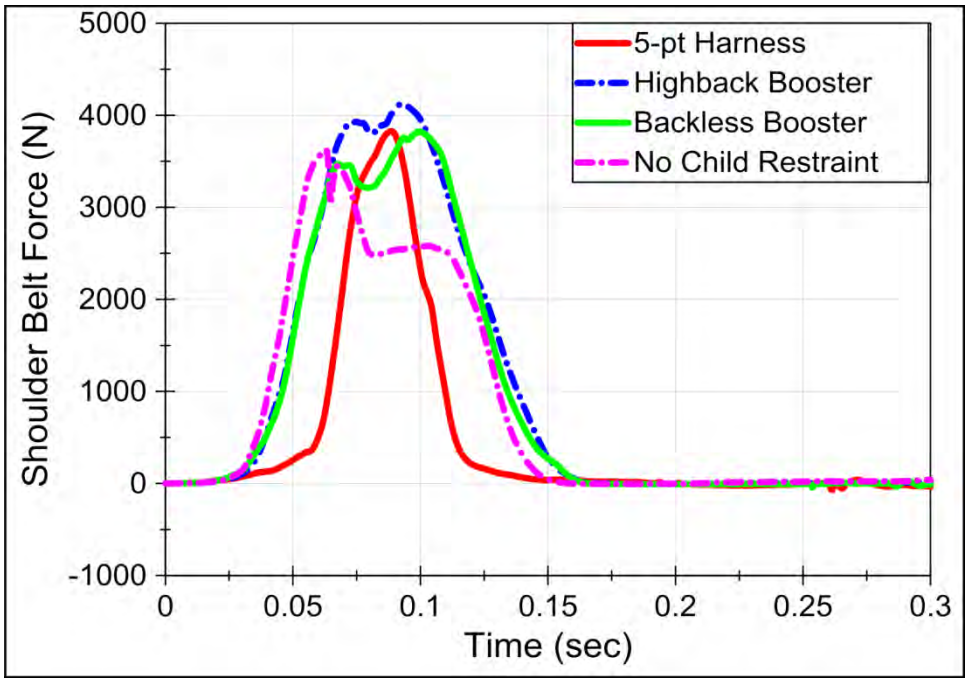

Figure 230. A comparison of shoulder belt forces in the LODC for all CRS configurations in 40 km/h test.

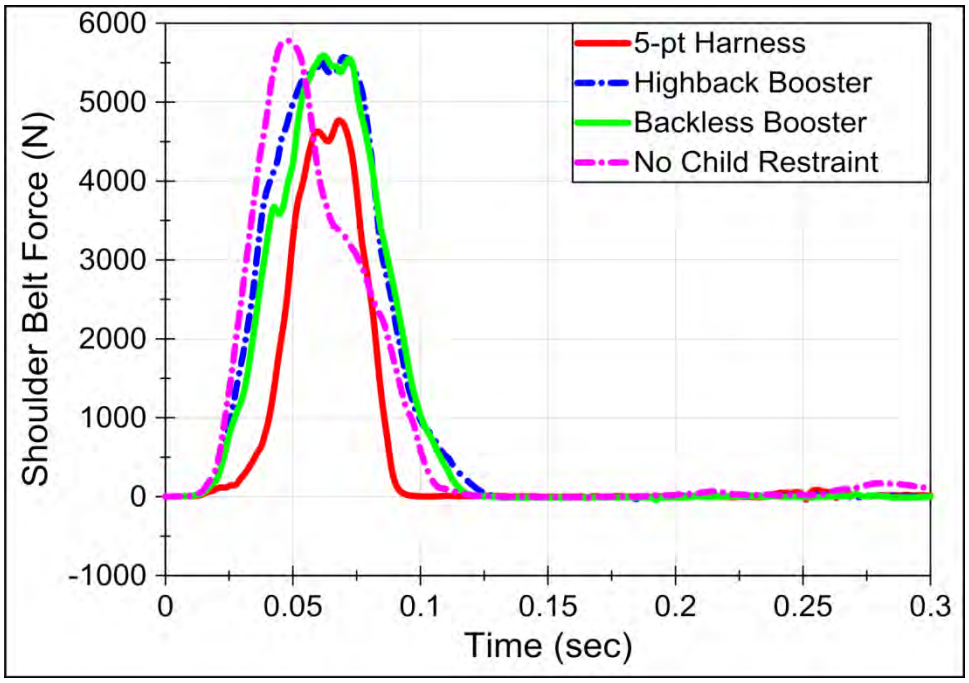

Figure 231. A comparison of shoulder belt forces in the LODC for all CRS configurations in 48 km/h (FMVSS No. 213) test.

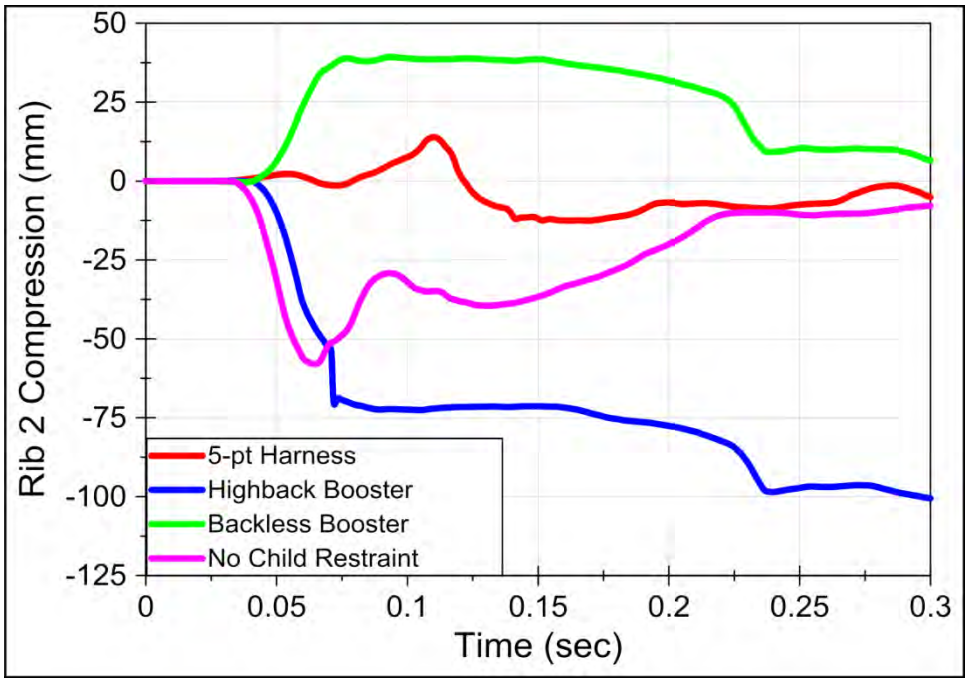

Figure 232. A comparison of rib 2 compressions in the LODC for all CRS configurations in 40 km/h test.

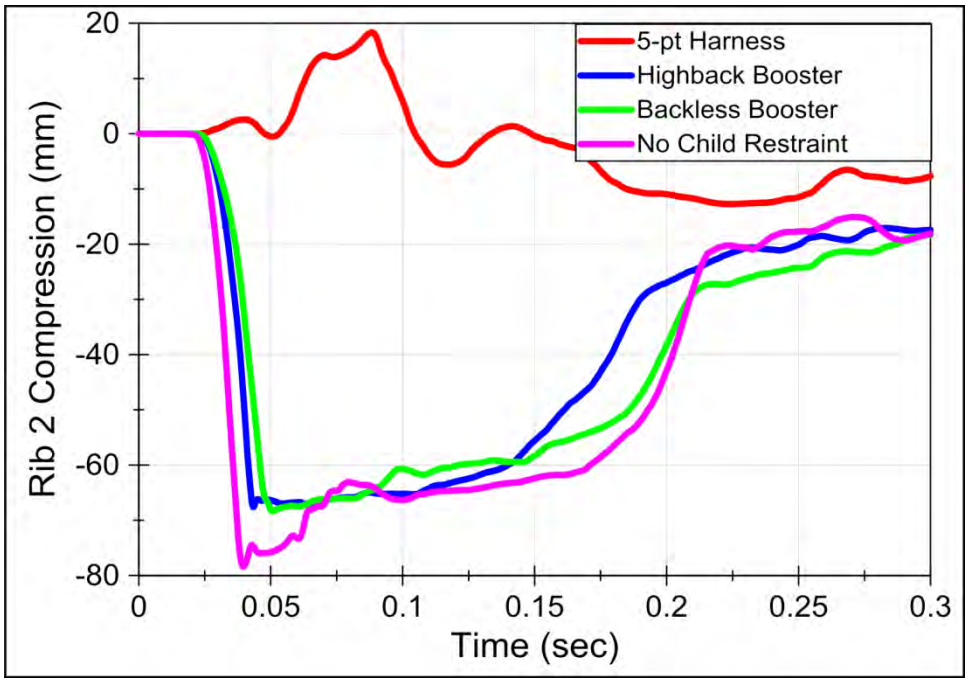

Figure 233. A comparison of rib 2 compressions in the LODC for all CRS configurations in 48 km/h (FMVSS No. 213) test.

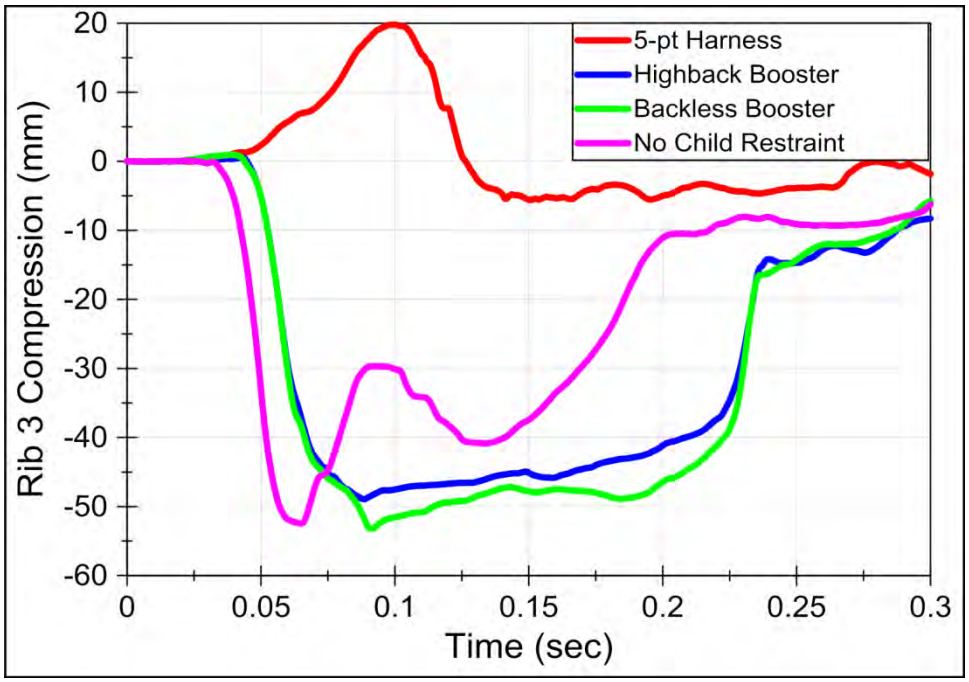

Figure 234. A comparison of rib 3 compressions in the LODC for all CRS configurations in 40 km/h test.

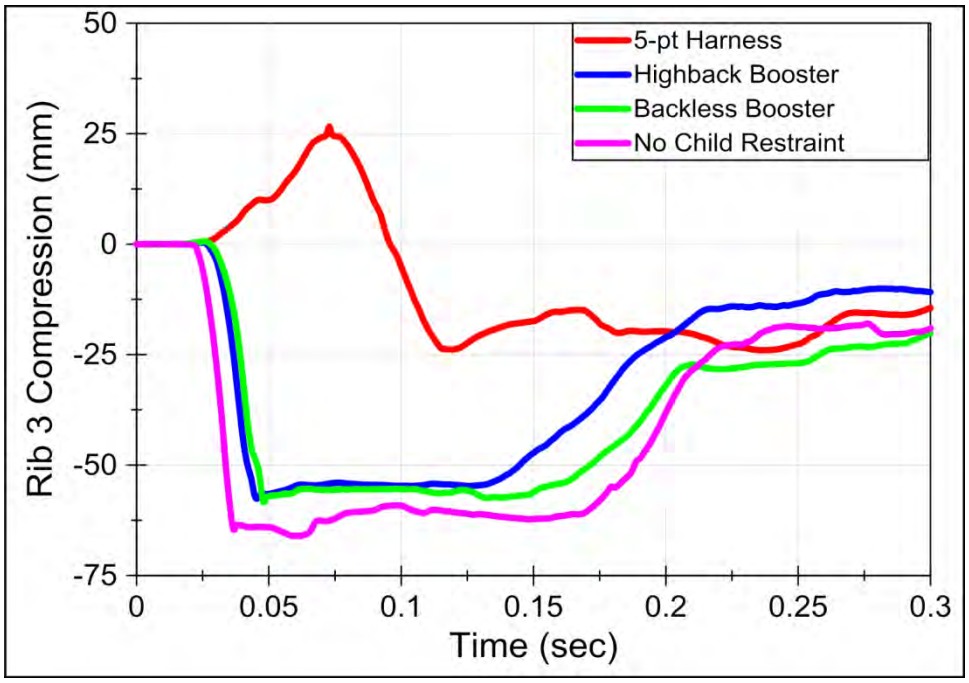

Figure 235. A comparison of rib 3 compressions in the LODC for all CRS configurations in 48 km/h (FMVSS No. 213) test.

DOT HS 812
December 2014

U.S. Department
of Transportation
**National Highway
Traffic Safety
Administration**

www.nhtsa.gov

11090-121514-v1b